

August 2020

Late Paleozoic Climatic Reconstruction of Western Argentina: Glacial Extent and Deglaciation of Southwestern Gondwana

Kathryn N. Pauls
University of Wisconsin-Milwaukee

Follow this and additional works at: <https://dc.uwm.edu/etd>



Part of the [Climate Commons](#), [Geochemistry Commons](#), and the [Geology Commons](#)

Recommended Citation

Pauls, Kathryn N., "Late Paleozoic Climatic Reconstruction of Western Argentina: Glacial Extent and Deglaciation of Southwestern Gondwana" (2020). *Theses and Dissertations*. 2576.
<https://dc.uwm.edu/etd/2576>

This Dissertation is brought to you for free and open access by UWM Digital Commons. It has been accepted for inclusion in Theses and Dissertations by an authorized administrator of UWM Digital Commons. For more information, please contact open-access@uwm.edu.

LATE PALEOZOIC CLIMATIC RECONSTRUCTION OF WESTERN ARGENTINA:
GLACIAL EXTENT AND DEGLACIATION OF SOUTHWESTERN GONDWANA

by

Kathryn N. Pauls

A Dissertation Submitted in
Partial Fulfillment of the
Requirements for the Degree of

Doctor of Philosophy
in Geosciences

at

The University of Wisconsin-Milwaukee

August 2020

ABSTRACT

LATE PALEOZOIC CLIMATE RECONSTRUCTION OF WESTERN ARGENTINA: GLACIAL EXTENT AND DEGLACIATION OF SOUTHWESTERN GONDWANA

by

Kathryn N. Pauls

The University of Wisconsin-Milwaukee, 2020
Under the Supervision of Professor John L. Isbell

Throughout its history Earth has experienced both icehouse and greenhouse conditions. Shifts and transitions from one end member to the other are driven by numerous driving mechanisms on global, orbital and more local scales. In particular, the late Paleozoic ice age (LPIA) is thought to have been driven by global drivers such as the drift of the Gondwanan continent across the South Pole, fluctuations in atmospheric CO₂ concentrations, and Milankovitch cycles. It was also affected by more local and regional drivers such as active tectonism along accretionary margins and changes in atmospheric and oceanic circulation patterns. South American Gondwana provides an excellent opportunity to examine and evaluate the effects that global versus local driving mechanisms had on regional climates during the shift from icehouse to greenhouse conditions around the Carboniferous-Permian boundary. Of particular interest to this study are the margin and foreland basins of western Argentina in comparison to their paleolatitudinal counterparts of Brazil and eastern Argentina (i.e. the Chaco-Paraná and Paraná basins). This study focuses on determining the extent of glaciation during the Serpukhovian-Bashkirian of the Paganzo and Calingasta-Uspallata basins, the subsequent and relatively early deglaciation and shift in climate from humid conditions to extreme aridity, and the driving

mechanisms for this change. This study tracks changes in facies, sediment dispersal, and climate indicators throughout the late Paleozoic strata in the Paganzo, Calingasta-Uspallata and Paraná basins, with special focus on the Paganzo Group strata. Here, we conclude that glaciation of the Paganzo and Calingasta-Uspallata basins was restricted to the Precordilleran region and nucleated on a significant uplift known as the Protoprecordillera and adjacent uplands. A paleoclimate reconstruction for the late Carboniferous using the Chemical Index of Alteration (CIA) indicates a shift from cold and arid to warm and humid following the deglaciation of the region, which is then succeeded by a drastic shift to an extremely arid environment. A provenance study using detrital zircon geochronology for selected units of the Paganzo Group strata indicates a restricted foreland basin setting in the early-middle Carboniferous that evolves and broadens through the Pennsylvanian and into the Permian as the active tectonic margin moves westward. With the accretion of a magmatic arc during the latest Carboniferous, the detrital zircon geochronology and the facies of the Paganzo Group record an enhancement, or an increase/expansion of the orographic effect originally created by the Protoprecordilleran range during the early-middle Carboniferous glaciation.

© Copyright by Kathryn N. Pauls, 2020
All Rights Reserved

TABLE OF CONTENTS

TABLE OF CONTENTS.....	v
LIST OF FIGURES	xi
ACKNOWLEDGEMENTS	xvii
Chapter 1. Introduction	1
The late Paleozoic ice age and Gondwana	1
Significance of western Gondwana basins.....	3
Paganzo Basin.....	4
Calingasta-Uspallata Basin.....	7
Paraná Basin	8
The Significance of the Protoprecordillera	9
Objectives.....	10
Significance of Research.....	11
Dissertation Structure	12
References	20
Chapter 2: Constraining late Paleozoic ice extent in the Paganzo Basin of western Argentina using U-Pb detrital zircon geochronology for the lower Paganzo Group strata	28
Abstract	28
1. Introduction	30
2. Background	31

3. Regional Geologic Setting	34
3.1 Geology of the Lower Paganzo Group strata	36
3.2. Olta-Malanzán paleovalley.....	37
3.3. Huaco locality.....	38
4. Methods.....	38
4.1. Lithofacies and Paleocurrent Analyses methods	38
4.2. Detrital zircon U-Pb geochronology analyses methods	39
5. Lithofacies analysis.....	41
5.1. Facies 1 – Diamictite Facies.....	43
5.2. Facies 2 – Conglomerate Facies	45
5.3. Facies 3 – Laminated Mudstone Facies.....	47
5.4. Facies 4 – Interbedded Mudstone and Sandstone.....	49
5.5. Facies 5 – Cross-bedded sandstone Facies.....	51
5.6. Facies 6 – Rippled Sandstone.....	53
6. Paleoflow and depositional environments.....	54
7. Detrital Zircon Geochronology Results	56
7.1. CDH0923-3S, Guandacol Formation, Huaco Locality	56
7.2. Previously published geochronology samples.....	57
8. Discussion	58
9. Evidence for mid-Carboniferous ice extent in the Paganzo Basin.....	62

9.1. Post-glacial sedimentation.....	66
10. Conclusions.....	68
Acknowledgements.....	69
References.....	80
Chapter 3: A paleoclimatic reconstruction of the Carboniferous-Permian paleovalley fill in the Eastern Paganzo Basin: Insights into glacial extent and deglaciation of southwestern Gondwana	
.....	95
Abstract.....	96
1. Introduction.....	97
2. Paganzo Basin.....	99
2.1. Eastern Paganzo Basin: Olta-Malanzán Paleovalley (OMPV).....	102
3. Chemical Index of Alteration as a Paleoclimatic Indicator.....	104
4. Methods.....	107
5. Stratigraphy of the OMPV.....	109
6. CIA Values for OMPV.....	113
7. Paleoclimate implications for the Eastern Paganzo Basin.....	114
8. Conclusion.....	119
Acknowledgements.....	120
Chapter 4. Late Paleozoic paleoclimate reconstruction of the Paganzo Basin of western Argentina: Controls on early Pennsylvanian deglaciation in western South American Gondwana	
.....	142

Abstract	142
1. Introduction	143
2. Regional Geologic Setting	146
2.1 Late Paleozoic basins of South America	146
2.2. Rise and fall of the Protoprecordillera.....	147
3. Geology of late Paleozoic South American basins	150
3.1. Strata of the western active margin basins	151
3.2. Paraná Basin strata.....	154
4. Bulk-rock major element geochemistry analyses.....	155
5. Geochemistry methods.....	156
6. CIA Analysis	158
7. Paleoclimate of Southern South American Basins.....	160
7.1. Western Margin Basins	160
7.2. Paraná Basin	165
8. Deglaciation of South American Gondwana during the LPIA	166
9. Tectonism as a control on climate change in southwestern Gondwana	168
10. Conclusions	172
References	184
Chapter 5. Provenance and paleogeography of the Paganzo Basin: Detrital zircon geochronology of the upper Paganzo Group strata.....	195

Abstract	195
1. Introduction	196
2. Regional Geologic Setting	197
3. Late Paleozoic strata of the Paganzo Basin.....	200
3.1. Agua Hedionda, Huaco locality.....	203
3.2. Olta-Malanzán paleovalley.....	203
4. Detrital zircon U-Pb geochronology analyses methods	204
5. Detrital Zircon Geochronology of the Paganzo Basin	206
6. Comparative detrital zircon sample.....	207
7. Provenance of the upper Paganzo Group Strata.....	209
7.1. Agua Hedionda, Huaco Provenance.....	209
7.2. Olta-Malanzán Provenance.....	211
8. Latest Pennsylvanian Paganzo Basin development	212
9. Implications for western Gondwana late Paleozoic climate	214
10. Future considerations	216
11. Conclusions	217
Chapter 6. Conclusions	237
Outcomes of stated project objectives.....	237
Implications of early deglaciation in western Gondwana	240
Future Directions.....	241

References	244
Appendix A: Detrital Zircon Geochronology Data	246
Appendix B. Bulk Rock Geochemistry Data	258
CURRICULUM VITAE.....	264

LIST OF FIGURES

Figure 1. A. Map of sedimentary basins of Gondwana during the Bashkirian stage. RBB – Río Blanco Basin, CUB – Calingasta-Uspallata Basin, CPB – Chaco-Paraná Basin, SGB – Sauce Grande Basin, TGB – Tepuel Genoa Basin. Modified from Isbell et al. (2012) and Montañez and Poulsen (2013). B. Map of the Paganzo and Calingasta-Uspallata basins where the localities of interest are located. CG – Cerro Guandacol, AH – Agua Hedionda Anticline, near the town of Huaco, OMPV – Olta-Malanzán Paleovalley system, and AJ – Agua de Jagüel. Modified from López Gamundí et al. (1994), Henry et al. (2008), Limarino et al. (2014). 16

Figure 2. Figure 2. Chronostratigraphic columns showing the units in the selected basins for this study. The grey triangles highlighted in blue represent the interpreted glacial diamictites for each locality. CG – Cerro Guandacol, AH – Agua Hedionda Anticline, near the town of Huaco, OMPV – Olta-Malanzán Paleovalley system, and AJ – Agua de Jagüel. Modified from Henry et al. (2008). 17

Figure 3. Map of the Paraná Basin and inset of the area in Rio Grande do Sul State where the samples were collected for this project. Modified from Fedorchuk et al. (2018). 18

Figure 4. The evolutive model of the Paganzo Basin development from the middle Carboniferous to the Permian. Modified from Moxness et al. (2018). 19

Figure 5. Correlation chart for the late Paleozoic Paganzo Group strata for the sites in the Paganzo Basin, Argentina mentioned in the text. Ages and units are based on Limarino et al. (2002a, 2002b, 2006, 2014), Césari et al. (2011, 2019). 70

Figure 6. A. Map of the Paganzo Basin during the late Paleozoic with arrows indicating paleoflow measurements from numerous publications, modified from Henry et al. (2008). Paleoflow data are from the following list of papers: (1) Agua Hedionda, Huaco - Bossi and Andreis (1981), Marensi et al. (2002, 2005), López Gamundí and Martínez (2000), this study (2) Olta-Malanzán Paleovalley - Andreis et al. (1986), this study (3) Los Pozuelos Creek - Marensi et al. (2005) (4) Loma de Los Piojos - López Gamundí and Martínez (2000), Alonso-Muruaga et al. (2012) (5) Cerro Bola, Cerro Guandacol - Andreis et al. (1975), López Gamundí et al. (1994), Dykstra et al. (2011), Fallgatter et al. (2019); (6) López Gamundí and Amos (1985), López Gamundí et al. (1994) (7) Cortaderas - Scalabrini Ortiz (1972), López Gamundí et al. (1994), Henry et al. (2010) (8) Talacasto - Aquino et al. (2014) (9) Henry et al. (2008) (10) Dykstra et al. (2006, 2007) (11) Quebrada Grande - Kneller et al. (2004), Dykstra et al. (2006), Valdez Buso et al. (2017), Fallgatter et al. (2019) (12) Hoyada Verde, Leoncito, Majaditas - González (1981), López Gamundí (1984), López Gamundí et al. (1994), López Gamundí and Martínez (2000, 2003); this study (13) Agua de Jagüel and Tramajo Creek - López Gamundí (1984), López Gamundí et al. (1994), Henry et al. (2008, 2010); this study (14) El Ratón Formation - López Gamundí et al. (1994). B. A plan-view and a cross-sectional view of discrete alpine glacial centers found throughout the Paganzo Basin (cf. Limarino et al., 2002a, 2006, 2014; Henry et al., 2008; Isbell et al., 2012). C. Extensive glaciation from an ice sheet centered in the Eastern Sierras Pampeanas that covered, and then drained through the uplands across the Paganzo Basin (cf. Valdez Buso et al., 2017; Milana and Bercowski, 1987, 1990, 1993; Milana, 1988; Milana et al., 1987; Aquino et al., 2014). Modified after Henry et al. (2008) and Moxness et al. (2018). 71

Figure 7. Google Earth aerial image with the geologic units of the Paganzo Group mapped showing the locations of the paleoflow measurements (white ellipsoids) and detrital zircon samples (yellow ellipsoids). A. The Olta-Malanzán paleovalley system (OMPV) with the Malanzán, Loma Larga, Solca, and La Colina formations (Andreis et al., 1986; Limarino et al., 2014; Moxness et al., 2018; Pauls et al., 2019). Detrital zircon sample ARG203 is from Craddock et al. (2019), and sample 29TR4 is from Enkelmann et al. (2014). B. The Agua Hedionda anticline, near the town of Huaco with the Guandacol, Tupe and Patquía formations. Mapped units are from Marensi et al., 2002. Detrital zircon sample ARG318 is from Craddock et al. (2019), and sample CDH0923-3S is from this study. 72

Figure 8. Simplified stratigraphic columns for the Guandacol and Malanzán formations. Detrital zircon sample within the sections indicated by stars. Paleoflow orientations collected from strata (at OMPV only) or striated pavements (at Huaco only) depicted using rose diagrams with number of measurements (n). The paleoflow locations reference those mapped in Figure 3. 73

Figure 9. Exposures of the Malanzán Formation at OMPV. A. Base of Malanzán Formation at OMPV locality. The diamictite facies (debris flow within the white dashed lines) overlying sandstone facies and basement (Olta phyllite and schist). Location of sample 29TR4 from Enkelmann et al. (2014). B. Conglomerate facies from a tributary paleovalley. Note dip of clinofolds to the right. C. Gilbert delta with a S-SW paleocurrent measurement from the upper Malanzán Formation, OMPV. Note the occurrence of topset, foreset and bottomset beds. D. Tool marks from interbedded mudstone and sandstone facies in the MPV: MVM1 locality near the location of sample ARG203 from Craddock et al. (2019). E. Interbedded mudstone and sandstone facies in the MPV. 74

Figure 10. Exposures of the Guandacol Formation and its contact with the San Juan Limestone at Huaco. A. Glacial grooves around siliceous nodules in San Juan Limestone (AH). Arrow indicates ice flow direction. B. Thin-bedded diamictite facies 4 meters above the contact with the San Juan Limestone with a marl bed. C. Thin-bedded diamictite facies directly overlying San Juan Limestone. D. Thick-bedded diamictite facies. E. Wavy bedding within the uppermost Guandacol Formation, near the location of sample CDH0923-3S. 75

Figure 11. Concordia plot of all analyzed concordant zircon U-Pb measurements for detrital zircon sample CDH0923-3S from the Malanzán Formation, OMPV locality. See Figure 3B for exact location. 76

Figure 12. Mesoproterozoic-Carboniferous igneous and metamorphic provinces for the Paganzo Basin area (demarcated by the dotted line) and their available zircon geochronology (n=398). Map is modified from Dahlquist et al. (2010). The four samples considered in this study come from the two areas highlighted by the yellow boxes: AH, Lower Guandacol Fm. – ARG318 (Craddock et al., 2019), Upper Guandacol Fm. – CDH0923-3S; OMPV, Lower Malanzán Fm. – 29TR4 (Enkelmann et al., 2014), Upper Malanzán Fm. – ARG203 (Craddock et al., 2019). The cited literature for the igneous and metamorphic zircon compilation is as follows: (1) Sierra de Pie de Palo - Vujovich et al., 2004; Naipauer et al., 2010a (2) Sierra de Umango - Varela et al., 2003, 2005 (3) Sierra de Valle Fértil - Pankhurst et al., 2000 (4) Sierra de Famatina - Pankhurst et al., 2000 (5) Sierra de Velasco - Toselli et al., 2003; Pankhurst et al., 2000 (6) Sierras de Chepes, Los Llanos - Pankhurst et al., 2000 (7) Sierra de San Luis - Vujovich and Ostera, 2003; Drobe et al., 2009 (8) Sierra de Córdoba - Rapela et al., 1998, Pankhurst et al., 2000 (9) Sierra Norte - Leal et al., 20003; Llambías et al., 2003. 77

Figure 13. Cumulative probability distribution for the four Paganzo Group samples and the basement units in the region. Lower Guandacol Fm. – ARG318 (Craddock et al., 2019), Upper Guandacol Fm. – CDH0923-3S, Lower Malanzán Fm. – 29TR4 (Enkelmann et al., 2014), Upper Malanzán Fm. – ARG203 (Craddock et al., 2019). The cited literature for the igneous and metamorphic zircon compilation is as follows: (1) Sierra de Pie de Palo - Vujovich et al., 2004; Naipauer et al., 2010a (2) Sierra de Umango - Varela et al., 2003, 2005 (3) Sierra de Valle Fértil - Pankhurst et al., 2000 (4) Sierra de Famatina - Pankhurst et al., 2000 (5) Sierra de Velasco - Toselli et al., 2003; Pankhurst et al., 2000 (6) Sierras de Chepes, Los Llanos - Pankhurst et al., 2000 (7) Sierra de San Luis - Vujovich and Ostera, 2003; Drobe et al., 2009 (8) Sierra de Córdoba - Rapela et al., 1998, Pankhurst et al., 2000 (9) Sierra Norte - Leal et al., 2000; Llambías et al., 2003. 78

Figure 14. The revised depositional environment and glacial extent model for the mid-Carboniferous Paganzo Basin. A. Ice centers and glacial deposition restricted to the western Paganzo Basin and Calingasta-Uspallata and Río Blanco basins. Paleoflow directions are from the same dataset as in Figure 1. Basin reconstruction map modified from López Gamundí et al. (1994). Paleoflow directions modified from Henry et al. (2008) and Moxness et al., (2018). B. Cross-section of the western margin of Gondwana with ice centers highlighted. Tectonic cross-section modified from Henry et al. (2008) and Moxness et al., (2018). 79

Figure 15. A. Plate reconstruction showing the location of the continents centered around the South Pole during the late Paleozoic. The Paganzo Basin, the area for this study, is highlighted by the arrow. RBB: Río Blanco Basin; CPB: Chaco-Paraná Basin; SGB: Sauce Grande Basin. TGB: Tepuel-Genoa Basin. (Modified from Moxness et al., 2018) B. Plan-view map showing the interpreted outline of the Paganzo Basin. The Olta-Malanzán paleovalley within the eastern portion of the basin is highlighted in the red box. (Modified from Limarino et al., 2006). 121

Figure 16. Simple stratigraphic column showing the Paganzo Group strata and correlations across the Paganzo Basin (modified after Henry et al. 2008; Taboada, 1985; Archangelsky and Lech, 1985; Archangelsky and Archangelsky, 1987; Fernandez-Seveso and Tankard, 1995; Azcuy et al., 1999; López Gamundí and Martínez, 2000; Gulbranson et al., 2010; Tedesco et al., 2010; Césari et al., 2011). 122

Figure 17. Map of the igneous and metamorphic basement units into which the late Paleozoic paleovalley is cut. (Modified from Pankhurst et al., 1998). 123

Figure 18. Simplified geologic map highlighting the late Paleozoic sedimentary fill of the two main paleovalley systems in the Sierra de Chepes and Sierra de los Llanos region (Modified after Net and Limarino, 1999; Moxness et al., 2018). 124

Figure 19. Generalized and simplified stratigraphic column for the strata in the paleovalley system. 125

Figure 20. Photos showing examples of the varying facies through the Malanzán and Loma Larga Formations. A. Conglomeratic and interbedded sand and mudstone facies at the base of the Malanzán Fm. Debris flow overlying the basement, followed by lake sediments. B. Stacked cross-bedded sandstone facies with overlying organic-rich mudstones. Fluvial dominant environment transitioning into a lacustrine setting. C. Stacked cross-bedded coarse sandstone facies with interbedded organic-rich mudstones of the Loma Larga Formation interpreted as

fluvial and vegetated lacustrine environments. D. Stacked cross-bedded coarse sandstone facies at the boundary between the Loma Larga and Solca Formations.	126
Figure 21. Photos showing the facies characteristics of the upper units of the paleovalley system: Solca Formation, Arroyo Totoral Formation, and La Colina Formation. A. Conglomerate facies interpreted as an alluvial fan amalgamation. B. Conglomerate facies cutting into a paleosol in the Solca Formation. This is interpreted to be a depositional hiatus followed by renewed deposition in the paleovalley. C. Weakly cross-bedded sandstone facies overlying the interbedded mudstone facies interpreted as lacustrine and fluvial settings in the Arroyo Totoral Formation. D. Interbedded sandstone and mudstone facies near the base of the La Colina Formation, overlying conglomeratic facies interpreted as alluvial fans transitioning into an ephemeral fluvial environment. E. Example of rill marks in the interbedded sandstone and mudstone facies of the La Colina Formation. F. Large cross-bedded sandstone facies at the top of the La Colina section interpreted as eolian dunes indicating desert-like conditions.	127
Figure 22. Ternary A-CN-K plot displaying the fresh Chepes Complex granodiorite and the late Paleozoic sedimentary fill samples based on their bulk geochemistry. Also plotted is the average granite and granodiorite compositions and the average granodiorite weathering trend line based on data from Nesbitt and Young (1989).	128
Figure 23. Generalized stratigraphic section from the Olta-Malanzán Paleovalley with the CIA values for each sample and a smoothed 3-point running average line (black) have been plotted next to their approximate location within the succession. Samples have been color-coded based on stratigraphic formation: green – Malanzán Formation, blue – Loma Larga Formation, red – Solca and La Colina formations, orange – Arroyo Totoral Formation. For the CIA scale, left to right indicates increased chemical weathering and an inferred humid paleoclimate (i.e. blue is more arid and orange is more humid).	129
Figure 24 A. Map of plate reconstruction for the Bashkirian stage. RBB: Río Blanco Basin; CUB: Calingasta-Uspallata Basin; CPB: Chaco-Paraná Basin; SGB: Sauce Grande Basin. TGB: Tepuel-Genoa Basin. Reconstruction modified from Moxness et al. (2018). B. Plan-view map showing the interpreted outline of the Paganzo Basin. The localities for this study are marked by black stars: AH – Agua Hedionda anticline near Huaco; CG – Cerro Guandacol; OMPV - Olta-Malanzán paleovalley; AJ – Agua de Jagüel. White star indicates Cerro Agua Negra Formation from Spalletti et al., (2012), data used in comparison to this study. Map modified from Limarino et al. (2006). C. Map of reconstruction of southeastern Paraná Basin with localities marked by black stars used in this study.	174
Figure 25. Generalized stratigraphic(white units) and basement rock (gray units) correlation chart for the western margin basins of Argentina and the Paraná Basin in Brazil. Modified from Limarino et al., 2014 with updated chronostratigraphic information for the Paraná Basin from Mottin et al. (2018) and Griffis et al. (2019).	175
Figure 26 Time distribution of the orogenic events that occurred along the western margin of Gondwana. Pampean and Famatinian orogenies resulted from the collision of the Cuyania Terrane. The Chañic orogeny resulted from the obduction of the Precordilleran terrane. The Carboniferous-Permian arc resulted from the collision of the Chilenia Terrane. Modified from Ramos, 1988, 1999.	176

Figure 27. Mesoproterozoic-Carboniferous igneous and metamorphic provinces for the Paganzo Basin area (demarcated by the black dashed line). Map is modified from Dahlquist et al. (2010). The cited literature for this compilation is as follows: (1) Vujovich et al., 2004; Naipauer et al., 2010a (2) Varela et al., 2003, 2005 (3) Pankhurst et al., 2000 (4) Pankhurst et al., 2000 (5) Toselli et al., 2003; Pankhurst et al., 2000 (6) Pankhurst et al., 2000 (7) Vujovich and Osters, 2003; Drobe et al., 2009 (8) Rapela et al., 1998, Pankhurst et al., 2000 (9) Leal et al., 20003; Llambías et al., 2003..... 177

Figure 28. Ternary plots of Al_2O_3 vs. CaO^*+Na_2O vs. K_2O (A=CN-K) system (Nesbitt and Young, 1989). The distribution of data points at each locality is consistent with loss of alkalinity through chemical weathering. Cerro Agua Negra Formation data is from Spalletti et al. (2012), and comparison data for the Paraná Basin is from Tedesco et al. (2019)..... 180

Figure 29. Generalized stratigraphic sections from Agua de Jagüel (AJ), Cerro Guandacol, Huaco (AH) based on the chronostratigraphic correlations from Césari et al. (2011), compared to the Olta-Malanzán Paleovalley (OMPV) data from Pauls et al. (2019). The Chemical Index of Alteration (CIA) values for each section have been plotted next to their approximate location within the succession and can also be found in Table 3. Left to right on the individual columns indicates increased chemical weathering and an inferred humid paleoclimate (i.e. blue is more arid and orange is more humid). The solid black line is a three-point moving average to give a better visual of the paleoclimate trend through time. 181

Figure 30. Glacial and cold intervals for South American Gondwana from west to east. Modified from Isbell et al. (2012), and based on data from Limarino and Spalletti (2006), Henry et al. (2008, 2010), Rocha-Campos et al. (2008), Gulbranson et al. (2010), Isbell et al. (2012), Limarino et al. (2014), Moxness et al. (2018), Fedorchuk et al. (2019), and Griffis et al. (2019). 182

Figure 31. Cross-sectional view of the western margin of Gondwana and the proposed tectonism model during the middle Carboniferous to the Permian. 183

Figure 32. Map of plate reconstruction for Bashkirian. RBB: Río Blanco Basin; CUB: Calingasta-Uspallata Basin; CPB: Chaco-Paraná Basin; SGB: Sauce Grande Basin. TGB: Tepuel-Genoa Basin. Reconstruction modified from Moxness et al. (2018). B. Plan-view map showing the interpreted outline of the Paganzo Basin. The localities for this study are marked by blue rectangles: AH – Agua Hedionda anticline near Huaco; OMPV - Olta-Malanzán paleovalley. Map modified from Limarino et al. (2006). 218

Figure 33. Correlation chart for the late Paleozoic Paganzo Group strata for the sites in the Paganzo Basin, Argentina mentioned in the text. Ages and units are based on Limarino et al. (2002a, 2002b, 2006, 2014), Césari et al. (2011, 2019). 219

Figure 34. Map of the igneous and metamorphic basement units that serve as potential source terranes for the detrital zircon populations of the late Paleozoic Paganzo Group strata, outlined in yellow boxes. 1 – Sierras de Chepes and Los Llanos, 2 – Sierra de Valle Fertil, 3 – Sierra de Pie de Palo, 4 – Sierras de Umango, Maz and Espinal, 5 – Sierras Famatina, 6 – Sierra de Velasco, 7- Sierras de Córdoba, 8 – Sierra de San Luis. (Modified from Dahlquist et al., 2010). The dotted line is the approximate outline of the Paganzo Basin. (Modified from Limarino et al., 2006).. 220

Figure 35. Simple stratigraphic column showing the selected Paganzo Group strata at the chosen localities. (Modified from Césari et al., 2011; Pauls et al., 2019). 221

Figure 36. Google Earth aerial image with the geologic units of the Paganzo Group mapped showing the locations of the detrital zircon samples (yellow ellipsoids). A. The Agua Hedionda anticline, near the town of Huaco with the Guandacol, Tupe and Patquía formations. Detrital zircon sample ARG318 is from Craddock et al. (2019), and sample CDH0923-3S is from Pauls et al. (in review). B. The Olta-Malanzán paleovalley system (OMPV) with the Malanzán, Loma Larga, Solca, and La Colina formations. Detrital zircon samples ARG175 and ARG203 are from Craddock et al. (2019), and sample 29TR4 is from Enkelmann et al. (2014). 222

Figure 37. Concordia plot of all analyzed concordant zircon U-Pb measurements for detrital zircon sample CDH0923-5S from the Tupe Formation, CDH0923-35S from the Patquía Formation at the AH locality; and LC0806 of the La Colina Formation, OMPV locality. See Figure 5 for exact locations of each sample..... 223

Figure 38. Cumulative probability distribution for the four Paganzo Group samples and the basement units in the region. Lower Paganzo Group strata samples are from other sources: Lower Guandacol Fm. – ARG318 (Craddock et al., 2019), Upper Guandacol Fm. – CDH0923-3S (Pauls et al., in review), Lower Malanzán Fm. – 29TR4 (Enkelmann et al., 2014), Upper Malanzán Fm. – ARG203 (Craddock et al., 2019). Upper Paganzo Group samples: Tupe Fm. – CDH0923-5S (this study), Patquía Fm. – CDH0923-35S (this study), Loma Larga Fm. – ARG175 (Craddock et al., 2019), La Colina Fm. – LC0806 (this study). The data for the igneous and metamorphic zircon compilation comes from the following literature: (1) Sierra de Pie de Palo - Vujovich et al., 2004; Naipauer et al., 2010a (2) Sierra de Umango - Varela et al., 2003, 2005 (3) Sierra de Valle Fértil - Pankhurst et al., 2000 (4) Sierra de Famatina - Pankhurst et al., 2000 (5) Sierra de Velasco - Toselli et al., 2003; Pankhurst et al., 2000 (6) Sierras de Chepes, Los Llanos - Pankhurst et al., 2000 (7) Sierra de San Luis - Vujovich and Ostera, 2003; Drobe et al., 2009 (8) Sierra de Córdoba - Rapela et al., 1998, Pankhurst et al., 2000 (9) Sierra Norte - Leal et al., 20003; Llambías et al., 2003..... 224

Figure 39. Mesoproterozoic-Carboniferous igneous and metamorphic provinces for the Paganzo Basin area (demarcated by the dotted line) and their available zircon geochronology (n=398). The studied sections are outlined by yellow boxes. Map is modified from Dahlquist et al. (2010). The cited literature for this compilation is as follows(1) Sierra de Pie de Palo - Vujovich et al., 2004; Naipauer et al., 2010a (2) Sierra de Umango - Varela et al., 2003, 2005 (3) Sierra de Valle Fértil - Pankhurst et al., 2000 (4) Sierra de Famatina - Pankhurst et al., 2000 (5) Sierra de Velasco - Toselli et al., 2003; Pankhurst et al., 2000 (6) Sierras de Chepes, Los Llanos - Pankhurst et al., 2000 (7) Sierra de San Luis - Vujovich and Ostera, 2003; Drobe et al., 2009 (8) Sierra de Córdoba - Rapela et al., 1998, Pankhurst et al., 2000 (9) Sierra Norte - Leal et al., 20003; Llambías et al., 2003..... 225

Figure 40. The proposed evolutive model of the Paganzo Basin development from the middle Carboniferous to the Permian. 226

ACKNOWLEDGEMENTS

This entire project was made possible by the assistance and guidance of many individuals, and I am immensely grateful. First, I would like to thank my advisor, Dr. John Isbell, for picking me up when everything fell apart, and for sticking with me through the years. I am appreciative of everything you have taught me in the field and in the classroom. I will never forget the countless field trips and countries we have been to, nor will I forget the memories we share. I am incredibly grateful for all the wonderful people you have introduced me to in Argentina and Brazil.

Speaking of, I would also like to thank Dr. C. Oscar Limarino for all of his guidance throughout this project, especially in the field. Without him, field work in Argentina would not have been possible. Over the years, I have learned a great deal from him: I will most certainly never forget how to measure “one Oscar” when estimating strata thicknesses. I am forever grateful to have been introduced to his former students, now colleagues: Dr. L. Jazmin Schencman and Dr. Pablo Alonso-Muruaga, as well as Dr. Carina Colombi in San Juan. I truly appreciated their knowledge, conversations and time spent on each of our trips.

I also appreciate the time my committee (Dr. Lindsay McHenry, Dr. Dyanna Czeck, Dr. Margaret Fraiser, and Dr. Mark Harris) has taken to help me along the doctoral milestones. Thank you for guiding me throughout the project, and for your constructive feedback through this process.

The fieldwork for this project was made possible by various grants and institutions, including the Geological Society of America, the Society for Sedimentary Geologists, the University of Wisconsin-Milwaukee (UWM) Center for Latin American and Caribbean studies,

the Wisconsin Geological Society, the University of Wisconsin-Milwaukee, the UWM Department of Geosciences, the Universidad de Buenos Aires, CONICET of Argentina, and specific grants from the USA National Science Foundation (Grants 1443557, 1559231, and 1729219).

Finally, and most importantly, I want to thank my family and friends. I especially need to thank a million times over my mom, my sister and my stepdad for constantly pushing me all these years and believing in me when I wanted to give up four years ago. I owe this to you.

Chapter 1. Introduction

The late Paleozoic ice age and Gondwana

The late Paleozoic ice age (LPIA) was the longest-lived ice age (372-259 million years ago) of the Phanerozoic. The LPIA is the only example of when a vegetated and biologically complex Earth shifted from an icehouse to a greenhouse state (Gastaldo et al., 1996; Montañez et al., 2007; Fielding et al., 2008a; Isbell et al., 2012; Montañez and Poulsen, 2013). Therefore, the LPIA helps to develop an understanding of the drivers influencing changing climatic regimes, which, in turn, provides insight on how such drivers affect modern climate change. One of the longstanding questions of the late Paleozoic centers around how different regions (i.e. low paleolatitude versus high paleolatitude) of Earth responded to a global shift in climate. Thus, regional studies at high chronostratigraphic resolution will add to our understanding of environmental responses to changing global climate.

Much of the research concerning the LPIA focuses on determining the timing and extent of the glaciations in Gondwana, the supercontinent that existed during the Paleozoic and Mesozoic, composed primarily of Africa, South America, Australia, India, and Antarctica (Fig. 1). Traditional LPIA hypotheses and models centered around the idea that there was one large ice sheet that covered Gondwana, and that it persisted for the 100 Ma duration of the LPIA (i.e. from the late Devonian to the late Permian; Frakes, 1979; Veevers and Powell, 1987; Frakes and Francis, 1988; Scotese, 1999; Blakey, 2008). As more studies were conducted over time, regional evidence has shown that the LPIA glaciation was more dynamic and complex than previously understood (Crowell and Frakes, 1970; López-Gamundí, 1997; Visser, 1997; Isbell et al., 2003, 2008, 2012; Fielding et al., 2008a,b; Heckel, 2008; Rygel et al., 2008; Gulbranson et

al., 2010; Taboada, 2010). The glacial intervals most likely occurred on much smaller scales (i.e. approximately one to several million years in length) and in different local regions across Gondwana, beginning in South America and northern Africa during the late Devonian (i.e. the Frasnian or Famennian), before spreading across the rest of Gondwana during the Carboniferous and into the Permian (Caputo and Crowell, 1985; Veevers and Powell, 1987; Eyles, 1993; López-Gamundí, 1997; Isbell et al., 2003, 2012; Caputo et al., 2008; Pérez Loinaze et al., 2010; Fielding et al. 2008c; Limarino et al., 2014; Frank et al., 2015; Metcalfe et al., 2015). Additionally, studies have highlighted potential driving mechanisms (i.e. the drift of Gondwana across the paleo South Pole, changes in the configurations of the continental plates, changes in atmospheric CO₂, and orogenic events) for these changing climatic conditions, focusing on the transition from icehouse to greenhouse conditions at the end of the LPIA (c.f. Caputo and Crowell, 1985; Eyles et al., 1993; Heckel, 1994, 2008; Isbell et al., 2003, 2008; 2012; Royer et al., 2004; Montañez et al., 2007; Rygel et al., 2008; Horton and Poulsen, 2009; Tabor and Poulsen, 2008; Gulbranson et al., 2010; Montañez and Poulsen, 2013; Limarino et al., 2014). Thus, an emerging perspective of the LPIA is forming, providing new insight into the glaciation-climate relationship and the forcing and feedback mechanisms that drive such global change. However, there is still much to be gained by understanding the climate drivers on a regional scale.

This dissertation aims to evaluate the effects that local tectonic changes in western Argentina had on the climate of the late Paleozoic strata in the Paganzo and Calingasta-Uspallata basins (Fig. 1). These strata, deposited in basins forming as result of the tectonic activity along the western (i.e. Panthalassan) margin of Gondwana, record drastic shifts in climate from glacial to temperate to desert during the Pennsylvanian, millions of years prior to the climatic shift

recorded in the Permian of more interior South American basins (i.e. Chaco-Paraná and Paraná basins of eastern Argentina Brazil; Fig. 1).

Significance of western Gondwana basins

South American Gondwanan basins provide ideal locations for an in-depth study of climate dynamics on a regional scale. Many of these basins contain glacial deposits and demonstrate a variation in the duration and timing of these glacial episodes (Crowell and Frakes, 1970; Visser, 1997; Isbell et al., 2003, 2012; Fielding et al., 2008a, 2008b; Henry et al., 2008, 2010; Rocha-Campos et al., 2008; Gonzalez and Diaz Saravia, 2010; Gulbranson et al., 2010; Taboada, 2010; Limarino et al., 2014; Fig. 2). Basins in Africa and Brazil experienced glaciation during the latest Devonian (late Famennian), but these centers diminished during the earliest Carboniferous (Caputo and Crowell, 1985). Glaciation, or local centers of ice, are recorded in the basins of western Argentina (i.e. Rio Blanco, Calingasta-Uspallata, and western Paganzo Basins) during the Mississippian (Visean), which is interpreted to be the onset of widespread glaciation across Gondwana, including glaciation occurring in the Paraná Basin in Brazil (López-Gamundí et al., 1994; López-Gamundí, 1997; Caputo et al. 2008; Henry et al., 2008; Holz and Iannuzzi, 2008; Rocha Campos et al., 2008; Limarino et al., 2014; Rosa et al., 2019). While glaciation in the Paraná Basin in Brazil appears to have continued until the Carboniferous-Permian boundary, and perhaps into the Early Permian, the western Argentina basins at similar paleolatitudes (Paganzo, Calingasta-Uspallata, and Rio Blanco Basins) experienced a climate shift from glacial to wet and humid conditions by the early Bashkirian stage and then to arid conditions during the late Pennsylvanian (Henry et al., 2008; Rocha-Campos et al., 2008; Holz et al., 2010; Césari et al., 2011; Limarino et al., 2014). Reasons are not known as to why terminal glaciation occurred

at different times across central South America. However, addressing this problem may provide important information on causes of long-term differences in climate change on a regional scale.

Paganzo Basin

The Paganzo Basin of western Argentina first developed as a relatively restricted foreland basin as the tectonic activity along the western (i.e. Panthalassan) margin of Gondwana created the Protoprecordillera uplift due to the collision of the Chilenia terrane into the Cuyania terrane on the western margin of Gondwana (Fig. 4 A). As subduction shifted westward toward the Panthalassan Ocean, extensional tectonics commenced, and the terranes that made up the highlands that bounded the basin—the Protoprecordillera in the west and the Famatina and Pampeanas Systems in the east— are interpreted to have collapsed and the Paganzo Basin evolved into a broader back-arc basin (Fig. 4 B; Ramos, 1988; Jordan et al., 1989; Lopéz-Gamundí et al., 1994; Limarino and Spalletti, 2006; Limarino et al., 2014).

However, there are differing interpretations of Paganzo Basin topographic and glaciation development. In one view, the paleotopography of the interior of the basin is thought to have been peneplained due to an overriding ice sheet that existed around 320 Ma (Astini et al., 2009). As the uplift of the Protoprecordillera occurred due to the collision of the Cuyania and Chilenia terranes, this ice sheet is thought to have diminished in size, leaving behind alpine glaciers carving out U-shaped valleys in both the eastern and western margins of the basin (Sterren and Martínez, 1996; Carignano et al., 1999; Astini et al., 2009; Astini, 2010). In an alternate view, these peneplained surfaces, though, were created later, and are much younger features than the late Paleozoic, more likely of Jurassic to Cenozoic age (cf. Carignano et al., 1999; Rabassa, 2014; Rabassa et al., 2014).). Further data in support of this alternate view is that while there is

abundant evidence for fjord-like and U-shaped valleys on the western margin of the Paganzo Basin (cf. Dykstra et al., 2006; Henry et al., 2008; Isbell et al., 2012; Aquino et al., 2014; Limarino et al., 2014), there is limited evidence for the same on the eastern margin of the basin (Sterren and Martinez, 1996; Net and Limarino, 1999; Net et al., 2002; Net and Limarino, 2006; Socha et al., 2014). Instead, much of this evidence comes from an isolated paleovalley that runs through the Sierra de Chepes and Sierra de Los Llanos, and the time-equivalent strata has recently been reinterpreted as non-glacigenic (cf. Moxness et al., 2018). The Paganzo Basin contains the Paganzo Group, which has been subdivided into numerous formations of time-equivalent strata. These different units are usually correlated using radiometric ages determined from the western units, along with palynological and fossil plant records from the various sections and the facies associated with each succession (Fig. 2.; cf. Gulbranson et al., 2010, 2015; Césari et al., 2011).

In the western portion of the Paganzo Basin, for example, the Paganzo Group is divided into the Guandacol (middle Serpukhovian-middle Baskirian), Tupe (middle Bashkirian-early Moscovian), and the Patquía (early Moscovian-early Permian) Formations (Limarino et al., 2006; Guena et al., 2010; Tedesco et al., 2010; Limarino et al., 2014). In the central Paganzo Basin, the Paganzo Group is divided into two formations: Lagares Formation (middle Serpukhovian-late Moscovian) and La Colina Formation (late Moscovian-Wuchiapingian) (Limarino et al., 2006; Guena et al., 2010; Tedesco et al., 2010; Limarino et al., 2014). In the eastern portion of the basin, the group is subdivided into the Malanzán Formation (middle Serpukhovian-middle Baskirian), Loma Larga Formation (middle Bashkirian-early Moscovian), Solca (middle Moscovian-late Moscovian), Arroyo Totoral (middle Moscovian-Wuchiapingian),

and La Colina Formation (late Moscovian-Wuchiapingian) (Pérez Loinaze, 2009; Césari et al., 2011; Limarino et al., 2014).

Within the Paganzo Basin, several formations have been interpreted as glacial. In the western Paganzo Basin, the base of the Guandacol Formation contains ice-proximal and subglacial deposits (Limarino et al., 2014). Diamictites identified in the eastern Paganzo Basin at the base of the Malanzán Formation within the Olta-Malanzán paleovalley are also interpreted as glacial deposits (Socha et al., 2014; Enkelmann et al., 2015; Enkelmann and Garver, 2015). For this reason, it has been inferred that there was widespread glaciation throughout the Paganzo Basin during the late Mississippian to early Pennsylvanian (Limarino et al., 2014). It is only recently that the diamictites of the Malanzán Formation were identified as non- glacial, formed as the result of debris flows associated with slope failure and mass transportation deposits off of the steep walls of the paleovalley (cf. Moxness et al., 2018).

The middle units (i.e. Tupe, Lagares, and Loma Larga Formations) are interpreted to be comprised of fluvial deposits that succeed the lowermost units (Andreis et al., 1986; Limarino et al., 2006; Guena et al., 2010; Tedesco et al., 2010; Limarino et al., 2014). Additionally, coal deposits are described from various levels within the middle units, which has led to the interpretation of a more humid post-glacial climate (Limarino et al., 2006; Guena et al., 2010; Tedesco et al., 2010; Limarino et al., 2014). In the eastern Paganzo Basin, the Solca Formation, which overlies the Loma Larga Formation, consists of mostly conglomeratic units and has a contentious interpretation history. It appears most similar in color (e.g. white sandstones alternating with red mudstones) and appearance to the lowermost Patquía Formation in the western part of the basin, but it is difficult to place the Carboniferous-Permian boundary within it. The uppermost units, Patquía and La Colina Formations, are found throughout the Paganzo

Basin (Limarino et al., 2006; Guena et al., 2010; Césari et al., 2011; Limarino et al., 2014).

These formations are interpreted to be indicative of eolian, ephemeral riverine and playa depositional environments. Additionally, the red beds of the La Colina and Patquía Formations indicate a drastic trend towards an arid climate that occurs in the western basins sooner than in the intracratonic basins, such as the Paraná, during the Permian.

Calingasta-Uspallata Basin

The Calingasta-Uspallata Basin is an arc-related basin formed in a tectonically and magmatically active region of the western Gondwana margin (Fig. 1). This basin is bounded in part to the east by the Protoprecordillera and to the west by a volcanic arc, which was located in present-day Chile (cf. Azcuy, 1999). Subsidence occurred in the basin from the Early Carboniferous through the late Carboniferous, until the early Permian, during the San Rafael orogeny, caused by continued subduction to the west (López-Gamundí et al., 1994; Azcuy et al., 1999; Limarino et al., 2014). The basin fill is predominantly marine in origin and contains a complete succession of the glacial to post-glacial stages (Limarino et al., 2014).

For a comparison of the glacial-to-post-glacial succession with the Paganzo Basin, one locality was chosen in the Calingasta-Uspallata Basin: the Agua de Jagüel locality (López Gamundí, 1984; López Gamundí et al., 1994; Henry et al., 2008; Fig. 2). The Agua de Jagüel contains three identified sequences that encompass the glacial to post glacial succession, and is approximately coeval to the Paganzo Group strata on the other side of the Protoprecordillera (Amos and Rolleri, 1965; Frakes and Crowell, 1969; González, 1981; López Gamundí, 1984; López Gamundí et al., 1994; Azcuy et al., 1999; Henry, 2007; Henry et al., 2008, 2010; Limarino et al., 2014; Fig. 2). However, not much information is published on the depositional

environments of the upper two sequences found at the Agua de Jagüel locality, so an in-depth study could provide insights into the progression of depositional and climatic shifts through the remainder of the LPIA.

Paraná Basin

The region of the intracratonic Paraná Basin stretches from present-day south-central Brazil southward into Paraguay, Argentina, and Uruguay, and during the late Paleozoic was adjacent to the western coast of Namibia, Africa (see Fig. 4 of Eyles and Eyles, 1993; Eyles et al., 1993; França, 1994; Milani et al., 1994; Rocha-Campos et al., 2008). To limit the variables considered for this study, only the southern portion of the Paraná Basin (i.e. the area of Rio Grande do Sul State; Fig. 3) will be considered. This region throughout the late Paleozoic experienced a wide variety of environments, including glaciation and the transgression and regression of an intracratonic sea. The Itararé Group is composed of intercalations of diamictite, mudstone, and sandstone (Rocha-Campos et al., 2008; Fig. 2). There are many names and varying subdivisions of the Itararé Group, but this project focuses on strata from the southeastern part of the basin (i.e. Rio Grande do Sul State). Overlying the uppermost Taciba Formation is the Rio Bonito Formation, which consists of fluvial sandstones, estuarine sandstones and shales, and coal packages. It is interpreted to represent the post-glacial succession and a shift to a more humid environment. The Palermo Formation interfingers with the Rio Bonito Formation in certain locations of the Paraná Basin, and contains deep-water and offshore deposits that are interpreted as an overall transgressive package.

The Significance of the Protoprecordillera

Numerous studies have found that mountain belts play an extremely important role in the moisture flow patterns across continents (Broccoli and Manabe, 1997; Ruddiman and Prell, 2007; Ruddiman et al., 1997; Newell et al., 1999; Tabor and Poulsen, 2008; Godard et al., 2014; Isbell et al., 2012; Limarino et al., 2014). Not only do mountain belts affect regions via the orographic effect and contribute to rain shadow regions, but they can also affect atmospheric circulation on a larger scale (Broccoli and Manabe, 1997 and references therein; Partridge, 1997; Ruddiman et al., 1997; Ruddiman and Prell, 2007). As the different paleotopographic highs in the western margin region of Argentine Gondwana changed in importance and elevation, the various atmospheric patterns would have been disrupted, which would have caused shifts in the regional climate regime (Ruddiman and Prell, 1997; Ruddiman et al., 1997; Newell et al., 1999; Broccoli and Manabe, 1997; Partridge, 1997; Tabor and Poulsen, 2008; Isbell et al., 2012; Godard et al., 2014; Limarino et al., 2014).

The Protoprecordillera was an ancient mountain belt that separated the western arc-related basins of Argentina (i.e. Calingasta-Uspallata and Río Blanco basins) from the interior foreland basin (i.e. Paganzo Basin; Ramos et al., 1984, 1986; Limarino et al., 2006; Henry et al., 2008; Isbell et al., 2012; Fig. 1). During the late Devonian to early Carboniferous (Mississippian), the Protoprecordillera is thought to have had significant topographic relief as the Chilenia terrane accreted to the Panthalassan margin of Gondwana (Ramos et al., 1984, 1986; Limarino et al., 2006; Isbell et al., 2012; Limarino et al., 2014). Incised paleovalleys, of up to 2,500 meters or more in relief, located along the Protoprecordillera contain records of glaciation at the base of each succession, which are then replaced by transgressive packages that are interpreted to represent a transition to post-glacial conditions (cf. López Gamundí, et al., 1994;

López Gamundí, 1997; Dykstra et al., 2006, 2007; Limarino and Spalletti, 2006; Limarino et al., 2006; Henry et al., 2010; Aquino et al., 2014; Limarino et al., 2014). The disappearance of these glacial packages occurs during the Early Pennsylvanian, and could possibly correspond to the collapse of the Protoprecordilleran mountain range, which is thought to have occurred during the Pennsylvanian to the Permian (Ramos, 1988; López-Gamundí et al., 1994; Limarino et al., 2002, 2006, 2014; Isbell et al., 2012; Fig. 4). Evidence for this collapse includes the disappearance of glacial deposits in the arc-related basins (i.e. Calingasta-Uspallata and Rio Blanco Basins) and in the western margin of the Paganzo Basin (Net and Limarino, 2006; Limarino et al., 2006). Volcanism occurred at the end of the Pennsylvanian and into the Permian, likely due to the accretion of a volcanic arc outboard of the western margin (cf. Limarino and Spalletti, 2006; Limarino et al., 2006; Spalletti et al., 2012; Limarino et al., 2014; Einhorn et al., 2015; Fig. 4). However, more evidence is needed to determine the timing and scale of the Protoprecordilleran collapse and the presence of the volcanic arc and unravel the influence of these topographic highs on regional climate and sedimentation processes.

Objectives

To compare the paleoclimate trends and depositional environments of the South American basins, this project had the following objectives:

1. *Conduct a detailed sedimentologic and stratigraphic analysis of the deposits within the eastern Paganzo Basin to refine our understanding of the extent and timing of glaciation during the Carboniferous.*
2. *Compare and contrast the glacial to post-glacial paleoclimate trends across the Paganzo Basin in southwestern Gondwana during the LPIA.*

3. *Assess the role of tectonics as a driver for climate shifts recorded in the western basins of Argentina during the late Paleozoic.*

Significance of Research

The work presented in this dissertation is valuable to a wide array of deep-time audiences. This project provides high-resolution data sets on the glacial to post-glacial transition across South American Gondwana, but specifically for the western margin and interior basins of Argentina. Prior to this work, knowledge of these basins was limited to reviews on the facies changes in select locations, limited petrologic studies (e.g. Net et al., 2002), and one climatic reconstruction from the Río Blanco Basin which has been evoked to represent the whole region (cf. Gulbranson et al., 2010, 2015). Furthermore, a single study (i.e. Gulbranson et al., 2010) is used widely in the literature as a comparison to contemporaneous basins that formed far from the Gondwanan margin such as the Paraná Basin in Brazil (cf. Césari et al., 2011; Enkelmann et al., 2014; Limarino et al., 2014; Enkelmann and Garver, 2015). Therefore, this research provides valuable information to scientists studying late Paleozoic geology in western Argentina and Brazil. Moreover, this project caters to a wide audience because it examines deep-time climate change and its relation to both local and global drivers during the early onset of the main phase of the LPIA, according to the current literature. Investigations such as this one will provide explanations on how various driving mechanisms and feedback systems affect regional climate, and how those compare on a continental scale.

This project also uses a tool not previously applied in this region of Gondwana: a major elemental geochemical analysis by x-ray fluorescence (XRF). Furthermore, this dissertation reconstructs paleoclimate using the Chemical Index of Alteration (CIA) of the LPIA strata in

Argentina, similar to previous studies for the Paraná Basin in Brazil (cf. Goldberg, 2001; Goldberg and Humayun, 2010; Fedorchuk et al., 2019). Similarly, there have been recent detrital zircon geochronology data for late Paleozoic strata in Brazil and other places in Gondwana, but relatively few in the Paganzo Basin (e.g. Craddock et al., 2019; Valdez Buso et al., 2020), and these have focused solely on the glacial deposits of the region. No study has been conducted on all late Paleozoic strata of the Paganzo Basin, let alone using provenance to test if tectonics was responsible for the climate shift during the Pennsylvanian and Permian. Therefore, the use of these methods provides new information and new perspectives on LPIA research in Argentina, as well as for other regions of South American Gondwana.

Dissertation Structure

This dissertation consists of four manuscripts written for publication in scientific journals, followed by a final concluding chapter that outlines the important findings of this dissertation. The formatting style of the Journal of South American Earth Sciences has been adopted for this dissertation, because the manuscripts of Chapter 2 (Constraining late Paleozoic ice extent in the Paganzo Basin of western Argentina using U-Pb detrital zircon geochronology for the lower Paganzo Group strata) and Chapter 3 (A paleoclimatic reconstruction of the Carboniferous-Permian paleovalley fill in the Eastern Paganzo Basin: Insights into glacial extent and deglaciation of southwestern Gondwana) have been published in and submitted to, respectively, this journal.

Chapter 2 of this study evaluates the current understanding of the ice extent within the Paganzo Basin. This chapter focuses on and presents evidence that glaciation was restricted to the western portion of the basin, along the active tectonic margin, rather than across the basin. This was done

using detrital zircon analyses to constrain drainage patterns and depositional centers for the Guandacol and Malanzán formations, which make up the basal formations of the Paganzo Group. Both stratigraphic units were deposited during cold climate conditions, but there is no indication for one centralized glacial center, as the detrital zircon populations indicate different provenance signatures. The detrital zircon populations also allude to disconnected depositional centers during the Visean-Bashkirian glaciation episode of the Paganzo Basin. This chapter was submitted to a special issue of the *Journal of South American Earth Sciences* in May 2020; it is currently under review.

Chapter 3 of this study investigates the applicability of the the Chemical Index of Alteration (CIA) as a paleoclimate proxy on the strata of late Paleozoic age in the Paganzo Basin. To do this, one section within the eastern portion of the Paganzo Basin in western Argentina were sampled for geochemical analyses. The Olta-Malanzán paleovalley system (OMPV) has been previously interpreted to have contained glacial deposits. Recent studies have shown that the paleovalley was not glaciated but owes its origin to extension and excavation by fluvial processes. The use of this paleoclimate proxy allowed for a quantitative paleoclimate analysis of a periglacial environment, which is then compared with time-equivalent glacial strata elsewhere in the basin in Chapter 4 of this dissertation. The results from the paleovalley samples show that this area was intermittently humid and arid through time, but with an overall arid profile.

However, it seems that the climate during the deposition of the late Pennsylvanian and Permian La Colina Formation was more humid than previously thought. This chapter has been published in the *South American Journal of Earth Sciences* in June of 2019.

Chapter 4 of this study is a regional paleoclimate reconstruction through two additional sections of Paganzo Group strata in the Paganzo Basin, and one locality in the Calingasta-Uspallata Basin

during the Carboniferous and early Permian. This study also compares paleoclimate of the western margin basins against samples from the southeastern Paraná Basin. These sections are used in conjunction with the section analyzed in Pauls et al. (2019), which is presented in the previous chapter (Chapter 3) of this dissertation. The aim of this paper is to quantify and better constrain the timing of the climate transition recorded in South American basins at the height of the LPIA. This chapter also explores the hypothesis that the collapse of the Protoprecordillera in the late-Mississippian and development of a volcanic arc in the late Carboniferous-early Permian was the main driver for the dramatic climate shift seen in the western basins (i.e. Paganzo, Calingasta-Uspallata, and Río Blanco basins) of Argentine Gondwana. For this purpose, the paleoenvironmental and paleoclimatic information presented in this chapter is discussed and used to build an updated conceptual model of the paleoclimatic evolution and provide a quantitative perspective of the middle Carboniferous to Permian transition in the Paganzo Basin.

Chapter 5 of this study analyzes shifts in provenance of six units of the Paganzo Group strata in two locations (i.e. Huaco and Olta-Malanzán) within the Paganzo Basin. To do this, three samples from the Tupe, Patquía and La Colina formations were analyzed using U-Pb detrital zircon geochronology methods in conjunction with samples published in the literature. Samples from the Tupe and Patquía and Loma Larga and La Colina formations were compared to the samples from the Guandacol and Malanzán formations analyzed in Chapter 2 of this dissertation. This paper also explores the timing of uplift and collapse of the Protoprecordillera belt and how this affects the development of the foreland basin region, and its ties to the climatic shift discussed in all chapters of this dissertation. The new detrital zircon age distributions show a strong source region shift towards the east for both sections in the basin. This points to subsidence in the west and a broadening of the depositional system for the foreland basin region.

Furthermore, both the samples for the Tupe and Patquía formations contained younger than expected detrital zircons, which can be linked to volcanism associated with the volcanic arc, which lies to the west of the region during this time. This new information may point to younger depositional ages for both units than were previously known, as well as indicate potential atmospheric circulation patterns.

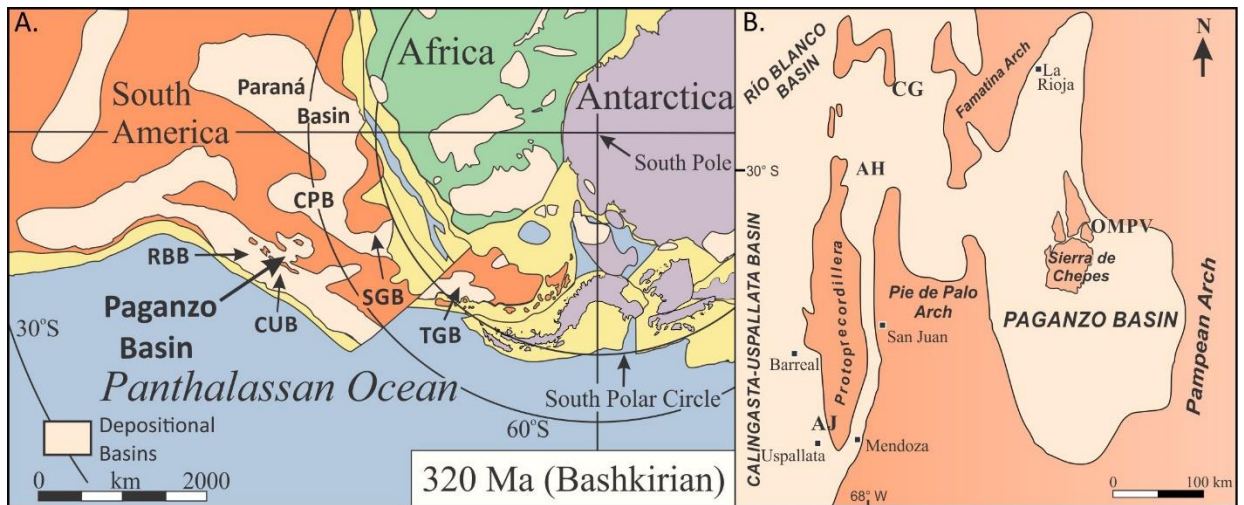


Figure 1. A. Map of sedimentary basins of Gondwana during the Bashkirian stage. RBB – Río Blanco Basin, CUB – Calingasta-Uspallata Basin, CPB – Chaco-Paraná Basin, SGB – Sauce Grande Basin, TGB – Tepuel Genoa Basin. Modified from Isbell et al. (2012) and Montañez and Poulsen (2013). B. Map of the Paganzo and Calingasta-Uspallata basins where the localities of interest are located. CG – Cerro Guandacol, AH – Agua Hedionda Anticline, near the town of Huaco, OMPV – Olta-Malanzán Paleovalley system, and AJ – Agua de Jagüel. Modified from López Gamundí et al. (1994), Henry et al. (2008), Limarino et al. (2014).

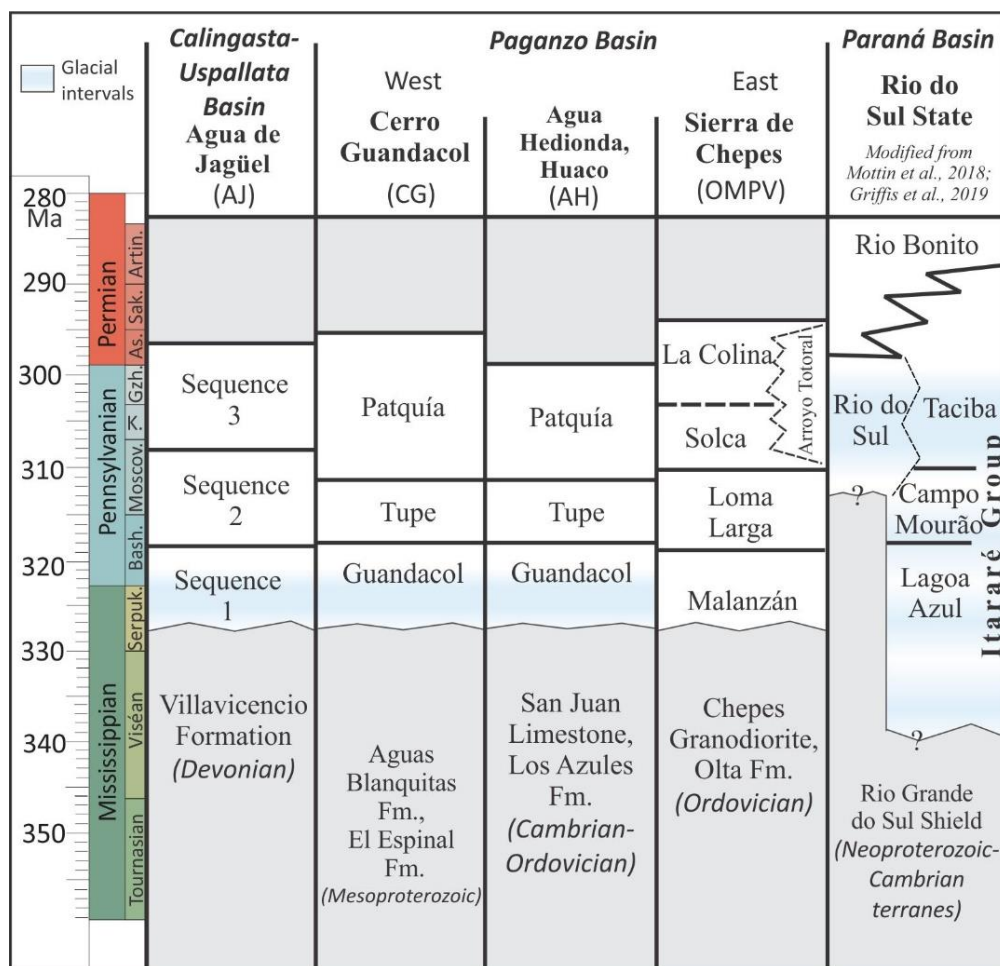


Figure 2. Chronostratigraphic columns showing the units in the selected basins for this study. The grey triangles highlighted in blue represent the interpreted glacial diamictites for each locality. CG – Cerro Guandacol, AH – Agua Hedionda Anticline, near the town of Huaco, OMPV – Olta-Malanzán Paleovalley system, and AJ – Agua de Jagüel. Modified from Henry et al. (2008).

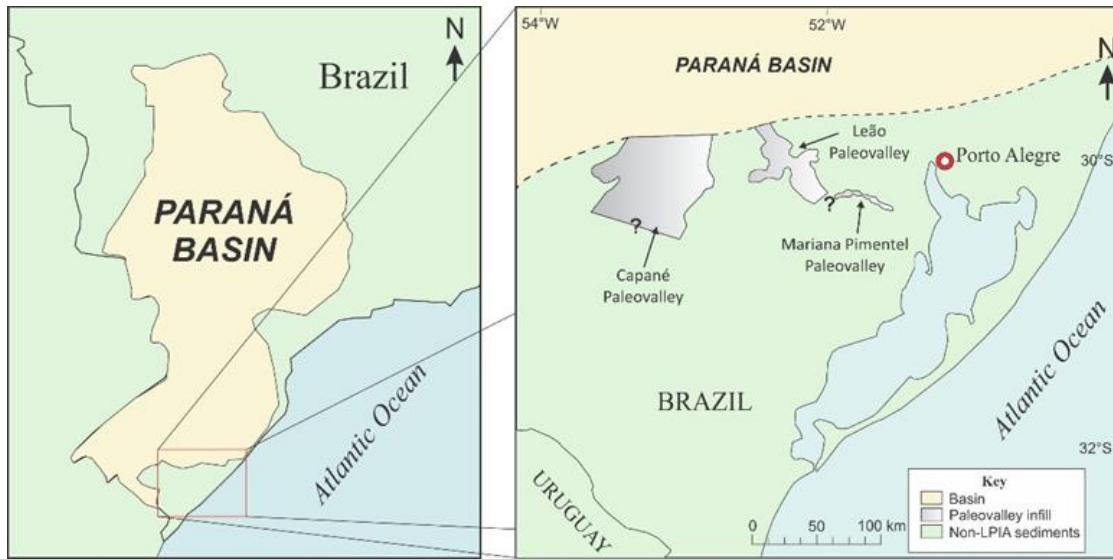


Figure 3. Map of the Paraná Basin and inset of the area in Rio Grande do Sul State where the samples were collected for this project. Modified from Fedorchuk et al. (2018).

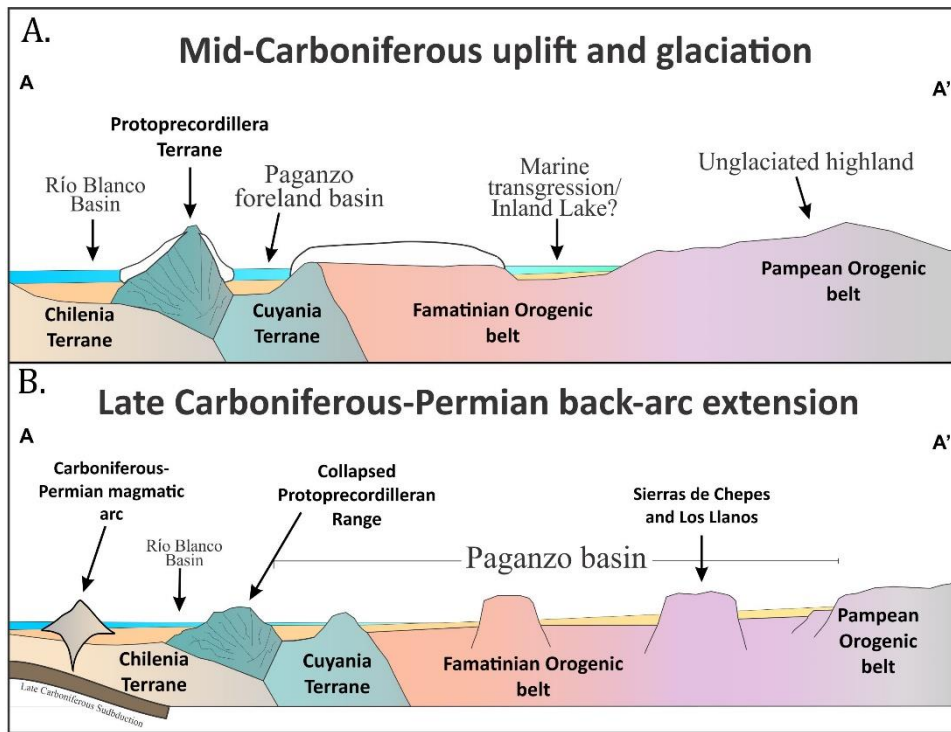


Figure 4. The evolutive model of the Paganzo Basin development from the middle Carboniferous to the Permian. Modified from Moxness et al. (2018)

References

- Amos, A.J., and Rolleri, E., 1965. El Carbónico marino en el valle Calingasta-Uspallata, San Juan-Mendoza: Boletín de Informaciones Petroleras 368, pp. 50–71.
- Andreis, R.R., Archangelsky, S., Leguizamón, R.R., 1986. El paleovalle de Malanzán: nuevos criterios para la estratigrafía del Neopaleozoico de la sierra de Los Llanos, La Rioja, República Argentina: Boletín de la Academia Nacional de Ciencias (Córdoba) 57, pp. 1-119.
- Aquino, C.D., Milana, J.P., Faccini, U.F., 2014. New glacial evidences at the Talacasto paleofjord (Paganzo basin, W-Argentina) and its implications for the paleogeography of the Gondwana margin. *Journal of South American Earth Sciences* 56, 278-300.
- Astini, R.A., Martina, F., Ezpeleta, M., Dávila, F.D., Cawood, P.A., 2009. Chronology from Rifting to Foreland Basin in the Paganzo Basin (Argentina), and a Reappraisal on the "eo- and Neohercynian" Tectonics along Western Gondwana., XII Congreso Geológico Chileno, Santiago, Chile. Universidad de Chile, Santiago, Chile, pp. 1–4 Extended Abstracts S9 010.
- Astini, R., 2010. Linked basins and sedimentary products across an accretionary margin: the case for the late history of the peri-Gondwanan Terra Australis orogen through the stratigraphic record of the Paganzo Basin. In: Papa, C., Astini, R. (eds.), *Field Excursion Guidebook, 18th International Sedimentological Congress*. International Association of Sedimentologists, Mendoza, Argentina, pp. 58.
- Azcuy, C.L., Carrizo, H.A., Caminos, R., 1999. Carbonífero y Pérmico de las Sierras Pampeanas, Famatina, Precordillera, Cordillera Frontal y Bloque de San Rafael. *Instituto de Geología y Recursos Minerales Geología Argentina*, v. 29, p. 261-318.
- Broccoli and Manabe, 1997, *Mountains and Midlatitude Aridity: In Ruddiman, W.F. (ed.) Tectonic uplift and climate change*, New York, NY, United States (USA), Plenum Press, New York, NY.
- Caputo, M.V., Crowell, J.C., 1985, Migration of glacial centers across Gondwana during Paleozoic Era. *Geological Society of America Bulletin* v. 96, p. 1020-1036.
- Caputo, M. V., de Melo, J. H. G., Streef, M., Isbell, J. L., 2008. Late Devonian and Early Carboniferous glacial records of South America, in Fielding, C. R., Frank, T. D., and Isbell, J. L., eds., *Resolving the Late Paleozoic Ice Age in Time and Space*: Boulder, CO, Geological Society of America Special Publication., p. 161-173.
- Carignano, C., Cioccale, M., Rabassa, J., 1999. Landscape antiquity of the central-eastern Sierras Pampeanas (Argentina): Geomorphological evolution since Gondwanic times: *Zeitschrift für Geomorphologie Neue Folge* 118, 245–268.
- Césari, S.N., Limarino, C.O., Gulbranson, E.L., 2011. An Upper Paleozoic bio-chronostratigraphic scheme for the western margin of Gondwana. *Earth Sci. Rev.* 106, p. 149-160.
- Craddock, J.P., Ojakangas, R.W., Malone, D.H., Konstantinou, A., Mory, A., Thomas, R.J., Craddock, S.D., Pauls, K.N., Zimmerman, U., Botha, G., Rocha-Campos, A., de Pazos, P.R.,

- Tohver, E., Riccomini, C.I., Martin, J., Redfern, J., Horstwood, M., Gehrels, G., 2019. Provenance of Permo-Carboniferous Diamictites across Gondwana. *Earth Science Reviews*. doi: 10.1016/j.earscirev.2019.01.01.
- Crowell, J.C., Frakes, L.A., 1970. Phanerozoic glaciation and the causes of ice ages. *American Journal of Science* 268, 193–224.
- Dykstra, M., Kneller, B., Milana, J.P., 2006. Deglacial and postglacial sedimentary architecture in a deeply incised paleovalley–paleofjord — the Pennsylvanian (late Carboniferous) Jejenes Formation, San Juan, Argentina. *Geological Society of America Bulletin* 118, pp. 913–937.
- Dykstra, M., Kneller, B., Milana, J.P., 2007. A high-resolution record of deep-water processes in a confined paleofjord, quebrada de Las Lajas, Argentina. In: Nilsen, T.H., Shew, R.D., Steffens, G.S., Studlick, J.R.J. (Eds.), *Atlas of Deep-Water Outcrops: AAPG Studies in Geology* 56, CD-ROM, 19 p.
- Einhorn, J.C., Gehrels, G.E., Vernon, A., and DeCelles, P.G., 2015. U-Pb zircon geochronology of Neoproterozoic–Paleozoic sandstones and Paleozoic plutonic rocks in the Central Andes (21°S–26°S). In: DeCelles, P.G., Ducea, M.N., Carrapa, B., and Kapp, P.A., eds., *Geodynamics of a Cordilleran Orogenic System: The Central Andes of Argentina and Northern Chile*. *Geological Society of America Memoir* 212, p. 115–124, doi: 10.1130/2015.1212(06).
- Enkelmann, E., Ridgway, K.D., Carignano, C., Linnemann, U., 2014. A thermochronometric view into an ancient landscape: tectonic setting, and inversion of the Paleozoic eastern Paganzo basin, Argentina. *Lithosphere* 6, pp. 93–107.
- Enkelmann, E., Garver, J.I., 2015. Low-temperature thermochronology applied to ancient settings. *Journal of Geodynamics* 93, pp. 17–30.
- Eyles, N., Eyles, C.H., 1993. Glacial geologic confirmation of an intraplate boundary in the Paraná basin of Brazil. *Geology* 21, pp. 459–462.
- Eyles, C.H., Eyles, N., França, A.B., 1993. Glaciation and tectonics in an active intracratonic basin: The late Paleozoic Itararé Group, Paraná Basin, Brazil. *Sedimentology* 40, pp. 1–25, doi: 10.1111/j.1365-3091.1993.tb01087.x.
- Fielding, C.R., Frank, T.D., Isbell, J.L., 2008a. The late Paleozoic ice age—A review of current understanding and synthesis of global climate patterns, in Fielding, C.R., Frank, T.D., and Isbell, J.L., eds., *Resolving the Late Paleozoic Ice Age in Time and Space*. *Geological Society of America Special Paper* 441, pp. 343–354.
- Fielding, C.R., Frank, T.D., Birgenheier, L.P., Rygel, M.C., Jones, A.T., Roberts, J., 2008b. Stratigraphic imprint of the Late Paleozoic Ice Age in eastern Australia: a record of alternating glacial and nonglacial climate regime. *Journal of the Geological Society, London*, v. 165, pp. 129–140.
- Fielding, C.R., Frank, T.D., Birgenheier, L.P., Rygel, M.C., Jones, A.T., Roberts, J., 2008c. Stratigraphic record and facies associations of the late Paleozoic ice age in eastern Australia (New South Wales and Queensland). In: Fielding, C.R., Frank, T., Isbell, J.L. (Eds.),

- Resolving the Late Paleozoic Ice Age in Time and Space. Geological Society of America Special Paper 441, pp. 41-57.
- Frakes, L.A., 1979, *Climates throughout geologic time*. Elsevier, Amsterdam, 310 p.
- Frakes, L.A., Crowell, J.C., 1969, Late Paleozoic glaciation: I, South America. Geological Society of America Bulletin 80, pp. 1007-1042.
- França, A.B., 1994, Itararé Group: Gondwanan Carboniferous-Permian of the Paraná Basin, Brazil, in Deynoux, M., Miller, J.M.G., Domack, E.W., Eyles, N., Fairchild, I.J., and Young, G.M., eds., *Earth's Glacial Record*: Cambridge, UK, Cambridge University Press, pp. 70–82.
- Frank, T. D., Shultis, A. I., Fielding, C. R., 2015, Acme and demise of the late Palaeozoic ice age: A view from the southeastern margin of Gondwana: *Palaeogeography Palaeoclimatology Palaeoecology* 418, pp. 176-192.
- Gastaldo, R.A., DiMichele, W.A., Pfefferkorn, H.W., 1996, Out of the icehouse into the greenhouse: a late Paleozoic analogue for modern global vegetational change. *GSA Today*, v. 10, p. 1-7.
- Godard, V., Bourlès, D.L., Spinabella, F., Burbank, D.W., Bookhagen, B., Burch Fisher, G., Moulin, A., Léanni, L., 2014, Dominance of tectonics over climate in Himalayan denudation: *Geology* 42, 3, pp. 243-246.
- Goldberg, K., 2001. The Paleoclimatic evolution of the Permian in the Paraná Basin in Southern Brazil. PhD Dissertation, University of Chicago, 234 p.
- Goldberg, K., Humayun, M., 2010. The applicability of the Chemical Index of Alteration as a paleoclimatic indicator: An example from the Permian of the Paraná Basin, Brazil. *Palaeogeography, Palaeoclimatology, Palaeoecology* 293, pp. 175-183.
- Guená, S.E., Escosteguy, L.D., 2010, Paleomagnetism of the Carboniferous-Permian Patquía Formation Paganzo basin, Argentina: implications for the apparent polar wander path for South America and Gondwana during the Late Paleozoic: *Geologica Acta* 8, 4, pp. 373-397.
- Gulbranson E.L., Montañez, I.P., Schmitz, M.D., Limarino, C.O., Isbell, J.L., Marensi, S.A., Crowley, J.L., 2010, High-precision U–Pb calibration of Carboniferous glaciation and climate history, Paganzo Group, NW Argentina. *Geological Society of America Bulletin* 122, 1480–1498.
- Gulbranson, E.L., Montañez, I.P., Tabor, N., Limarino, C.O., 2015. Late Pennsylvanian aridification on the southwestern margin of Gondwana (Paganzo Basin, NW Argentina): A regional expression of a global climate perturbation. *Palaeogeography Palaeoclimatology Palaeoecology* 417, pp. 220-235.
- Heckel, P.H., 1994. Evaluation of evidence for glacio-eustatic control over marine Pennsylvanian cyclothems in North America and consideration of possible tectonic effects: In: Dennison, J.M., Ettensohn, F.R. (Eds.), *Tectonic and eustatic controls on sedimentary cycles*: Tulsa, Oklahoma, SEPM (Society for Sedimentary Geology) Concepts in Sedimentology and Paleontology 4, pp. 65–87.

- Heckel, P.H., 2008. Pennsylvanian cyclothems in midcontinent North America as far-field effects of waxing and waning of Gondwana ice sheets. In: Fielding, C.R., Frank, T., Isbell, J.L. (Eds.), *Resolving the Late Paleozoic Ice Age in Time and Space: Geological Society of America Special Paper 441*, pp. 275–289.
- Henry, L.C., 2007. Carboniferous glaciogenic deposits of the Hoyada Verde and Tramojo Formations of the Calingasta-Uspallata Basin, west central Argentina. M.S. Thesis, University of Wisconsin-Milwaukee, 151 p.
- Henry, L.C., Isbell, J.L., Limarino, C.O., 2008, Carboniferous glaciogenic deposits of the Protoprecordillera of west central Argentina. In: Fielding, C.R., Frank, T.D., Isbell, J.L. (Eds.), *Resolving the Late Paleozoic Ice Age in Time and Space*. Geological Society of America Special Paper 441, pp. 131–142.
- Henry L.C., Isbell, J.L., Limarino, C.O., McHenry, L.J., Fraiser, M.L., 2010. Mid-Carboniferous deglaciation of the Protoprecordillera, Argentina, recorded in the Agua de Jagüel paleovalley. *Palaeogeography, Palaeoclimatology, Palaeoecology* 298, pp. 112–129.
- Holz, M., Souza, P. A., Iannuzzi, R., 2008. Sequence stratigraphy and biostratigraphy of the Late Carboniferous to Early Permian glacial succession (Itarare Subgroup) at the eastern-southeastern margin of the Parana Basin, Brazil. *Geological Society of America Special Paper 441*, pp. 115-129.
- Holz, M., Franca, A. B., Souza, P. A., Iannuzzi, R., and Rohn, R., 2010. A stratigraphic chart of the Late Carboniferous/Permian succession of the eastern border of the Paraná Basin, Brazil, *South Americaa: Journal of South American Earth Sciences*, v. 29, no. 2, p. 381-399.
- Horton D.E., Poulsen, C.J., 2009. Paradox of late Paleozoic glacioeustasy. *Geology* 37, pp. 715–718.
- Isbell, J.L., Miller, M.F., Wolfe, K.L. & Lenaker, P.A., 2003. Timing of late Paleozoic glaciation in Gondwana: was glaciation responsible for the development of northern hemisphere cyclothems?: in *Extreme depositional environments: mega end members in geologic time*, eds. M. A. Chan & A. W. Archer Boulder, Colorado: Geological Society of America Special Paper, pp. 5-24.
- Isbell, J.L., Fraiser, M.L., Henry, L.C., 2008. Examining the complexity of environmental change during the late Paleozoic and early Mesozoic: *Palaios* 23, 5-6, pp. 267-269.
- Isbell, J.L., Henry, L.C., Gulbranson, E.L., Limarino, C.O., Fraiser, M.L., Koch, Z.J., Ciccioioli, P.L. & Dineen, A.A., 2012. Glacial paradoxes during the late Paleozoic ice age: Evaluating the equilibrium line altitude as a control on glaciation. *Gondwana Research* 22, pp. 1-19.
- Jordan, T.E., Zeitler, P., Ramos, V., Gleadow, A.J.W., 1989, Thermochronometric data on the development of the basement peneplain in the Sierras Pampeanas, Argentina: *Journal of South American Earth Sciences* 2, 3, pp. 207-222.

- Limarino, C.O., Marensi, S.A., Tripaldi, A., Caselli, A.T., 2002. Evolution of the Upper Paleozoic basins of western Argentina during the maximum extent of Gondwana. 16th International Sedimentological Congress, Abstracts, pp. 224-225.
- Limarino, C.O., Spalletti, L.A., 2006. Paleogeography of the Upper Paleozoic basins of southern South America: an overview. *Journal of South American Earth Sciences* 22, pp. 134–155.
- Limarino, C.O., Tripaldi, A., Marensi, S., Fauqué, L., 2006. Tectonic, sea level, and climatic controls on late Paleozoic sedimentation in the western basins of Argentina. *Journal of South American Earth Sciences* 33, pp. 205–226.
- Limarino, C.O., Césari, S.N., Spalletti, L.A., Taboada, A.C., Isbell, J.L., Geuna, S., Gulbranson, E.L., 2014. A paleoclimatic review of southern South America during the late Paleozoic; A record from icehouse to extreme greenhouse conditions: *Gondwana Research* 25, pp. 1396-1421.
- López-Gamundí, O. R., 1987. Depositional models for the glaciomarine sequences of Andean late Paleozoic basins of Argentina: *Sedimentary Geology* 52, pp. 109–126.
- López-Gamundí, O.R., Espejo, I.S., Conaghan, P.J., Powell, C.McA., Veevers, J.J., 1994. Southern South America. In: Veevers, J.J., Powell, C.McA. (Eds.), *Permian–Triassic Pangean basins and foldbelts along the Panthalassan margin of Gondwanaland*. Boulder, Colorado: Geological Society of America Memoir 184, pp. 281–329.
- López-Gamundí, O.R., 1997. Glacial–postglacial transition in the late Paleozoic basins of southern South America. In: Martini, I.P. (Ed.), *Late Glacial and Postglacial Environmental Changes: Quaternary, Carboniferous–Permian, and Proterozoic*. Oxford University Press, Oxford, UK, pp. 147–168.
- Metcalfe, I., Crowley, J. L., Nicoll, R. S., and Schmitz, M., 2015. High-precision U-Pb CA-TIMS calibration of Middle Permian to Lower Triassic sequences, mass extinction and extreme climate-change in eastern Australian Gondwana: *Gondwana Research* 28, 61-81.
- Milani, E.J., França, A.B., and Schneider, R.L., 1994. Bacia do Paraná: *Boletim de Geociências da Petrobras*, v. 8, p. 69–82.
- Montañez, I.P., Tabor, N.J., Niemeier, D., DiMichele, W.A., Frank, T.D., Fielding, C.R., Isbell, J.L., Birgenheir, L.P., Rygel, M.C., 2007. CO₂-forced climate and vegetative instability during late Paleozoic deglaciation. *Science* 315, pp. 87–91.
- Montañez, I.P., Poulsen, C.J., 2013. The late Paleozoic ice age: An evolving paradigm. *Annual Review of Earth and Planetary Sciences*, 41, pp. 24.1-24.
- Montanez, I.P., McElwain, J.C., Poulsen, C.J., White, J.D., DiMichele, W.A., Wilson, J.P., Griggs, G., Hren, M.T., 2016. Climate, pCO₂ and terrestrial carbon cycle linkages during late Palaeozoic glacial-interglacial cycles. *Nature Geosciences*, 9, 11, pp. 824-828.
- Moxness, L.D., Isbell, J.L., Pauls, K.N., Limarino, C.O., Schencman, J., 2018, Sedimentology of the mid-Carboniferous fill of the Olta paleovalley, eastern Paganzo Basin, Argetina: Implications for glaciation and controls on diachronous deglaciation in western

- Gondwana during the late Paleozoic Ice Age. *Journal of South American Earth Sciences* 84, pp. 127-148. doi/10.1016/j.jsames.2018.03.015.
- Nesbitt, H.W., Young, G.M., 1982, Early Proterozoic climates and plate motions inferred from major element chemistry from lutites: *Nature*, v. 199, p. 715-717.
- Net, L.I., Alonso, M.S., Limarino, C.O., 2002. Source rock and environmental control on clay mineral associations, lower section of Paganzo group (Carboniferous), northwest Argentina. *Sedimentary Geology* 152, 183–199.
- Newell, A.J., Tverdokhlebov, V.P., Benton, M.J., 1999, Interplay of tectonics and climate on a transverse fluvial system, Upper Permian, Southern Uralian Foreland Basin, Russia: *Sedimentary Geology*, v. 127, p. 11-29.
- Patridge, T., 1997. Late Neogene uplift in eastern and southern Africa and its paleoclimatic implications: In Ruddiman, W.F. (ed.) *Tectonic uplift and climate change*, New York, NY, United States (USA), Plenum Press, New York, NY.
- Pérez Loinaze, V.P., 2009. New palynological data from the Malanzán Formation (Carboniferous), La Rioja Province, Argentina. *Ameghiniana* 46, p. 495–512.
- Pérez Loinaze, V.S., Limarino, C.O., Césari, S.N., 2010. Glacial events in Carboniferous sequences from Paganzo and Río Blanco Basins (Northwest Argentina): palynology and depositional setting. *Geologica Acta* 8, 399–418.
- Poulsen, C.J., Pollard, D., Montañez, I.P., Rowley, D., 2007, Late Paleozoic tropical climate response to Gondwanan deglaciation: *Geology*, v. 35, p. 771–74.
- Rabassa, J., Carignano, C., Cioccale, M., 2014. A general overview of Gondwana landscapes in Argentina. In: Rabassa, J., Ollier, C. (Eds.), *Gondwana Landscapes in Southern South America: Argentina, Uruguay and southern Brazil*. Springer Earth System Science, Dordrecht, Heidelberg, New York, London, 201–245.
- Ramos, V., Jordan, T., Allmendinger, R., Kay, S., Cortés, J., Palma, M., 1984. Chilenia: un terreno alóctono en la evolución paleozoica de los Andes Centrales. In: 10° Congreso Geol, 2. Actas, Argentino, pp. 84–106.
- Ramos, V., Jordan, T., Allmendinger, R., Mpodozis, C., Kay, S., Cortés, J., Palma, M., 1986. Paleozoic terranes of the central Argentine-Chilean Andes. *Tectonics* 5, pp. 855–888.
- Ramos, V.A., 1988. Tectonics of the Late Proterozoic–Early Paleozoic: a collisional history of Southern South America. *Episodes* 11, pp. 168–174.
- Rocha Campos, A.C., dos Santos, P.R., Canuto, J.R., 2008. Late Paleozoic glacial deposits of Brazil; Parana Basin. In: Fielding, C.R., Frank, T.D., Isbell, J.L. (Eds.), *Resolving the Late Paleozoic Ice Age in Time and Space: Geological Society of America Special Paper*, 441, pp. 97–114.
- Ramos, V.A., Dallmeyer, D. y Vujovich, G., 1998. Time constraints on the Early Paleozoic docking of the Precordillera, Central Argentina. In: Pankhurst, R. y Rapela, C. (Eds.): *The Proto-Andean Margin of Gondwana*, Geological Society, London, Special Publication, 142, 143-158.

- Rolleri, E.O., Baldis, B.A., 1969. Paleogeography and distribution of Carboniferous deposits in the Argentine Precordillera. *Gondwana Stratigraphy, Ciencias de la Tierra*, vol. 2, pp. 1005–1024.
- Rosa, E.L.M., Vesely, F.F., Isbell, J.L., Kipper, F., Fedorchuk, N.D., Souza, P.A., 2019. Constraining the timing, kinematics and cyclicity of Mississippian-Early Pennsylvanian glaciations in the Paraná Basin, Brazil. *Sedimentary Geology* 384, pp. 29-49. doi:10.1016/j.sedgeo.2019.03.001.
- Royer, D. L., Berner, R. A., Montañez, I. P., Tabor, N. J., and Beerling, D. J., 2004, CO₂ as a primary driver of Phanerozoic climate: *GSA Today*, v. 14, no. 3, p. 4-10.
- Ruddiman, W. F., and Prell, W. L., 1997, *Introduction to the uplift-climate connection*, New York, NY, United States (USA), Plenum Press, New York, NY, Tectonic uplift and climate change.
- Ruddiman, W. F., Raymo, M. E., Prell, W. L., and Kutzbach, J. E., 1997, *The uplift-climate connection: a synthesis*, New York, NY, United States (USA), Plenum Press, New York, NY, Tectonic uplift and climate change.
- Rygel, M.C., Fielding, C.R., Frank, T.D., Birgenheier, L.P., 2008. The magnitude of late Paleozoic glacioeustatic fluctuations: a synthesis. *Journal of Sedimentary Research* 78, 500–511.
- Scotese, C.R., 1997. *The PALEOMAP Project: paleogeographic atlas and plate tectonic software*. Department of Geology, University of Texas, TX.
- Socha et al., 2014. Gondwana glacial paleolandscape, diamictite record of Carboniferous valley glaciation and preglacial remnants of an ancient weathering front in Northwestern Argentina, in *Gondwana Landscapes in southern South America*.
- Sterren, A.F., Martínez, M., 1996. El paleovalle de Olta (Carbonífero): paleoambientes y paleogeografía. 13° Congreso Geológico Argentino y 3° Congreso Exploración de Hidrocarburos (Buenos Aires), Actas 2, 89-103.
- Taboada, A.C. 2010. Mississippian-Early Permian brachiopods from western Argentina: Tools for middle- to high-latitude correlation, paleobiogeographic and paleoclimatic reconstruction. *Palaeogeography, Palaeoclimatology, Palaeoecology* 298, 152-73.
- Tabor, N. J., and Poulsen, C. J., 2008, Palaeoclimate across the Late Pennsylvanian-Early Permian tropical palaeolatitudes; a review of climate indicators, their distribution, and relation to palaeophysiographic climate factors: *Palaeogeography, Palaeoclimatology, Palaeoecology*, v. 268, no. 3-4, p. 293-310.
- Tedesco, A., Ciccioli, P., Suriano, J., Limarino, C., 2010, Changes in the architecture of fluvial deposits in the Paganzo Basin (Upper Paleozoic of San Juan Province): an example of sea level and climatic controls on the development of coastal fluvial environments. *Geologica Acta*.
- Valdez Buso, V., Milana, J.P., di Pasquo, M., Paim, P.S.G., Philipp, R.P., Aquino, C.D., Caligari, J., Junior, F.C., Kneller, B., 2020. Timing of the late Palaeozoic glaciation in

western Gondwana: New ages and correlations from Paganzo and Paraná basins.
Palaeogeography, Palaeoclimatology, Palaeoecology 544.
doi:10.1016/j.palaeo.2020.109624.

Veevers, J.J., Powell, M., 1987. Late Paleozoic glacial episodes in Gondwanaland reflected in transgressive–regressive depositional sequences in Euramerica. *Geological Society of America Bulletin* 98, 475–487.

Visser, J.N.J., 1997. Deglaciation sequences in the Permo-Carboniferous Karoo and Kalahari basins of southern Africa: a tool in the analysis of cyclic glaciomarine basin fills. *Sedimentology* 44, 507–521.

Chapter 2: Constraining late Paleozoic ice extent in the Paganzo Basin of western Argentina using U-Pb detrital zircon geochronology for the lower Paganzo Group strata

Kathryn N. Pauls¹, John L. Isbell¹, C. Oscar Limarino², Pablo J. Alonso-Murauga², David H. Malone³, L. Jazmin Schencman², Carina E. Colombi⁴, Levi D. Moxness^{1*}

1: University of Wisconsin-Milwaukee, 3209 N. Maryland Ave., Milwaukee, WI 53211.

* Current Address: North Dakota Geological Survey, 600 East Boulevard, Dept. 405, Bismarck, ND 58505-0840

2: Universidad de Buenos Aires-IGEB (UBA-CONICET), Facultad de Ciencias Exactas y Naturales, Departamento de Ciencias Geológicas, Ciudad Universitaria Pab. 2, 1° piso, CABA.

3 : Department of Geography, Geology and the Environment, Illinois State University, Normal, IL 61790-4400, USA

4 : Instituto y Museo de Ciencias Naturales, Universidad Nacional de San Juan, Centro de Investigaciones de la Geosfera y la Biosfera - Conicet, España 400 (Norte), San Juan, Argentina

Authors' email addresses: kpauls@uwm.edu , jisbell@uwm.edu, limar@gl.fcen.uba.ar, pablojoaquin3@gmail.com, dhmalone@ilstu.edu, jazminsch@gmail.com, ccolombi@unsj.edu.ar, ldmoxness@gmail.com

Abstract

The western margin of Gondwana records evidence of mid-Carboniferous glaciation (Viséan-Bashkirian) in the strata of the Paganzo Basin and adjacent areas. Previous studies focused on constraining the orientations of ice flow and generalizing the extent and occurrence of glacial ice in the basin. However, there is uncertainty occurs concerning the location and extent of glaciation and the locations of glacial centers during deposition of the Guandacol Formation

located in the western portion and the time correlative Malanzán Formation in the and eastern parts of the basin respectively. Understanding these strata and the conditions that led to the deposition of these strata has important implications for understanding paleoclimatic conditions along the western margin of Gondwana during the late Paleozoic Ice age. To refine the glaciation history, we present new paleocurrent, facies, and a comparative analysis of previously published and one new detrital zircon geochronology data set. Together, these data provide new insight into sediment dispersal patterns and glacial centers within the basin. Our data indicate that both units were deposited under cold climatic conditions that occurred across the entire basin, but that glaciers were restricted to the western portion of the basin. The facies analysis for both formations indicates very different depositional environments for the two units: glacial and glaciomarine environments in the west and non-glacial alluvial, alluvial fan and lacustrine and/or marine environments in the east. Detrital zircon geochronology indicates separate localized provenance signatures for the two formations. Furthermore, the detrital zircon populations allude to disconnected depositional centers. At Huaco, glacial flow in the Guandacol is oriented toward the northwest (i.e. 313°) and appears to be draining from an uplift that contains similar zircon age populations as the Sierra de Valle Fértil and Sierra de Pie de Palo ranges. In the Olta-Malanzán paleovalley system, drainage was off valley walls and down the valley axis (i.e. south and southwest) within the Sierras de Chepes region with limited sediment sourced from the east just beyond the paleovalley system. Paleoflow measurements reported from other known glacial localities along the western portion of the basin reflect a radial flow pattern within and away from deeply incised valleys that clearly point to upland glacial centers within the Cuyania and Precordilleran terranes.

1. Introduction

Over the past several decades, research on the late Paleozoic ice age (LPIA; 372-259 million years ago) has led to a better understanding of the development and termination of glaciation(s) across Gondwana. The LPIA is the only example of when a vegetated and biologically complex Earth shifted from an icehouse to a greenhouse state (Gastaldo et al., 1996; Montañez et al., 2007, 2016; Fielding et al., 2008a; Isbell et al., 2012; Montañez and Poulsen, 2013). Therefore, further research on the LPIA will help in understanding drivers that influence changing climatic regimes.

In the Paganzo Basin, located along the Panthallassan margin of western Argentina, glaciers developed during the Middle Mississippian (Visean) and disappeared in the early Pennsylvanian (Bashkirian; López-Gamundí et al., 1994; López-Gamundí, 1997; Holz et al., 2008; Caputo et al., 2008; Henry et al., 2008, 2010; Isbell et al., 2012; Limarino et al., 2014). However, other places in Gondwana at similar paleo-latitudes (e.g. southern Paraná Basin in Brazil) persisted until the end of the Carboniferous (Caputo and Crowell, 1985; Rocha Campos et al., 2008; Isbell et al., 2012; Griffis et al., 2018), or perhaps until the Early Permian (early Cisuralian, eastern Paraná Basin; Mottin et al., 2018). For these purposes, we used paleoenvironmental, paleocurrent, and geochronological information to address the timing and location of glaciation in the Paganzo Basin. We 1) examined published and new evidence for glaciers using paleoflow and facies analyses; 2) compared published and newly obtained detrital zircon age populations for samples from different locations within the Paganzo Basin to assess provenance; 3) used this data to test various hypotheses regarding the extent and location of ice centers within the basin; and 4) evaluated and discussed the current understanding of the location

and extent of the uplands within and surrounding the basin during the early-middle Carboniferous.

2. Background

Western Argentina contains evidence of glaciation during the LPIA (Viséan to early Bashkirian), concentrated within several basins along the Panthalassan margin. Following Limarino et al. (2002b) and Marensi et al. (2005), these basins can be broken into paleogeographic domains of open marine, transitional and continental dominated basin settings. The Paganzo Basin incorporates two of these settings: transitional and continental-dominated. This basin, which spans an area of approximately 144,000 km² at its largest extent, is bounded today by the Sierras Pampeanas to the east, north and south, and the Precordilleran range in the west. The development and structure of the Paganzo Basin is still under debate. Various studies identified it as a retroarc foreland basin (Ramos et al., 1988), a rift basin (Astini et al., 1995, 2009; Astini, 2010), or as a pull-apart basin due to strike-slip activity along the Panthalassan margin of Gondwana (Limarino et al., 2002a, 2014; Milana and Di Pasquo, 2019). Regardless of the exact type of basin, it was a major catchment for late Paleozoic sediments, and records early evidence of glaciation during the peak Mid-Carboniferous phase of the LPIA.

This evidence is recorded at the base of the late Paleozoic strata of the Paganzo Basin, which contains both ice-proximal and subglacial deposits (López-Gamundí, 1987; Limarino and Gutiérrez, 1990; Net, 1999; López-Gamundí and Martínez, 2000; Limarino et al., 2002b; Henry, 2007; Henry et al., 2008, 2010; Césari et al., 2011; Limarino et al., 2014; Alonso-Muruaga et al., 2018; Valdez Buso et al., 2017, 2020). The Paganzo Group strata cover the entire basin and are broken up into regional formations (Fig. 5). The basal part of the Paganzo Group is the subject of

this paper. In the west, the glacial units are known as the Jejenes and the Guandacol formations, in the central portion of the basin, this unit is referred to as the Lagares Formation, and in the east the Malanzán Formation is the time-equivalent unit (Limarino et al., 2002a, 2006). The various formations are correlated using palynological and fossil plant remains, as well as some radiometric ages determined from strata in the western Paganzo and Río Blanco basins (cf. Gulbranson et al., 2010, 2015; Césari et al., 2011, 2019; Valdez Buso et al., 2020). The correlations between these units, and previous interpretations of these deposits as glacial in origin, has provided grounds for a few hypotheses concerning the extent of glaciation during the Visean and Bashkirian stages in the Paganzo Basin. One of the goals of this study is to test hypotheses on the extent of glaciation in the basin.

One such hypothesis maintains that there were several potentially separate glacial centers in the basin. In the western domain, there was a glaciated upland in the Precordilleran region of the western Sierras Pampeanas, known as the Protoprecordillera (cf. proto-Precordillera of Amos and Rolleri, 1965; González, 1975; Fig. 6). This region is a small terrane that was uplifted as a fold-and-thrust belt during the Chañic orogeny (middle Devonian to earliest Mississippian), which occurred due to the accretion of the Chilenia terrane to Gondwana (Ramos et al., 1984, 1986; López-Gamundí et al., 1994; Limarino et al., 2006, 2014; Henry et al., 2008; Isbell et al., 2012; Moxness et al., 2018). The Protoprecordilleran range is considered by certain studies to be an ancient mountain belt and significant paleotopographic high that developed from the fold-and-thrust belt, and today underlies the present Precordilleran range of the Andes Mountains (González Bonorino, 1975; Ramos, 1988; López-Gamundí et al., 1994; Limarino et al., 2002, 2006; Isbell et al., 2012). Glaciomarine deposition occurred during the Visean-early Bashkirian in deeply-incised paleovalleys that emanated from the Protoprecordilleran region (Fig. 6B) and

into the surrounding Paganzo, Calingasta-Uspallata and Rio Blanco basins (cf. López-Gamundí et al., 1997; Limarino et al., 2002a, 2002b, 2006; Kneller et al., 2004; Dykstra et al., 2006, 2007; Limarino and Spalletti; Henry, 2007; Henry et al., 2008, 2010; Astini, 2010; Gulbranson et al., 2010; Césari et al., 2011; Isbell et al., 2012; Aquino et al., 2014; Alonso-Muruaga et al., 2018). The diamictites at the base of the Lagares Formation in the central Paganzo Basin at least indicate a potential for glacial influence along the proto-Famatina arch (Fig. 6B; Limarino et al., 2002a, 2006; Limarino and Spalletti; Astini, 2010; Tedesco et al., 2010; Limarino et al., 2014). There are also reported diamictites in the eastern domain, at the base of the Malanzán Formation, which contain outsized clasts and sparse debris flows, but these diamictites lack the traditional characteristics of true subglacial and proglacial deposits, such as faceted and striated clasts and the occurrence of sheared horizons (Andreis et al., 1986; Sterren and Martínez, 1996; Socha et al., 2014; Limarino et al., 2014; Moxness et al., 2018). Nevertheless, the presence of diamictites has led to the interpretation of glaciation throughout the Paganzo Basin, but in the form of alpine glaciation centered on the various ancient highlands (Fig. 6).

A second hypothesis contends that there was extensive regional uplift for this region during the Devonian and earliest Carboniferous (340-325 Ma; Astini, 2009; Astini et al., 2010), followed by an extensive peneplain (Jordan et al., 1989). In this scenario, the Protoprecordillera was not a significant uplift, and therefore did not host glacial ice centers. The peneplain surface in the Paganzo Basin region was instead thought to have been formed by a large ice sheet that was centered in the eastern Sierras Pampeanas, or on the Pampean arch (Milana and Berscowski, 1987, 1990, 1993; Milana, 1988; Milana et al., 1987; Astini, 2010; Aquino et al., 2014; Valdez Buso et al., 2017, 2020; Milana and Di Pasquo, 2019). This ice sheet would have advanced across the uplands, and as the ice sheet collapsed, it carved through a chain of uplands that was

known as the Zonda and Tontal arches in the west, as well as the Sierras de Chepes region in the east (Fig. 6C). These uplands were dissected by glacial valleys that drained the ice sheet and deposited the glacial strata of the Paganzo Group (i.e. the Guandacol, Lagares and Malanzán formations).

This paper will test these hypotheses to better determine the mid-Carboniferous glacial history of the western margin of Gondwana. We will use paleoflow measurements and detrital zircon geochronology to refine the current understanding of depositional environments and provenance of the lower Paganzo Group and time-equivalent strata.

3. Regional Geologic Setting

The western margin of Argentine Gondwana is an assemblage of terranes (the Pampia, Precordillera and Chilenia terranes), igneous intrusions, and subsequent metamorphosed units (Ramos, 1988; Pankhurst et al., 1998; Ramos et al., 1998, 2010, 2015; Rapela et al., 1998; Ramos, 1999, 2008; Rapalini, 2005; Dahlquist et al., 2010; Einhorn et al., 2015). The resulting paleotopographic highs created terrane accretion have been implicated in the climate and depositional histories of the subsequent basins (cf. Limarino et al., 2002a, 2002b, 2006).

The Sierras Pampeanas today make up most of the highlands between the Precordillera terrane and the Rio de la Plata craton and are divided into magmatic belts that correspond to different accretionary events of western Argentina (Fig. 12). The easternmost Sierras Pampeanas were formed during the Cambrian as the Pampia terrane docked to the Rio de La Plata craton, and therefore contain zircon ages between 500 and 600 Ma (Rapela et al., 1998, 2007; Ramos et al., 2015). The ranges include the Sierra de Córdoba, Sierra del norte de Córdoba, Sierra

Ambato, Sierra Ancasti and others (Rapela et al., 1998; Leal et al., 2003; Llambías et al 2003; Toselli et al., 2003)

The Sierras Pampeanas also include the Ordovician Famatina magmatic belt (490-450 Ma, with the main magmatism occurring between 490-470 Ma) and the eastern portion of the Cuyania Terrane (Pankhurst et al., 1998, 2000; Ramos et al., 1998; Keller, 1999; Ramos, 1999). The Famatina orogenic belt runs north-south between the Pampean orogenic belt and the Cuyania composite terrane, and encompasses Sierra de Valle Fértil, Sierras Famatina, Sierra de San Luis, and the Sierras de Chepes, Los Llanos, and Malanzán (Pankhurst et al., 1998, 2000; Toselli et al., 2003; Vujovich and Ostera 2003; Dahlquist et al., 2010; Einhorn et al., 2015). The Sierras de Chepes region contains crystallization ages from 477-497 Ma (Pankhurst et al., 1998; Stuart-Smith et al., 1999; Enkelmann et al., 2014). The western Famatina belt was also subject to metamorphism around 469 Ma, and contains some younger ages north of the Sierra de Valle Fértil region (Pankhurst et al., 1998, 2000; Ramos et al., 1998, 2010, 2015; Rapela et al., 1998, 2001; Rapalini, 2005; Dahlquist et al., 2010; Einhorn et al., 2015). Additionally, these Ordovician granites were intruded by post-orogenic granitic bodies during the Devonian-early Carboniferous (365-345 Ma; Dahlquist et al., 2010; Martina et al., 2018).

The Cuyania terrane is a microplate that either rifted from another region of Gondwana or rifted from Laurentia during the Cambrian or earliest Ordovician (Kay et al., 1996; Keller et al., 1998; Keller, 1999; Ramos, 2000; Casquet et al., 2001; Willner et al., 2008). The Cuyania terrane accreted to the western margin of Gondwana around 460-435 Ma, and contains sedimentary packages of “Grenville-age” (1165-980 Ma) and occur in the western Sierras Pampeanas ranges of the Sierra de Pie de Palo and the Sierras de Umango, Maz and Espinol (Huff et al., 1998; Ottone et al., 2001; Dahlquist et al., 2010; Sial et al., 2013; Verdecchia et al.,

2014, 2018). Superimposed upon Cuyania is a fold-and-thrust belt that is known as the Precordillera terrane, which contains Cambrian-Ordovician sedimentary units (i.e. the San Juan Limestone and Los Azules Formation) that represent carbonate and siliciclastic platform depositional environments (Kay et al., 1996; Huff et al., 1998; Keller et al., 1998; Keller, 1999; Ottone et al., 2001; Willner et al., 2008). The Precordillera terrane is interpreted to be part of a tectonic belt that made up either the proto-Precordilleran range or the Tontal Arch during the early Carboniferous (cf. Amos and Rolleri, 1965; Limarino et al., 2006; Aquino et al., 2014; Valdez Buso et al., 2017, 2020). The Cambrian and Ordovician deposits of the Precordillera and Cuyania terranes are overlain conformably or unconformably by sedimentary packages that range in age from Silurian to Triassic (cf. Keller et al., 1998; Keller, 1999; Willner et al., 2008).

3.1 Geology of the Lower Paganzo Group strata

Purported glacial deposits of the Paganzo Group strata are reported all throughout the Paganzo Basin and are interpreted to be mostly fjord-like or glacial valley environments (Marenssi et al., 2005; Limarino et al., 2002a, 2002b, 2014; Aquino et al., 2014; Valdez Buso et al., 2017; Alonso-Muruaga et al., 2018; Fallgatter et al., 2019; Milana and di Pasquo, 2019). In this study, we measured detailed stratigraphic sections at two localities on the western (Huaco locality) and eastern (i.e. the Olta-Malanzán paleovalley) margins of the Paganzo Basin for an evaluation of the extent of glacial deposits within the basin. While much is known about the glacial deposits of the Paganzo Group strata, new understandings of the climate and depositional environments across the basin have come to light (cf. Valdez Buso et al., 2017, 2020; Alonso-Muruaga et al., 2018; Moxness et al., 2018; Pauls et al., 2019; Fallgatter et al., 2019; Milana and di Pasquo, 2019). Recent studies suggest that glacial strata may not be present throughout the

basin (cf. Moxness et al., 2018; Pauls et al., 2019). To evaluate the interconnection between the eastern and western margins of the basin and to refine the extent of glaciation, we present lithofacies analyses and detrital zircon geochronology results from the Malanzán Formation of the Olta-Malanzán region in the eastern Paganzo Basin and from the Guandacol Formation at Huaco on the western margin (Fig. 7).

3.2. Olta-Malanzán paleovalley

The Olta-Malanzán paleovalley (OMPV) occurs in an isolated uplift of the Famatina orogenic belt of the Sierras Pampeanas (Fig. 7A). The paleovalley developed in an alpine or mountain valley setting, either carved by glacial ice (cf. Sterren and Martinez, 1996; Enkelmann et al., 2014; Rabassa et al., 2014; Socha et al., 2014) or formed as the result of a fault-bounded basin (Braccacini, 1948; Andreis et al., 1986; Buatois and Mangano, 1995; Net and Limarino, 1999; Moxness et al. 2018). The Paleozoic valley fill overlies various granitic-granodioritic and metamorphic complexes (the Chepes granodiorite, Tuaní and Asperezas granite suites, and the Olta schist and phyllite). The paleovalley is ~40 km long and trends northeast-southwest between the towns of Olta (northeastern end) and Malanzán (southwestern end). The paleovalley ranges from 500-5500 m in width and widens to the southwest. The Río Olta drains this paleovalley to the east, but paleocurrent data from the Paganzo Group strata indicate a westerly drainage during the late Paleozoic. The paleovalley is exposed in a syncline, with the oldest (i.e. Serpukhovian-Bashkirian) material at the easternmost and westernmost ends, and the youngest (i.e. Permian) strata exposed toward the center (Fig. 7A). Therefore, the paleovalley is often divided into two segments, the Olta paleovalley (OPV) to the northeast and the Malanzán paleovalley (MPV) to the southwest. The Malanzán Formation is the basal unit of the Paganzo Group in the paleovalley

system and is the strata of interest for this study (Braccacini, 1948; Azcuy, 1975; Andreis et al., 1986; Azcuy et al., 1987; Buatois and Mángano, 1995; Sterren and Martinez, 1996; Net and Limarino, 1999; Gutiérrez and Limarino, 2001; Net et al., 2002).

3.3. Huaco locality

Strata of the Guandacol Formation are exposed on either flank of the Agua Hedionda anticline (cf. Bossi and Andreis, 1985; López-Gamundí et al., 1994; Martínez, 1993; López-Gamundí and Martínez, 2000; Pazos, 2000, 2002a, 2002b; Marensi et al., 2002; Limarino et al., 2002a; Marensi et al., 2005). Sections were measured at Cuesta de Huaco, along the eastern flank of the anticline, north and south of the Huaco River and Route 40 (Fig. 7B). Strata were measured here as this section represents one of the most complete records of late Paleozoic strata in northwestern Argentina. The Guandacol Formation overlies the Ordovician San Juan Formation, which serves as the basement for the area. Multiple studies at the Cuesta de Huaco and Los Pozuelos Creek localities have interpreted this area as a fjord setting containing advance and retreat cycles, that is succeeded by a final glacial withdrawal, and a transition to deltaic settings (López-Gamundí and Martínez, 2000; Pazos, 2000, 2002a, 2002b; Marensi et al., 2002; Limarino et al., 2002).

4. Methods

4.1. Lithofacies and Paleocurrent Analyses methods

Field work was conducted in March 2015, August 2016 and August 2017 and used standard stratigraphic and sedimentological techniques to examine and measure 24 sections of the Malanzán Formation and seven sections of the Guandacol Formation. Poorly sorted clastic

material was identified using the classification scheme developed by Hambrey and Glasser (2012). Careful attention was paid to the presence and absence of striated pavements and striated clasts, and the characteristics of diamictites and conglomerates. Facies distribution was accomplished by extensive mapping at both localities. To track changes in sediment dispersal and transport direction through time, paleoflow and paleocurrent measurements were taken at multiple levels within the Malanzán and Gundacol formations. Paleoflow and paleoslope measurements were taken as flow directions from striated pavements, flutes, grooves, tool marks, and fold noses, and paleocurrent measurements were taken as dip and dip direction on cross-laminations, cross-beds, and macroform foresets. A total of 57 measurements (12 in the Guandacol Formation at Huaco and 45 in the Malanzán Formation at OMPV) were taken (Fig. 8). At OMPV, sections were measured in both segments of the paleovalley system to obtain a full understanding of upstream and downstream (proximal and distal) depositional environments.

4.2. Detrital zircon U-Pb geochronology analyses methods

This study makes use of previously published detrital zircon data for the strata in question, with one additional sample from the upper Guandacol Formation to allow for a full comparison of provenance through time during the glacial-to-post-glacial transition (Fig. 7, 8). One sandstone sample (CDH0923-3S) for detrital zircon analysis was collected from the AH locality. The sample was prepared according to methods laid out by Gehrels (2011) and U-Pb ages were determined for all zircons at the University of Arizona LaserChron laboratory (ALC). Zircons were extracted by traditional methods of crushing and grinding, and were separated using a Wilfley table, heavy liquids, and a Frantz magnetic separator to remove high-U zircons that could yield discordant results (Sircombe and Stern, 2002; McKay et al., 2018). The sample

analyzed at ALC contained 75 zircons, which were hand-picked and mounted from a sieved 63-250 μm size-fraction. U-Pb geochronology of the zircons was conducted by laser ablation inductively coupled plasma mass spectrometry (LA-ICPMS). The sample was analyzed using a Thermo Element2 single-collector ICPMS. Data collected at the ALC were reduced using their Excel age calculation program (see Gehrels et al., 2008; Gehrels and Pecha, 2014; ALC website: <https://sites.google.com/a/laserchron.org/laserchron/>). To eliminate results of analyses with common-Pb contamination or Pb loss, criteria for rejection included the following:

1. High errors (>10% uncertainty) of $^{206}\text{Pb}/^{207}\text{Pb}$ and $^{206}\text{Pb}/^{238}\text{U}$ isotope ratios
2. High ^{204}Pb values
3. Low $^{206}\text{Pb}/^{204}\text{Pb}$ ratios
4. High discordance (>20%) or reverse discordance (>5%)

The analyses that presented these criteria were removed from interpretations and are listed with the full list of analyses in Appendix A.

Once the data were obtained, all accepted analyses were used to create Concordia diagrams using Isoplot 4.15, a Microsoft Excel add-in from Ludwig (2012). The data here are discussed in the context of previously published ages from other strata of the Paganzo Group (cf. Enkelmann et al., 2014; Craddock et al., 2019). The data are also compared to published ages of igneous and metamorphic basement lithologies to determine provenance through time in the Paganzo Basin (e.g. Huff et al., 1998; Pankhurst et al., 1998; Rapela et al., 1998; Ottone et al., 2001; Dahlquist et al., 2010; Drobe et al., 2011; Verdecchia et al., 2011, 2014, 2018; Sial et al., 2013; Einhorn et al., 2015; Rapela et al., 2018).

Three out of the four samples used here are previously published data. For the Guandacol Formation, the oldest-strata (i.e. lowermost) sample was previously reported in Craddock et al.

(2019; ARG318) from a glaciogenic diamictite above the contact with the San Juan Limestone (Figs. 7, 8). The second post-glacial Guandacol sample is newly presented here (CDH0923-3S) and is from a wavy-bedded sandstone in the uppermost Guandacol Formation. The two Malanzán Formation samples (i.e. lowermost and middle) used for reference in this contribution are previously reported (Fig. 7). The first Malanzán Formation sample is from a study conducted by Enkelmann et al. (2014; 29TR4) and comes from a sandstone at the base of the formation near section OV1 (Figure 9A) described in Moxness et al. (2018). The second Malanzán Formation sample is from a compilation published by Craddock et al. (2019) and is sampled from the middle part of the formation, in a thick succession of interbedded mudrock and sandstone beds. The samples from Craddock et al. (2019; ARG318 and ARG203) were also analyzed at ALC using the same criteria and methods. The sandstone sample used for reference for the lowermost Malanzán Formation comes from Enkelmann et al. (2014; 29TR4), and was analyzed using LA-ICP-MS (at the Museum für Mineralogie und Geologie in Germany) according to the methods described in Enkelmann et al. (2014), and the raw data can be found in the Data Repository file (GSA Data Repository Item 2014126, www.geosociety.org/pubs/ft2014.htm).

5. Lithofacies analysis

Outcrops of the Paganzo Group strata are exposed at the surface along both the western and eastern margins of the Paganzo Basin. At Olta-Malanzán, the base of the Malanzán Formation overlies basement, but is only exposed at the surface in the easternmost (i.e. towards Olta; OPV) portion of the paleovalley system (Fig. 7). The Malanzán Formation was measured at several locations throughout both the eastern and western (i.e. towards Malanzán; MPV) ends to get a full picture of the changes in depositional environments. At the base, the Malanzán

Formation is dominated by sandstones and conglomerates (depending on location in the paleovalley) that directly overlie basement material without any grooves or striations to indicate glacial activity. The middle units of the formation at both ends of the paleovalley system record either an abrupt or an overall fining upward trend, indicating a local flooding event (Fig. 8). The upper members of the Malanzán Formation record a coarsening-upward and a progradational setting as indicated by a transition from interbedded mudstone and sandstones to sandy clinofolds and conglomerates or conglomeratic sandstones (Figs. 8, 9).

At Huaco, the base of the Guandacol Formation is exposed along the core of the anticline and is accessible in several locations south of Route 49 (formerly Route 40; Fig. 7). The Guandacol Formation was measured at several locations along the eastern and western limbs of the anticline (Fig. 7). The base of the formation overlies the San Juan Formation, which is an Ordovician limestone unit that comprises the core of the anticline. There are a few exposed striated pavements directly underlying the basal beds of the Guandacol Formation along this eastern limb and that were used to determine paleoflow direction (Figs. 7, 10A). The base of the Guandacol Formation is dominated by thick- and thin-bedded and massive diamictites that tend to interfinger with each other indicating changes in proximal and more distal depositional settings. The diamictites transition into sandstones and mudstones that comprise a fining upward trend which culminates in a black shale. Above the black shale, interbedded sandstone and mudstones dominate the formation and contain evidence of soft sediment deformation and grooves. The top of the Guandacol Formation contains a coarsening-upward succession with the introduction of sandstones near the boundary with the overlying Tupe Formation.

5.1. Facies 1 – Diamictite Facies

5.1.1. Description

The diamictite facies is found at each of the sections and can be divided into two distinguishing groups: thick-bedded diamictites and thin-bedded diamictites. The clast-rich thick-bedded diamictite subfacies at OMPV overlies the sandstone facies near the contact with basement material (OV1 of Moxness et al., 2018; Fig. 9A). This diamictite is primarily a sandy diamictite, and it is massive with little to no internal structures, but in some areas inverse grading is noted and contains boulders that protrude into the overlying facies. Additionally, some wedge-shaped bodies are present, but are otherwise tabular in shape; this subfacies contains beds up to 1 meter thick. The grains and clasts are angular to subrounded clast shapes, and range in size from coarse sand, and granules to cobbles, as well as boulders. All grains and clasts are granitic or granodiorite and metamorphic (schist or phyllite) in lithology. No striated clasts were observed. The contacts are sharp with boulders and cobbles protruding into overlying sandstone, while lateral boundaries either wedge out or end in an overhanging boulder nose with graded, granule to coarse-grained sandstone beds onlapping onto the nose.

At Huaco, the clast-rich to clast-poor, matrix-supported thin-bedded diamictite overlies the basement rock, the San Juan Limestone. This subfacies consists of coarse-grained clast sizes (granules to cobbles with rare boulders) within a silt-sand matrix (Fig. 10B, C). The clasts are primarily limestone with rare granitic and metamorphic lithologies, and most displayed either facets or striations and are on occasion bullet-shaped. Sub-decimeter scale marl beds are infrequently interbedded within the stratified diamictite units. The thin-bedded units are approximately one meter thick and are cut into by a sandstone facies that vertically fines into

interbedded mudstones and sandstones. Above this is a transition into 2-3 meters of thick-bedded and more massive diamictite units that become more clast-supported than matrix-supported upward (Fig. 10D). The clast lithologies do alternate in dominance between the two subfacies (i.e. carbonate rocks dominate the diamictite facies, and granitic and metamorphic lithologies in other facies), but clast size on average seems to increase with smaller boulder and cobbles becoming more frequent upward in the section.

5.1.2. Interpretation

Diamictites are generated by numerous processes and do not always indicate the presence of glaciers (Lawson, 1979; Visser 1983; Ashley et al., 1985; Powell and Domack, 2002; Eyles and Eyles, 2010; Vesely et al., 2018; Dietrich et al., 2019). In this study we present two diamictite facies that are genetically different. To determine the exact depositional processes, and therefore the depositional environment, a list of criteria was noted for each of the two localities: diamictite characteristics (thickness, class size trends, support mechanisms, presence/absence of internal shear planes, deformational structures etc.), the shape of outsized clasts, the presence or absence of striations on clasts, the presence of grooves and striae (i.e. iceberg keel marks or striated/grooved pavements) on underlying facies or basement material, and clast lithology. Using these features as a guide, a glacial/nonglacial environment can be inferred.

At OMPV, the thick-bedded sandy diamictite is interpreted as a mass transport deposit, specifically as subaqueous debris flows (Potsma et al., 1988; Mulder and Alexander, 2001; Sohn, 2000; Talling et al., 2012; Moxness et al., 2018; Fig. 9A). The clasts within this subfacies are often subrounded to angular and are poorly sorted, and in some instances are inversely graded within the diamictite bodies, but none were striated. Furthermore, the wedge-shaped bodies have

preserved flow noses as well as boulders protruding from the tops of the deposits, indicating they are debris flows. The lack of any striated, bulleted or faceted clasts, the overwhelming dominance of local clast lithologies, as well as the complete lack of any striated pavements indicates that the debris flows are not resedimented glacial diamictites. Instead, the Olta-Malanzán paleovalley is housed within narrow, steep valley walls, which presents the ideal conditions for debris flows off the valley walls and into standing bodies of water within the central axis of the paleovalley (Van Steijn, 1996; Godt and Coe, 2007).

At Huaco, the thin-bedded diamictites are also interpreted as mass transport deposits, but in this case, these debris flows are resedimented deposits in distal glaciomarine depositional settings (Fig. 10B, C). There are numerous lines of evidence to support this interpretation. The outsized clasts in this subfacies are striated, and some are bullet-shaped and faceted. The clast lithologies were predominantly local (i.e. carbonate), and to a lesser degree granitic and metamorphic, which are considered to be exotic as these lithologies do not occur within this area of the Precordilleran terrane (Keller, 1999; Marensi et al., 2005). Furthermore, directly underlying this subfacies are numerous striated and grooved pavements on the San Juan Limestone, which serves as the basement for this locality.

5.2. Facies 2 – Conglomerate Facies

5.2.1. Description

The conglomerate facies is found only at OMPV and comprises a large portion of the lower member of the Malanzán Formation in areas where tributary paleovalleys join the main paleovalley (Fig. 9B). The base of this facies is erosional and overlies various other facies. This facies often cuts into finer-grained facies and laterally interfingers with finer-grained facies

towards and down the axis of the paleovalley. The sandy matrix in the lower part of this facies gives way to thick bedded, cobble and boulder-supported conglomerates in the upper portion. The beds themselves are on average internally massive, but some beds display normal grading while others display inverse grading (Fig. 9B). Downlapping onto other facies is abundant, and undeformed beds display inclinations, or depositional dips (Fig. 9B). Some of the packages within this facies are wedge shaped, and decrease in thickness (i.e. pinch out) towards the paleovalley axis going from several meters to 1 meter or less in thickness over a distance of tens to a hundred meters along exposures. All clast and boulder lithologies are dominated by granitic or granodiorite (i.e. Chepes granodiorite, Tuaní granite) and schist and phyllite cobbles (i.e. Olta metamorphic complex). Laterally and vertically, these conglomerates interstratify with sandstone facies and laminated mudstone facies. Internally these conglomerates cut down into underlying sediment packages, especially where they meet the valley walls. Towards the central axis of the paleovalley system, these conglomerates normally grade into finer-grained facies (i.e. sandstone facies and interbedded mudstone and sandstone facies).

5.2.2. Interpretation

The conglomerate facies in the Olta paleovalley is thoroughly described and discussed in Moxness et al. (2018). Since this facies downlaps, interfingers with, and grades laterally into finer-grained facies, and also contains boulder conglomerate clinofolds, the overall facies is interpreted as fan deltas, or where they may be subaerially exposed, alluvial fans. As such, these conglomerate bodies are the result of deposition in a high-energy environment subjected to numerous sediment gravity flows and rock falls from valley walls and tributary paleovalleys. These deposits then transition to sheet floods, non-cohesive and cohesive sediment gravity flows

(i.e. coarse-grained debris flows) that are associated with high discharge events in a multi-channel fan delta system. The conglomerate facies is also found in the Malanzán paleovalley, but to a lesser degree.

5.3. Facies 3 – Laminated Mudstone Facies

5.3.1. Description

The base of this facies at both localities is gradational with underlying interbedded mudstone and sandstone facies. At the OMPV, this facies consists of silt and clay-sized particles and is punctuated occasionally by fine to very-fine grained sandstone beds that pinch out laterally into the mudstone. At Huaco, this facies is silt and clay at the base and fines into a black shale at the top. Throughout the OMPV system, the mudstone facies contains frequent impressions of plant fossils (i.e. cordaites sp.), and in some sections contains hummocky cross-laminated, very fine-grained sandstones. At Huaco, the base of this facies drapes over the ripples that occur where this facies overlies the interbedded mudstone and sandstone facies, but is otherwise dominated by centimeter-scale laminations throughout without any other discernable internal structures. In the OPV, the mudstones are continuous, several meters thick, and rarely interrupted by granule to boulder outsized clasts of granodiorite and schist lithologies in areas proximal to the valley walls. In the MPV, this facies occurs in meter to sub-meter scale packages that are punctuated by units 3-10 cm thick of massive sandstone bodies. The upper boundary of this facies at both localities interfingers with the sandstone facies as well as the interbedded mudstone and sandstone facies above. Towards the upper part of the section measured in the MPV, this facies is also associated with centimeter-decimeter scale marl beds.

5.3.2. Interpretation

The mudstone facies at both localities represents a transition to a lower energy environment and deposition in an overall deeper water setting, below normal wave base. Both sections record flooding events. At Huaco, this has been interpreted to be a marine transgression (i.e. a late Mississippian-Early Pennsylvanian transgressive episode of Limarino et al., 2002a, 2006), and the mudstone facies at OMPV may be correlated to a regional rise in base level due to a potential marine transgression across the basin. It may also be due to the damming of the paleovalley by rock falls or by progradation of an alluvial fan across the valley. A marine interpretation of these deposits at OMPV has been supported by the presence of acritarchs within the middle member of the Malanzán Formation, and an interpretation of brackish marine conditions (Gutiérrez and Limarino, 2001). The mudstone facies at OMPV contains some outsized clasts, which are interpreted here as either a product of falling detritus from the paleovalley walls, or rafting from surface ice formation (cf. Andreis and Bossi, 1981; Powell, 1984; Thomas and Connell, 1985; Gilbert, 1990; Bennet et al., 1994; Kempema et al., 2001; Powell and Domack, 2002). Several processes can transport clasts in inundated narrow valleys such as rock fall, the seasonal formation of lake or sea ice with an accumulation of clasts from mass-wasting and other alluvial processes, or by clasts trapped in root systems of floating plants. Some sections containing these outsized clasts were located near valley walls, and were composed of local, exposed bedrock, so we interpret the transport mechanism to be either surface ice formation, or rock falls. The loss of outsized clasts through the vertical succession is interpreted here as a cessation in either/or tectonic activity, or a change in climatic conditions that did not allow for the formation of surface ice. The mudstone facies associated with the sandstone stringers are most likely the result of distal hyperpycnal flows from periodic fluvial

discharge events or from underflows potentially corresponding to storm activity where rare hummocky cross-stratification is noted within cm-scale sandstone horizons (cf. Lambert and Giovanoli, 1988; Martinsen, 1990; Bhattacharya, 2006; Crookshanks and Gilbert, 2008).

5.4. Facies 4 – Interbedded Mudstone and Sandstone

5.4.1. Description

This facies is found at both localities, with some notable differences. Additionally, the interbedded mudstone and sandstone facies most often display sheet geometries, and less often as discontinuous bodies that had erosional to sharp bases at both localities. At OMPV, this facies is often comprised of 2-5 meter-thick exposures of fine or medium-grained sandstones that grade into mudstones (i.e. high percentages of silt and clay, and at times with a very small percentage of lower very-fine grained sand size fraction; Fig. 9D, E). The centimeter to decimeter-scale medium-grained sandstone bodies are mostly internally-massive, but often also display sole marks along base of these packages and cross-laminations along the upper boundaries. At Huaco, the massive sandstone beds range in thickness from 10 to 25 cm. At both localities, the beds often contain medium-grained sand. Both in the Malanzán and Guandacol formations, some beds contain groove and prod marks as well as other soft sediment deformation at their base but internally, the beds are massive. At Huaco, these beds tend to be stacked vertically within 1-meter thick packages and may display faint laminations just above the flute and grooves at the base. However, in some cases within the Malanzán Formation, these beds can occur as isolated folded and deformed pods within a finer-grained (very fine-grained sandstone to mudstone) matrix and are associated laterally with deformed units. Additionally, the facies at Huaco displayed grain-size differences that were less pronounced, with fine sand layers interspersed

with silt-to very-fine sand interbeds. In the MPV, there are several levels of grooves, tool marks (i.e. prod marks), and flutes (Fig. 9D). Rare gutter casts were also noted. These disappear up-section. One level of intense deformation within this facies was recorded. In areas proximal to the valley walls in the OPV, infrequent outsized clasts become rare and are finally lost altogether as the facies grades upward into the laminated mudstone facies at section OV14 in Moxness et al. (2018). At OMPV the dominant clast lithology was granitic/granodiorite within this facies, followed by schist and phyllite, all of which are local bedrock lithologies. In contrast, extremely rare to no outsized clasts were recorded within this facies at Huaco. At both localities, the facies grades normally into overlying facies or is cut into by overlying facies.

5.4.2. Interpretation

The presence of the thin planar and interbedded mudstone and sandstone facies association at both localities indicates a rapid and fluctuating change in environmental and depositional energy that is interpreted as gravity-driven deposits and rhythmites, more specifically turbidites (Talling et al., 2012; Talling, 2014). The appearance of horizontally laminated and massively-bedded sandstone bodies is consistent with the definition of the TD turbidite interval as described by Talling et al. (2012). The massive sandstone facies is found in both localities and records intervals of high-density flow deposition (Talling et al., 2012; Talling, 2014). Horizontally laminated sandstones are also deposited by geostrophic currents that represent return flow of water along the sea bottom away from coastlines during storm surges. Such events result in deep water deposition from episodic underflow currents (Basilici et al., 2012). The fine-grained horizontally laminated sandstone beds were most likely deposited by turbidity currents, hyperpycnal flows, or possibly underflows, and could have been triggered by

slope failure or storm activity (López Gamundí, 1997; Gani, 2004; Winsemann et al., 2007; Talling et al., 2012; Talling, 2014). The erosional lower contacts of the sandstones are likely due to scouring caused by turbulent currents (Powell and Cowan, 1986; Boulton, 1990; Powell and Domack, 2002). The flutes and grooves found at the base of this facies represent current scour and scour by tools carried at the base of the flow in a distal deltaic environment. The deformed level at MPV displayed fold noses and axes that imparted a down-valley transport direction is interpreted as a down-slope mass transport deposit, and as there was internal deformation, it is classified as a slump (Talling et al., 2012; Talling, 2014). The association of deformed sandstones and mudstones within this facies indicates mass movements and sediment-gravity deposits from downslope movement of material off the valley walls, introduction by hyperpycnal flow off of the Gilbert Deltas, or storm-generated bottom currents down the paleovalley axis.

5.5. Facies 5 – Cross-bedded sandstone Facies

5.5.1. Description

The cross-bedded sandstone facies is found at both localities. The base of the cross-bedded sandstone facies at several sections is erosional, and cuts into multiple underlying facies, such as the interbedded mudstone and sandstone facies and the rippled sandstone facies. At OMPV this facies is noted at both ends of the paleovalley system within the middle member and also comprises most of the uppermost member of the Malanzán Formation. In the middle member of the MPV, the facies occurs in small, 0.5-meter or less medium-grained sand size lenticular bodies within other facies, such as the interbedded mudstone and sandstone facies. In the uppermost member, the facies is found in gently to steeply-dipping clinoform bodies and foresets that fine and extend across outcrops as bottomset beds (Fig. 9C). Individual foresets can

be traced into the underlying bottomsets in a down-valley direction. The facies in the OMPV is found in the middle member of the Malanzán Formation, where tributary valleys enter into the main paleovalley, and in a narrow portion of the main valley axis just before the valley increases in width. The facies is also present in the upper member of the Malanzán Formation throughout the paleovalley. At both ends of the paleovalley, the clinofolds are coarse-grained, and can range in grain size from granular and pebbly to conglomeratic. At Huaco, the facies is represented by medium-to-coarse-grained sandstone crossbeds within 0.5-meter stacked bodies with erosional upper and lower boundaries. The sandstone facies cuts down into the symmetrically rippled sandstone facies (see section 5.6. below).

5.5.2. Interpretation

The cross-bedded sandstone facies represents periods of prograding or aggrading deltaic environments at both localities. In the lower and middle members of the Malanzán Formation (i.e. at both the Olta and Malanzán ends of the paleovalley), intervals of stacked cross-bedded sandstone bodies indicate deltaic systems building out into bodies of water most likely created by damming from the conglomeratic facies (cf. Moxness et al., 2018). They might also indicate progradation into a brackish marine embayment (cf. Gutierrez and Limarino, 2001; Buatois et al., 2010). Toward the top of the Guandacol Formation at Huaco, the cross-bedded facies overlies a symmetrically rippled sandstone, which indicates the progradation of deltaic systems into the area, and indicates a transition to more continental depositional processes, as this facies is erosionally overlain by fluvial sandstones of the Tupe Formation (Limarino et al., 2002b; Marensi et al., 2005). The uppermost Malanzán Formation is preserved at both ends of the OMPV and contains this facies in 10+ meters-long sandy clinofolds that have both their topsets

and bottomsets preserved. These sandstones represent prograding Gilbert-type deltas of high-gradient stream systems that are flowing into cold, dense waters of a proximal lacustrine or marine environment within the paleovalley system producing laterally extensive hyperpycnal (underflows) flows (cf. Stanley and Surdam, 1978; Colella et al., 1987; Nemeč, 1990; Winsemann et al., 2007; Moxness et al., 2018). The preservation of extensive bottomset beds indicates that incoming waters continued away from the delta front as turbulent underflows.

5.6. Facies 6 – Rippled Sandstone

5.6.1. Description

The rippled sandstone facies can be found at both localities and can be broken down into two subfacies groups. Here we present symmetrically rippled subfacies, and asymmetrically-rippled sandstone facies. At Huaco, the two subfacies are found toward the upper portion of the formation. The base of the symmetrically rippled sandstone subfacies is erosional into the underlying asymmetrically rippled sandstone facies (Fig. 10E). On average, the ripples have a ripple index (RI) of 1 and are considered symmetrical, but in some cases are slightly asymmetrical. At OMPV, successions of symmetrically rippled sandstones are found to alternate with and gradationally overlie successions of asymmetrically-rippled sandstones. The asymmetrically rippled sandstone subfacies is present in both ends of the paleovalley and occurs in upper fine to medium-grained sand deposits. In some sections, this subfacies occurs gradationally above the massive sandstone facies, where in other locations it occurs gradationally above and below the symmetrically-rippled sandstone subfacies. In all sections, these ripples are often overlain by silt, or very-fine sand drapes.

5.6.2. Interpretation

The rippled sandstone subfacies is present at both localities and represents modification of sands by both wave and current activity. At Huaco, the symmetrical wave ripples are part of a coarsening- and shallowing-upward succession near the top of the Guandacol formation, indicating a progradation of a deltaic environment (cf. Schatz et al., 2011). At OMPV, the symmetrically-rippled sandstones suggest the reworking of a unidirectional flow deposit, or a bi-directional flow from wave activity (Baird, 1962; Reineck and Singh, 1980; Moxness et al., 2018). As indicated by Moxness et al. (2018), numerous levels of wave-rippled sandstones are found throughout the Olta paleovalley. However, the Malanzán end of the paleovalley is instead dominated by asymmetrical ripples and are the result of unidirectional flow associated with turbidity or hyperpycnal currents.

6. Paleoflow and depositional environments

The base of the Guandacol Formation at all Huaco localities contains subglacial and ice-proximal deposits and features (Marenssi et al., 2005; Limarino et al., 2014). There, the Guandacol Formation has been measured and described in multiple studies (cf. López-Gamundí and Martínez, 2000; Limarino et al., 2002, 2005; Pazos, 2002; Marenssi et al., 2005; Henry et al., 2008). Our observations of this section do not dispute previous findings, and the measured sections contain ample evidence of glacial processes, from striated pavements along the Cambrian-Ordovician San Juan Limestone, to stratified diamictites with striated and faceted clasts at the base of the section (Fig. 8). The paleoflow measurements are from a glaciated and striated pavement that exists on the upper surface of the San Juan Limestone (Fig. 8). The striations allow for interpretation of true glacial flow as there were grooves with plucking around

siliceous nodules in the San Juan Limestone (Fig. 8). The paleoflow of the glacier at Huaco was to the NW (i.e. 310-320°, with a vector mean direction of 313°; Fig. 8). The glacial deposits of the lower Guandacol Formation here are overlain by thick successions of shales, interspersed with sandstones. The shales and sandstones are interpreted as a local post-glacial transgression (i.e. a change in relative sea-level; Powell and Cooper, 2002) by multiple studies (Limarino et al., 2002, 2005, 2014). The shales are overlain by increasingly thicker packages of wavy-bedded sandstones and by planar laminated sandstones (Fig. 8). The depositional environment interpretation for the upper Guandacol Formation at Huaco is a progradational succession from offshore, to offshore-transition and then tidewater and deltaic packages at the uppermost boundary with the overlying Tupe Formation.

The Malanzán Formation is the time-equivalent unit in the easternmost part of the Paganzo Basin, which occurs in the Olta-Malanzán paleovalley (Braccacini, 1948; Azcuy, 1975; Andreis et al., 1986; Acuy et al., 1987; Buatois and Mángano, 1995; Sterren and Martínez, 1996; Net and Limarino, 1999; Net et al., 2002; Moxness et al., 2018; Pauls et al., 2019). These deposits have been reinterpreted as conglomerates, diamictites, sandstones and shales related to alluvial, fluvial, and lacustrine processes (Moxness et al., 2018; Pauls et al., 2019). The base of the section overlies basement material, Olta phyllite and schist, in an erosive manner and onlaps the Chepes granodiorite in some exposed locations (Fig. 9A; Moxness et al., 2018; Pauls et al., 2019). No striated pavement, nor striations of any kind were recorded in the paleovalley where the Malanzán Formation overlies bedrock. Unlike glacial valleys, the OMPV narrows near tributary paleovalleys from several km wide down to less than 200 m wide. These tributary paleovalleys have coarse fan faces emanating from them indicating that they are of fluvial origin (Moxness et al., 2018). Additionally, the clasts present in the diamictite and conglomerate facies

of the Malanzán Formation are not striated nor faceted, and paleocurrent measurements range from S-SW, parallel to the axis of the paleovalley throughout the Malanzán Formation (Fig. 7). While glacially-carved valleys are generally classified by their profile shape (i.e. U-shaped; MacGregor et al., 2000), the OMPV does not appear to display this geometry for the late Paleozoic sedimentary fill. The floor of the paleovalley narrows to less than 200 m across where paleotributary valleys appear to enter the main axis, which has not been recorded in glacial erosion models, nor in more recent glacially-excavated valleys (Montgomery, 2000; MacGregor et al., 2002; Anderson et al., 2006). Moxness et al. (2018) concluded that with the lack of glacial evidence and the geometry of the paleovalley at this location, the paleovalley could not have been carved by a glacier, or by glacial processes.

7. Detrital Zircon Geochronology Results

7.1. CDH0923-3S, Guandacol Formation, Huaco Locality

One sandstone sample was collected from a wavy-bedded meter-thick sandstone package from within a shoreface succession in the uppermost Guandacol Formation (Figs.7, 8). This sample contained 75 concordant zircons ranging in age from 2616.4 ± 8.9 Ma to 381.4 ± 3.3 Ma (Fig. 11). One primary age peak ranges from 480-440 Ma (Ordovician), with a component from 500-600 Ma (Cambrian-late Neoproterozoic), and a secondary peak at 1160-960 Ma (Fig. 11, 12). In this sample, 1% of the zircons analyzed were Carboniferous, 5% were Devonian, 3% were Silurian, 20% were Ordovician, 10% were Cambrian, 27% were Neoproterozoic, and 28% were Mesoproterozoic.

7.2. Previously published geochronology samples

ARG318, Lowermost Guandacol Formation, Huaco Locality (Craddock et al., 2019)

This sample was collected from a glacial diamictite at the base of the Guandacol Formation and is interpreted to be from a proglacial glaciomarine environment (Figs. 7, 8). This sample contained 36 concordant zircons that range in age from 2059 ± 7.5 to 385.2 ± 5.9 Ma. For this sample, 3% of the zircons were Devonian, 20% were Ordovician, 44% were Cambrian, 19% were Neoproterozoic, 8% were Mesoproterozoic, and 3% were Paleoproterozoic (Fig. 12).

29TR4, Lowermost Malanzán Formation, Olta-Malanzán Paleovalley (Enkelmann et al., 2014)

This sample was collected from a debris flow deposit at the base of the Malanzán Formation (Figs. 7, 8). The sample contained 93 concordant detrital zircons with ages ranging from 2203 ± 36 Ma to 333 ± 4.5 . For this sample, 3% of the analyzed zircons were Carboniferous, 12% were Devonian, 3% were Silurian, 24% were Ordovician, 29% were Cambrian, 19% were Neoproterozoic, 3% were Mesoproterozoic, and 7% were Paleoproterozoic (Fig. 12).

ARG203, Middle-Upper Malanzán Formation, Olta-Malanzán Paleovalley (Craddock et al., 2019)

This sample was collected from a sandstone within a succession of interbedded mudstones and sandstones that are interpreted to be a prograding/fluctuating delta front system (Figs. 7, 8). The sample contained 50 zircons that range in age from 937.3 ± 26.1 Ma to 362.7 ± 8.6 Ma. For this sample, 8% of the zircons were Devonian, 2% were Silurian, 54% were Ordovician, 20% were Cambrian, and 16% were Neoproterozoic (Fig. 12).

8. Discussion

The wide variety of clast lithologies, such as carbonates, granites and metamorphic rocks, in both the glacial diamictites and post-glacial deposits of the Guandacol Formation at Huaco indicate a mixture of potential source areas (cf. Marensi et al., 2005; this study). The detrital zircon age populations for the Guandacol Formation samples (ARG318, CDH0923-3S) indicate a relatively local provenance, with a primary age peak showing an Ordovician age source (470-450 Ma), and a secondary peak with Mesoproterozoic ages (1200-900 Ma). Huaco is located within the Cuyania terrane, and just to the west of the westernmost Famatinian-aged granites in the Sierra de Valle Fértil, which contain crystallization ages within the range of the primary age peak for the detrital zircons of the Guandacol Formation (cf. Pankhurst et al., 2000; Dahlquist et al., 2010). However, the glacial diamictites could also contain reworked sediments from the Ordovician and Cambrian sedimentary deposits of the Precordillera and Cuyania terranes (Huff et al., 1998; Ottone et al., 2001; Vujovich et al., 2004; Naipauer et al., 2010a; Sial et al., 2013). Together, these early Paleozoic sources of the Precordilleran and Cuyania terranes provide the appropriate age range for the majority of the detrital zircons found in the Guandacol Formation at Huaco. The clast compositions found in the basal Guandacol sediments are consistent with these interpretations.

The older, less prominent peak of Mesoproterozoic ages can only be associated with basement material of that same age along the eastern margin of the Precordilleran and Cuyania terranes where there is known Mesoproterozoic basement, such as is found within the Sierra de Pie de Palo (Vujovich et al., 2004; Dahlquist et al., 2010; Naipauer et al., 2010a; Einhorn et al., 2015). Therefore, the Guandacol Formation at Huaco is likely derived from basement material similar in age to material from the Cuyania terrane and the westernmost edge of the Famatina

magmatic belt (cf. Pankhurst et al., 2000; Vujovich et al., 2004; Dahlquist et al., 2010; Naipauer et al., 2010a; Einhorn et al., 2015), as these ranges contain material of both age sets.

Furthermore, the NW paleoflow measurements from the striated and grooved surface cut on the San Juan Limestone discussed above also support this interpretation (cf. López-Gamundí and Martínez, 2000; Henry et al., 2008; this study; Figs. 7, 8).

The upper Guandacol sample (CDH0923-3S) is from the uppermost part the formation, after the post-glacial marine transgressive shales (Figs. 7, 8). The sandstones here represent a wave-dominated deltaic environment, and there are no more striated clasts, nor oversized clasts recorded, and as such, any influence glacial ice had on the system is minimal to none. The detrital zircons, nonetheless, still indicate the same provenance signature, with a primary Ordovician peak and a secondary Mesoproterozoic peak (Fig 12). Thus, the depositional system is still localized and reworking from the same system that sourced the glacial units.

The Olta-Malanzán samples also represent deposition during both glacial/cold-climate and post-glacial phases in the western Paganzo Basin, but indirectly, as there is no evidence of glaciation occurring in this paleovalley (Moxness et al., 2018; Pauls et al., 2019). The basement material that underlies this paleovalley contains late Cambrian to Ordovician metamorphic and granitoid rocks (Pankhurst et al., 1998, 2000; Dahlquist et al., 2010). The lowermost sample is from the base of the Malanzán Formation, and based on its primary age peak, reflects the early Ordovician Sierra de Chepes basement material (477-497 Ma; Pankhurst et al., 1998; Enkelmann et al., 2014; Fig. 8). The local lithology of the clasts (i.e. granodiorite, granite, schist, and phyllite) within the conglomerate and diamictite facies further supports this interpretation. The second Malanzán Formation sample is from the middle part of the formation, in a thick succession of interbedded mudrock and sandstone beds, which is correlated with the post-glacial

transgression across the Paganzo Basin (Gutiérrez and Limarino, 2001). The detrital zircon age populations for both Malanzán samples are very similar and reflect ages found within the igneous and metamorphic provinces within the Sierra de Chepes and Los Llanos ranges (Figs. 12, 13), and therefore represent a local provenance. The detrital zircon analyses have been interpreted by both Enkelmann et al. (2014) and Craddock et al. (2019) to represent local provenance, and the results from this study agree with their interpretations (Fig. 12). Furthermore, the samples are found along the main valley axis, with much of the depositional fill sourcing from the valley walls and tributary paleovalleys within the paleovalley system (Fig. 8; Moxness et al., 2018).

Nevertheless, the fact that these two lower samples from the Guandacol and Malanzán formations have similar detrital zircon populations is not unexpected since most of the western margin of Argentine Gondwana is composed of metamorphic and igneous units of similar ages (Fig. 12, 13; Huff et al., 1998; Pankhurst et al., 1998, 2000; Ramos et al., 1998, 2010, 2015; Rapela et al., 1998; Ottone et al., 2001; Sato et al., 2001, 2006; Vujovich et al., 2004; Rapalini, 2005; Dahlquist et al., 2010; Naipauer et al., 2010a,b; Sial et al., 2013; Verdecchia et al., 2011, 2014; Einhorn et al., 2015). The main peaks for all four samples represent the sedimentary deposits following the Pampean orogeny (520-570 Ma; Pankhurst et al., 2000; Willner et al., 2008), as well as the Famatinian magmatic belt (500-440 Ma; Pankhurst et al., 2000; Enkelmann et al., 2014), and sediments derived from those igneous bodies. A similar study conducted by Einhorn et al. (2015) looked at Neoproterozoic through Permian sedimentary deposits to the north of the Paganzo Basin, in Argentina and Bolivia. Comparing the results from this study to those of Einhorn et al. (2015), it is clear that all of the strata along the Panthalassan margin of Gondwana during this timeframe contains very similar detrital zircon populations (Fig 13).

However, one stark difference between the two sample sets is the presence of early Carboniferous detrital zircons in the Malanzán Formation samples and the absence of these ages in the Guandacol Formation samples. This difference points to potentially separate depositional centers, as Devonian to Early Carboniferous intrusive post-orogenic granites are found throughout the central Famatina magmatic belt (cf. Dahlquist et al., 2010; Martina et al., 2018), which corresponds to the central portion of the Paganzo Basin. If there were an ice sheet that drained from the eastern Sierras Pampeanas, then detrital zircons of early Carboniferous ages would be expected at both localities. Detrital zircons of these ages are only present at OMPV and not at Huaco (Fig. 12), providing evidence that these two localities do not share a depositional connection.

Another major difference between the two Paganzo Basin sample sets is the lack of prominent peaks of Mesoproterozoic detrital zircons for the Malanzán Formation, where in contrast to both of the Guandacol Formation samples which contain strong detrital zircon Mesoproterozoic peaks (Fig. 12). In the Cuyania and Precordilleran terranes, many studies have found Mesoproterozoic crust underlying the Sierra de Pie de Palo, Sierra de Umango and Sierra de Maz, and is therefore interpreted to be a remnant of the Brasiliano-Pan-African belt (Vujovich et al., 2004; Dahlquist et al., 2010; Thomas et al., 2015; Rapela et al., 2018), or a part of Laurentia (Fig. 12). We interpret these ranges to be the sources for the Mesoproterozoic zircon populations in the Guandacol Formation samples, but not the Malanzán Formation samples. Instead, the Mesoproterozoic zircons within the Malanzán Formation are most likely sourced and subsequently reworked from Mesoproterozoic-aged metamorphic rocks that have been mapped and identified to the east, south and north and of the Sierra de Chepes and Los Llanos ranges, in the Sierra de San Luis and Sierras de Córdoba (Sato et al., 2001, 2006; Drobe et al., 2009, 2011;

Rapela et al., 2018). Mesoproterozoic ages are also found in older metasedimentary units, such as the Puncoviscana Formation further to the north in northern Argentina and Bolivia (Rapela et al., 2018). The paleocurrent data indicate (i.e. SW; Fig. 8) that the Sierra de San Luis and the Puncoviscana Formation would likely not have been a source for the Carboniferous strata. That is not to say that there could not be recycling of these grains from the Neoproterozoic-Cambrian metamorphic units in the Sierras de Chepes and Los Llanos, as well as to the east in the Sierras de Córdoba, which certainly could have supplied the limited number of grains that were measured in the lowermost sample.

9. Evidence for mid-Carboniferous ice extent in the Paganzo Basin

The Guandacol Formation at Huaco presents several lines of evidence for glacial presence in the western margin of the Paganzo Basin. First is the presence of the striated pavement along the uppermost surface of the San Juan Limestone, which serves as the contact with basement in this location of the Guandacol Formation (Fig. 8). The directions of the striae from that study (i.e. 300°-120°; Marensi et al., 2005) are in agreement with the NW-SE directions we recorded on the eastern limb (ranging from 310°-320°; Fig. 8), and also aligns with descriptions from López Gamundí and Martínez (2000). The inferred flow direction of glacial ice at the base of the Guandacol Formation was in a NW (mean vector of 313°; Fig. 8) direction based on the measurements taken from grooves around eroded nodules on the limestone surface (Fig. 10A). Additionally, directly above the striated contact with the San Juan Limestone, several meters of thin and thick-bedded diamictite were measured and these strata contained numerous striated and faceted clasts, some with characteristic bullet shapes. With the occurrence of each of

these lines of evidence, we can conclude that glacial ice was present in the vicinity of the Huaco locality during the Serpukhovian-Bashkirian glacial phase of the Paganzo Basin.

In contrast to the ample lines of glacial evidence in the lower Guandacol units at Huaco, as well as other localities along the western margin of the Paganzo Basin (cf. Scalabrini Ortiz, 1972; Andreis et al., 1975; López-Gamundí and Amos, 1985; Buatois and Mángano, 1994; López-Gamundí and Martínez, 2000; Kneller et al., 2004; Henry, 2007; Henry et al., 2008, 2010; Isbell et al., 2012; Aquino et al., 2014; Valdez-Buso et al., 2017, 2020; Limarino et al., 2014; Alonso-Muruaga et al., 2018), the Malanzán Formation does not display any evidence of glaciation within the basal and middle units (this study; Moxness et al., 2018; Pauls et al., 2019). There is a lack of any glacial evidence, such as faceted and/or striated clasts; there were no striae found on exposed basement lithologies, even where there was direct contact with the Malanzán Formation; and the diamictite morphology at the base of the Malanzán Formation is indicative of formation via debris flows in an alluvial fan and lacustrine environment rather than from morainal bank or pro-glacial depositional processes (cf. Andreis et al., 1986; Buatois and Mangano, 1995; Socha et al., 2014; Moxness et al., 2018). Paleocurrent measurements from the base of the Malanzán Formation indicate a more south-southwesterly direction (Fig. 8), which indicates flow within the confines of the paleovalley, and does not correspond to the paleoflow measurements in the western proto-Precordilleran domain of the Paganzo Basin.

When comparing the clast lithologies for the two localities, the sections record very different clast lithologies. For example, at Huaco, the Guandacol Formation contains clasts comprised of carbonates, high-grade metamorphic rocks, and granites. As noted in our descriptions, and also supported by Marensi et al. (2005), the diamictite facies are dominated by carbonate clast lithologies, while the interbedded sand and mudstone facies are dominated by the

high-grade metamorphic and granitic lithologies. The dominant lithology appears to correspond to changes in depositional settings, which is a reflection of the change in source materials and erosional patterns, and ultimately, provenance. In the literature, it is interpreted that the carbonate clasts of the glacial deposits represent local basement lithology within the Precordilleran terrane, such as the San Juan Limestone, and Los Azules and Talacasto formations (Huff et al., 1998; Ottone et al., 2001; Sial et al., 2013), while the other lithologies (i.e. the metamorphic and igneous clasts) in the ice-retreat facies are representative of more distal sources from the Sierras Pampeanas (cf. Marensi et al., 2005). Once ice retreated from exposures of Cambrian-Ordovician limestones, there would no longer be a carbonate source. Icebergs, however, would transport clasts that the retreating glacier was eroding and transport them to the Agua Hedionda anticline area after calving and iceberg transit. The detrital zircon geochronology results of the lower Guandacol Formation samples (ARG318; Craddock et al., 2019) further support the interpretation that the glacial deposits are likely sourced from more local basement lithologies found within, and possibly just beyond, the Cuyania terrane (Fig. 12). Cambrian ages are the dominant ages (44%), followed by Ordovician and Neoproterozoic ages (20 and 19% respectively; Fig. 12). These ages also correspond to findings from a detrital zircon geochronology study presented by Valdez Buso et al. (2020), where samples of the Guandacol Formation at other localities have similar Mesoproterozoic age populations (Figs. 12, 13). We can therefore conclude that the sources for these grains are coming from local sources within the Cuyania and Precordilleran terrane regions, and not from further to the east in the Paganzo Basin, such as the eastern Sierras Pampeanas.

On the other side of the basin, the Malanzán Formation records a similar trend of provenance based upon the clast lithologies. The clasts in the lower Malanzán Formation are

predominantly granodiorite with lesser amounts of schist and phyllite clasts. All three clast types can be traced to bedrock lithologies in the Sierras de Chepes (Pankhurst et al., 1998, 2000). The detrital zircon geochronology results further support this interpretation. The bedrock of this paleovalley system is Cambrian-Ordovician in age, and the age peaks from these samples are predominantly Cambrian and Ordovician (29% and 24% respectively in sample 29TR4; and 20%, 54% respectively in sample ARG203), followed by Neoproterozoic ages (19% in sample 29TR4, and 16% in sample ARG203). The Sierra de Chepes region is approximately 475-480 Ma, and therefore can account for the dominant ages in the samples (Pankhurst et al., 2000). The Neoproterozoic ages most likely come from the Olta schist and phyllite that is found within the Sierras de Chepes range, and could also potentially be sourced from rocks that are mapped further to the east, such as those identified in the Sierras de Córdoba (Rapela et al., 1998; Leal et al., 2003; Llambías et al 2003; Toselli et al., 2003). A few more prominent age populations occur in the Malanzán Formation samples that are not as prevalent or even present in the Guandacol Formation samples, and correspond to Silurian, and Devonian to early Carboniferous ages (Fig 8). These ages likely correspond to early-middle Paleozoic post-orogenic granites that exist within and along the Famatina belt, and into the eastern Sierras Pampeanas, interpreted to be the result of active transtensional or extensional tectonism throughout the area during the Devonian and early Carboniferous (Martina et al., 2018).

While there was synchronous deposition along both margins of the Paganzo Basin, there does not appear to have been any drainage connectivity between the two depocenters during the time of glaciation. Based on an extensive compilation of paleoflow directions from multiple studies, there appears to be a separation or pattern of flow directions (cf. Scalabrini Ortiz, 1972; Andreis et al., 1975; López-Gamundí and Amos, 1985; Buatois and Mángano, 1994; López-

Gamundí et al., 1994; López-Gamundí and Martínez, 2000; Kneller et al., 2004; Henry et al., 2008; Alonso-Muruaga et al., 2011; Aquino et al., 2014; Valdez-Buso et al., 2017, 2020; Limarino et al., 2014; Fallgatter et al., 2019; Milana and di Pasquo, 2019; Fig. 14). Along the western margin, the flow directions indicate a more radial pattern away from a central area, from which a series of uplifted blocks, or elevated nucleation points, can be inferred (Fig. 14). Additionally, several studies along the Precordilleran region describe paleovalleys with depths of 1,000- 2,500 meters and filled with glacial and glacially influenced deposits up to 450 meters thick (cf. Dykstra et al., 2006, 2007; Henry et al., 2008, 2010; Aquino et al., 2014; Valdez Buso et al., 2017, 2020; Milana and di Pasquo, 2019). This body of evidence seems to support the hypothesis that there existed a mountain belt or upland along the western margin of the Paganzo Basin, at least during the Serpukhovian-Bashkirian glaciation phase during the LPIA in Argentine Gondwana. Paleovalleys that are over 2.5 km deep, along with the radial distribution of paleoflow, indicate substantial relief in the Precordilleran region during the mid-Carboniferous. Such relief is characteristic of a substantial upland rather than the occurrence of a gentle topographic arch.

9.1. Post-glacial sedimentation

Along the western margin of the basin, the basal diamictites of the Guandacol are replaced by shales interpreted as a flooding event, which corresponds to a post-glacial transgression that is recorded at several other localities across the Paganzo Basin (Limarino et al., 2002b; Marensi et al., 2005; Net and Limarino, 2006; Limarino et al., 2014; Pauls et al., 2019). The metamorphic and granitic clast lithologies from the post-glacial facies of the Guandacol Formation are interpreted to represent a more distal provenance (cf. Marensi et al.,

2005). Similar to our interpretation for the lower Guandacol Formation sample, we interpret these clasts as sourced from a location to the east of the Precordilleran Terrane, probably from the Sierra de Pie de Palo or Sierra Valle Fértil areas (cf. Pankhurst et al., 1998, 2000; Ramos et al., 1998, 2010, 2015; Rapela et al., 1998; Vujovich et al., 2004; Rapalini, 2005; Dahlquist et al., 2010; Sial et al., 2013; Verdecchia et al., 2011, 2014; Einhorn et al., 2015). The age peaks from the detrital zircon geochronology results correspond to the Mesoproterozoic ages found within the Sierra de Pie de Palo complex, as well as the Sierra de Maz and Umango ranges (Mesoproterozoic age ranges: 1000-1200 Ma; Varela et al., 2003, 2005; Vujovich et al., 2004; Naipauer et al., 2010a, 2010b; Figs. 8, 9). The Ordovician ages correspond well with ages found in granites and gneisses from the Sierra de Valle Fértil (Cambrian-Ordovician age ranges: 500-450 Ma; Pankhurst et al., 2000). The age population range of the upper Guandacol Formation sample (CDH0923-3S) indicates a drainage shift, or unroofing of basement material in an eastward direction, as proximal depositional environments prograde westward (Limarino et al., 2002a, 2002b, 2006, 2014; Tedesco et al., 2010).

There is no record of striated pavements nor striated or faceted clasts in the Olta-Malanzán paleovalley, but that does not preclude a cold environment, with the occasional development of lake ice as there is evidence of potential ice-rafted debris. The limestones could also have been from rock fall off of valley walls into the narrow paleovalley (cf. Moxness et al., 2018), as physical weathering and rock fall is prevalent in cold climate environments. Paleocurrent measurements at the base of the Malanzán Formation point to flow through the narrow paleovalley in a south-southwest direction. The large conglomeratic deltas of the upper Malanzán Formation at the interpreted paleomouth near the town of Malanzán indicate that paleoflow is to the west, but these deltas are considered to be post-glacial deposits, and therefore

cannot be used to infer paleoflow from a glacier across the Paganzo Basin from east to west. Furthermore, the paleovalley narrows where tributary valleys connect with the main axis, and the paleoflow measurements follow the S-SW and lazy-S shape of the valley walls. This trend suggests internal and localized flow within a confined alpine valley setting rather than a paleofjord or glacially-carved valley system. While the detrital zircon sample sets contain similar age peaks, this is not wholly unexpected based on the similarities in age suites of the igneous and metamorphic basement complexes found throughout the Paganzo Basin region (Figs. 12, 13). The absence of early Carboniferous detrital zircons in the Guandacol Formation, and the presence of these ages within the Malanzán Formation, indicates that an ice center did not drain from the eastern Sierras Pampeanas and across the Paganzo Basin. The most important difference between the two formations, which provides clear evidence that these two localities do not share the same provenance, is the appearance of the Mesoproterozoic peaks in the Guandacol Formation samples, which point to a Cuyania terrane provenance. The evidence accumulated by the lithofacies and paleoflow analyses indicates that there were most likely separate depositional centers throughout the Paganzo Basin during the Visean and Serpukhovian-Bashkirian glaciations (Fig. 14). Further analyses are needed to further constrain glacial centers in the Protoprecordilleran and Sierra de Pie de Palo ranges, or if there were other glacial centers located in the Famatina arch system in the north-central region.

10. Conclusions

Detrital zircon populations and new paleoflow measurements demonstrate that there was more than one depositional center in the Paganzo Basin during the middle Carboniferous. There was one localized catchment for the Guandacol Formation at Huaco that drained westward off

the Sierra de Pie de Palo or Sierra Valle Fértil. The strata at Olta-Malanzán paleovalley are sourced from the Sierra de Chepes and Los Llanos ranges, with a minor component source region further to the east. The compiled paleoflow measurements provide clear evidence that there were discrete glaciated uplands centered on the Protoprecordilleran fold-and-thrust belt, while the eastern Sierras Pampeanas remained unglaciated.

Acknowledgements

Financial support for this study was provided by various grants from numerous agencies including the Geological Society of America, the Society for Sedimentary Geologists, the University of Wisconsin-Milwaukee Center for Latin American and Caribbean studies, the Wisconsin Geological Society, University of Wisconsin-Milwaukee (RGI grant), the University of Wisconsin-Milwaukee Department of Geosciences, the Universidad de Buenos Aires, CONICET, and grants from the USA National Science Foundation (Grants 1443557, 1559231, and 1729219).

Age (Ma)	Time Scale		Paganzo Basin		
	Period	Stage	Huaco	Paganzo	Sierra de Chepes
295	Permian	Cisuralian		La Colina/ Patquía	La Colina
300	Carboniferous	Gzhelian	Patquía	Lagares	Solca
305		Kasimovian			
310		Moscovian			
315		Bashkirian	Tupe	Loma Larga	
320			Guandacol	Malanzán	
325		Serpukhovian			
330	Mississippian	Viséan			
335					

Figure 5. Correlation chart for the late Paleozoic Paganzo Group strata for the sites in the Paganzo Basin, Argentina mentioned in the text. Ages and units are based on Limarino et al. (2002a, 2002b, 2006, 2014), Césari et al. (2011, 2019).

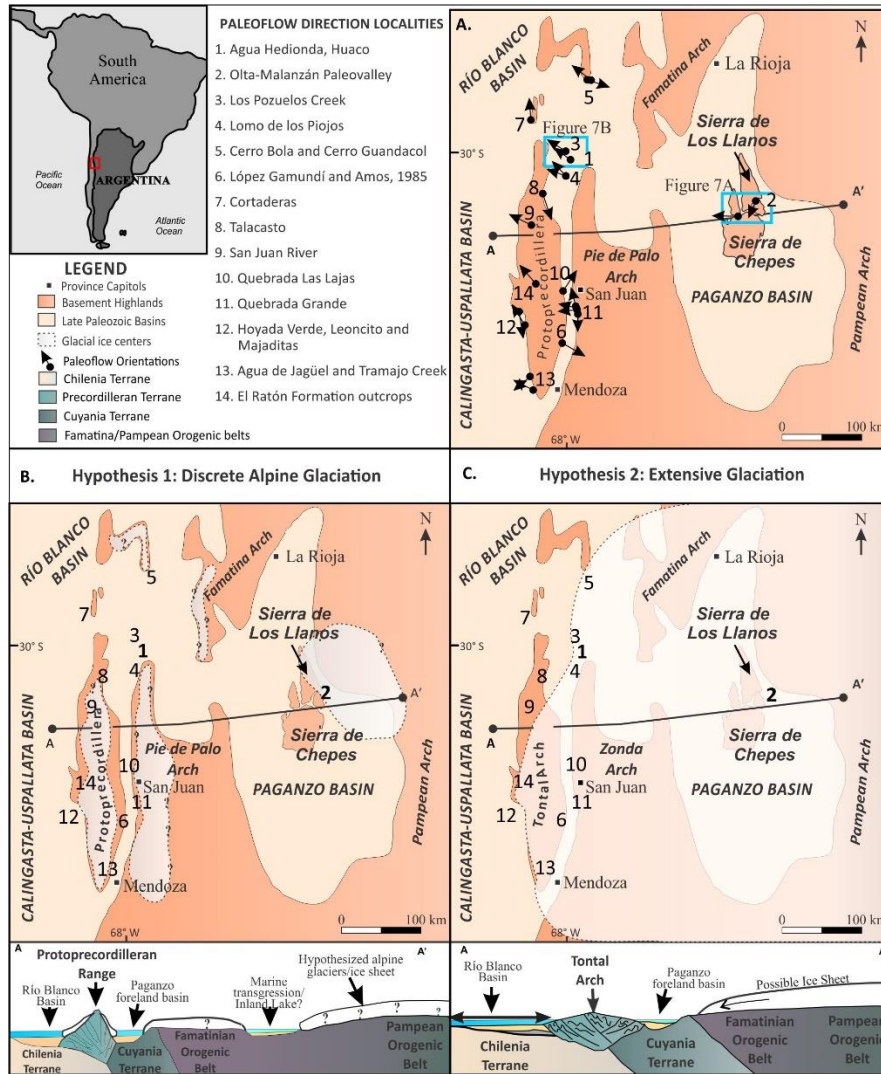


Figure 6. A. Map of the Paganzo Basin during the late Paleozoic with arrows indicating paleoflow measurements from numerous publications, modified from Henry et al. (2008). Paleoflow data are from the following list of papers: (1) Agua Hedionda, Huaco - Bossi and Andreis (1981), Marensi et al. (2002, 2005), López Gamundí and Martínez (2000), this study (2) Olta-Malanzán Paleovalley - Andreis et al. (1986), this study (3) Los Pozuelos Creek - Marensi et al. (2005) (4) Loma de Los Piojos - López Gamundí and Martínez (2000), Alonso-Muruaga et al. (2012) (5) Cerro Bola, Cerro Guandacol - Andreis et al. (1975), López Gamundí et al. (1994), Dykstra et al. (2011), Fallgatter et al. (2019); (6) López Gamundí and Amos (1985), López Gamundí et al. (1994) (7) Cortaderas - Scalabrini Ortiz (1972), López Gamundí et al. (1994), Henry et al. (2010) (8) Talacasto - Aquino et al. (2014) (9) Henry et al. (2008) (10) Dykstra et al. (2006, 2007) (11) Quebrada Grande - Kneller et al. (2004), Dykstra et al. (2006), Valdez Buso et al. (2017), Fallgatter et al. (2019) (12) Hoyada Verde, Leoncito, Majaditas - González (1981), López Gamundí (1984), López Gamundí et al. (1994), López Gamundí and Martínez (2000, 2003); this study (13) Agua de Jagüel and Tramajo Creek - López Gamundí (1984), López Gamundí et al. (1994), Henry et al. (2008, 2010); this study (14) El Ratón Formation - López Gamundí et al. (1994). B. A plan-view and a cross-sectional view of discrete alpine glacial centers found throughout the Paganzo Basin (cf. Limarino et al., 2002a, 2006, 2014; Henry et al., 2008; Isbell et al., 2012). C. Extensive glaciation from an ice sheet centered in the Eastern Sierras Pampeanas that covered, and then drained through the uplands across the Paganzo Basin (cf. Valdez Buso et al., 2017; Milana and Bercowski, 1987, 1990, 1993; Milana, 1988; Milana et al., 1987; Aquino et al., 2014). Modified after Henry et al. (2008) and Moxness et al. (2018).

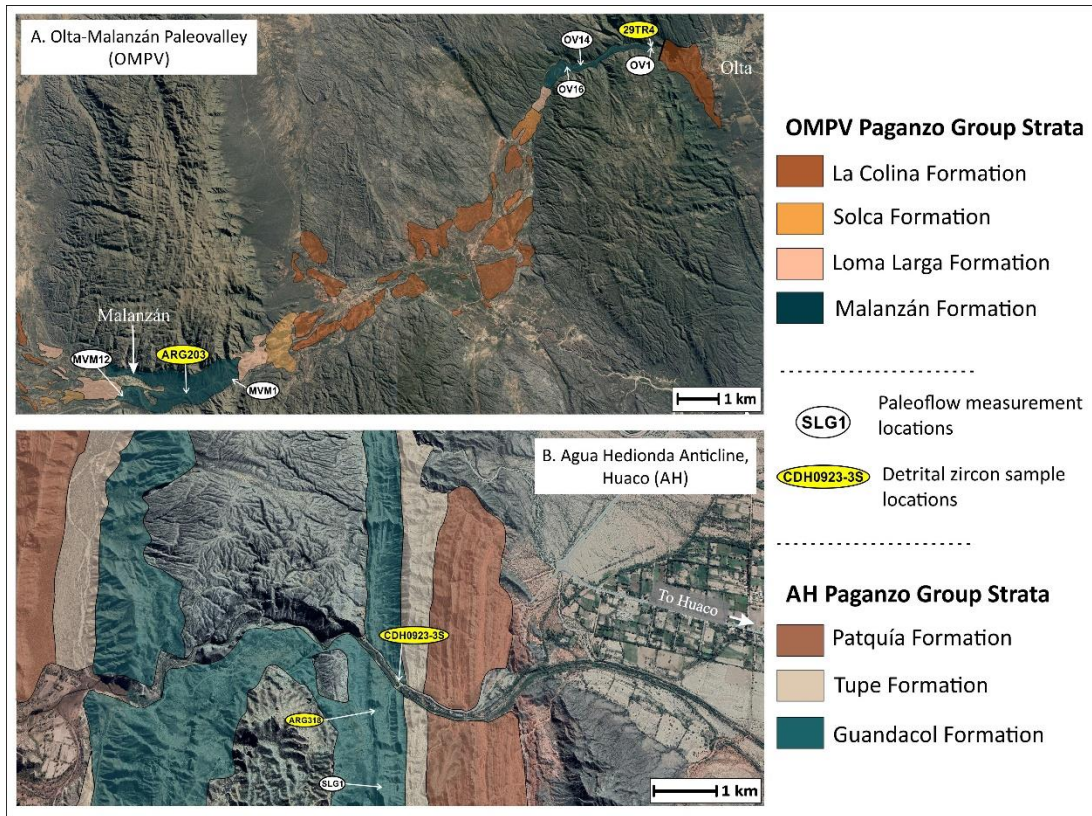


Figure 7. Google Earth aerial image with the geologic units of the Paganzo Group mapped showing the locations of the paleoflow measurements (white ellipsoids) and detrital zircon samples (yellow ellipsoids). A. The Olta-Malanzán paleovalley system (OMPV) with the Malanzán, Loma Larga, Solca, and La Colina formations (Andreis et al., 1986; Limarino et al., 2014; Moxness et al., 2018; Pauls et al., 2019). Detrital zircon simple ARG203 is from Craddock et al. (2019), and sample 29TR4 is from Enkelmann et al. (2014). B. The Agua Hedionda anticline, near the town of Huaco with the Guandacol, Tupe and Patquía formations. Mapped units are from Marensi et al., 2002. Detrital zircon sample ARG318 is from Craddock et al. (2019), and sample CDH0923-3S is from this study.

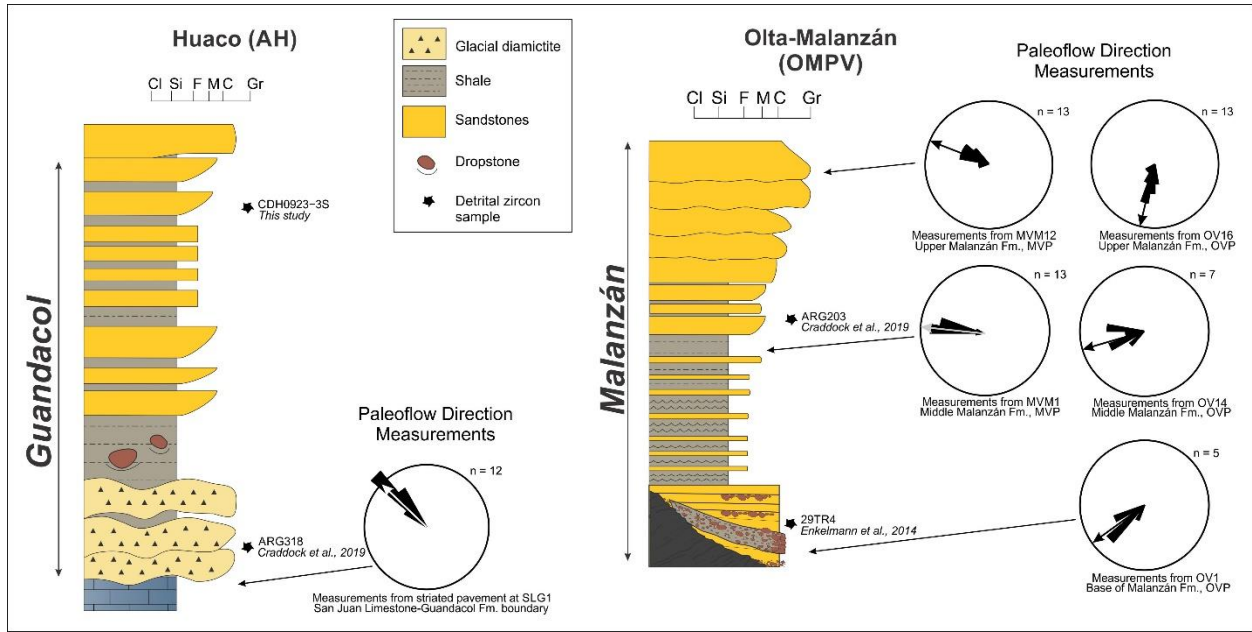


Figure 8. Simplified stratigraphic columns for the Guandacol and Malanzán formations. Detrital zircon within the sections indicated by stars. Paleoflow orientations collected from strata (at OMPV only) or striated pavements (at Huaco only) depicted using rose diagrams with number of measurements (n). The paleoflow locations reference those mapped in Figure 3.

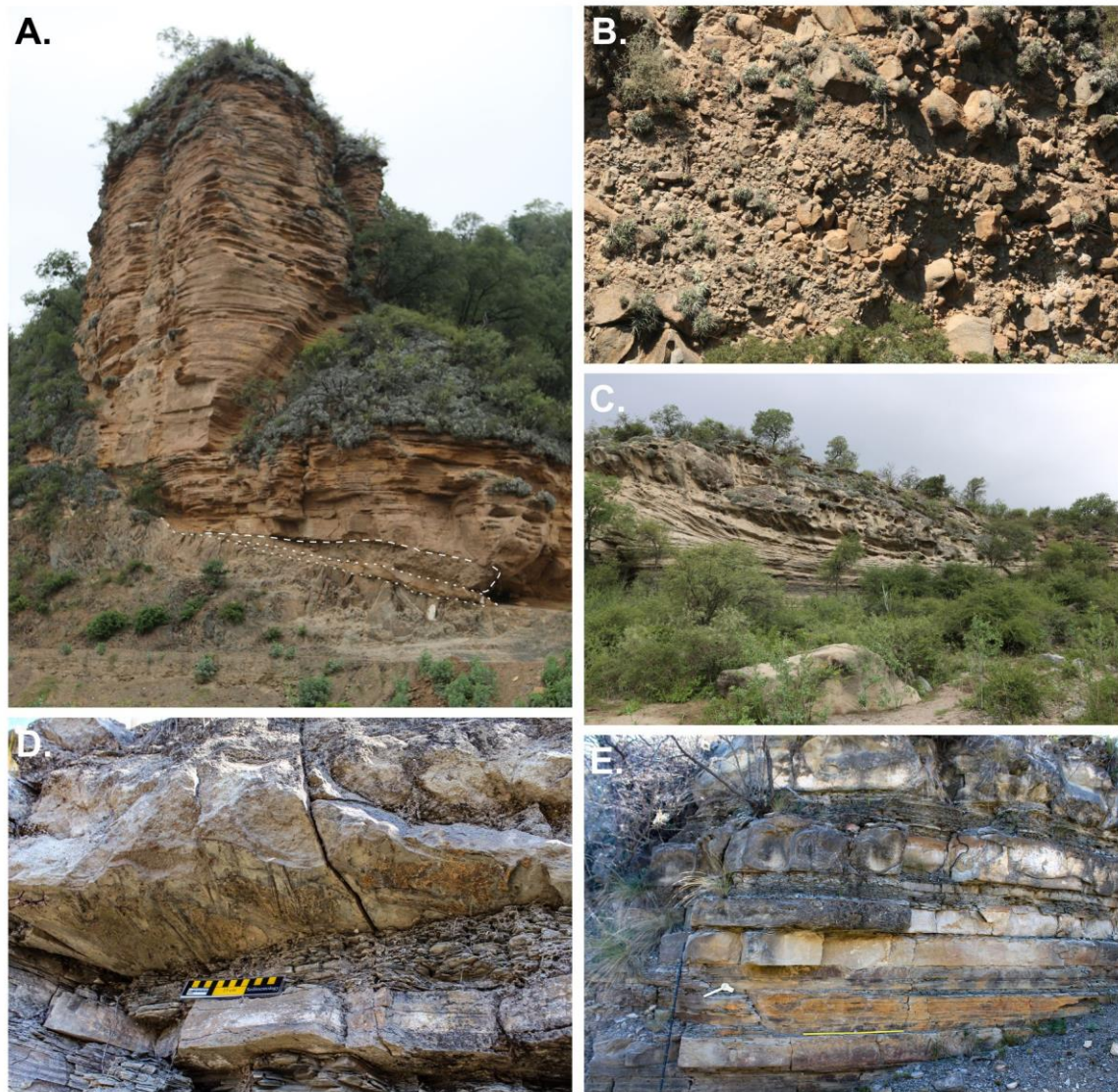


Figure 9. Exposures of the Malanzán Formation at OMPV. A. Base of Malanzán Formation at OMPV locality. The diamictite facies (debris flow within the white dashed lines) overlying sandstone facies and basement (Olta phyllite and schist). Location of sample 29TR4 from Enkelmann et al. (2014). B. Conglomerate facies from a tributary paleovalley. Note dip of clinofolds to the right. C. Gilbert delta with a S-SW paleocurrent measurement from the upper Malanzán Formation, OMPV. Note the occurrence of topset, foreset and bottomset beds. D. Tool marks from interbedded mudstone and sandstone facies in the MPV: MVM1 locality near the location of sample ARG203 from Craddock et al. (2019). E. Interbedded mudstone and sandstone facies in the MPV.

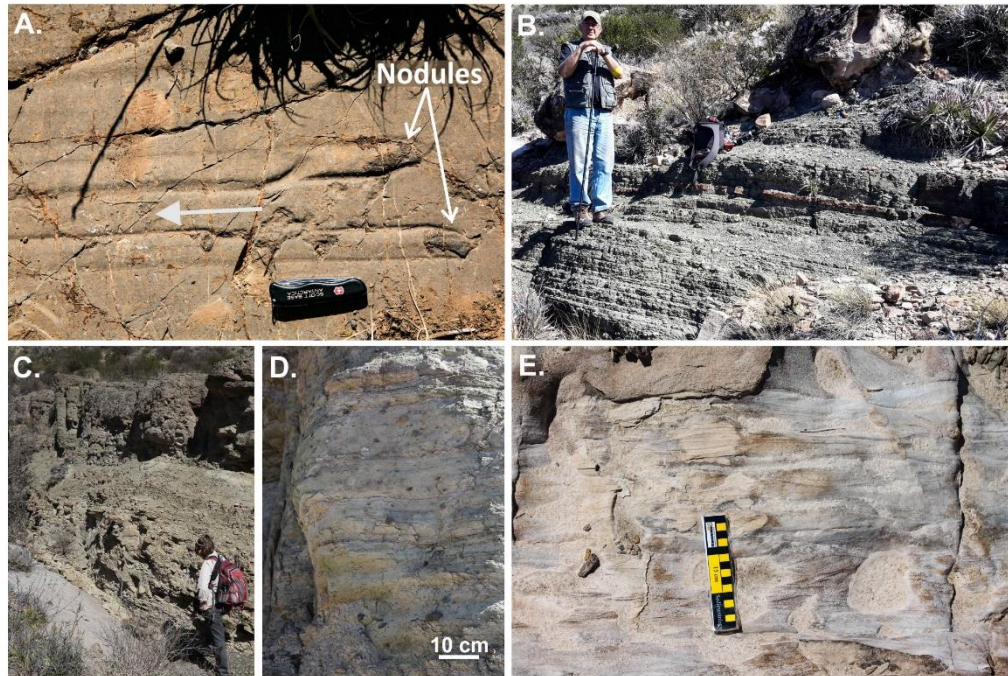


Figure 10. Exposures of the Guandacol Formation and its contact with the San Juan Limestone at Huaco. A. Glacial grooves around siliceous nodules in San Juan Limestone (AH). Arrow indicates ice flow direction. B. Thin-bedded diamictite facies 4 meters above the contact with the San Juan Limestone with a marl bed. C. Thin-bedded diamictite facies directly overlying San Juan Limestone. D. Thick-bedded diamictite facies. E. Wavy bedding within the uppermost Guandacol Formation, near the location of sample CDH0923-3S.

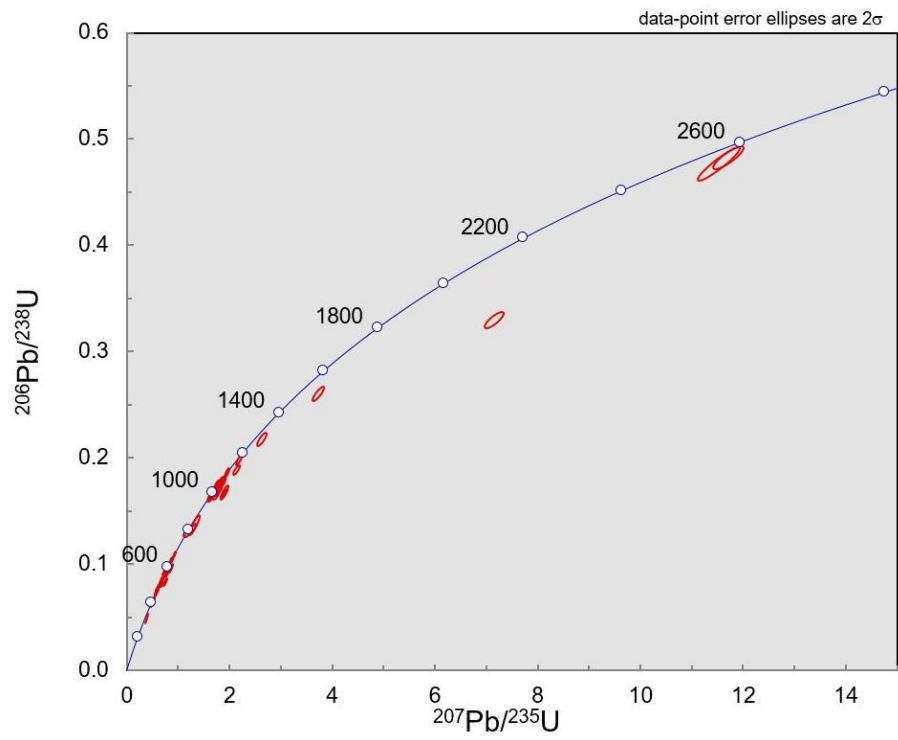


Figure 11. Concordia plot of all analyzed concordant zircon U-Pb measurements for detrital zircon sample CDH0923-3S from the Malanzán Formation, OMPV locality. See Figure 3B for exact location.

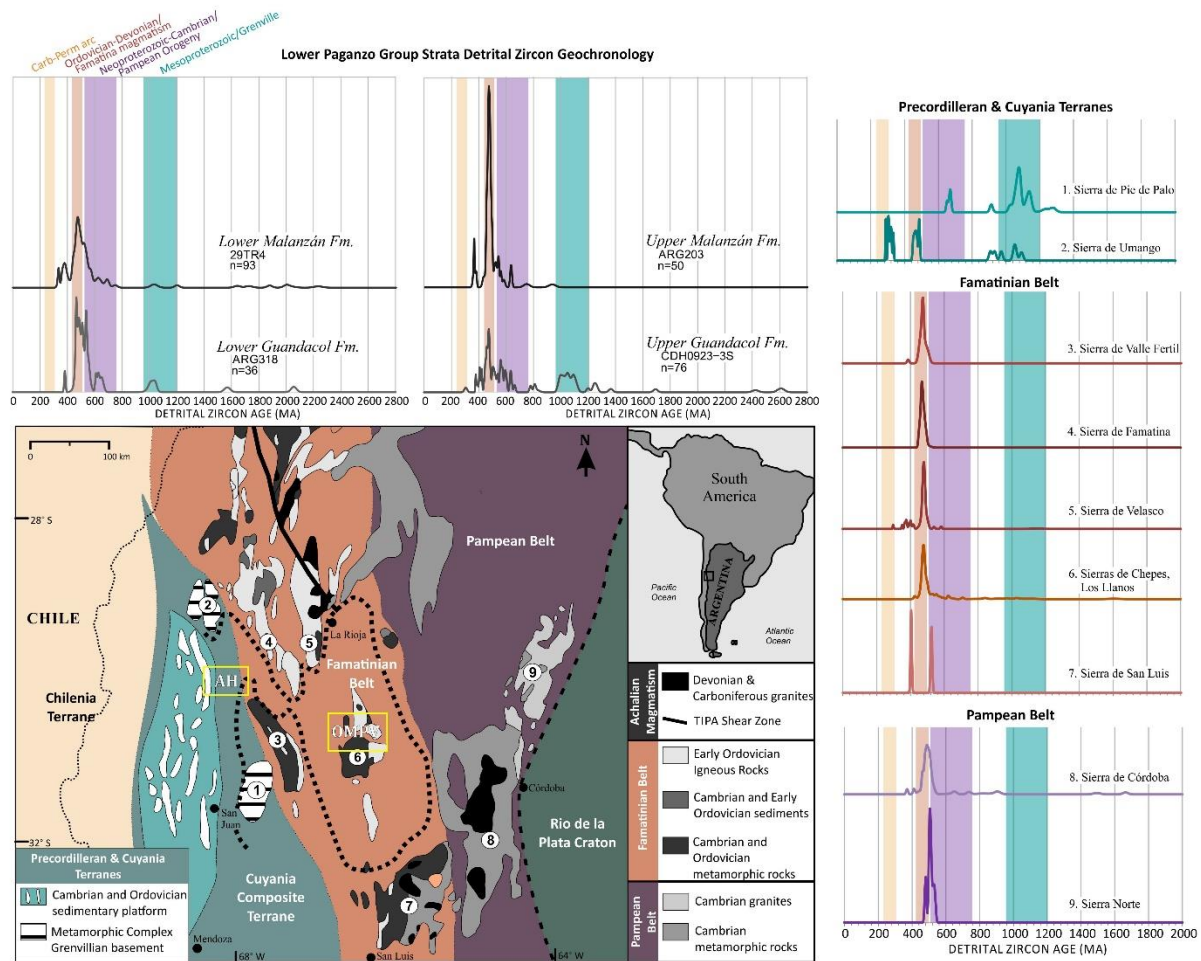


Figure 12. Mesoproterozoic-Carboniferous igneous and metamorphic provinces for the Paganzo Basin area (demarcated by the dotted line) and their available zircon geochronology (n=398). Map is modified from Dahlquist et al. (2010). The four samples considered in this study come from the two areas highlighted by the yellow boxes: AH, Lower Guandacol Fm. – ARG318 (Craddock et al., 2019), Upper Guandacol Fm. – CDH0923-3S; OMPV, Lower Malanzán Fm. – 29TR4 (Enkelmann et al., 2014), Upper Malanzán Fm. – ARG203 (Craddock et al., 2019). The cited literature for the igneous and metamorphic zircon compilation is as follows: (1) Sierra de Pie de Palo - Vujovich et al., 2004; Naipauer et al., 2010a (2) Sierra de Umango - Varela et al., 2003, 2005 (3) Sierra de Valle Fértil - Pankhurst et al., 2000 (4) Sierra de Famatina - Pankhurst et al., 2000 (5) Sierra de Velasco - Toselli et al., 2003; Pankhurst et al., 2000 (6) Sierras de Chepes, Los Llanos - Pankhurst et al., 2000 (7) Sierra de San Luis - Vujovich and Ostera, 2003; Drobe et al., 2009 (8) Sierra de Córdoba - Rapela et al., 1998, Pankhurst et al., 2000 (9) Sierra Norte - Leal et al., 20003; Llambías et al., 2003.

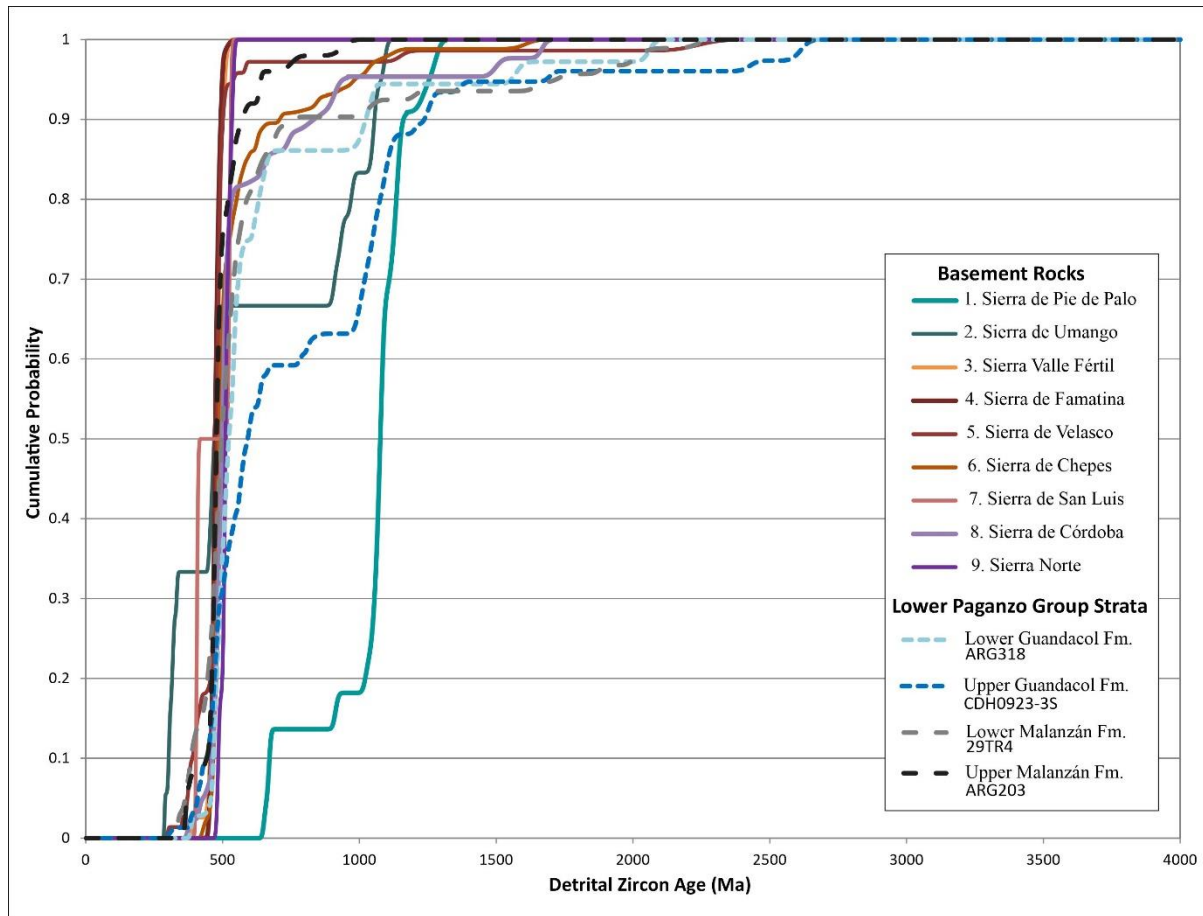


Figure 13. Cumulative probability distribution for the four Paganzo Group samples and the basement units in the region. Lower Guandacol Fm. – ARG318 (Craddock et al., 2019), Upper Guandacol Fm. – CDH0923-3S, Lower Malanzán Fm. – 29TR4 (Enkelmann et al., 2014), Upper Malanzán Fm. – ARG203 (Craddock et al., 2019). The cited literature for the igneous and metamorphic zircon compilation is as follows: (1) Sierra de Pie de Palo - Vujovich et al., 2004; Naipauer et al., 2010a (2) Sierra de Umango - Varela et al., 2003, 2005 (3) Sierra de Valle Fértil - Pankhurst et al., 2000 (4) Sierra de Famatina - Pankhurst et al., 2000 (5) Sierra de Velasco - Toselli et al., 2003; Pankhurst et al., 2000 (6) Sierras de Chepes, Los Llanos - Pankhurst et al., 2000 (7) Sierra de San Luis - Vujovich and Ostera, 2003; Drobe et al., 2009 (8) Sierra de Córdoba - Rapela et al., 1998, Pankhurst et al., 2000 (9) Sierra Norte - Leal et al., 20003; Llambías et al., 2003.

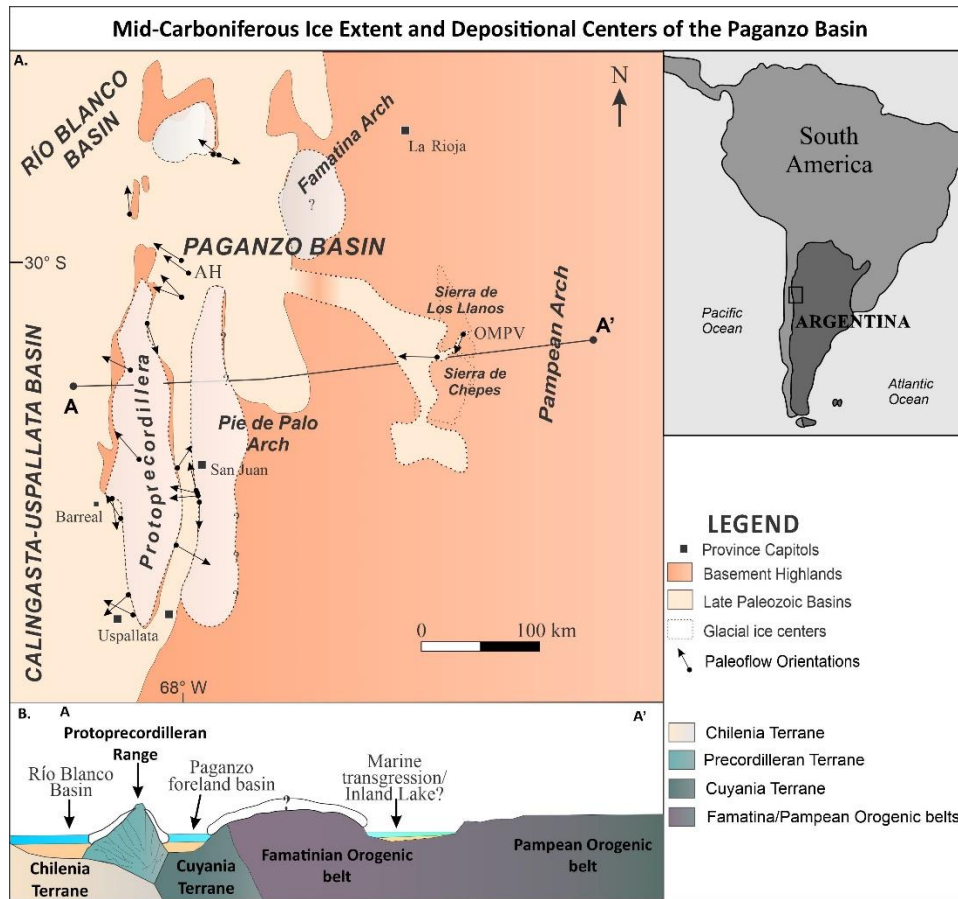


Figure 14. The revised depositional environment and glacial extent model for the mid-Carboniferous Paganzo Basin. A. Ice centers and glacial deposition restricted to the western Paganzo Basin and Calingasta-Uspallata and Río Blanco basins. Paleoflow directions are from the same dataset as in Figure 1. Basin reconstruction map modified from López Gamundí et al. (1994). Paleoflow directions modified from Henry et al. (2008) and Moxness et al., (2018). B. Cross-section of the western margin of Gondwana with ice centers highlighted. Tectonic cross-section modified from Henry et al. (2008) and Moxness et al., (2018).

References

- Alonso-Muruaga, P.J., Limarino, C.O., Spalletti, L.A., Colombo Piñol, F., 2011. Findings of intraformational striated pavements in the Late Carboniferous glacial deposits of the Andean Precordillera, Argentina. *Latin American Journal of Sedimentology and Basin Analysis* 18, pp.151–157.
- Alonso-Muruaga, P.J., Limarino, C.O., Spalletti, L.A., Piñol, F.C., 2018. Depositional settings and evolution of a fjord system during the carboniferous glaciation in Northwest Argentina. *Journal of South American Earth Sciences* 369, pp. 28-45.
- Anderson, R. S., Riihimaki, C.A., Safran, E.B., MacGregor, K.R., 2006. Facing reality: Late Cenozoic evolution of smooth peaks, glacially ornamented valleys and deep river gorges of Colorado's Front Range, in *Tectonics, Climate and Landscape Evolution*, edited by S. D. Willett et al., *Special Papers Geological Society of America* 398, 397– 418.
- Andreis, R.R., Bossi, G.E., 1981. Algunos ciclos lacustres en la Formación Malanzán (Carbónico superior) en la región de Malanzán, sierra de Los Llanos, provincia de La Rioja [artículos de libros]. Publicado en: 8o. Congreso Geológico Argentino. San Luis. Actas 4, pp. 639-655.
- Andreis, R.R., Spalletti, L.A., Mazzoni, M.M., 1975. Estudio geológico del subgrupo Sierra de Maz (Paleozoico Superior), Sierra de Maz, Provincia de La Rioja, República Argentina. *Revista de la Asociación Geológica Argentina* 30, 3, pp. 247-273.
- Andreis, R.R., Archangelsky, S., Leguizamón, R.R., 1986, El paleovalle de Malanzán: nuevos criterios para la estratigrafía del Neopaleozoico de la sierra de Los Llanos, La Rioja, República Argentina: *Boletín de la Academia Nacional de Ciencias (Córdoba)* 57, pp. 1-119.
- Aquino, C.D., Milana, J.P., Faccini, U.F., 2014. New glacial evidences at the Talacasto paleofjord (Paganzo basin, W-Argentina) and its implications for the paleogeography of the Gondwana margin. *Journal of South American Earth Sciences* 56, pp. 278-300.
- Ashley, G.M., Shaw, J., Smith, N.D., 1985. *Glacial Sedimentary Environments*. SEPM Short Course No. 16. Society of Paleontologists and Mineralogists, Tulsa, OK, pp. 246.
- Astini, R.A., Benedetto, J. L., & Vaccari, N. E. 1995. The Early Paleozoic evolution of the Argentine Precordillera as a Laurentian rifted, drifted and collided terrane: a geodynamic model. *Geological Society of America Bulletin*, 107, pp. 253-273. doi: 10.1130/0016-7606(1995)107<0253:TEPEOT>2.3.CO;2
- Astini, R.A., Martina, F., Ezpeleta, M., Dávila, F.D., Cawood, P.A., 2009. Chronology from Rifting to Foreland Basin in the Paganzo Basin (Argentina), and a Reappraisal on the "eo- and Neohercynian" Tectonics along Western Gondwana., XII Congreso Geológico Chileno, Santiago, Chile. Universidad de Chile, Santiago, Chile, pp. 1–4 Extended Abstracts S9 010.
- Astini, R., 2010. Linked basins and sedimentary products across an accretionary margin: the case for the late history of the peri-Gondwanan Terra Australis orogen through the stratigraphic record of the Paganzo Basin. In: Papa, C., Astini, R. (eds.), *Field Excursion Guidebook*, 18th International Sedimentological Congress. International Association of Sedimentologists, Mendoza, Argentina, pp. 58.

- Azcuy, C.A., 1975. Miosporas del Namuriano y Westfaliano de la comarca de Malanzán-Loma Larga, provincia de La Rioja, Argentina. II, vol. 12. Descripciones sistemáticas y significado estratigráfico de las microfloras, Ameghiniana, pp. 113–163.
- Azcuy, C.L., Carrizo, H.A., Caminos, R., 1999. Carbonífero y Pérmico de las Sierras Pampeanas, Famatina, Precordillera, Cordillera Frontal y Bloque de San Rafael. Instituto de Geología y Recursos Minerales Geología Argentina, v. 29, pp. 261-318.
- Baird, D. M., 1962, Ripple Marks: *Journal of Sedimentary Petrology* 32, 2, pp. 332-334.
- Basilici, G., Luca, P.H.V.d., and Poiré, D.G., 2012, Hummocky cross-stratification-like structures and combined-flow ripples in the Punta Negra Formation (Lower-Middle Devonian, Argentine Precordillera): A turbiditic deep-water or storm-dominated prodelta inner-shelf system?. *Sedimentary Geology* 267-268, pp. 73-92.
- Bennett, M.R., Doyle, P., Mather, A.E., Woodfin, J., 1994. Testing the climatic significance of dropstones: an example from the Miocene of the Sorbas Basin, south east Spain. *Geology* 131, pp. 845-848.
- Bhattacharya, J.P., 2006. Deltas. In: Posamentier, H., Walker, R.G. (Eds.), *Facies Models Revisited*. SEPM Special Publication 84, pp. 237–292.
- Bossi, G. and Andreis, R.R., 1985. Secuencias deltaicas y lacustres del Carbonífero del centro-oeste argentino. X International Congress on Carboniferous Stratigraphy and Geology, Madrid, pp. 285-309.
- Boulton, G.S., 1990, Sedimentary and sea level changes during glacial cycles and their control on glaciomarine facies architecture, in Dowdeswell, J.A., Scourse, J.D., eds., *Glaciomarine Environments: Processes and Sediments*, v. 53. Geological Society of London, Special Publications, pp. 15-52.
- Braccini, I.O., 1948. Los Estratos de Paganzo y sus niveles plantíferos en la sierra de los Llanos (provincia de La Rioja). *Revista de la Asociación Geológica Argentina* 1, 19-61.
- Buatois, L.A., and Mángano, M.G., 1994. Lithofacies and depositional processes from a Carboniferous lake of Gondwana, Sierra de Narvéez, northwest Argentina: *Sedimentary Geology* 93, pp. 25–49, doi: 10.1016/0037-0738(94)90027-2.
- Buatois, L.A., Mángano, M.G., 1995. Post-glacial lacustrine event sedimentation in an ancient mountain setting: Carboniferous Lake Malanzán (western Argentina). *Journal of Paleolimnology* 14, pp. 1–22.
- Buatois, L.A., Netto, R.G., Mángano, M.G., 2010. Ichnology of late Paleozoic postglacial transgressive deposits in Gondwana: Reconstructing salinity conditions in coastal ecosystems affected by strong meltwater discharge. *Geological Society of America Special Papers* 468, pp. 149-173. doi: 10.1130/2010.2468(07).
- Caputo, M.V., Crowell, J.C., 1985. Migration of glacial centers across Gondwana during Paleozoic Era. *Geological Society of America Bulletin* 96, pp. 1020-1036.
- Caputo, M. V., de Melo, J. H. G., Streel, M., Isbell, J. L., 2008. Late Devonian and Early Carboniferous glacial records of South America, in Fielding, C. R., Frank, T. D., and Isbell,

- J. L., eds., *Resolving the Late Paleozoic Ice Age in Time and Space*: Boulder, CO, Geological Society of America Special Publication., pp. 161-173.
- Casquet, C., Rapela, C.W., Pankhurst, R.J., Baldo, E.G., Galindo, C., Fanning, C.M., Dahlquist, J.A., Saavedra, J., 2012. A history of Proterozoic terranes in southern South America: from Rodinia to Gondwana. *Geoscience Frontiers* 3, pp. 137–145. doi: 10.1016/j.gsf.2011.11.004.
- Césari, S.N., Limarino, C.O., Gulbranson, E.L., 2011. An Upper Paleozoic bio-chronostratigraphic scheme for the western margin of Gondwana. *Earth Sci. Rev.* 106, p. 149-160.
- Colella, A., De Boer, P.L., Nio, S.D., 1987. Sedimentology of a marine intermontane Pleistocene Gilbert-type fan-delta complex in the Crati Basin, Calabria, southern Italy. *Sedimentology* 34, pp. 721-736.
- Craddock, J.P., Ojakangas, R.W., Malone, D.H., Konstantinou, A., Mory, A., Thomas, R.J., Craddock, S.D., Pauls, K.N., Zimmerman, U., Botha, G., Rocha-Campos, A., de Pazos, P.R., Tohver, E., Riccomini, Cl., Martin, J., Redfern, J., Horstwood, M., Gehrels, G., 2019. Provenance of Permo-Carboniferous Diamictites across Gondwana. *Earth Science Reviews*. doi: 10.1016/j.earscirev.2019.01.01.
- Crookshanks, S., Gilbert, R., 2008. Continuous, diurnally fluctuating turbidity currents in Kluane Lake, Yukon Territory. *Canadian Journal of Earth Science* 45, pp. 1123–1138.
- Dahlquist, J.A., Alasino, P.H., Nelson Eby, G., Galindo, C., Casquet, C., 2010. Fault controlled Carboniferous A-type magmatism in the proto-Andean foreland (Sierras Pampeanas, Argentina): Geochemical constraints and petrogenesis. *Lithos* 115, pp. 65-81.
- Dietrich, P., Franchi, F., Setlhabi, R.P., Bamford, M., 2019. The nonglacial diamictite of Toutswe Mogala Hill (Lower Karoo Supergroup, Central Botswana): Implications on the extent of the late Paleozoic ice age in the Kalahari-Karoo Basin. *Journal of Sedimentary Research* 89, pp. 875-889. doi: 10.2110/jsr.2019.48.
- Drobe, M., Lopez de Luchi, M.G., Steenken, A., Frei, R., Naumann, R., Siegesmund, S. & Wemmer, K. 2009. Provenance of the late Proterozoic to early Cambrian metaclastic sediments of the Sierra de San Luis (Eastern Sierras Pampeanas) and Cordillera Oriental, Argentina. *Journal of South American Earth Sciences*, 28, pp. 239–262.
- Drobe, M., López de Luchi, M., Steenken, A., Wemmer, K., Naumann, R., Frei, R., Siegesmund, S., 2011. Geodynamic evolution of the Eastern Sierras Pampeanas (Central Argentina) based on geochemical, Sm–Nd, Pb–Pb and SHRIMP data. *Int. J. Earth Sciences* 100, pp. 631-657.
- Dykstra, M., Kneller, B., Milana, J.P., 2006. Deglacial and postglacial sedimentary architecture in a deeply incised paleovalley–paleofjord — the Pennsylvanian (late Carboniferous) Jejenos Formation, San Juan, Argentina. *Geological Society of America Bulletin* 118, pp. 913–937.
- Dykstra, M., Kneller, B., Milana, J.P., 2007. A high-resolution record of deep-water processes in a confined paleofjord, quebrada de Las Lajas, Argentina. In: Nilsen, T.H., Shew, R.D., Steffens, G.S., Studlick, J.R.J. (Eds.), *Atlas of Deep-Water Outcrops: AAPG Studies in Geology* 56, CD-ROM, 19 p.

- Dykstra, M., Garyfalou, K., Kertznus, V., Kneller, B., Milana, J.P., Molinaro, M., Szuman, M., Thompson, P., 2011. Mass-transport deposits: Combining Outcrop studies and seismic forward modeling to understand lithofacies distributions, deformation and their seismic expression. In: Shipp, R.C., Weimer, P., Posamentier, H.W. (Eds.), *Mass transport Deposits in Deepwater Settings*. 96. SEPM Special Publications, pp. 293-310.
- Einhorn, J.C., Gehrels, G.E., Vernon, A., and DeCelles, P.G., 2015. U-Pb zircon geochronology of Neoproterozoic–Paleozoic sandstones and Paleozoic plutonic rocks in the Central Andes (21°S–26°S). In: DeCelles, P.G., Ducea, M.N., Carrapa, B., and Kapp, P.A., eds., *Geodynamics of a Cordilleran Orogenic System: The Central Andes of Argentina and Northern Chile*. Geological Society of America Memoir 212, p. 115–124, doi: 10.1130/2015.1212(06).
- Enkelmann, E., Ridgway, K.D., Carignano, C., Linnemann, U., 2014. A thermochronometric view into an ancient landscape: tectonic setting, and inversion of the Paleozoic eastern Paganzo basin, Argentina. *Lithosphere* 6, pp. 93–107.
- Enkelmann, E., Garver, J.I., 2015. Low-temperature thermochronology applied to ancient settings. *Journal of Geodynamics* 93, pp. 17-30.
- Eyles, C.H., Eyles, N., França, A.B., 1993. Glaciation and tectonics in an active intracratonic basin: The late Paleozoic Itararé Group, Paraná Basin, Brazil: *Sedimentology* 40, pp. 1–25, doi: 10.1111/j.1365-3091.1993.tb01087.x.
- Eyles, C.H., Eyles, N., 2010. Glacial deposits. In: James, N.P., Dalrymple, R.W. (Eds.), *Facies Models 4*. GEOtext 6. Geological Association of Canada, St. John's, Newfoundland, pp. 73–104.
- Fallgatter, C., Valdez Buso, V., Paim, P.S.G., Milana, J.P., 2019. Stratigraphy and depositional architecture of lobe complexes across a range of confinements: Examples from the late Paleozoic Paganzo Basin, Argentina. *Marine and Petroleum Geology* 110, pp. 254-274. doi: 10.1016/j.marpetgeo.2019.07.020.
- Fielding, C.R., Frank, T.D., Isbell, J.L., 2008a. The late Paleozoic ice age—A review of current understanding and synthesis of global climate patterns, in Fielding, C.R., Frank, T.D., and Isbell, J.L., eds., *Resolving the Late Paleozoic Ice Age in Time and Space*. Geological Society of America Special Paper 441, p. 343-354.
- Gani, M. R., 2004. From Turbid to Lucid: A Straightforward Approach to Sediment Gravity Flows and Their Deposits. *The Sedimentary Record* 2, 3, pp. 4-8.
- Gastaldo, R.A., DiMichele, W.A., Pfefferkorn, H.W., 1996. Out of the icehouse into the greenhouse: a late Paleozoic analogue for modern global vegetational change. *GSA Today* 10, pp. 1-7.
- Gehrels, G.E., Valencia, V., Ruiz, J., 2008, Enhanced precision, accuracy, efficiency, and spatial resolution of U-Pb ages by laser ablation–multicollector–inductively coupled plasma–mass spectrometry: *Geochemistry, Geophysics, Geosystems* 9, Q03017, doi:10.1029/2007GC001805.

- Gehrels, G., 2011. Detrital Zircon U-Pb Geochronology: Current Methods and New Opportunities, in *Recent Advances in Tectonics of Sedimentary Basins*, C. Busby and A. Azor, editors, Blackwell Publishing.
- Gehrels, G., Pecha, M., 2014. Detrital zircon U-Pb geochronology and Hf isotope geochemistry of Paleozoic and Triassic passive margin strata of western North America: *Geosphere*, v. 10, pp. 49-65.
- Gilbert, R., 1990. Rafting in glacial marine environments. In: J.A. Dowdeswell and J.D. Scourse (Editors), *Glacial Marine Environments: Processes and Sediments*. Geological Society London Special Publications 53, pp. 105-120.
- Godt, J.W., Coe, J.A., 2007. Alpine debris flows triggered by a 28 July 1999 thunderstorm in the central Front Range, Colorado. *Geomorphology* 84, pp. 80–97.
- Gonzalez Bonorino, G., 1975. Acerca de la existencia de la Protoprecordillera de Cuyo. in *actas. VI congreso geológico Argentino*. Bahía Blanca 1, pp. 101-107.
- Griffis, N.P., Mundil, R., Montañez, I.P., Isbell, J., Fedorchuk, N., Vesely, F., Iannuzzi, R., Qing-Zhu, Y., 2018. A new stratigraphic framework built on U-Pb single zircon TIMS ages with implications for the timing of the Penultimate Icehouse (Paraná Basin, Brazil): *Earth and Planetary Science Letters*.
- Gulbranson E.L., Montañez, I.P., Schmitz, M.D., Limarino, C.O., Isbell, J.L., Marensi, S.A., Crowley, J.L., 2010. High-precision U–Pb calibration of Carboniferous glaciation and climate history, Paganzo Group, NW Argentina. *Geological Society of America Bulletin* 122, pp. 1480–1498.
- Gulbranson, E.L., Montañez, I.P., Tabor, N., Limarino, C.O., 2015. Late Pennsylvanian aridification on the southwestern margin of Gondwana (Paganzo Basin, NW Argentina): A regional expression of a global climate perturbation. *Palaeogeography Palaeoclimatology Palaeoecology* 417, pp. 220-235.
- Gutiérrez, P. R., and Limarino, C. O., 2001. Palinología de la Formación Malanzán (Carbonífero Superior), La Rioja, Argentina; nuevos datos y consideraciones paleoambientales: *Ameghiniana* 38, 1, pp. 99-118.
- Hambrey, M.J., Glasser, N.F., 2012. Discriminating glacier thermal and dynamic regimes in the sedimentary record. *Sedimentary Geology* 251–252, pp. 1–33.
- Henry, L.C., 2007. Carboniferous glacial deposits of the Hoyada Verde and Tramojo Formations of the Calingasta-Uspallata Basin, west central Argentina: M.S. Thesis, University of Wisconsin-Milwaukee, 151 p.
- Henry, L.C., Isbell, J.L., Limarino, C.O., 2008. Carboniferous glacial deposits of the Protoprecordillera of west central Argentina. In: Fielding, C.R., Frank, T.D., Isbell, J.L. (Eds.), *Resolving the Late Paleozoic Ice Age in Time and Space*: Geological Society of America Special Paper, 441, pp. 131–142.

- Henry L.C., Isbell, J.L., Limarino, C.O., McHenry, L.J., Fraiser, M.L., 2010. Mid-Carboniferous deglaciation of the Protoprecordillera, Argentina, recorded in the Agua de Jagüel paleovalley. *Palaeogeography, Palaeoclimatology, Palaeoecology* 298, pp. 112–129.
- Holz, M., Souza, P. A., Iannuzzi, R., 2008. Sequence stratigraphy and biostratigraphy of the Late Carboniferous to Early Permian glacial succession (Itarare Subgroup) at the eastern-southeastern margin of the Parana Basin, Brazil. *Special Paper - Geological Society of America* 441, pp. 115-129.
- Huff, W.D., Davis, D., Bergström, S.M., Krekeler, M.P.S., Kolata, D.R., Cingolani, C.A., 1998. A biostratigraphically well-constrained K-bentonite U–Pb zircon age of the lowermost Darriwillian Stage (Middle Ordovician) from the Argentine Precordillera. *Episodes* 20, pp. 29–33.
- Isbell, J.L., Henry, L.C., Gulbranson, E.L., Limarino, C.O., Fraiser, M.L., Koch, Z.J., Ciccioli, P.L. & Dineen, A.A., 2012. Glacial paradoxes during the late Paleozoic ice age: Evaluating the equilibrium line altitude as a control on glaciation. *Gondwana Research* 22, pp. 1-19.
- Jordan, T.E., Zeitler, P., Ramos, V., Gleadow, A.J.W., 1989. Thermochronometric data on the development of the basement peneplain in the Sierras Pampeanas, Argentina: *Journal of South American Earth Sciences*, v. 2, no. 3, p. 207-222.
- Kay, S.M., Orrel, S., Abbruzzi, J.M., 1996. Zircon and whole rock Nd-Pb isotopic evidence for a Greenville age and Laurentian origin for the basement of the Precordillera terrane in Argentina. *J. Geol.*, v. 104, pp. 637-648.
- Keller, M., 1999. Argentine Precordillera: Sedimentary and plate tectonic history of a Laurentian crustal fragment in South America: *Geological Society of America Special Paper* 341, 131 p., doi: 10.1130 /0-8137-2341-8.1.
- Keller, M., Buggisch, W., Lehnert, O., 1998. The stratigraphical record of the Argentine Precordillera and its plate-tectonic background. In: Pankhurst, R. J. & Rapela, C. W. (eds) *The Proto-Andean Margin of Gondwana*. Geological Society, London, Special Publications 142, 35-56.
- Kempema, E.W., Reimnitz, E., Barnes, P.W., 2001. Anchor-ice formation and ice rafting in southwestern Lake Michigan, U.S.A. *Journal of Sedimentary Research* 71, 346–354.
- Kneller, B., Milana, J.P., Buckee, C., Al Ja'aidi, O.S., 2004. A depositional record of deglaciation in a paleofjord (Late Carboniferous [Pennsylvanian] of San Juan Province, Argentina): the role of catastrophic sedimentation. *Geological Society of America Bulletin* 116, pp. 348–367.
- Lambert, A., Giovanoli, F., 1988. Records of riverborne turbidity currents and indications of slope failures in the Rhone Delta of Lake Geneva. *Limnology and Oceanography* 33, pp. 458–468.
- Lawson D.E., 1979. Sedimentological analysis of the western terminus región of the Matanuska Glacier, Alaska. *Cold Regions Research and Engineering Laboratory Report* 79-9, pp. 112.

- Leal, P.R., Hartmann, L.A., Santos, J.O.S., Miró, R.C., Ramos, V.A., 2003. Volcanismo postorogénico en el extremo norte de las Sierras Pampeanas Orientales: Nuevos datos geocronológicos y sus implicancias tectónicas. *Revista Asociación Geológica Argentina* 58, pp. 593–607.
- Limarino, C., and Gutiérrez, P., 1990. Diamictites in the Agua Colorada Formation (northwestern Argentina); new evidence of Carboniferous glaciation in South America: *Journal of South American Earth Sciences* 3, 1, pp. 9-20.
- Limarino, C.O., Marensi, S.A., Tripaldi, A., Caselli, A.T., 2002a. Evolution of the Upper Paleozoic basins of western Argentina during the maximum extent of Gondwana. 16th International Sedimentological Congress, Abstracts, 224-225.
- Limarino, C.O., Césari, S.N., Net, L.I., Marensi, S.A., Gutiérrez, P.R., Tripaldi, A., 2002b. The Upper Carboniferous postglacial transgression in the Paganzo and Río Blanco Basins (northwestern Argentina): facies and stratigraphic significance. *Journal of South American Earth Sciences* 15, pp. 445–460.
- Limarino, C.O., Spalletti, L.A., 2006. Paleogeography of the Upper Paleozoic basins of southern South America: an overview. *Journal of South American Earth Sciences* 22, pp. 134–155.
- Limarino, C.O., Tripaldi, A., Marensi, S., Fauqué, L., 2006. Tectonic, sea level, and climatic controls on late Paleozoic sedimentation in the western basins of Argentina. *Journal of South American Earth Sciences* 33, pp. 205–226.
- Limarino, C.O., Césari, S.N., Spalletti, L.A., Taboada, A.C., Isbell, J.L., Geuna, S., Gulbranson, E.L., 2014. A paleoclimatic review of southern South America during the late Paleozoic: A record from icehouse to extreme greenhouse conditions: *Gondwana Research*, 25, pp. 1396-1421.
- Llambías, E.J., Gregori, D., Basei, M.A., Varela, R., Prozzi, C., 2003. Ignimbritas riolíticas neoproterozoicas en la Sierra Norte de Córdoba: ¿evidencia de un arco magmático temprano en el ciclo Pampeano?. *Revista Asociación Geológica Argentina* 58, 4, pp. 572-582.
- López-Gamundí, O. R., 1987. Depositional models for the glaciomarine sequences of Andean late Paleozoic basins of Argentina: *Sedimentary Geology* 52, pp. 109–126.
- López-Gamundí, O.R., Espejo, I.S., Conaghan, P.J., Powell, C.McA., Veevers, J.J., 1994. Southern South America. In: Veevers, J.J., Powell, C.McA. (Eds.), *Permian–Triassic Pangean basins and foldbelts along the Panthalassan margin of Gondwanaland*. Boulder, Colorado: Geological Society of America Memoir 184, pp. 281–329.
- López Gamundí, O.R., 1997. Glacial–postglacial transition in the late Paleozoic basins of southern South America. In: Martini, I.P. (Ed.), *Late Glacial and Postglacial Environmental Changes: Quaternary, Carboniferous–Permian, and Proterozoic*. Oxford University Press, Oxford, UK, pp. 147–168.
- López-Gamundí, O.R., and Amos, A.J., 1985, Consideraciones paleoambientales de las secuencias carbónicas del sector Precordillerano de la Cuenca Calingasta-Uspallata, San

- Juan y Mendoza: Primeras Jornadas sobre Geología de la Precordillera, Serie "A" Monografías y Reuniones, Asociación Geológica Argentina, Actas, no. 2, pp. 289–294.
- López-Gamundí, O.R., Martínez, M., 2000. Evidence of glacial abrasion in the Calingasta–Uspallata and western Paganzo Basins, mid-Carboniferous of western Argentina. *Palaeogeography, Palaeoclimatology, Palaeoecology* 159, pp. 145–165.
- Ludwig, K.R., 2012. *Isoplot 3.75, A Geochronological Toolkit for Excel*: Berkeley Geochronology Center Special Publication 5, 75.
- MacGregor, K. R., Anderson, R.S., Anderson, S. P., Waddington, E.D., 2000. Numerical simulations of glacial-valley longitudinal profile evolution, *Geology* 28, pp. 1031– 1034.
- Marensi, S.A., Limarino, C.O., Césai, S.N., Tripaldi, A., Caselli, A.T., 2002. Glacial and postglacial sedimentation in western Paganzo Basin, Northwest Argentina. 16th International Sedimentological Congress, Abstracts, Johannesburg, pp. 236-237.
- Marensi, S.A., Tripaldi, A., Limarino, C.O., Caselli, A.T., 2005. Facies and architecture of a Carboniferous grounding-line system from the Guandacol Formation, Paganzo Basin, northwestern Argentina. *Gondwana Res.* 8, 187–202.
- Martina, F., Canelo, H.N., Dávila, F.M., Hollanda, M.H.B.M, Teixeira, W., 2018. Mississippian lamprhyre dikes in western Sierras Pampeanas, Argentina: Evidence of transtensional tectonics along the SW margin of Gondwana. *Journal of South American Earth Sciences* 83, pp. 68-80.
- Martinsen, O.J., 1990. Fluvial, inertia-dominated deltaic deposition in the Namurian (Carboniferous) of northern England. *Sedimentology* 37, pp. 1099–1113.
- Martínez, M., 1993. Hallazgo de fauna marina en la Formación Guandacol (Carbonífero) en la localidad de Agua Hedionda, San Juan, Precordillera Nororiental, Argentina. *Compte Rendus XII Congrès International de la Stratigraphie et Géologie du Carbonifère et Permien* 2, pp. 291–296.
- McKay, M.P., Weislogel, A.L., Jackson, W.T., Jr., Dean, J., Fildani, A., 2018. Structural and magmatic controls on the turbidites of the Karoo Basin, South Africa. In: Ingersoll, R.V., Graham, S.A., Lawton, T.F. (eds), *Tectonics, Sedimentary Basins, and Provenance: A Celebration of William R. Dickinson's Career*: Geological Society of America Special Paper 540, pp. 689-705.
- Milana, J.P., 1988. Sedimentación estuarina carbonífera tardía en la Precordillera central, San Juan, Argentina. 2 Reunión Argent. Sedimentol. (Buenos Aires). Actas 185-188.
- Milana, J.P., Berscowski, F., 1987. Rasgos erosivos y depositacionales glaciales en el neopaleozoico de la precordillera central, San Juan, Argentina. 4a Reun. Internac. Work.roup PICG-211 (IUGS-UNESCO), St. Cruz Sierra, Bolivia, Abstracts, pp. 46-48.
- Milana, J.P., Berscowski, F., 1990. Facies y geometría de depósitos glaciales en un paleovalle Carbonífero de Precordillera Central, San Juan, Argentina, 3 Reunión Argentina de Sedimentología (San Juan). Actas, pp. 199-204.

- Milana, J.P., Bercowski, F., 1993. Late Palaeozoic Glaciation in Paganzo Basin, Western Argentina: Sedimentological Evidence. *Comptes Rendus XII ICC-P, Bs. As.*, v.1, pp. 325-335.
- Milana, J.P., Bercowski, F., Lech, R.R., 1987. Análisis de una secuencia marinocontinental Neopaleozoica en la región del Río San Juan, Precordillera Central, San Juan. In: 10th Cong. Geológ. Argent., Tucumán, Argentina, Actas III, pp. 113–116.
- Milana, J.P., di Pasquo, M.M., 2019. New chronostratigraphy for a Lower to Upper Carboniferous strike-slip basin of W-Precordillera (Argentina): its paleogeographic, tectonic and glacial importance. *Journal of South American Earth Sciences* 96. <https://doi.org/10.1016/j.jsames.2019.102383>.
- Montañez, I.P., Tabor, N.J., Niemeier, D., DiMichele, W.A., Frank, T.D., Fielding, C.R., Isbell, J.L., Birgenheir, L.P., Rygel, M.C., 2007. CO₂-forced climate and vegetative instability during late Paleozoic deglaciation. *Science* 315, pp. 87–91.
- Montañez, I.P., Poulsen, C.J., 2013, The late Paleozoic ice age: An evolving paradigm. *Annual Review of Earth and Planetary Sciences*, 41, pp. 24.1-24.
- Montanez, I.P., McElwain, J.C., Poulsen, C.J., White, J.D., DiMichele, W.A., Wilson, J.P., Griggs, G., Hren, M.T., 2016. Climate, pCO₂ and terrestrial carbon cycle linkages during late Palaeozoic glacial-interglacial cycles. *Nature Geosciences*, 9, 11, pp. 824-828.
- Montgomery, D.R., 2000. Valley formation by fluvial and glacial erosion. *Geology* 30, 11, pp. 1047-1050.
- Mottin, T.E., Vesely, F.F., Rodrigues, M.C.N.L., Kipper, F., Souza, P.A., 2018. The paths and timing of late Paleozoic ice revisited: New stratigraphic and paleo-ice flow interpretations from a glacial succession in the upper Itararé Group (Paraná Basin, Brazil). *Palaeogeography, Palaeoclimatology, Palaeoecology* 490, pp 488-504. doi: 10.1016/j.palaeo.2017.11.031
- Moxness, L.D., Isbell, J.L., Pauls, K.N., Limarino, C.O., Schencman, J., 2018. Sedimentology of the mid-Carboniferous fill of the Olta paleovalley, eastern Paganzo Basin, Argentina: Implications for glaciation and controls on diachronous deglaciation in western Gondwana during the late Paleozoic Ice Age. *Journal of South American Earth Sciences* 84, pp. 127-148. doi/10.1016/j.jsames.2018.03.015.
- Mulder, T., Alexander, J., 2001. The physical character of subaqueous sedimentary density flows and their deposits. *Sedimentology* 48, pp. 269–299.
- Naipauer, M., Vujovich, G.I., Cingolani, C.A., McClelland, W.C., 2010a. Detrital zircon analysis from the Neoproterozoic-Cambrian sedimentary cover (Cuyania terrane), Sierra de Pie de Palo, Argentina: evidence of a rift and passive margin system? *Journal of South American Earth Sciences* 29, pp. 306-326.
- Naipauer, M., Cingolani, C.A., Vujovich, G.I., Chemale Jr., F., 2010b. Geochemistry of Neoproterozoic-Cambrian metasedimentary rocks of the Caucete Group, Sierra de Pie de Palo, Argentina: Implications for their provenance. *Journal of South American Earth Sciences* 30, pp. 84-96. doi:10.1016/j.jsames.2010.03.002.

- Nemec, W., 1990. Aspects of sediment movement on steep delta slopes. In: Colella, A., Pior, D.B. (Eds.), *Coarse-grained Deltas*. IAS. Special Publication 10, pp. 29–73.
- Net, L.I., 1999. Petrografía, diagénesis y procedencia de areniscas de la sección inferior del Grupo Paganzo (carbonífero) en la cuenca homónima. PhD Thesis, Universidad de Buenos Aires, pp.49.
- Net, L.I., Limarino, C.O., 1999. Paleogeografía y correlación estratigráfica del Paleozoico Tardío de la Sierra de Los Llanos, provincia de La Rioja, Argentina: *Revista de la Asociación Geológica Argentina* 54 (3), pp. 229–239.
- Net, L.I., Alonso, M.S., Limarino, C.O., 2002. Source rock and environmental control on clay mineral associations, lower section of Paganzo group (Carboniferous), northwest Argentina. *Sedimentary Geology* 152, pp. 183–199.
- Net, L.I., Limarino, C.O., 2006. Applying sandstone petrofacies to unravel the Upper Carboniferous evolution of the Paganzo Basin, northwest Argentina. *Journal of South American Earth Sciences* 22, 239–254.
- Ottone, E.G., Holfeltz, G.D., Albanesi, G.L., Ortega, G., 2001. Chitinozoans from the Ordovician Los Azules Formation, Central Precordillera, Argentina. *Micropaleontology* 47, pp. 97-110.
- Pankhurst, R.J., Rapela, C.W., Saavedra, J., Baldo, E., Dahlquist, J., Pascua, I., Fanning, C.M., 1998. The Famatinian magmatic arc in the Central Sierras Pampeanas: An early to mid-Ordovician continental arc on the Gondwana margin. In: Pankhurst, R.J., Rapela, C.W. (Eds.), *The Proto-Andean Margin of Gondwana*. Geological Society of London Special Publication 142, pp. 343-367.
- Pankhurst, R.J., Rapela, C.W., Fanning, C.M., 2000. Age and origin of coeval TTG, I- and S-type granites in the Famatinian belt of NW Argentina. *Earth and Environmental Science Transactions of the Royal Society of Edinburgh* 91, pp. 151-168.
- Pauls, K.N., Isbell, J.L., McHenry, L., Limarino, C.O., Moxness, L.D., Schencman, L.J., 2019. A paleoclimatic reconstruction of the Carboniferous-Permian paleovalley fill in the Eastern Paganzo Basin: Insights into glacial extent and deglaciation of southwestern Gondwana. *Journal of South American Earth Sciences* 95. doi:10.1016/j.jsames.2019.102236.
- Pazos, P.J. (2000) Análisis litofacial y trazas fósiles de las Formaciones Guandacol y Tupe, en el ámbito occidental de la Cuenca Paganzo. Unpub. PhD Thesis, Univ. Buenos Aires, Buenos Aires, Argentina, 467p.
- Pazos, P.J., 2002a. The Late Carboniferous glacial to postglacial transition: facies and sequence stratigraphy, western Paganzo Basin, Argentina. *Gondwana Research* 5, pp. 467–487.
- Pazos, P.J., 2002b. Palaeoenvironmental framework of the glacial-postglacial transition (Late Paleozoic) in the Paganzo-Calingasta Basin (southern South America) and the Great Karoo-Kalahari Basin (southern Africa): ichnological implications. *Gondwana Research* 5, pp. 619-640.
- Postma, G., Nemec, W., Kleinspehn, K.L., 1988. Large floating clasts in turbidites: a mechanism for their emplacement. *Sedimentary Geology* 58, pp. 47-61.

- Powell, R.D., 1984. Glacimarine processes and inductive lithofacies modeling of ice shelf and tidewater glacier sediments based on Quaternary examples. *Marine Geology* 57, pp. 1-52.
- Powell, R.D., and Cowan, E.A., 1986. Depositional processes at McBride Inlet and Riggs glacier. In: Anderson, P.G., Goldthwait, R.P., McKenzie, G.D. (Eds.), *Observed processes of glacial deposition in Glacier Bay, Alaska*: Ohio State University, Institute of Polar Studies, Miscellaneous Publications, 256, pp. 140–156.
- Powell, R.D., Cooper, J.M., 2002. A glacial sequence stratigraphic model for temperate, glaciated continental shelves. In: Dowdeswell, J.A., Ó Cofaigh, C. (Eds.), *Glacier-influenced Sedimentation on High-latitude Continental Margins*: Geological Society of London Special Publication 203, pp. 215-244.
- Powell, R.D., Domack, E.W., 2002. Modern glacimarine environments. In: Menzies, J. (Ed.), *Modern and Past Glacial Environments*. Butterworth-Heinemann Ltd., Oxford, pp. 361–389.
- Rabassa, J., Carignano, C., Cioccale, M., 2014. A general overview of Gondwana landscapes in Argentina. In: Rabassa, J., Ollier, C. (Eds.), *Gondwana Landscapes in Southern South America: Argentina, Uruguay and southern Brazil*. Springer Earth System Science, Dordrecht, Heidelberg, New York, London, pp. 201-245.
- Ramos, V., Jordan, T., Allmendinger, R., Kay, S., Cortés, J., Palma, M., 1984. Chilenia: un terreno alóctono en la evolución paleozoica de los Andes Centrales. In: 10° Congr. Geol., vol. 2. Actas, Argentino, pp. 84–106.
- Ramos, V.A., 1988. Tectonics of the Late Proterozoic–Early Paleozoic: a collisional history of Southern South America. *Episodes* 11, pp. 168–174.
- Ramos, V.A., Dallmeyer, D. y Vujovich, G., 1998. Time constraints on the Early Paleozoic docking of the Precordillera, Central Argentina. In: Pankhurst, R. y Rapela, C. (Eds.): *The Proto-Andean Margin of Gondwana*, Geological Society, London, Special Publication, 142, pp. 143-158.
- Ramos, V.A., 1999. Evolución tectónica de la Argentina. In: *Rasgos Estructurales del Territorio Argentino*. Instituto de Geología y Recursos Minerales, Geología Argentina Anales 29 (24), pp. 715-784.
- Ramos, V.A., 2000. The southern central Andes. In: Cordani, U.G., Milani, E.J., Thomaz Filho, A., Campos, D.A. (Eds.), *International Geological Congress Rio de Janeiro. Tectonic evolution of South America* 31, pp. 561–604.
- Ramos, V.A., 2008. The basement of the Central Andes: the Arequipa and related terranes. *Annual Review Earth and Planetary Sciences* 36, pp. 289–324.
- Ramos, V.A., 2009. The Grenville-Age Basement of the Andes. *Journal of South American Earth Sciences*. doi:10.1016/j.jsames.2009.09.004.
- Ramos, V.A., Vujovich, G., Martino, R. & Otamendi, J. 2010. Pampia: a large cratonic block missing in the Rodinia supercontinent. *Journal of Geodynamics*, 50, pp. 243–255.

- Ramos, V.A., Escayola, M., Leal, P., Pimentel, M.M., Santos, J.O.S., 2015. The late stages of the Pampean Orogeny, C_ordoba (Argentina): Evidence of postcollisional Early Cambrian slab break-off magmatism. *Journal of South American Earth Sciences* 64, pp. 351-364. doi: 10.1016/j.jsames.2015.08.002.
- Rapalini, A.E., 2005. The accretionary history of southern South America from the latest Proterozoic to the late Paleozoic: Some paleomagnetic constraints, in Vaughan, A.P.M., Leat, P.T., and Pankhurst, R.J. (Eds.) *Terrane Processes at the Margins of Gondwana: Geological Society London Special Publication 246*, pp. 305–328.
- Rapela, C.W., Pankhurst, R.J., Casquet, C., Baldo, E., Saavedra, J., Galindo, C., Fanning, C.M., 1998. The Pampean orogeny of the southern proto-Andes: evidence for Cambrian continental collision in the Sierras de Córdoba. In: Pankhurst, R.J., Rapela, C.W. (Eds.), *The Proto-Andean Margin of Gondwana*. Geological Society of London, pp. 181–217.
- Rapela, C.W., Pankhurst, R.J., Baldo, E., Casquet, C., Galindo, C., Fanning, C.M., Saavedra, J., 2001. Ordovician metamorphism in the Sierras Pampeanas: New U-Pb SHRIMP ages in Central-East Valle Fértil and the Velasco Batholith. III Simposio Sudamericano de Geología Isotópica (III SSAGI). Publicación en CD-ROM.
- Rapela, C.W., Pankhurst, R.J., Casquet, C., Fanning, C.M., Baldo, E.G., González-Casado, J.M., Galindo, C., Dahlquist, J., 2007. The Río de la Plata craton and the assembly of SW Gondwana. *Earth-Science Reviews* 83, pp. 49–82.
- Rapela, C.W., Pankhurst, R.J., Casquet, C., Dahlquist, J.A., Fanning, M., Baldo, E.G., Galindo, C., Alasino, P.H., Ramacciotti, C.D., Verdecchia, S.O., Murra, J.A., Basei, M.A.S., 2018. A review of the Famatinian Ordovician magmatism in southern South America: evidence of lithosphere reworking and continental subduction in the early proto-Andean margin of Gondwana. *Earth-Science Reviews* 187, pp. 259-285.
- Reineck, H. E., and Singh, I. B., 1980. *Depositional sedimentary environments*, Berlin, Springer-Verlag, 551 p.
- Rocha Campos, A.C., dos Santos, P.R., Canuto, J.R., 2008. Late Paleozoic glacial deposits of Brazil; Parana Basin. In: Fielding, C.R., Frank, T.D., Isbell, J.L. (Eds.), *Resolving the Late Paleozoic Ice Age in Time and Space: Geological Society of America Special Paper*, 441, pp. 97–114.
- Sato, A.M., González, P.D., Sato K., 2001. First indication of Mesoproterozoic age from the western basement of the Sierra de San Luis, Argentina, 3rd South American Symposium on Isotope Geology, Extended Abstracts (CD edition), Soc. Geol. Chile, Santiago, pp. 64–67.
- Sato, A.M., González, P.D., Basei, M.A.S., Llambías, E.J., 2006. U-Pb ages of Komatiitic Rocks from Sierra de San Luis, Argentina, 5th SSAGI, Short Papers, pp. 169–173.
- Scalabrini Ortiz, J., 1972. El Carbónico en el sector septentrional de la Precordillera Sanjuanina: *Revista Asociación Geológica Argentina* 27, pp. 351–377.

- Schatz, E.R., Mángano, M.G., Buatois, L.A., Limarino, C.O., 2011. Life in the late Paleozoic ice age: Trace fossils from glacially influenced deposits in a late Carboniferous fjord of western Argentina. *Journal of Paleontology* 85, 3, pp. 502-518.
- Sial, A.N., Peralta, S., Gaucher, C., Toselli, A.J., Ferreira, V.P., Frei, R., Parada, M.A., Pimentel, M.M., Pereira, N.S., 2013. High-resolution stable isotope stratigraphy of the upper Cambrian and Ordovician in the Argentine Precordillera: Carbon isotope excursions and correlations. *Gondwana Research* 24, pp. 330-348.
- Sircombe, K.N., Stern, R.A., 2002. An investigation of artificial biasing in detrital zircon U-Pb geochronology due to magnetic separation in sample preparation. *Geochimica et Cosmochimica Acta*, 66 (13), pp. 2379-2397.
- Socha, B.J., Carignano, C., Rabassa, J., Mickelson, D.M., 2014. Gondwana glacial paleolandscape, diamictite record of Carboniferous valley glaciation, and preglacial remnants of an ancient weathering front in northwestern Argentina. In: Rabassa, J., Ollier, C. (Eds.), *Gondwana landscapes in southern South America*. Springer, Dordrecht, pp. 331–363.
- Sohn, Y.K., 2000. Depositional processes of submarine debris flows in the Miocene fan deltas, Pohang Basin, SE Korea with special reference to flow transformation. *Journal of Sedimentary Research* 70, pp. 491–503.
- Sterren, A.F., Martínez, M., 1996. El paleovalle de Olta (Carbonífero): paleoambientes y paleogeografía. 13° Congreso Geológico Argentino y 3° Congreso Exploración de Hidrocarburos (Buenos Aires), Actas 2, pp. 89-103.
- Stanley, K.O., Surdam, R.C., 1978. Sedimentation on the front of Eocene Gilbert-type deltas, Washakie Basin, Wyoming. *Journal of Sedimentary Petrology* 48: 557-573.
- Stuart-Smith, P.G., Camacho, A., Sims, J.P., Skirrow, R.G., Pieters, P.E., Black, L.P., Miró, R., 1999. U–Pb, Th–Pb and Ar–Ar geochronology from the southern, 1999. Uranium–Lead dating of felsic magmatic cycles in the southern Sierras Pampeanas, Argentina: implications for the tectonic development of the proto-Andean Gondwana margin. *Laurentia Gondwana connections before Pangea*: In: Ramos, V.A., Keppe, I.D. (Eds.), *Geological Society of America, Special Paper*, vol. 336, pp. 87–114.
- Talling, P.J., 2014. On the triggers, resulting flow types and frequencies of subaqueous sediment density flows in different settings. *Marine Geology* 352, pp. 155–182.
- Talling, P.J., Masson, D.G., Sumner, E.J., Malgesini, G., 2012. Subaqueous sediment density flows: Depositional processes and deposit types, *Sedimentology* 59, pp. 1937–2003.
- Tedesco, A., Cicciooli, P., Suriano, J., Limarino, C., 2010. Changes in the architecture of fluvial deposits in the Paganzo Basin (Upper Paleozoic of San Juan Province): an example of sea level and climatic controls on the development of coastal fluvial environments. *Geologica Acta*.
- Thomas, G.S.P., Connell, R.J., 1985. Iceberg drop, dump, and grounding structures from Pleistocene glacio-lacustrine sediments, Scotland. *Journal of Sedimentary Petrology* 55, 2, pp. 243-249.

- Thomas, W.A., Astini, R.A., Mueller, P.A., McClelland, W.C., 2015. Detrital-zircon geochronology and provenance of the Ocoyic synorogenic clastic wedge, and Ordovician accretion of the Argentine Precordillera terrane. *Geosphere* 11, 6, pp. 1749-1769. doi: 10.1130/GES01212.1.
- Toselli, A.J., Basei, M.A., Rossi de Toselli, J.N., Rudas, R., 2003. Análisis geoquímico-geocronológico de rocas granulíticas y calcosilicáticas de las Sierras Pampeanas Noroccidentales. *Revista de la Asociación Geológica Argentina*, 58, 4, pp. 629-642.
- Valdez Buso, V., Pasquo, M.D., Milana, J.P., Kneller, B., Fallgatter, C., Chemale, F.J., Paim, P.S.G., 2017. Integrated U-Pb zircon and palynological/palaeofloristic age determinations of a Bashkirian palaeofjord fill, Quebrada Grande (Western Argentina). *Journal of South American Earth Sciences* 73, pp. 202–222.
- Valdez Buso, V., Milana, J.P., di Pasquo, M., Paim, P.S.G., Philipp, R.P., Aquino, C.A., Cagliari, J., Junior, F.C., Kneller, B., 2020. Timing of the Late Paleozoic glaciation in western Gondwana: New ages and correlations from Paganzo and Paraná basins. *Palaeogeography, Palaeoclimatology, Palaeoecology* 544. doi:10.1016/j.palaeo.2020.109624.
- Van Steijn, H., 1996. Debris-flow magnitude—frequency relationships for mountainous regions of Central and Northwest Europe. *Geomorphology* 15, pp. 259–273.
- Varela, R., Basei, M.A.S., Sato, A.M., González, P.D., Siga Jr, O., Campos Neto, M.C., Cingloani, C.A., 2003. Grenvillian basement and Famatinian events of the Sierra de Umango (29°S): A review and new geochronological data. IV South American Symposium on Isotope Geology- Short Papers, pp. 304-306.
- Verdecchia, S. O., Casquet, C., Baldo, E. G., Pankhurst, R. J., Rapela, C. W., Fanning, M., Galindo, C., 2011. Mid- to Late Cambrian docking of the Rio de la Plata Craton to southwestern Gondwana; age constraints from U-Pb SHRIMP detrital zircon ages from Sierras de Ambato and Velasco (Sierras Pampeanas, Argentina). *Journal of the Geological Society of London* 168, pp. 1061-1071.
- Verdecchia, S.O., Murra, J.A., Baldo, E.G., Casquet, C., Pascua, I., Saavedra, J., 2014. Geoquímica de las rocas metasedimentarias del Cámbrico medio al Ordovícico temprano de la Sierra de Los Llanos (Sierras Pampeanas, Argentina): Fuente de sedimentos, correlación y ambiente geotectónico. *Andean Geology* 41, 2, pp. 380-400. doi: 10.5027/andgeoV41n2-a06.
- Vesely, F.F., Rodrigues, M.C.N.L., da Rosa, E.L.M., Amato, J.A., Trzaskos, B., Isbell, J.L., Fedorchuk, N.D., 2018. Recurrent emplacement of non-glacial diamictite during the late Paleozoic ice age. *Geology* 46, 7, pp. 615-618.
- Visser, J.N.J., 1983. The problems of recognizing ancient sub- aqueous debris flow deposits in glacial sequences: *Transactions of the Geological Society of South Africa* 86, pp. 127-135.

- Vujovich, G.I., Osters, H.A., 2003. Evidencias del ciclo Pampeano en el basamento del sector noroccidental de la sierra de San Luis. *Revista de la Asociación Geológica Argentina* 58, 4, pp. 541-548.
- Vujovich, G.I., Van Staal, C.R. & Davis, W., 2004. Age constraints and the tectonic evolution and provenance of the Pie de Palo Complex, Cuyania composite terrane, and the Famatinian orogeny in the Sierra de Pie de Palo, San Juan, Argentina. *Gondwana Research* 7, pp. 1041–1056.
- Willner, A.P., Gerdes, A., Massonne, H.-J., 2008. History of crustal growth and recycling at the Pacific convergent margin of South America at latitudes 29° -36° S revealed by a U-Pb and Lu-Hf isotope study of detrital zircon from late Paleozoic accretionary systems. *Chemical Geology* 253, pp. 114-129. doi:10.1016/j.chemgeo.2008.04.016
- Winsemann, J., Aspöck, U., Meyer, T., Schramm, C., 2007. Facies characteristics of Middle Pleistocene (Saalian) ice-margin subaqueous fan and delta deposits, glacial Lake Leine, NW Germany. *Sedimentary Geology* 193, pp. 105–129.

Chapter 3: A paleoclimatic reconstruction of the Carboniferous-Permian paleovalley fill in the Eastern Paganzo Basin: Insights into glacial extent and deglaciation of southwestern Gondwana

Kathryn N. Pauls¹, John L. Isbell¹, Lindsay McHenry¹, C. Oscar Limarino², Levi D. Moxness^{1*},

L. Jazmin Schencman²

1: Department of Geosciences, University of Wisconsin-Milwaukee, 3209 N. Maryland Ave., Milwaukee, WI 53211, U.S.A.

2: Departamento de Ciencias Geológicas, Universidad de Buenos Aires-IGEBBA (UBA-CONICET), Facultad de Ciencias Exactas y Naturales, Ciudad Universitaria Pab. 2, 1° piso, CABA.

* Current Address: North Dakota Geological Survey, 600 East Boulevard, Dept. 405, Bismarck, ND 58505-0840

Corresponding Author: Kathryn N. Pauls, Department of Geosciences, University of Wisconsin-Milwaukee, 3209 N. Maryland Ave., Milwaukee, WI 53211, U.S.A.

kpauls@uwm.edu

Authors' email addresses: John Isbell - jisbell@uwm.edu

[Lindsay McHenry – lmchenry@uwm.edu](mailto:lmchenry@uwm.edu)

[Carlos O Limarino – limar@gl.fcen.uba.ar](mailto:limar@gl.fcen.uba.ar)

[Levi D. Moxness – ldmoxness@gmail.com](mailto:ldmoxness@gmail.com)

[L. Jazmin Schencman – jazminsch@gmail.com](mailto:jazminsch@gmail.com)

Abstract

During the mid-Carboniferous, ice centers located in present-day western Argentina disappeared until the late Cenozoic with glaciation of the Andes. The disappearance of mid-Carboniferous glaciers and the subsequent climate shift, recorded in the Paganzo Basin, has been attributed to global events and drivers, such as increased atmospheric CO₂ concentrations and the shifting position of Gondwana across the South Pole. However, glaciers continued at the same paleolatitude in eastern South America and did not disappear from Gondwana until the Late Permian. This study investigates links to local drivers that acted in combination with other global drivers to explain the early deglaciation along the western margin of Gondwana. To do this, several outcrops within the eastern portion of the Paganzo Basin in western Argentina were sampled for the Chemical Index of Alteration (CIA) geochemical analyses. Here, we test the applicability of the CIA as a paleoclimate proxy on strata in the Olta-Malanzán paleovalley that historically was thought to have been glaciated. A recent study by the authors has shown that the paleovalley was not glaciated, but owes its origin to extension and excavation by fluvial processes. However, the late Paleozoic stratigraphy of this paleovalley system is similar to the rest of the Paganzo Basin. The results from the paleovalley samples show that this area was intermittently humid and arid through time, but with an overall arid profile. This signature is predominantly due to the nature of the paleovalley, which was subjected to rapid burial from frequent rock falls, progradation alluvial fans/fan deltas, and lacustrine sediment gravity flows (Malanzán Fm.), which prevented any significant chemical weathering. While the overall Pennsylvanian climatic signature appears to be relatively arid (Malanzán, Loma Larga, and Solca Fms.), it seems that the climate during the deposition of the late Pennsylvanian and Permian La Colina Formation was more humid than previously thought.

Keywords

late Paleozoic ice age; Carboniferous; Permian; Paleoclimate; Paleovalley; Gondwana
Glaciation; Argentina

1. Introduction

The climatic shift from icehouse to greenhouse of the late Paleozoic is of great interest to scientists due to its potential analogue to current global climate change (cf. Gastaldo et al., 1996). The late Paleozoic ice age (LPIA) was the longest-lived ice age (approximately 360-255 million years ago) of the Phanerozoic (cf. Gastaldo et al., 1996). The LPIA is the only example of when a vegetated and biologically complex Earth shifted from an icehouse to a greenhouse state (Gastaldo et al., 1996; Montañez et al., 2007; Fielding et al., 2008a; Isbell et al., 2012; Montañez and Poulsen, 2013; Limarino et al., 2014). Because of this, the LPIA will aid in developing an understanding of the drivers influencing changing climatic regimes, which in turn will provide insight on how such drivers affect modern climate change.

One of the longstanding questions of the late Paleozoic centers around how different regions (i.e. low paleolatitude versus high paleolatitude) of Earth responded to a global shift in climate. Thus, regional studies at high chronostratigraphic resolution will add to our understanding of environmental responses to changing global climate. Much of the research concerning the LPIA focuses on determining the timing and extent of the glaciations in Gondwana. Traditional LPIA hypotheses and models centered around the idea that there was one large ice sheet that covered Gondwana, and that it persisted for the 100 Ma duration of the LPIA (i.e. from the late Devonian to the late Permian; Frakes, 1979; Veevers and Powell, 1987; Frakes and Francis, 1988; Frakes et al., 1992; Ziegler et al., 1997; Hyde et al., 1999; Scotese, 1997;

Blakey, 2008). As more studies were conducted over time, more and more regional evidence has shown that the LPIA glaciation was more dynamic and complex than previously understood (Crowell and Frakes, 1970; López-Gamundí, 1997; Visser, 1997; Isbell et al., 2003, 2008, 2012; Fielding et al., 2008a, 2008b; Heckel, 2008; Rygel et al., 2008; Gulbranson et al., 2010; Taboada, 2010; Montanez and Paulson, 2013; Griffis et al., 2018). The glacial intervals occurred on much smaller scales (i.e. approximately one to several million years in length) and in different regions across Gondwana, beginning in South America and northern Africa during the late Devonian (the Frasnian or Famennian), and then spreading across the rest of Gondwana during the Carboniferous and into the Permian (Caputo and Crowell, 1985; Veevers and Powell, 1987; Eyles et al., 1993; López-Gamundí, 1997; Isbell et al., 2003, 2012; Caputo et al., 2008; Pérez Loinaze et al., 2010; Fielding et al. 2008c; Limarino et al., 2014; Frank et al., 2015; Metcalfe et al., 2015). Additionally, there have been studies highlighting potential driving mechanisms (i.e. the drift of Gondwana across the paleo South Pole, changes in the configurations of the continental plates, changes in atmospheric CO₂, changes in insolation due to orbital parameters, and orogenic events) for these changing climatic conditions (c.f. Caputo and Crowell, 1985; Scotese and Barrett, 1990; Eyles et al., 1993; Heckel, 1994, 2008; Isbell et al., 2003, 2008; 2012; Royer et al., 2004; Montañez et al., 2007; Rygel et al., 2008; Horton and Poulsen, 2009; Tabor and Poulsen, 2008; Gulbranson et al., 2010; Montañez and Poulsen, 2013; Limarino et al., 2014). An emerging perspective of the LPIA is forming from these studies, providing new insight into the glaciation-climate relationship and the forcing and feedback mechanisms that drive such global change. However, there is still much to be gained by understanding the climate-drivers on a regional scale. This paper aims to develop a high-resolution record of paleoclimate using the Chemical Index of Alteration (CIA) in a complex basin of southwestern Gondwana. The

Paganzo Basin presents a unique problem in that glacial ice develops at the onset of the Visean stage and then disappears in the Early Pennsylvanian while other parts of Gondwana at similar paleo-latitudes, such as the southern Paraná Basin in Brazil, persisted (López-Gamundí et al., 1994; López-Gamundí, 1997; Holz et al., 2008; Caputo et al., 2008; Henry et al., 2008; Rocha-Campos et al., 2008; Limarino et al., 2014; Griffis et al., 2018; Fig. 15).

2. Paganzo Basin

It is generally accepted that the Paganzo Basin of western Argentina developed as a broken foreland basin as the tectonic activity along the western (i.e. Panthalassan) margin of Gondwana evolved due to flatbed (progressively shallowing) subduction (Limarino et al., 2002, 2014; Ramos and Folguera, 2009; Astini, 2010; Fig. 15). Transpressional mechanisms for basin subsidence have also been proposed (Ramos and Folguera, 2009; Martina et al., 2018). From the Cambrian through the early Carboniferous, there were various terranes that accreted to western Gondwana (Pankhurst et al., 1998; Ramos et al., 1998; Ramos, 1999; Ramos et al., 2015). The ancestral Sierras Pampeanas belt that bounds the Paganzo Basin to east was formed during the Cambrian, as the Pampia terrane docked to the Rio de La Plata craton (Rapela et al., 1998; Ramos et al., 2015). The Famatina system developed in the Ordovician, created by the thrusting and uplift associated with the accretion of the Cuyania arc terrane (Pankhurst et al., 2000; Ramos, 1999). The uplift of the Protoprecordillera range is associated with the western margin shifting westward as the Chilenia terrane docked (Ramos et al., 1998; Ramos, 1999).

Although much is known about the timing of the orogenic events, there are still differing interpretations of the development and nature of glaciation within the Paganzo Basin. According to Astini et al. (2009), the paleotopography of the interior of the basin is thought to have been

pleneplained due to an overriding ice sheet that existed around 320 Ma. As the uplift of the Protoprecordillera mountain belt occurred due to the accretion of Chilenia to South America, this ice sheet is thought to have diminished in size, leaving behind alpine glaciers carving out U-shaped valleys in both the eastern and western margins of the basin (Sterren and Martínez, 1996; Carignano et al., 1999; Astini et al., 2009; Astini, 2010). These pleneplained surfaces, though, have been shown to have been created later, and are much younger features than the late Paleozoic, more likely to be Jurassic to Cenozoic in age (Carignano et al., 1999; Rabassa, 2014; Rabassa et al., 2014). Additionally, while there is abundant evidence for fjord-like and U-shaped valleys on the western margin of the Paganzo Basin (cf. Dykstra et al., 2006; Henry et al., 2008; Isbell et al., 2012; Aquino et al., 2014; Limarino et al., 2014), there is limited evidence for the same on the eastern margin of the basin (Sterren and Martínez, 1996; Net and Limarino, 1999; Net et al., 2002; Net and Limarino, 2006; Socha, 2007; Socha et al., 2014). Instead, much of this evidence comes from an isolated paleovalley that runs through the Sierra de Chepes and Sierra de Los Llanos (Fig. 15).

The Paganzo Basin contains the strata of the Paganzo Group, which has been subdivided into numerous formations of time-equivalent strata over time (Fig. 16). The correlations of these different units are usually made by using lithological similarities, palynological and fossil plant records from the various sections, and radiometric ages obtained from the western units (cf. Gulbranson et al., 2010, 2015; Césari et al., 2011). In recent literature, most of what is written about the Paganzo Basin comes from the western units of the Paganzo Group, the Guandacol, the Tupe, and the Patquía Formations, and these depositional processes and environments are often then extrapolated basin-wide. It has been suggested that as early as the Kasimovian the Paganzo Basin experienced widespread and pervasive aridity, where in some portions erg-like dune fields

developed (Limarino et al., 1984; Morelli et al., 1984; Guena et al., 2010; Gulbranson et al., 2010; Krapovickas et al., 2010; Césari et al., 2011). No study has been conducted on the deposits across the basin to establish a high-resolution record of the paleoclimate as the glacial centers retracted and ultimately disappeared through the Carboniferous-Permian boundary.

Here we focus on a paleovalley and uplift in the eastern portion of the Paganzo Basin, first to test a paleoclimate reconstruction method, and second to determine whether the generalization of the paleoclimate interpretations made from the western margin localities are similar or different from those of the eastern sections. For the eastern margin, it is currently understood (e.g. Moxness et al., 2018) that the paleovalley was not carved by glaciers, and is therefore not considered a sub-or pro-glacial environment. For the purpose of this study, we instead propose to use the term “periglacial,” as it relates to environments that are under the influence or within the realm of recurrent freeze-thaw cycles (Slaymaker and Kelly, 2007).

Paleotopographic highs along the western basin margin (i.e. the Precordillera region and a developing arc farther west; Ramos et al., 1988; Mpodozis and Ramos, 1989) likely played a role in the changing climatic conditions within the basin, based on evidence from sedimentological and stratigraphy studies conducted in the Paganzo Basin (Limarino et al., 2014; Moxness et al., 2018). This study aims to assess whether the various ancestral mountain belts (i.e. the Sierras de Cordoba and Sierra de San Luis of the Pampean orogeny in the east, the Famatina magmatic arc system in the central portion, and the Protoprecordilleran range in the west; Fig. 15) indeed played a role in this unique transition from glacial to post-glacial to arid conditions along the western margin, and from periglacial to intensely arid conditions in the eastern ranges during the end of the Carboniferous.

2.1. Eastern Paganzo Basin: Olta-Malanzán Paleovalley (OMPV)

The Olta-Malanzán paleovalley presents an idealized location to test the applicability of a high-resolution paleoclimate reconstruction using geochemistry analyses such as the CIA because it represents a continuous depositional and localized succession. The paleovalley is cut through a series of uplifted blocks that are known by different names: Sierra de Chepes, Sierra de los Llanos, Sierra de Malanzán, and the Sierra de los Luján (Fig. 17). The valley cuts through Ordovician (470-450 Ma) I-type and S-type granitoid bodies (i.e. Chepes Granodiorite and The Olta-Malanzán paleovalley presents an idealized location to test the applicability of a high-resolution paleoclimate reconstruction using geochemistry analyses such as the CIA because it represents a continuous depositional and localized succession. The paleovalley is cut through a series of uplifted blocks that are known by different names: Sierra de Chepes, Sierra de los Llanos, Sierra de Malanzán, and the Sierra de los Luján (Fig. 17). The valley cuts through Ordovician (470-450 Ma) I-type and S-type granitoid bodies (i.e. Chepes Granodiorite and Porphyritic Granodiorite, Tuani Granite, Asperezas Granite), Tama Gabbro, as well as a few metasedimentary units (Olta Phyllite and Schist), and some units of gneiss and migmatite (Pankhurst et al., 1998, 2000). The granitoid batholith of these sierras was emplaced at about the same time, approximately middle-late Ordovician, as part of the continental Famatinian magmatic arc that developed prior to the docking of the allochthonous Protoprecordillera terrane (Astini et al., 1995; Astini, 1998; Pankhurst et al., 1998). The S-type granites (e.g. Tuaní and Asperezas Granites) and metamorphic complexes (e.g. phyllite, schist, gneiss and migmatite) are considered to represent the remnants of the country rock into which the I-type granitoids were emplaced (Pankhurst et al., 1998, 2000), but on the whole, these basement complexes do not contribute heavily to the geochemistry of the paleovalley system strata due to the limited areal

extent (Net and Limarino, 1999; Net and Limarino, 2006; Fig. 17). The late Paleozoic sediments are derived from the surrounding granitoid batholith units and fill the valley until it was overtopped sometime during the early Permian (Andreis et al., 1986, 1998). The paleovalley was re-exhumed due to flat-slab subduction of the Cenozoic Andean orogeny events (Jordan et al., 1989; López-Gamundí et al., 1994; Dávila et al., 2007; Enkelmann et al., 2014; Enkelmann and Garver, 2015). The late Paleozoic paleovalley system is currently exposed as the present day Olta and Malanzán valleys and tributary systems exhume it (Fig. 18).

The main trunk of the paleovalley system runs from east to west, starting near the town of Olta, to the town of Malanzán in the west (Fig. 18). There are other smaller tributary valleys that fed into the main valley, and vary in size and importance in terms of sedimentary contribution, with the largest being the Anzulón paleovalley (Fig. 18), which is interpreted to have developed sometime during the Permian, after sediment overtopped the valley walls (cf. Andreis et al., 1984; Cuneo and Archangelsky, 1996). The exhumed valley is approximately 40 km long along its axis, and varies greatly in its width, from less than 200 m in the east to more than 5000 m in the west.

The paleovalley itself was initially interpreted as having been developed along a graben due to extensive tectonic activity during the Carboniferous (Andreis et al., 1986). Later studies implied a glacier-proximal origin (Sterren and Martínez, 1996; Net, 1999; Net and Limarino, 1999; Net et al., 2002), and a more recent study by Socha et al. (2014) has interpreted the paleovalley as having been carved by a glacier, citing evidence of the presence of a U-shaped valley and subglacial deposits throughout the Malanzán Formation. The present U-shape of the valley is cut on top of the Paleozoic fill and is therefore not representative of the original shape and formation of the valley (Moxness et al., 2018). The Olta-Malanzán succession consists of the

Malanzán, Loma Larga, Solca, and La Colina Formations (Fig. 16, 18), and was redefined in the literature as more recent studies on the LPIA have been conducted in the Paganzo Basin, as summarized below. The base of the Malanzán Formation in particular has long been interpreted as a glacial diamictite (Sterren and Martínez, 1996; Limarino et al., 2014; Socha et al., 2014), or as conglomeratic units of alluvial fan deposits (Andreis et al., 1986; Net and Limarino, 1999; Net et al., 2002; Net and Limarino, 2006). Other studies also include evidence of marine depositional environments within the Malanzán Formation, leading to the interpretation that the paleovalley was a paleofjord (Buatois and Mángano, 1995; Net et al., 2002). However, recent work by Moxness et al. (2018) has questioned this assertion by concluding that an initial lacustrine setting was truncated by prograding alluvial fans and fluvial systems, which ultimately filled and overtopped the valley walls, based on the sedimentological features and facies analysis (Fig. 19). These interpreted depositional processes do not indicate that there were glaciers nearby during the time of deposition.

3. Chemical Index of Alteration as a Paleoclimatic Indicator

The Chemical Index of Alteration (CIA) has been used in many studies to ascertain the humidity of an environment in the ancient rock record (cf. Nesbitt and Young, 1982; Maynard, 1992; Fedo et al., 1995; Bauluz et al., 2000; Price and Vebl, 2003; Sheldon, 2006; Soreghan and Soreghan, 2007; Sheldon and Tabor, 2009; Goldberg and Humayun, 2010). The CIA was originally created to determine the amount of chemical weathering that takes place during the deposition of clastic sediments in varying depositional environments (Nesbitt and Young, 1982). Nesbitt and Young developed the equation

$$\text{CIA} = (\text{Al}_2\text{O}_3 / \text{Al}_2\text{O}_3 + \text{CaO}^* + \text{Na}_2\text{O} + \text{K}_2\text{O}) \times 100$$

where CaO* represents the calcium content within silicate minerals. They operated under the assumption that the degradation of feldspars into clay minerals constitutes the main process during chemical weathering. This process is enhanced under humid climatic conditions, which leads to higher CIA values in muds deposited in these environments. Conversely, in arid environments, this degradation process would presumably be negligible, and therefore, these sediments would result in lower CIA values. Nesbitt and Young (1982) geochemically analyzed a variety of typical clastic sedimentary rock types and calculated average CIA values. For average shale and mudrock, the CIA values range from 70 to 75 and correspond to the high content of illite and chlorite that are contained in those types of rocks. On the other hand, muds that develop in tropical environments result in values from 80 to 100, and generally contain high percentages of kaolinite. Those deposits from glacial and arid environments have values ranging from 50 to 70, which correspond to the presence of unweathered K-feldspar and plagioclase mineral clasts (Nesbitt and Young, 1982).

Knowing the mineralogical composition of the source rock and calculating its CIA value is of utmost importance, because different minerals produce varying CIA values (Price and Vebl, 2003; Garzanti and Resentini, 2016). Nesbitt and Young (1996) determined that comparing the mineralogy of bedrock, soils and sediments must be completed to understand weathering effects. For example, in the case of a granite, the CIA value would depend entirely on the geochemistry and mineral composition of the granite itself (Nesbitt and Young, 1989). Each mineral in a granite has its own CIA value, i.e. feldspars and biotite are 50, muscovite and illite are 75, and kaolinite is 100 (Nesbitt and Young, 1989). As illite is a common alteration product of K-feldspar, and illites generally form as granite weathers, this could potentially skew the subsequent material weathered into having a higher CIA value (Weaver, 1967; Weaver and

Pollard, 1973; Brock, 1943; Wahlstrom, 1948; Sand and Bates, 1953; Grant, 1963; Nesbitt et al., 1980; Nesbitt and Young, 1989).

Chemical weathering of bedrock materials is the reaction of inorganic and organic acids of water, groundwater or even perhaps precipitation, with the minerals contained in the rock (Nesbitt et al., 1997). For igneous rocks, each mineral will weather at a different rate, and will weather to different clay minerals, and because each igneous rock contains a different percentage of each mineral, the chemical index value can vary from rock type to rock type (Figure 4). Illite, for example, is a common alteration product of K-feldspar, and illites will generally form as granitic rocks weather, where as gabbros and tonalites contain more plagioclase, and will weather to smectite clays (Brock, 1943; Wahlstrom, 1948; Sand and Bates, 1953; Grant, 1963; Weaver, 1967; Weaver and Pollard, 1973; Nesbitt et al., 1980; Nesbitt and Young, 1989).

Furthermore, Nesbitt and Young (1989) and Nesbitt and Markovics (1997) show that mature weathering profiles, while complex mineralogically, follow similar trends regardless of the climatic conditions of the environment, as a certain mineral will weather in more or less a linear progression through time. Therefore, igneous rocks of like mineral composition (i.e. granites and granodiorites vs. tonalites and gabbros) tend to display similar weathering trends, but they will plot in different locations on A-CN-K plots (Nesbitt and Young, 1989). Average fresh granites and granodiorites will plot, using an A-CN-K diagram, between 45 and 55 (Nesbitt and Young, 1989; Fedo et al., 1995; Nesbitt and Markovics, 1997; Bahlburg and Dobrzinski, 2011). Because granites and granodiorites tend to contain higher percentages of plagioclase and K-feldspars, these rocks will weather to illite and kaolinite, which could result in higher CIA values for the resulting material developed from the breakdown of the parent material. Tonalites

and gabbros contain more CaO and very little K₂O, and therefore will weather to smectites and kaolinite (Nesbitt and Young, 1989).

There are, however, a few processes that could complicate this simple weathering progression, such as winnowing or infiltration of fines and diagenetic reactions associated with the introduction and interaction with groundwater. Regardless, it may prove to be difficult to constrain climate from a CIA value alone without knowledge of the mineral constituents of the parent material first. Taking into consideration other factors and processes that could lead to skewed results (i.e. metasomatism and illitization leading to increased K⁺ concentrations, hydraulic sorting and inclusion of a wide variety of grain sizes analyzed, as well as including CaO contents of carbonates), using the CIA proves to be a powerful paleoclimate proxy (Maynard, 1992; Fedo et al., 1995; Bauluz et al., 2000; Price and Veblen, 2003; Sheldon, 2006; Soreghan and Soreghan, 2001; Retallack, 2009; Sheldon and Tabor, 2009; Goldberg and Humayun, 2010).

4. Methods

Field work was conducted in March of 2015 and August of 2016. Standard stratigraphic measurements and methods to examine the strata, such as section measurements, identification of sedimentary structures, contacts, and stratigraphic surfaces, as well as lithological and facies analyses were used. These measurements were taken in order to determine depositional environment evolution through time and to compare the CIA results with the environments as determined from physical sedimentology. Careful attention was paid to the presence or absence of the following features: striated pavements, striated clasts, sheared diamictites versus clast-supported conglomerates, inverse versus normal grading within foresets, fine-grained large-scale

cross-bedded sandstone (i.e. eolian dunes), paleosol development. The occurrence of these features are indicated in Table 1. In order to establish the occurrence of glaciers in the eastern Paganzo Basin, a facies and environmental analysis of the Malanzán Formation in the Olta valley was conducted concurrently to this study (Moxness et al., 2018) and is used to complement the facies analysis of the upper section (Loma Larga through La Colina Formations) that is presented here. No glacial signatures were found in the Malanzán Formation. A total of 45 sections were measured along the roads that follow along the main axis of the paleovalley. To reduce a weathering bias during sample collection, which could potentially skew the dataset towards low or high CIA values, only clay to silt-sized samples (i.e. $< 0.004 - 0.0062$ mm) were collected from trenches dug >10 cm into the outcrops, thus providing fresh, unweathered material. Rock units that contained outsized clasts were also avoided, so as not to create a “fresh-material” bias in the results. As such, an equal distribution of samples throughout the measured sections could not be achieved, especially within coarse-clastic horizons. Samples were instead collected from every unit that had the desired grain size (i.e. mudrocks). Because of this, some parts of the measured sections contain a higher sample abundance, and therefore provide a higher-resolution record of the CIA values.

The CIA analysis was conducted using the calculations found in Nesbitt and Young (1982) and the geochemical preparations and x-ray fluorescence (XRF) and diffraction (XRD) methodologies found in McHenry (2009) and McHenry et al. (2017). Samples of mudrock and shales were ground and crushed using a tungsten-carbide shatterbox, left to dry overnight in a drying oven, and then heated to 1050° C to determine loss on ignition. XRD results (Bruker D8 Focus diffractometer) were used to determine the mineralogy of the samples, which indicated if a sample was viable for further study (i.e. contains less than 20% calcite as per Goldberg and

Humayun [2010]). XRF analyses using a Bruker S4 Pioneer were then conducted on the appropriate samples, after which the data was used in order to determine the CIA values.

5. Stratigraphy of the OMPV

At the base of the stratigraphic section there have been several facies of the Malanzán Formation described in detail in Moxness et al. (2018; Fig. 20A). The Malanzán Formation outcrops in both portions of the paleovalley (Fig. 18). In the western Malanzán portion, the middle and upper members of the Malanzán Formation appear. In the eastern Olta paleovalley, the whole succession is present, and samples were primarily collected from this portion used for this study (Fig. 19). There is no continuous outcrop from one end of the paleovalley to the other, so the exact position of the middle members is based on the stratigraphic correlation of Braccacini (1948), Azcuy (1975), and Andreis et al. (1986).

The lowermost Malanzán Formation contains thick clast-supported conglomerates, thick medium-coarse-grained rippled and graded sandstones suggesting deposition within a standing body of water that has been interpreted as lacustrine in origin (Andreis et al., 1986; Buatois and Mángano, 1994; Moxness et al., 2018). The middle member of the Malanzán Formation contains thicker packages of interbedded mudstones and sandstone, contains evidence of marine life with the appearance of acritarchs, and is interpreted as a regional or local rise in relative sea level (Net and Limarino, 1999; Gutiérrez and Limarino, 2001; Fig. 20B). Both ends of the paleovalley contain the upper member, which consists of large cross-bedded conglomeratic facies. These have been identified and interpreted as gilbert deltas, are thought to have formed due to cold conditions, and have been interpreted in the literature to correspond to a post-glacial

transgression across the basin (Sterren and Martínez, 1996; Net and Limarino, 1999; Net, 2002; Gutiérrez and Limarino, 2001; Limarino et al., 2014; Moxness et al., 2018).

The overlying Loma Larga Formation consists of stacked cross-bedded sandstone units and finer-grained, silty sandstones (Fig. 19). The cross-bedded sandstone facies contains coarse-medium grained beds with sharp erosional boundaries. The grains themselves are predominantly quartz, plagioclase and altered K-feldspar with some beds containing muscovite mica, and are considerably whiter in appearance than the sandstones of the Malanzán Formation. The siltier facies often contain horizontal beds with no structures preserved. This facies also contained layers of fossilized plant remains, and are identified as Cordaitales, calamites, lycopods, and pteridosperms (Césari et al., 2011). The Loma Larga Formation crops out in both portions of the paleovalley, but the units that are located in the Malanzán valley are at a steep subvertical structural dip toward the east. For the purposes of this paper, the samples were all taken from the Olta valley (Andreis et al., 1986). These units are all interpreted as stacked fluvial systems flowing through the paleovalley with occasional fluvial flooding that led to thin splay deposits along vegetated banks (Fig. 20C-D; Andreis, 1998).

In the overlying Solca Formation, the most dominant facies is boulder conglomerate (Fig. 21A). The conglomerates are often clast-supported and contain sand as the matrix. The clasts range widely, from gravel-sized to cobbles to boulders that are meters in diameter. However, though reported as Malanzán glacial deposits in Socha et al. (2014), these conglomerates are interpreted here, and in other works (e.g. Andreis et al., 1986; Limarino et al., 2014), as alluvial fan deposits. Some of these fans are preserved as amalgamated lens complexes, and one complex appears to have convex geometries stacked on top of one another, and is interpreted here as an alluvial fan entering into the main axis of the valley from a tributary (Fig. 21A). There are few

places where a coarse-grained sandstone facies occurs within the Solca Formation, which is immediately overlain by a fine-grained siltstone facies that contains abundant horizons of fossil plant material. The fossils in the siltstone facies were recorded as pteridosperm, conifer needles, and lycopods. This section also contains poorly developed ripples and is interpreted here as fluvial to lacustrine depositional environments, respectively, with associated vegetated flood plain environments (Andreis et al., 1986; Cúneo, 1987; Cúneo, 1990; Limarino et al., 1996). There was one paleosol recorded in the measured section of the Solca Formation, and it accounts for the finest-grained facies within the stratigraphic column in this portion of the paleovalley (Fig. 21B). According to the criteria established in Mack et al. (1993), the paleosol here is considered to be an argillosol, with some horizon development and clay content accumulated. Overlying the paleosol is another series of stacked conglomeratic units, and as the formation nears its upper boundary with the La Colina Formation, the boulders increase in size. The dip of the formation also decreases from 8° at its base to nearly horizontal at its upper boundary.

The neighboring Permian Anzulón paleovalley has outcrops of the lower Permian Arroyo Totoral Formation. Andreis et al. (1984) described two sections measured from near the boundary of the two units. The first section contained two facies: a fine-grained mudstone facies and a coarse-grained sandstone facies with outsized clasts (Fig. 21C). The boundary between the two facies is sharp and erosional. The finer-grained mudstone facies records/displays a color change from white-gray at the base to red at the top, and contains very fine sand lenses (Fig. 21C). The sandstone facies contains weak cross-bedding. The second Arroyo Totoral Formation section records a very similar coarsening-upward trend. The base of the section is also a mudstone facies, but is characterized by silt interbeds and organic-rich layers containing abundant plant remains. The plant remains are similar to those recorded near the middle of the

Solca Formation: Calamites, cordaitaleans and conifer needles (Cúneo, 1984; Cúneo and Archangelsky, 1996). The cross-bedded sandstone facies has an erosive contact into the underlying mudstone facies. Overall, both sections display coarsening-upward patterns suggesting a fluvial progradation into a floodplain or lacustrine system, or a return to a braided fluvial system (Andreis et al., 1984; Cuneo and Archangelsky, 1996; Andreis, 1998).

The La Colina Formation is a classical red bed succession composed of interbedded mudstone and sandstone facies, coarse-grained sandstones, and fine-grained cross-bedded sandstone facies (Fig. 21D). The base of the formation contains intercalated sand and mud beds with cross-bedded medium sandstones. The alternating sand and mudstone units contain very fine-grained sand beds with silt and clay-sized particles contained in the alternating mudstone beds (Figs. 21D, E). These units contain ripples, rill marks, and adhesion warts, indicating subaerial exposure. The alternating layers are interpreted here as splay deposits or as floodplain deposits, where water has spilled over and out of the channels and results in thin, fine-grained units. Higher in the succession, the mudcracks, rill marks, and adhesion structures (i.e. adhesion ripples and adhesion warts) recorded in this facies become scarce, which is here taken to indicate alternating dry and wet periods (Kocurek and Fielder, 1982; Mountney, 2006).

The coarser-grained trough-cross-bedded sandstone facies are found in the middle of the paleovalley, are in stacked and amalgamated geometries, and often display some scouring into the units below. These units are on average a few meters thick, and also contain some outsized clasts of granitoid and basalt composition. These are interpreted as braided fluvial units, and a return to higher energy within the paleovalley system. Fine-grained sandstone cross-bedded tabular bodies that have knife-sharp upper and lower boundaries overlie the coarse-grained cross-bedded facies (Fig. 21F). These are the uppermost units of the La Colina Formation, and are

quite extensive throughout the middle of the paleovalley system. The centimeter-scale foresets of the sandstones display inverse-grading and range between 5 and 10 meters in length. The units themselves are at least three meters thick. Because of the geometry, grain size and boundary type, this sandstone facies is interpreted as eolian dunes (Fryeberger, 1993; Mountney, 2006).

6. CIA Values for OMPV

The raw data were compiled and then sorted based on the formation and sampling location, see Table 2. These results were then compared to the geochemical data of the fresh igneous components published in the studies of the Famatina and Pampeanas ranges by Pankhurst et al. (1998, 2000) using an A-CN-K plot to demonstrate the weathering trend of the resulting sediments (Fig. 22). The dominant igneous rock types in the Olta-Malanzán paleovalley area are primarily granodiorite (Chepes Complex), followed by a metasedimentary suite (phyllite and schist), and granite (Tuaní Granite) (Pankhurst et al., 1998).

Overall, the lower strata of the paleovalley have relatively low CIA values (Fig. 23). In a few instances the values increase including within the uppermost Malanzán Formation through the lowermost Loma Larga Formation. In general, the CIA values for the Malanzán Formation range from 58 to 78, with an average CIA value of 67. The samples in the upper units of the Loma Larga Formation have similar CIA values to average shale and range from 55 to 71 with an average of 65. The Solca and La Colina Formations samples have CIA values that range from 58 to 91, with an average of 70. The paleosol of the Solca Formation has a wide range in CIA values, but overall its average CIA value is 66. The two La Colina Formation samples were collected from the middle strata of the unit and are thus higher than all of the older formations for the Olta-Malanzán paleovalley system. In addition to the main valley samples, a few samples

from the Arroyo Totoral Formation in the Permian tributary Anzulón paleovalley also resulted in relatively higher CIA values of 70 and 78.

7. Paleoclimate implications for the Eastern Paganzo Basin

The strata of the Olta-Malanzán paleovalley system were chosen to test the applicability of CIA as a high-resolution proxy for paleoclimate because of the renewed interest in the timing and extent of the glacial centers of Gondwana. While past researchers (e.g. Socha et al., 2014) interpreted it to have been carved by glaciers, recent evidence (e.g. Moxness et al., 2018) shows that the valley only contains fluvial, alluvial, deltaic, lacustrine, and shallow marine deposits (Andreis et al., 1986; Gutiérrez and Limarino, 2001). Although the base of the succession (i.e. Malanzán Formation) differs from those of the western Paganzo Basin units, the rest of the succession (Loma Larga through La Colina formations) still records the same shift in climate: post-glacial to increasing aridity. The Olta-Malanzán paleovalley system provides ideal conditions in which to conduct this type of study because the strata are all locally-derived. Any chemical weathering that occurred in this paleovalley affected the Famatinian granitoids through which the valley is cut. It is thus possible to ascertain any diagenetic effects on the sedimentary units through time by comparing the samples to an average weathering trend for the corresponding granite type. As can be seen in the A-CN-K plot (Nesbitt and Young, 1984; Nesbitt and Markovics, 1997) in Figure 22, the samples follow a chemical weathering trend of increased weathering intensities over time, as predicted. The fresh basement samples plot between the average granite and granodiorite and the samples from the sedimentary rocks follow a linear trend of progressive weathering (Nesbitt and Young, 1984; Pankhurst et al., 1998). Therefore, these units can provide a reliable paleoclimate reconstruction for this system, and

perhaps for the eastern margin of the Paganzo Basin, and at the very least be used to compare to paleoclimate reconstructions for the middle and western units of the Paganzo Group (i.e. Gulbranson et al., 2010; Limarino et al., 2014; Gulbranson et al., 2015).

The sedimentology of the Malanzán Formation indicates that the paleovalley was dominated by non-glacial debris-flows and rock falls, which led to the occasional damming of the central valley axis and the formation of lakes (Andreis et al., 1986; Andreis, 1998; Moxness et al., 2018). As displayed in Figure 23, the base of the Malanzán Formation has CIA values in the middle-to-upper 60s. This increase appears to coincide with a transgression during the Serpukhovian that has been interpreted to have crossed the Paganzo Basin and would have raised local base level (Net et al., 2002; Limarino et al., 2002, 2006, 2014). Coupled with a shifting climate, from a cold periglacial environment to more temperate climatic conditions, a rise in local base level could have increased chemical weathering processes due to the introduction of a more humid environment as there is evidence of organic-rich beds. However, the values are still relatively low and do not represent any significant chemical weathering of the plagioclase to clays, such as illite, smectite and kaolinite, which have CIA values ranging from 75- 80 (Nesbitt and Young, 1982, 1984; Nesbitt and Markovics, 1997). From these low values, it can be asserted that there was initial weathering of the feldspars from the granodiorite, which consistently plot at 49 and 50, but the overall climate was dry, rather than humid, and represents a cold arid environment at the termination of the glacial episode in the western Paganzo Basin. This is consistent with the facies that have been described both here and in Moxness et al. (2018).

The CIA values show an increasing trend within the upper Malanzán Formation and lower Loma Larga Formation boundary. Here we see the values increase from upper 60s and lower 70s to upper 70s. This is interpreted here as a transition to a humid climate during the

formation of the carbon-rich layers, and coincides chronostratigraphically with the other coal deposits (e.g., in the Tupe and Lagares formations) across the Paganzo Basin (López-Gamundí, 1997; Net et al., 2002; Limarino et al., 2002, 2006, 2014). The carbon-rich beds here are relatively thin, on the orders of centimeter-thick beds, and are found just below the Gilbert delta packages and again between the stacked fluvial systems of the lowermost Loma Larga Formation (Figure 20). The higher CIA values combined with the formation of coal and organic-rich terrestrial deposits affirms that the basin was firmly in a post-glacial humid climate during the latest Bashkirian.

The sandstone packages of the Loma Larga Formation are relatively coarse-grained and tend to consist of mostly quartz and plagioclase grains. The finer-grained packages between the fluvial sandstones of the Loma Larga Formation display similar values to those in the lower Malanzán Formation. This trend could be representative of either more arid conditions, or a return to rapid-burial style deposition in a seasonal climate regime as the paleovalley continues to fill. Rapid burial would prevent further alteration of the feldspars within the near-surface environments (Nesbitt and Markovics, 1997; Andreis, 1998; Net et al., 2002; Bahlburg and Dobrzinski, 2011).

Although the Solca Formation is dominated by conglomerates and sandstones, a paleosol level is exposed close to the Solca and La Colina Formations boundary, and appears to have developed alongside, or on top of the valley wall. Along with the nearly horizontal dip of the strata, the development of this paleosol directly on top of the basement, or paleovalley wall, indicates non-deposition during a time when the paleovalley was being overtopped (Sheldon and Tabor, 2009). The average CIA value, though, for the whole paleosol is only 66, which does not

indicate a very humid environment, but does provide evidence of clay development (Nesbitt and Young, 1982; Goldberg and Humayun, 2010; Bahlburg and Dobrzinski, 2011).

The climate at the Carboniferous-Permian boundary in the eastern Paganzo Basin was probably a fluctuating seasonal or temperate one. The Arroyo Totoral Formation outcrop samples have higher CIA values (70 and 78), and along with the facies and paleoflora assemblage, indicate a humid lacustrine setting (Andreis et al., 1986; Cuneo and Archangelsky, 1996; Andreis, 1998). The paleoclimate record from strata of the La Colina Formation presents an interesting deviation from the expected trend of the succession. Where we expect an increase in aridity according to the model developed by Gulbranson et al. (2010), CIA values of 91 and 78 indicate a brief period where the paleoclimate was warm-humid. The mineralogy of the interbedded sand and mudstone facies consists of primarily kaolinite and hematite. The facies together with the mineralogy and therefore resulting CIA values, though, indicate that there may have been a much higher precipitation rate than first implied by the sedimentary structures, and therefore increased chemical weathering (Nesbitt and Young, 1982, 1984; Nesbitt and Markovics, 1997). As there does not appear to be an abundance of organic material, which could contribute to the chemical alteration of the feldspathic minerals in the system, we conclude that the climate during the earliest Permian, in the eastern portion of the Paganzo Basin, was briefly extremely humid. The top of this interbedded facies shows a coarsening upward signature and marked increase in subaerial structures (i.e. rill marks, adhesion structures, mud cracks). The overlying facies of the La Colina Formation contain very small amounts of fine-grained deposits, and the depositional style returns to a more braided fluvial environment, which could indicate a more seasonal climate.

At the very top of the succession in the paleovalley system, the climate finally gives way to an extremely arid environment (Andreis, 1998; Limarino et al., 2014). This is evidenced by the large dunes developing over the braided fluvial systems, and even cross-cutting one another. There were no fine-grained beds to sample, so it is assumed that minimal chemical alteration occurred due to little to no precipitation, and that any fines that did develop were subsequently winnowed away (Nesbitt and Young, 1984; Goldberg and Humayun, 2010).

As the western margin of Gondwana developed, the active tectonic margin continued to shift westward through the Paleozoic (Ramos, 1988; Pankhurst et al., 1998; Ramos et al., 1998; Limarino et al., 2002, 2006; Astini et al., 2009; Astini, 2010). While the exact significance of the Protoprecordillera as a topographic high is disputed (c.f. Limarino et al., 2002, 2006; Astini et al., 2009; Astini, 2010; Valdez Buso et al., 2017), it played a role in the nucleation and persistence of glaciers along the western margin of the Paganzo Basin during the middle Carboniferous (López-Gamundí et al., 1994; Limarino et al., 2014; Net and Limarino, 2006; Kneller et al., 2004; Dykstra et al., 2006; Henry et al., 2008; Aquino et al., 2014). The disappearance of the glacial centers and the transgression deposits across the basin signal the collapse of the Protoprecordilleran range as the active tectonic margin shifted westward. The rain shadow effect of the Protoprecordilleran range on the eastern Paganzo Basin in the Carboniferous would have been intensified as the Panthalassan Ocean margin moved further westward (cf. Ramos, 1988; Pankhurst et al., 1998; Ramos et al., 1998; Ramos, 1999; Limarino et al., 2002, 2006; Astini et al., 2009; Astini, 2010), and could account for the arid conditions that prevailed into the Permian. The record of increasing aridity at the end of the Carboniferous and into the early Permian established in the CIA record of the Olta-Malanzán paleovalley in this study clearly demonstrates this trend.

8. Conclusion

The stratigraphic section in the Olta-Malanzán paleovalley system provides an excellent opportunity for a high-resolution test of the CIA as a paleoclimate proxy due to well-documented changing post-glacial conditions within the Paganzo Basin. The CIA is a powerful geochemical proxy, especially when considered in conjunction with sedimentological and stratigraphic measurements and interpretations, and is used here to quantitatively assess paleoclimate changes in the late Paleozoic succession of the eastern Paganzo Basin. The strata in the paleovalley record a transition from periglacial conditions to increasingly arid conditions in the eastern portion of the Paganzo Basin. The results from this study demonstrate that the paleoclimate in the intermontane paleovalley fluctuated between humid and arid over time. This shows that the climate transition of the Paganzo Basin was more dynamic than previously thought.

The base of the succession has low CIA values due to the nature of the depositional environments within paleovalley, which was subject to rapid burial from frequent rock falls, prograding alluvial fans/fan deltas, and lacustrine sediment gravity flows (Malanzán Formation), which seem to have prevented significant chemical weathering. While the overall Pennsylvanian climatic signature appears to be relatively arid (Malanzán, Loma Larga, and Solca Formations), the results indicate that the climate during the deposition of the late Pennsylvanian and Permian La Colina Formation was more humid than previously inferred from the facies.

This shift in climate does not align with global drivers at the Carboniferous-Permian boundary, and is likely more tied to regional tectonic drivers, such as the ongoing subduction and accretion of terranes onto the Panthalassan margin of Argentine Gondwana.

Acknowledgements

Financial support for this study was provided by various grants from numerous agencies including the Geological Society of America, the Society for Sedimentary Geologists, the University of Wisconsin-Milwaukee Center for Latin American and Caribbean studies, the Wisconsin Geological Society, University of Wisconsin-Milwaukee (RGI grant), the University of Wisconsin-Milwaukee Department of Geosciences, the Universidad de Buenos Aires, CONICET, and grants from the USA National Science Foundation (Grants 1443557, 1559231, and 1729219).

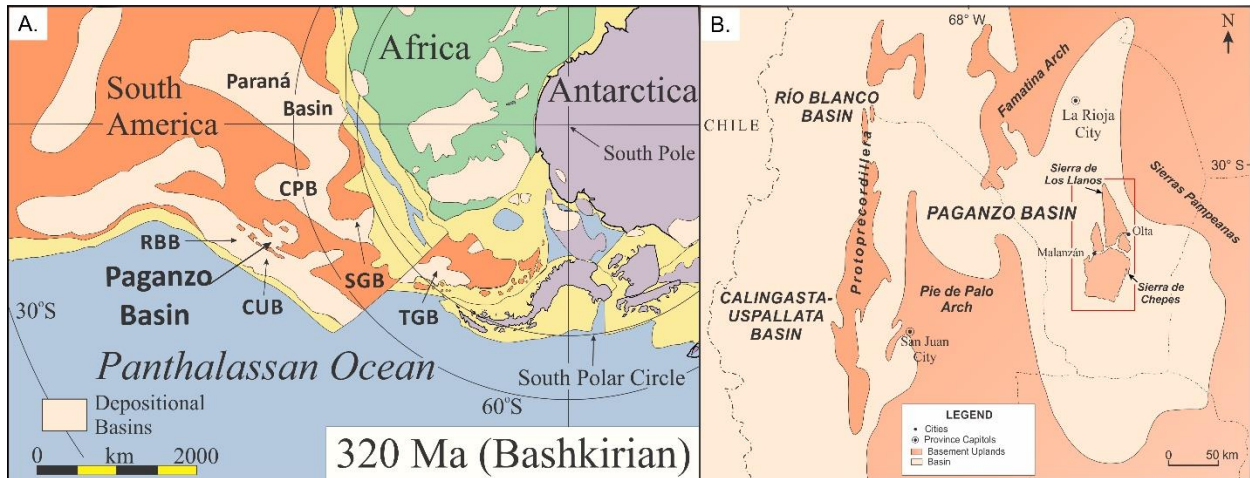


Figure 15. A. Plate reconstruction showing the location of the continents centered around the South Pole during the late Paleozoic. The Paganzo Basin, the area for this study, is highlighted by the arrow. RBB: Río Blanco Basin; CPB: Chaco-Paraná Basin; SGB: Sauce Grande Basin. TGB: Tepuel-Genoa Basin. (Modified from Moxness et al., 2018) B. Plan-view map showing the interpreted outline of the Paganzo Basin. The Olta-Malanzán paleovalley within the eastern portion of the basin is highlighted in the red box. (Modified from Limarino et al., 2006).

Age (Ma)	Time Scale			Paganzo Basin		
	Period		Stage	Huaco	Paganzo	Sierra de Chepes
295	Permian	Cisuralian	Sakmarian			
			Asselian		La Colina/ Patquía	La Colina
300	Carboniferous	Pennsylvanian	Gzhelian	Patquía		Lagares
			Kasimovian		Solca	
Moscovian			Loma Larga			
Bashkirian					Malanzán	
325		Mississippian	Serpukhovian	Guandacol ▲▲▲▲▲ ▲▲▲▲▲		▲▲▲▲▲
330		Mississippian	Viséan			
335						

Figure 16. Simple stratigraphic column showing the Paganzo Group strata and correlations across the Paganzo Basin (modified after Henry et al. 2008; Taboada, 1985; Archangelsky and Lech, 1985; Archangelsky and Archangelsky, 1987; Fernandez-Seveso and Tankard, 1995; Azcuy et al., 1999; López Gamundí and Martínez, 2000; Gulbranson et al., 2010; Tedesco et al., 2010; Césari et al., 2011).

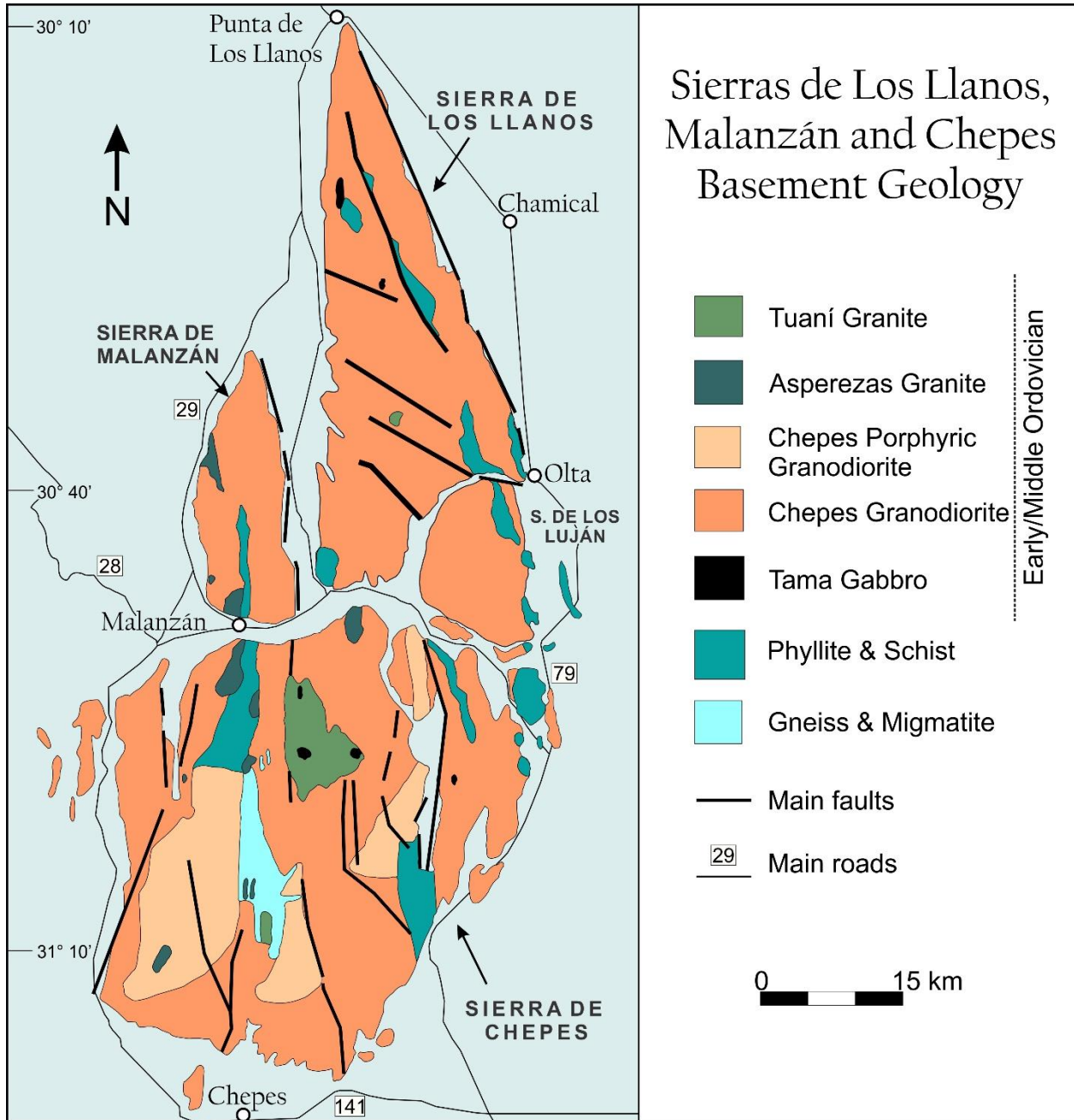


Figure 17. Map of the igneous and metamorphic basement units into which the late Paleozoic paleovalley is cut. (Modified from Pankhurst et al., 1998).

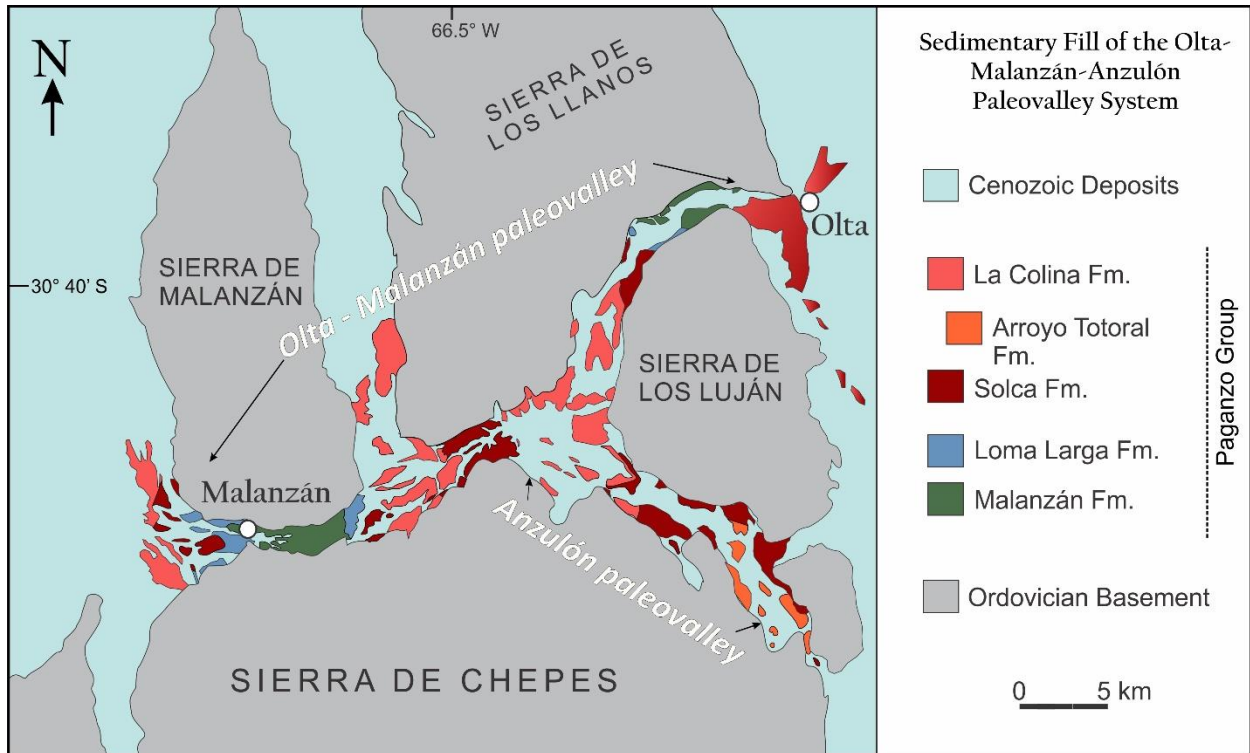


Figure 18. Simplified geologic map highlighting the late Paleozoic sedimentary fill of the two main paleovalley systems in the Sierra de Chepes and Sierra de los Llanos region (Modified after Net and Limarino, 1999; Moxness et al., 2018).

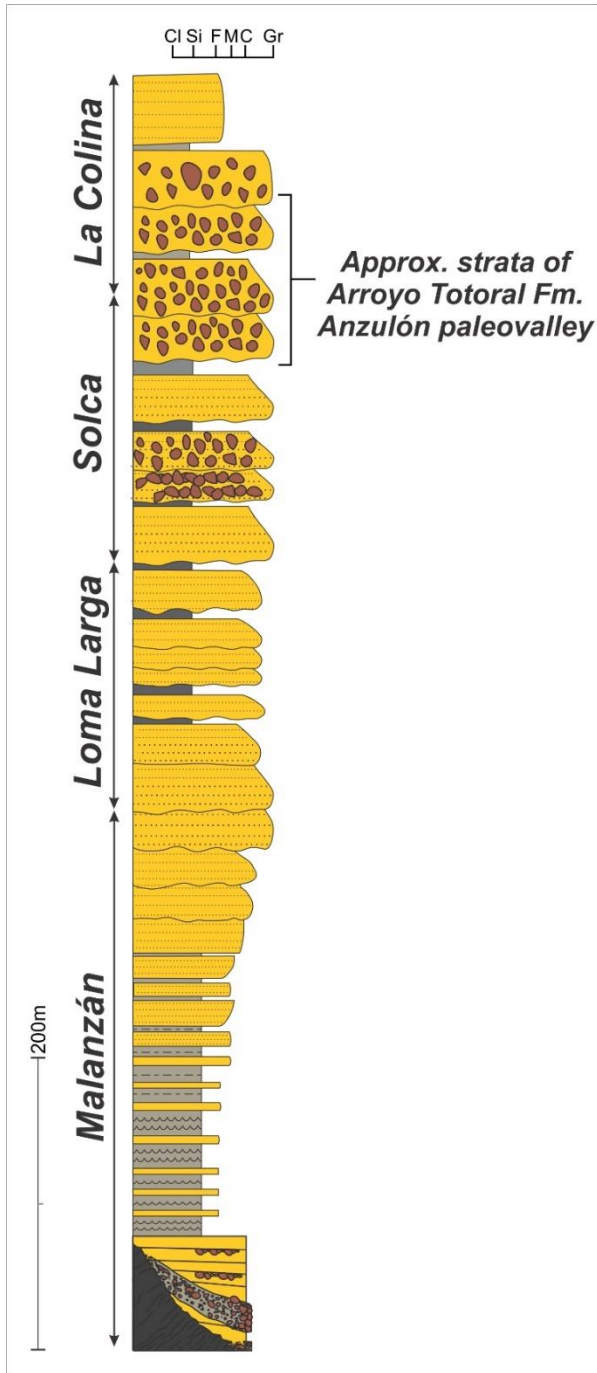


Figure 19. Generalized and simplified stratigraphic column for the strata in the paleovalley system.

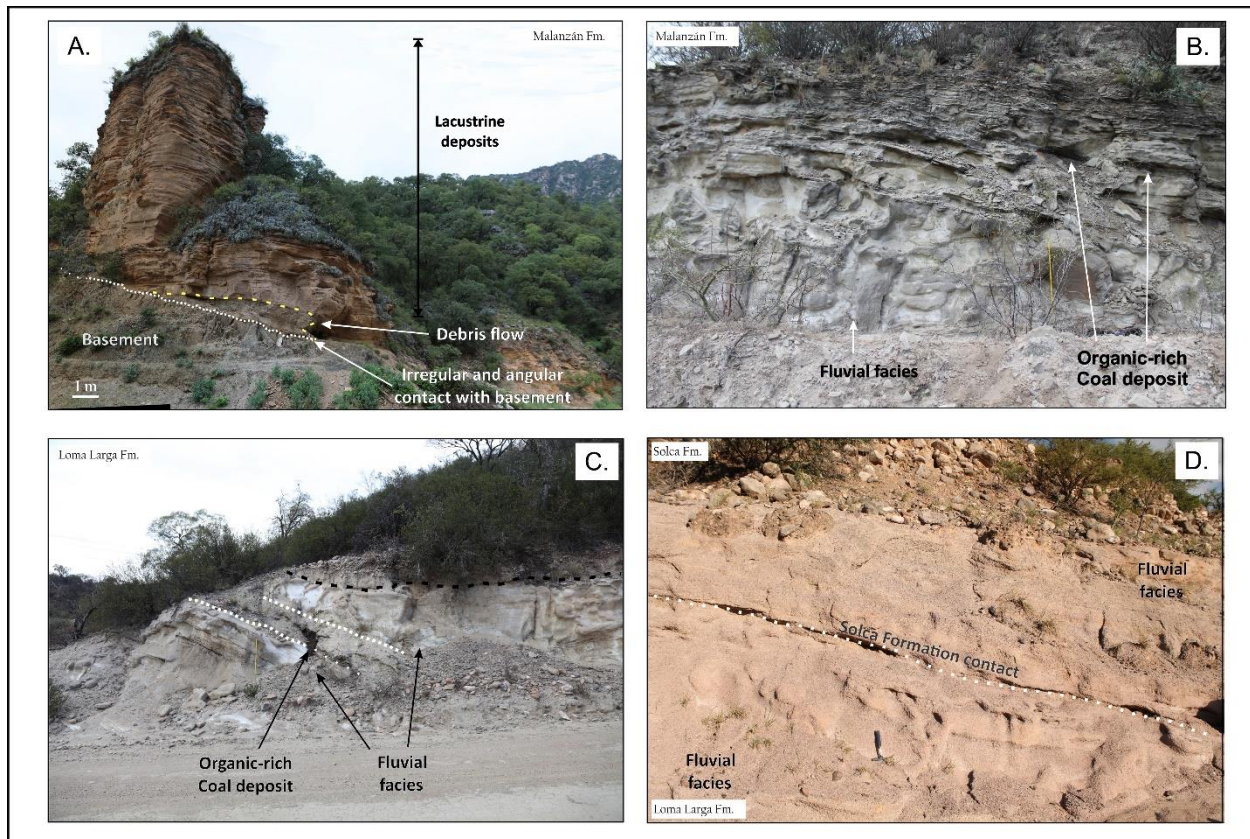


Figure 20. Photos showing examples of the varying facies through the Malanzán and Loma Larga Formations. A. Conglomeratic and interbedded sand and mudstone facies at the base of the Malanzán Fm. Debris flow overlying the basement, followed by lake sediments. B. Stacked cross-bedded sandstone facies with overlying organic-rich mudstones. Fluvial dominant environment transitioning into a lacustrine setting. C. Stacked cross-bedded coarse sandstone facies with interbedded organic-rich mudstones of the Loma Larga Formation interpreted as fluvial and vegetated lacustrine environments. D. Stacked cross-bedded coarse sandstone facies at the boundary between the Loma Larga and Solca Formations.

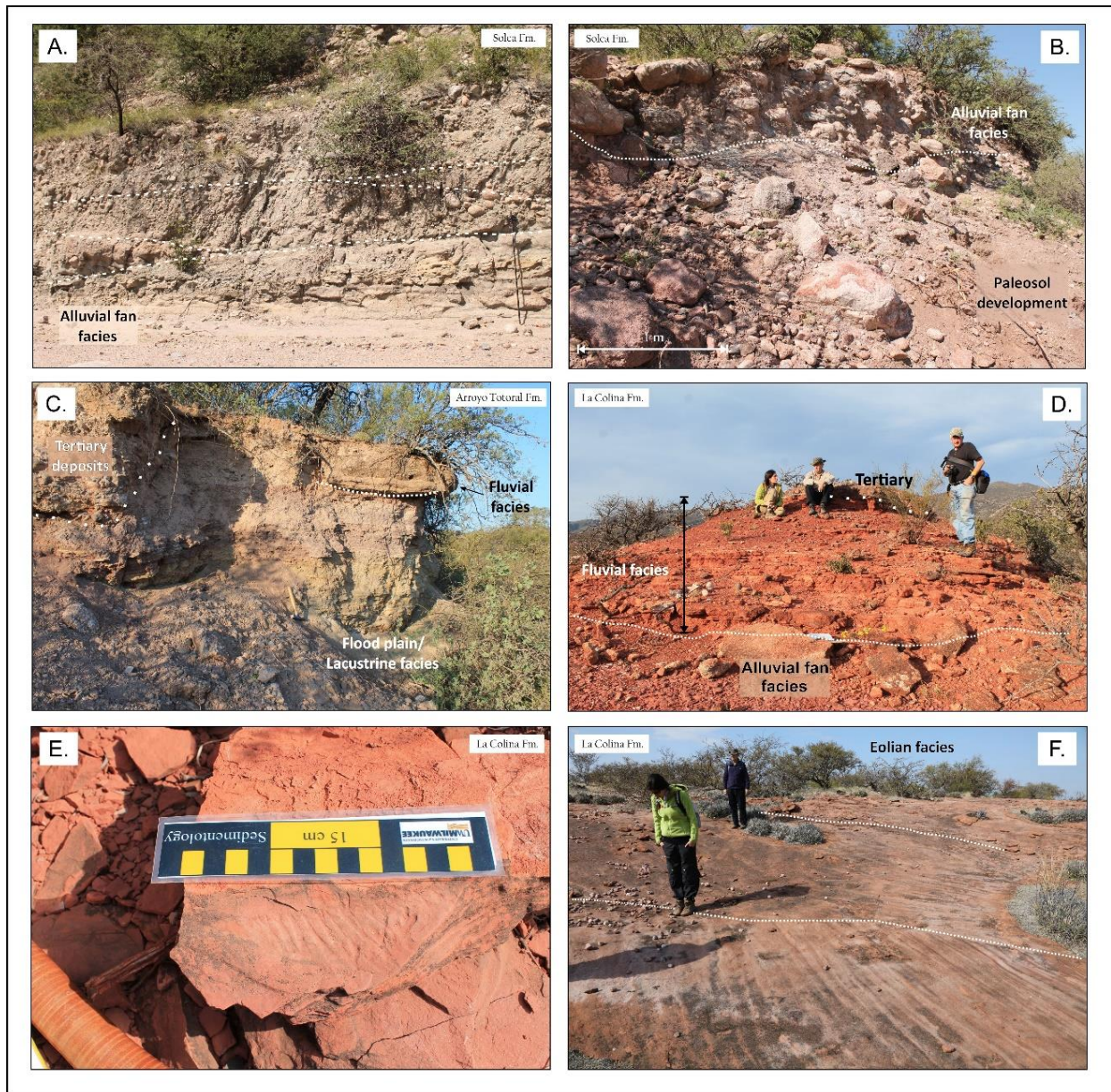


Figure 21. Photos showing the facies characteristics of the upper units of the paleovalley system: Solca Formation, Arroyo Totoral Formation, and La Colina Formation. A. Conglomerate facies interpreted as an alluvial fan amalgamation. B. Conglomerate facies cutting into a paleosol in the Solca Formation. This is interpreted to be a depositional hiatus followed by renewed deposition in the paleovalley. C. Weakly cross-bedded sandstone facies overlying the interbedded mudstone facies interpreted as lacustrine and fluvial settings in the Arroyo Totoral Formation. D. Interbedded sandstone and mudstone facies near the base of the La Colina Formation, overlying conglomeratic facies interpreted as alluvial fans transitioning into an ephemeral fluvial environment. E. Example of rill marks in the interbedded sandstone and mudstone facies of the La Colina Formation. F. Large cross-bedded sandstone facies at the top of the La Colina section interpreted as eolian dunes indicating desert-like conditions.

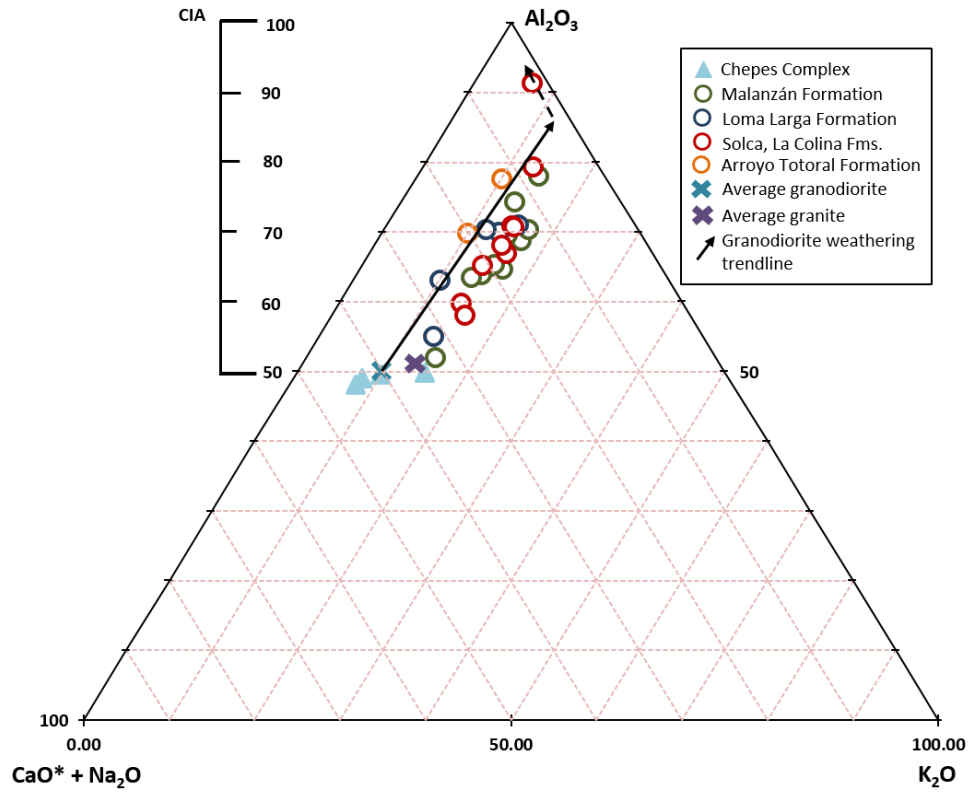


Figure 22. Ternary A-CN-K plot displaying the fresh Chepes Complex granodiorite and the late Paleozoic sedimentary fill samples based on their bulk geochemistry. Also plotted is the average granite and granodiorite compositions and the average granodiorite weathering trend line based on data from Nesbitt and Young (1989).

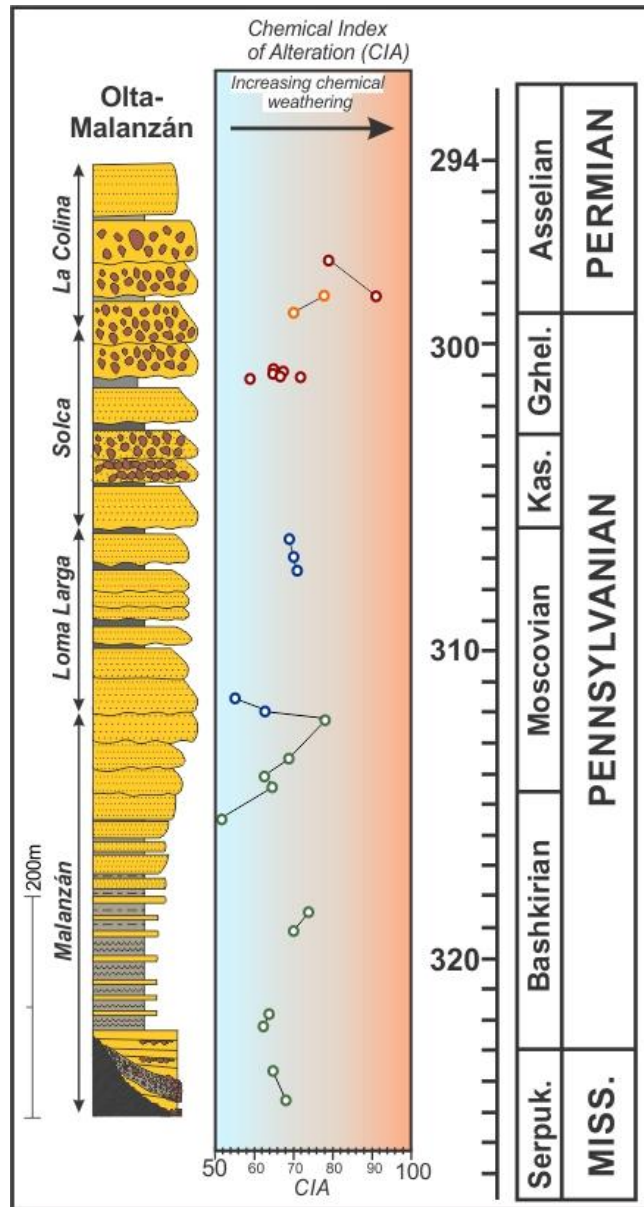


Figure 23. Generalized stratigraphic section from the Olta-Malanzán Paleovalley with the CIA values for each sample and a smoothed 3-point running average line (black) have been plotted next to their approximate location within the succession. Samples have been color-coded based on stratigraphic formation: green – Malanzán Formation, blue – Loma Larga Formation, red – Solca and La Colina formations, orange – Arroyo Totoral Formation. For the CIA scale, left to right indicates increased chemical weathering and an inferred humid paleoclimate (i.e. blue is more arid and orange is more humid).

Sedimentary Features	Interpretations	Formation Names				
		Malanzán	Loma Larga	Solca	Arroyo Totoral	La Colina
Striated pavements	Sub-glacial erosion	-	-	-	-	-
Striated Clasts	Glacial transport	-	-	-	-	-
Sheared Diamictites	Sub-glacial deformation (till deposits)	-	-	-	-	-
Clast-supported Conglomerates	Fluvial-alluvial fan deposition	x	-	x	-	x
Inversely graded foresets	Eolian grain-flow	-	-	-	-	x
Fine-grained large-scale crossbeds	Eolian dune deposition	-	-	-	-	x
Paleosol features	Subaerial soil development	-	-	x	-	-

Table 1.. Record of sedimentary features described in the measured section through the Olta-Malanzán paleovalley. Here, “x” indicates feature was present, and “-” indicates that the feature was not present.

Sample ID	Formation	SiO ₂	TiO ₂	Al ₂ O ₃	Fe ₂ O ₃	MnO	MgO	CaO	Na ₂ O	K ₂ O	P ₂ O ₅	LOI	Total	CIA
BMM	Malanzán Fm.	59.09	0.82	19.58	6.52	0.10	2.43	1.09	1.47	4.45	0.14	4.41	100.1	69
Malanzán1	Malanzán Fm.	62.77	0.64	17.47	17.47	0.05	1.71	0.52	2.94	3.71	0.17	3.28	98.36	65
OPV0808-2C	Malanzán Fm.	69.9	0.52	14.9	4.16	0.07	1.43	0.51	2.74	3.10	0.15	2.43	99.91	64
OPV0803-3C	Malanzán Fm.	50.57	1.00	19.28	8.63	0.14	2.79	4.15	1.97	5.06	2.40	4.51	98.19	65
MPV0807-1C	Malanzán Fm.	57.89	0.9	20.01	5.57	0.11	2.62	0.95	1.31	4.54	0.14	4.62	100.09	70
MPV0807-4C	Malanzán Fm.	60.50	0.68	17.5	5.57	0.05	1.57	1.11	0.83	2.97	0.23	8.15	99.17	74
OG5B	Malanzán Fm.	79.3	0.21	10.9	1.81	0.04	0.67	1.39	2.87	2.71	0.06	1.43	101.39	52
OPV0804-6C	Malanzán Fm.	53.73	0.9	16.46	6.42	0.06	2.24	0.67	2.46	3.62	0.18	13.2	99.94	65
OPV0805-2C	Malanzán Fm.	56.61	0.61	18.08	5.28	0.1	2.13	2.09	1.84	3.47	0.07	9.75	100.03	63
OPV0805-4C	Malanzán Fm.	51.78	1.14	20.2	7.36	0.1	3.6	0.96	1.94	4.01	0.18	8.65	99.92	70
MPV0808-2C	Malanzán Fm.	51.96	0.87	18.08	2.42	0.02	1.07	0.2	0.86	3.16	0.05	22.0	100.66	78
OPV0317-1	Loma Larga Fm.	72.8	0.6	12.3	4.3	0.07	1.75	0.71	2.02	2.68	0.13	2.73	97.54	63
OPV0805-6C	Loma Larga Fm.	52.03	0.78	16.31	4.87	0.09	2.48	4.4	1.20	3.38	0.14	12.0	97.68	55
OPV0805-7C	Loma Larga Fm.	57.36	0.9	18.98	5.71	0.05	2.34	0.62	1.68	3.85	0.14	8.54	100.17	71
OPV0805-9C	Loma Larga Fm.	64.24	0.75	17.02	4.49	0.05	2.01	1.16	1.35	3.06	0.15	6.11	100.39	70
OPV0318-8C	Loma Larga Fm.	59.59	0.63	19.9	4.22	0.06	1.47	0.96	2.16	3.11	0.11	6.78	98.99	70
OPV0318-1	Solca Fm.	64.9	0.73	14.6	4.89	0.13	2.22	2.2	1.60	3.06	0.05	5.51	99.89	60
OPV0318-3	Solca Fm.	67.3	0.57	15.9	4.79	0.08	1.6	1.23	0.63	3.04	0.02	5.77	100.94	71
OPV0318-2	Solca Fm.	66.6	0.7	15.4	4.49	0.1	1.97	1.29	1.04	3.35	0.04	4.13	99.11	67
OPV0318-4	Solca Fm.	65.5	0.68	15.8	5.89	0.1	1.88	1.68	1.34	3.05	0.06	4.75	100.73	65
OPV0318-7	Solca Fm.	66.34	0.55	15.21	5.05	0.06	1.59	1.52	0.71	3.01	0.04	5.19	99.27	68
OPV0318-5	Solca Fm.	67.9	0.59	14.7	4.13	0.09	1.59	1.29	0.43	2.85	0.04	5.26	98.87	71
OPV0318-6	Solca Fm.	68	0.5	13.2	3.59	0.08	1.41	2.92	0.60	3.05	0.04	6.59	99.98	58
OPV0805-11C	La Colina Fm.	53.73	1.01	26.3	7.58	0.04	0.18	0.24	0.04	1.91	0.04	8.90	99.97	91
LC0806-3C	La Colina Fm.	71.7	0.77	15.33	4.29	0.03	0.74	0.39	0.50	2.40	0.06	4.48	100.69	79
AT0806-1C	Arroyo Totoral Fm.	69.42	0.72	12.69	3.88	0.06	0.87	1.46	0.75	1.65	0.08	5.41	96.99	70
AT0806-2C	Arroyo Totoral Fm.	49.45	0.76	13.65	2.42	0.02	1.01	0.71	0.58	1.68	0.06	28.3	98.64	78

Table 2. Elemental abundances, loss-on-ignition (LOI), total analyzed abundances, CIA values for samples from the Oltá-Malanzán paleovalley sedimentary fill.

References

- Andreis, R.R., Cúneo, R., Rolón, A.D., 1984. Definición formal de los "Estratos de Arroyo Totoral" Pérmico inferior, Sierra de Los Llanos, Provincia de La Rioja. In: Actas del Congreso Geológico Argentino 9, p. 209–229.
- Andreis, R.R., Archangelsky, S., Leguizamón, R.R., 1986. El paleovalle de Malanzán: nuevos criterios para la estratigrafía del Neopaleozoico de la sierra de Los Llanos, La Rioja, República Argentina. *Boletín de la Academia Nacional de Ciencias (Córdoba)* 57, p. 1-119.
- Andreis, R.R., 1998. Evolution of fluvial systems in a late Paleozoic intramontane basin, Sierra de los Llanos, La Rioja Province, northwestern Argentina. 15th International Sedimentological Congress. International Association of Sedimentologists, Alicante, Spain, pp. 139.
- Archangelsky, A., Archangelsky, S., 1987. Tafoflora de la formación Tramojo, Paleozoico tardío, en la región de Uspallata, provincia de Mendoza, República Argentina. *Ameghiniana* 24, 251–256.
- Archangelsky, A., Archangelsky, S., 1987. Tafoflora de la formación Tramojo, Paleozoico tardío, en la región de Uspallata, provincia de Mendoza, República Argentina. *Ameghiniana* 24, 251–256.
- Archangelsky, S., Cúneo, R., 1991. Late Paleozoic floristic succession from northwestern Argentina. In Ulbrich, H., Rocha Campos, A.C. (eds.) *Gondwana 7th, Proceedings*, Instituto de Geociencias, USP, Brazil. 469 -481.
- Archangelsky, S., Sabbatini, N., Aceñolaza, F., Buatois, L.A., González, C., García, G., Césari, S., Ottone, E., Cúneo, R., Hünicken, M., Mazzoni, A., Gutiérrez, P., 1996. Paleontología y Bioestratigrafía de las Cuencas Paganzo, Calingasta-Uspallata, Río Blanco y San Rafael. In Archangelsky, S. (ed.) *El Sistema Pérmico en la República Argentina y en la República Oriental del Uruguay*. Academia Nacional de Ciencias, Córdoba. 177-201.
- Astini, R.A., Benedetto, J. L., & Vaccari, N. E. 1995. The Early Paleozoic evolution of the Argentine Precordillera as a Laurentian rifted, drifted and collided terrane: a geodynamic model. *Geological Society of America Bulletin*, 107, 253-273. doi: 10.1130/0016-7606(1995)107<0253:TEPEOT>2.3.CO;2
- Astini, R.A. 1998. Stratigraphical evidence supporting the rifting, drifting and collision of the Laurentian Precordillera terrane of western Argentina. In: Pankhurst, R. J. & Rapela, C. W. (eds) *The Proto-Andean Margin of Gondwana*. Geological Society, London, Special Publications, 142, 11-33. doi /10.1144/GSL.SP.1998.142.01.02
- Astini, R.A., Martina, F., Ezpeleta, M., Dávila, F.D., Cawood, P.A., 2009. Chronology from Rifting to Foreland Basin in the Paganzo Basin (Argentina), and a Reappraisal on the "eo- and Neohercynian" Tectonics along Western Gondwana., XII Congreso Geológico Chileno, Santiago, Chile. Universidad de Chile, Santiago, Chile, pp. 1–4 Extended Abstracts S9 010.
- Astini, R., 2010. Linked basins and sedimentary products across an accretionary margin: the case for the late history of the peri-Gondwanan Terra Australis orogen through the stratigraphic

- record of the Paganzo Basin. In: Papa, C., Astini, R. (eds.), Field Excursion Guidebook, 18th International Sedimentological Congress. International Association of Sedimentologists, Mendoza, Argentina, pp. 58.
- Aquino, C.D., Milana, J.P., Faccini, U.F., 2014. New glacial evidences at the Talacasto paleofjord (Paganzo basin, W-Argentina) and its implications for the paleogeography of the Gondwana margin. *Journal of South American Earth Sciences* 56, p. 278-300.
- Azcuy, C.A., 1975. Miosporas sel Namuriano y Westfaliano de la comarca de Malanzán-Loma Larga, provincia de La Rioja, Argentina. II, vol. 12. Descripciones sistemáticas y significado estratigráfico de las microfloras, Ameghiniana, pp. 113–163.
- Azcuy, C.L., Carrizo, H.A., Caminos, R., 1999. Carbonífero y Pérmico de las Sierras Pampeanas, Famatina, Precordillera, Cordillera Frontal y Bloque de San Rafael. *Instituto de Geología y Recursos Minerales, Geología Argentina* 29, 261–318.
- Bahlburg, H., Dobrzinski, N., 2011. A review of the Chemical Index of Alteration (CIA) and its application to the study of Neoproterozoic glacial deposits and climate transitions. In: Arnaud E., Halverson, G.P., Shields-Zhou, G. (Eds.) *The Geological Record of Neoproterozoic Glaciations*, Geological Society, London, *Memoirs* 36, p. 81-92.
- Bauluz, B., Mayayo, M.J., Fernandez-Nieto, C., Lopez, J.M.G., 2000. Geochemistry of Precambrian and Paleozoic siliciclastic rocks from the Iberian Range (NE Spain): implications for source-area weathering, sorting, provenance, and tectonic setting. *Chemical Geology* 168, p. 135–150.
- Brock, R. W., 1943. Weathering of igneous rocks near Hong Kong. *Geological Society of America Bulletin* 54, p. 717-738.
- Buatois, L.A., Mángano, M.G., 1995. Post glacial lacustrine event sedimentation in an ancient mountain setting: Carboniferous Lake Malanzán (western Argentina). *Journal of Paleolimnology* 14, p. 1–22.
- Caputo, M.V., Crowell, J.C., 1985. Migration of glacial centers across Gondwana during Paleozoic Era. *Geological Society of America Bulletin* 96, p. 1020-1036.
- Caputo, M. V., de Melo, J. H. G., Streef, M., Isbell, J. L., 2008. Late Devonian and Early Carboniferous glacial records of South America, in Fielding, C. R., Frank, T. D., and Isbell, J. L., eds., *Resolving the Late Paleozoic Ice Age in Time and Space: Boulder, CO*, Geological Society of America Special Publication, p. 161-173.
- Carignano, C., Cioccale, M., Rabassa, J., 1999. Landscape antiquity of the central-eastern Sierras Pampeanas (Argentina). *Geomorphological evolution since Gondwanic times: Zeitschrift für Geomorphologie Neue Folge* 118, p. 245–268.
- Césari, S.N., Limarino, C.O., Gulbranson, E.L., 2011. An Upper Paleozoic bio-chronostratigraphic scheme for the western margin of Gondwana. *Earth Sci. Rev.* 106, p. 149-160.
- Crowell, J.C., Frakes, L.A., 1970. Phanerozoic glaciation and the causes of ice ages. *American Journal of Science* 268, p. 193–224.

- Cúneo, R., 1984. Primeros resultados fitopaleoecológicos de la Formación Arroyo Totoral, Pérmico inferior de La Rioja, Argentina. *Actas IX del Congreso Geológico Argentino* 4: 318-336.
- Cúneo, R., 1986. Ecología de las floras neopaleozoicas argentinas. *Actas IV del Congreso Geológico Argentino Paleontología y Bioestratigrafía*, 1: 195-204. Mendoza
- Cúneo, R., 1987. Tafofloras de las Formaciones Solca y La Colina, Paleozoico superior de la Sierra de los Llanos, La Rioja, Argentina. *Annual Meeting Working Group, Project 211-IGCP (Abstracts)*, 72-75.
- Cúneo, 1990. Paleoecología de la Formación Solca, Carbonífero superior (Trampeaderense) de la sierra de Los Llanos, La Rioja. *Annual Meeting Working Group, Project 211-IGCP*. Buenos Aires.
- Cúneo, R., Archangelsky, A., 1996. Nuevos resultados fitopaleoecológicos de la Formación Arroyo Totoral, Pérmico inferior, Provincia de La Rioja. *Ameghiniana* 3 (2), p. 145-154.
- Dávila, F.M., Astini, R.A., Jordan, T.E., Gehrels, G., Ezpeleta, M., 2007. Miocene forebulge development previous to broken foreland partitioning in the southern Central Andes, west-central Argentina. *Tectonics* 26, TC5016, doi:10.1029/2007TC002118.
- Dykstra, M., Kneller, B., Milana, J.P., 2006. Deglacial and postglacial sedimentary architecture in a deeply incised paleovalley–paleofjord — the Pennsylvanian (late Carboniferous) Jejenes Formation, San Juan, Argentina. *Geological Society of America Bulletin* 118, p. 913–937.
- Enkelmann, E., Ridgway, K.D., Carignano, C., Linnemann, U., 2014. A thermochronometric view into an ancient landscape: tectonic setting, and inversion of the Paleozoic eastern Paganzo basin, Argentina. *Lithosphere* 6, p. 93–107.
- Enkelmann, E., Garver, J.I., 2015. Low-temperature thermochronology applied to ancient settings. *Journal of Geodynamics* 93, p. 17-30.
- Eyles, C.H., Eyles, N., França, A.B., 1993. Glaciation and tectonics in an active intracratonic basin: The late Paleozoic Itararé Group, Paraná Basin, Brazil: *Sedimentology* 40, p. 1–25, doi: 10.1111/j.1365-3091.1993.tb01087.x.
- Fedo, C.M., Nesbitt, H.W., Young, G.M., 1995. Unraveling the effects of potassium metasomatism in sedimentary rocks and paleosols, with implications for paleoweathering conditions and provenance: *Geology* 23, p.921-924.
- Fernandez-Seveso, F., Tankard, A.J., 1995. Tectonics and stratigraphy of the late Paleozoic Paganzo Basin of western Argentina and its regional implications. In: Tankard, A.J., Soruco, R.S., Welsink, H.J. (Eds.), *Petroleum Basins of South America: AAPG Memoir*, 62, pp. 285–301.
- Fielding, C.R., Frank, T.D., Isbell, J.L., 2008a. The late Paleozoic ice age—A review of current understanding and synthesis of global climate patterns, in Fielding, C.R., Frank, T.D., and Isbell, J.L., eds., *Resolving the Late Paleozoic Ice Age in Time and Space*. *Geological Society of America Special Paper* 441, p. 343-354.

- Fielding, C.R., Frank, T.D., Birgenheier, L.P., Rygel, M.C., Jones, A.T., Roberts, J., 2008b. Stratigraphic imprint of the Late Paleozoic Ice Age in eastern Australia: a record of alternating glacial and nonglacial climate regime. *Journal of the Geological Society, London* 165, p. 129-140.
- Fielding, C.R., Frank, T.D., Birgenheier, L.P., Rygel, M.C., Jones, A.T., Roberts, J., 2008b. Stratigraphic record and facies associations of the late Paleozoic ice age in eastern Australia (New South Wales and Queensland). In: Fielding, C.R., Frank, T., Isbell, J.L. (Eds.), *Resolving the Late Paleozoic Ice Age in Time and Space*. Geological Society of America Special Paper 441, pp. 41-57.
- Frakes, L.A., 1979. *Climates throughout geologic time*. Elsevier, Amsterdam, 310 p.
- Frakes, L.A., Crowell, J.C., 1969. Late Paleozoic glaciation: I, South America. *Geological Society of America Bulletin* 80, p. 1007-1042.
- Frank, T. D., Shultis, A. I., Fielding, C. R., 2015, Acme and demise of the late Palaeozoic ice age: A view from the southeastern margin of Gondwana: *Palaeogeography Palaeoclimatology Palaeoecology* 418, p. 176-192.
- Garzanti, E., Resentini, A., 2016. Provenance control on chemical indices of weathering. *Sedimentary Geology* 336, p. 81-95.
- Gastaldo, R.A., DiMichele, W.A., Pfefferkorn, H.W., 1996. Out of the icehouse into the greenhouse: a late Paleozoic analogue for modern global vegetational change. *GSA Today* 10, p. 1-7.
- Goldberg, K., Humayun, M., 2010. The applicability of the Chemical Index of Alteration as a paleoclimatic indicator: An example from the Permian of the Paraná Basin, Brazil. *Palaeogeography, Palaeoclimatology, Palaeoecology* 293, p. 175-183.
- González, C.R., Díaz Saravia, P., 2010. Bimodal character of the Late Paleozoic glaciations in Argentina and bipolarity of climatic changes. *Palaeogeography, Palaeoclimatology, Palaeoecology* 298, p. 101-111.
- Grant, W. H., 1963. Weathering of Stone Mountain Granite, in Ingersoll, E., ed., *Clays and Clay Minerals*: Oxford, Pergamon, p. 65-73.
- Griffis, N.P., Mundil, R., Montañez, I.P., Isbell, J., Fedorchuk, N., Vesely, F., Iannuzzi, R., Qing-Zhu, Y., 2018. A new stratigraphic framework built on U-Pb single zircon TIMS ages with implications for the timing of the Penultimate Icehouse (Paraná Basin, Brazil). *Geological Society of America Bulletin* 130, p. 848-858. doi: 10.1130/B31775.1.
- Güena, S.E., Escosteguy, L.D., Limarino, C.O., 2010, Paleomagnetism of the Carboniferous-Permian Patquía Formation Paganzo basin, Argentina: implications for the apparent polar wander path for South America and Gondwana during the Late Paleozoic: *Geologica Acta* 8 (4), p. 373-397.
- Gulbranson E.L., Montañez, I.P., Schmitz, M.D., Limarino, C.O., Isbell, J.L., Marensi, S.A., Crowley, J.L., 2010, High-precision U–Pb calibration of Carboniferous glaciation and

- climate history, Paganzo Group, NW Argentina. *Geological Society of America Bulletin* 122, p. 1480–1498.
- Gulbranson, E.L., Montañez, I.P., Tabor, N., Limarino, C.O., 2015. Late Pennsylvanian aridification on the southwestern margin of Gondwana (Paganzo Basin, NW Argentina): A regional expression of a global climate perturbation. *Palaeogeography Palaeoclimatology Palaeoecology* 417, p. 220–235.
- Gutiérrez, P. R., and Limarino, C. O., 2001. Palinología de la Formación Malanzán (Carbonífero Superior), La Rioja, Argentina; nuevos datos y consideraciones paleoambientales. *Ameghiniana* 38 (1), p. 99-118.
- Heckel, P.H., 1994, Evaluation of evidence for glacio-eustatic control over marine Pennsylvanian cyclothems in North America and consideration of possible tectonic effects: In: Dennison, J.M., Ettensohn, F.R. (Eds.), *Tectonic and eustatic controls on sedimentary cycles. SEPM (Society for Sedimentary Geology) Concepts in Sedimentology and Paleontology* 4, p. 65–87.
- Heckel, P.H., 2008. Pennsylvanian cyclothems in midcontinent North America as far-field effects of waxing and waning of Gondwana ice sheets. In: Fielding, C.R., Frank, T., Isbell, J.L. (Eds.), *Resolving the Late Paleozoic Ice Age in Time and Space: Geological Society of America Special Paper* 441, p. 275–289.
- Henry, L.C., Isbell, J.L., Limarino, C.O., 2008, Carboniferous glaciogenic deposits of the Protoprecordillera of west central Argentina. In: Fielding, C.R., Frank, T.D., Isbell, J.L. (Eds.), *Resolving the Late Paleozoic Ice Age in Time and Space. Geological Society of America Special Paper* 441, p. 131–142.
- Henry L.C., Isbell, J.L., Limarino, C.O., McHenry, L.J., Fraiser, M.L., 2010. Mid-Carboniferous deglaciation of the Protoprecordillera, Argentina, recorded in the Agua de Jagüel paleovalley. *Palaeogeography, Palaeoclimatology, Palaeoecology* 298, p. 112–129.
- Horton D.E., Poulsen, C.J., 2009. Paradox of late Paleozoic glacioeustasy. *Geology* 37, p. 715–718.
- Isbell, J.L., Miller, M.F., Wolfe, K.L. & Lenaker, P.A., 2003, Timing of late Paleozoic glaciation in Gondwana: was glaciation responsible for the development of northern hemisphere cyclothems?. In: Chan, M.A., Archer, A.W. (Eds.), *Extreme depositional environments: mega end members in geologic time. Geological Society of America Special Paper*, 5-24.
- Isbell, J.L., Fraiser, M.L., Henry, L.C., 2008, Examining the complexity of environmental change during the late Paleozoic and early Mesozoic. *Palaios* 23 (5-6), p. 267-269.
- Isbell, J.L., Henry, L.C., Gulbranson, E.L., Limarino, C.O., Fraiser, M.L., Koch, Z.J., Ciccioli, P.L. & Dineen, A.A., 2012. Glacial paradoxes during the late Paleozoic ice age: Evaluating the equilibrium line altitude as a control on glaciation. *Gondwana Research* 22, p. 1-19.
- Jordan, T.E., Zeitler, P., Ramos, V., Gleadow, A.J.W., 1989. Thermochronometric data on the development of the basement peneplain in the Sierras Pampeanas, Argentina. *Journal of South American Earth Sciences* 2 (3), p. 207-222.

- Kneller, B., Milana, J.P., Buckee, C., Al Ja'aidi, O.S., 2004. A depositional record of deglaciation in a paleofjord (Late Carboniferous [Pennsylvanian] of San Juan Province, Argentina): the role of catastrophic sedimentation. *Geological Society of America Bulletin* 116, 348–367.
- Krapovickas, V., Mancuso, A.C., Arcucci, A., Caselli, A., 2010. Fluvial and eolian ichnofaunas from the Lower Permian of South America (Patquía Formation, Paganzo Basin). *Geologica Acta* 8 (4), p. 449-462.
- Lawver, L.A., Dalziel, I.W.D., Norton, I.O., Gahagan, L.M., 2008. The Plates 2007 Atlas of Plate Reconstructions (750 Ma to Present Day), Plates Progress Report No. 305–0307. University of Texas Technical Report No. 195, 160 pp.
- Limarino, C.O., Andreis, R.R., Ferrando, L., 1996. Paleoclimas del Paleozoico Tardío. In In Archangelsky, S. (ed.) *El Sistema Pérmico en la República Argentina y en la República Oriental del Uruguay*. Academia Nacional de Ciencias, Córdoba. 177-201.
- Limarino, C.O., Césari, S.N., Net, L.I., Marensi, S.A., Gutiérrez, P.R., Tripaldi, A., 2002. The Upper Carboniferous postglacial transgression in the Paganzo and Río Blanco Basins (northwestern Argentina): facies and stratigraphic significance. *Journal of South American Earth Sciences* 15, p. 445–460.
- Limarino, C.O., Tripaldi, A., Marensi, S., Fauqué, L., 2006. Tectonic, sea level, and climatic controls on late Paleozoic sedimentation in the western basins of Argentina. *Journal of South American Earth Sciences* 33, p. 205–226.
- Limarino, C.O., Césari, S.N., Spalleti, L.A., Taboada, A.C., Isbell, J.L., Geuna, S., Gulbranson, E.L., 2014. A paleoclimatic review of southern South America during the late Paleozoic; A record from icehouse to extreme greenhouse conditions. *Gondwana Research*, v. 25, p. 1396-1421.
- López-Gamundí, O.R., Espejo, I.S., Conaghan, P.J., Powell, C.McA., Veevers, J.J., 1994. Southern South America. In: Veevers, J.J., Powell, C.McA. (Eds.), *Permian–Triassic Pangean basins and foldbelts along the Panthalassan margin of Gondwanaland*. Boulder, Colorado: Geological Society of America Memoir 184, p. 281–329.
- López Gamundí, O.R., 1997. Glacial–postglacial transition in the late Paleozoic basins of southern South America. In: Martini, I.P. (Ed.), *Late Glacial and Postglacial Environmental Changes. Quaternary, Carboniferous–Permian, and Proterozoic*. Oxford University Press, Oxford, UK, pp. 147–168.
- López Gamundí, O.R., Martínez, M., 2000. Evidence of glacial abrasion in the Calingasta–Uspallata and western Paganzo Basins, mid-Carboniferous of western Argentina. *Palaeogeography, Palaeoclimatology, Palaeoecology* 159, 145–165.
- Mack, G.H., James, W.C., Monger, H.C., 1993. Classification of paleosols. *Geological Society of America Bulletin* 105, 129–136.
- Martina, F., Canelo, H.N., Dávila, F.M., Hollanda, M.H.B.M, Teixeira, W., 2018. Mississippian lamprhyre dikes in western Sierras Pampeanas, Argentina: Evidence of transtensional

- tectonics along the SW margin of Gondwana. *Journal of South American Earth Sciences* 83, 68-80.
- Maynard, J.B., 1992. Chemistry of modern soils as a guide to interpreting Precambrian paleosols. *Journal of Geology* 100, 279–289.
- McHenry, L.J., 2009. Element mobility during zeolitic and argillic alteration of volcanic ash in a closed-basin lacustrine environment: case study Olduvai Gorge, Tanzania. *Chemical Geology* 265, p. 540–552.
- McHenry, L.J., Carson, G.L., Dixon, D.T., Vickery, C.L., 2017. Secondary minerals associated with Lassen fumaroles and hot springs: Implications for martian hydrothermal deposits. *American Mineralogist* 102, p. 1418-1434. Doi: 10.2138/am-2107-5839
- Metcalfe, I., Crowley, J. L., Nicoll, R. S., and Schmitz, M., 2015. High-precision U-Pb CA-TIMS calibration of Middle Permian to Lower Triassic sequences, mass extinction and extreme climate-change in eastern Australian Gondwana. *Gondwana Research* 28, p. 61-81.
- Montañez, I.P., Tabor, N.J., Niemeier, D., DiMichele, W.A., Frank, T.D., Fielding, C.R., Isbell, J.L., Birgenheir, L.P., Rygel, M.C., 2007, CO₂-forced climate and vegetative instability during late Paleozoic deglaciation: *Science* 315, p. 87–91.
- Montañez, I.P., Poulsen, C.J., 2013, The late Paleozoic ice age: An evolving paradigm. *Annual Review of Earth and Planetary Sciences* 41, p. 24.1-24.
- Moxness, L.D., Isbell, J.L., Pauls, K.N., Limarino, C.O., Schencman, J., 2018, Sedimentology of the mid-Carboniferous fill of the Olta paleovalley, eastern Paganzo Basin, Argentina: Implications for glaciation and controls on diachronous deglaciation in western Gondwana during the late Paleozoic Ice Age. *Journal of South American Earth Sciences* 84, p 127-148. doi/10.1016/j.jsames.2018.03.015
- Nesbitt, H.W., Markovics, G., Price, R. C., 1980. Chemical processes affecting alkalis and alkaline earths during continental weathering. *Geochimica et Cosmochimica Acta* 44, p. 1659-1666.
- Nesbitt, H.W., Young, G.M., 1982, Early Proterozoic climates and plate motions inferred from major element chemistry from lutites. *Nature* 199, p. 715-717.
- Nesbitt, H.W., Young, G.M., 1989. Formation and diagenesis of weathering profiles. *Journal of Geology* 97, p. 129-147.
- Nesbitt, H.W., Young, G.M., 1996. Petrogenesis of sediments in the absence of chemical weathering: effects of abrasion and sorting on bulk composition and mineralogy. *Sedimentology*, v. 42, p. 341-358.
- Nesbitt, H.W., Fedo, C.M., Young, G.M., 1997. Quartz and feldspar stability, steady and non-steady-state weathering, and petrogenesis of siliciclastic sands and muds. *Journal of Geology* 105, p. 173-192.

- Nesbitt, H.W., Markovics, G., 1997. Weathering of granodioritic crust, long-term storage of elements in weathering profiles and petrogenesis of siliciclastic sediments. *Geochimica et Cosmochimica Acta* 61 (8), p. 1653-1670.
- Net, L.I., Limarino, C.O., 1999. Paleogeografía y correlación estratigráfica del Paleozoico Tardío de la Sierra de Los Llanos, provincia de La Rioja, Argentina. *Revista de la Asociación Geológica Argentina* 54 (3), p. 229-239.
- Net, L.I., Alonso, M.S., Limarino, C.O., 2002. Source rock and environmental control on clay mineral associations, lower section of Paganzo group (Carboniferous), northwest Argentina. *Sedimentary Geology* 152, p. 83-199.
- Net, L.I., Limarino, C.O., 2006. Applying sandstone petrofacies to unravel the Upper Carboniferous evolution of the Paganzo Basin, northwest Argentina. *Journal of South American Earth Sciences* 22, p. 239-254.
- Pankhurst, R.J., Rapela, C.W., Saavedra, J., Baldo, E., Dahlquist, J., Pascua, I., Fanning, C.M., 1998. The Famatinian magmatic arc in the Central Sierras Pampeanas: An early to mid-Ordovician continental arc on the Gondwana margin. In: Pankhurst, R.J., Rapela, C.W. (Eds.) *The Proto-Andean Margin of Gondwana*. Geological Society of London Special Publication 142, 343-367.
- Pankhurst, R.J., Rapela, C.W., Fanning, C.M., 2000. Age and origin of coeval TTG, I- and S-type granites in the Famatinian belt of NW Argentina. *Earth and Environmental Science Transactions of the Royal Society of Edinburgh*, 91, 151-168.
- Pérez Loinaze, V.P., 2009. New palynological data from the Malanzán Formation (Carboniferous), La Rioja Province, Argentina. *Ameghiniana* 46, p. 495-512.
- Price, J.R., Velbel, M.A., 2003. Chemical weathering indices applied to weathering profiles developed on heterogeneous felsic metamorphic parent rocks. *Chemical Geology* 202, 397-416.
- Rabassa, J., Carignano, C., Cioccale, M., 2014. A general overview of Gondwana landscapes in Argentina. In: Rabassa, J., Ollier, C. (Eds.), *Gondwana Landscapes in Southern South America: Argentina, Uruguay and southern Brazil*. Springer Earth System Science, Dordrecht, Heidelberg, New York, London, 201-245.
- Ramos, V.A., 1988. Tectonics of the Late Proterozoic-Early Paleozoic: a collisional history of Southern South America. *Episodes* 11, 168-174.
- Ramos, V.A., Dallmeyer, D. y Vujovich, G., 1998. Time constraints on the Early Paleozoic docking of the Precordillera, Central Argentina. In: Pankhurst, R. y Rapela, C. (Eds.): *The Proto-Andean Margin of Gondwana*, Geological Society, London, Special Publication, 142, 143-158.
- Ramos, V.A., 1999. Evolución tectónica de la Argentina. In: *Rasgos Estructurales del Territorio Argentino*. Instituto de Geología y Recursos Minerales, Geología Argentina Anales 29 (24), 715-784.

- Ramos, V.A., Folguera, A., 2009. Andean flat-slab subduction through time. Geological Society, London, Special Publication 327, 31-54.
- Ramos, V.A., Escayola, M., Leal, P., Pimentel, M.M., Santos, J.O.S., 2015. The late stages of the Pampean Orogeny, C_ordoba (Argentina): Evidence of postcollisional Early Cambrian slab break-off magmatism. *Journal of South American Earth Sciences* 64, 351-364. doi: 10.1016/j.jsames.2015.08.002.
- Royer, D. L., Berner, R. A., Montañez, I. P., Tabor, N. J., and Beerling, D. J., 2004, CO₂ as a primary driver of Phanerozoic climate, *GSA Today* 14 (3), 4-10.
- Rygel, M.C., Fielding, C.R., Frank, T.D., Birgenheier, L.P., 2008. The magnitude of late Paleozoic glacioeustatic fluctuations: a synthesis. *Journal of Sedimentary Research* 78, 500–511.
- Sand, L. B., and Bates, T. L., 1953. Mineralogy of the residual kaolins of the Southern Appalachians. *Am. Mineral.* 38, 358-372.
- Scotese, C.R., 1997. The PALEOMAP Project: paleogeographic atlas and plate tectonic software. Department of Geology, University of Texas, TX.
- Scotese, C.R., Barrett, S.F., 1990. Gondwana's movement over the South Pole during the Palaeozoic: evidence from lithological indicators of climate. In: McKerrow, W.S., Scotese, C.R. (Eds.), *Palaeozoic Palaeogeography and Biogeography*, Geological Society, London, *Memoirs* 12, 75–85.
- Sheldon, N.D., 2006. Abrupt chemical weathering increase across the Permian–Triassic boundary. *Palaeogeography, Palaeoclimatology, Palaeoecology* 231, 315–321.
- Sheldon, N.D., Tabor, N.J., 2009. Quantitative paleoenvironmental and paleoclimatic reconstruction using paleosols. *Earth Science Reviews* 95, 1–52.
- Slaymaker, O., Kelly, R.E., 2007. The transience of the cryosphere and transitional landscapes. In: *The Cryosphere and Global Environmental Change*. Blackwell Publishing, Massachusetts, Oxford, Australia, 158-195.
- Socha B., Carignano, C., Rabassa, J., Mickelson, D., 2014. Gondwana glacial paleolandscape, diamictite record of Carboniferous valley glaciation and preglacial remnants of an ancient weathering front in Northwestern Argentina, in *Gondwana Landscapes in southern South America*. In: Rabassa, J., Ollier, C. (Eds.), *Gondwana Landscapes in Southern South America*. Springer, Dordrecht, 331-363.
- Soreghan, M.J., Soreghan, G.S., 2007. Whole-rock geochemistry of upper Paleozoic loessite, western Pangaea: implications for paleo-atmospheric circulation. *Earth and Planetary Science Letters* 255, 117–132.
- Sterren, A.F., Martínez, M., 1996. El paleovalle de Olta (Carbonífero): paleoambientes y paleogeografía. 13° Congreso Geológico Argentino y 3° Congreso Exploración de Hidrocarburos (Buenos Aires), *Actas* 2, 89-103.

- Taboada, A.C., 1985. Estratigrafía Y contenido paleontológico de la Formación Agua del Jagüel, Pérmico Inferior de la Precordillera Mendocina. Primeras Jornadas Sobre Geología de Precordillera, San Juan Acta I, San Juan.
- Taboada, A.C. 2010. Mississippian-Early Permian brachiopods from western Argentina: Tools for middle- to high-latitude correlation, paleobiogeographic and paleoclimatic reconstruction. *Palaeogeography, Palaeoclimatology, Palaeoecology* 298, 152-73.
- Tabor, N. J., and Poulsen, C. J., 2008, Palaeoclimate across the Late Pennsylvanian-Early Permian tropical palaeolatitudes; a review of climate indicators, their distribution, and relation to palaeophysiographic climate factors. *Palaeogeography, Palaeoclimatology, Palaeoecology* 268 (3-4), 293-310.
- Tedesco, A., Ciccioli, P., Suriano, J., Limarino, C., in press. Changes in the architecture of fluvial deposits in the Paganzo Basin (Upper Paleozoic of San Juan Province): an example of sea level and climatic controls on the development of coastal fluvial environments. *Geologica Acta*. doi: [10.1344/105.000001583](https://doi.org/10.1344/105.000001583)
- Veevers, J.J., Powell, M., 1987. Late Paleozoic glacial episodes in Gondwanaland reflected in transgressive–regressive depositional sequences in Euramerica. *Geological Society of America Bulletin* 98, 475–487.
- Visser, J.N.J., 1997. Deglaciation sequences in the Permo-Carboniferous Karoo and Kalahari basins of southern Africa. a tool in the analysis of cyclic glaciomarine basin fills. *Sedimentology* 44, 507–521.
- Wahlstrom, E. E., 1948. Pre-Fountain and recent weathering on Flagstaff Mountain near Boulder, Colorado. *Geological Society of America Bulletin* 59, 1173-1190.
- Weaver, C. E., 1967. Potassium, illite, and the oceans. *Geochimica et Cosmochimica Acta* 31, 281-296.
- Weaver, C. E., Pollard, L. D., 1973. *The Chemistry Minerals*. Amsterdam, Elsevier, 213 p.

Chapter 4. Late Paleozoic paleoclimate reconstruction of the Paganzo Basin of western Argentina: Controls on early Pennsylvanian deglaciation in western South American Gondwana

Abstract

While the late Paleozoic ice age was the result of a combination of both global and regional drivers, the subsequent glaciation and deglaciation were asynchronous across Gondwana, specifically along the southwest margin. Testing in the mid-paleolatitude basins of South American Gondwana (i.e. Paganzo, Calingasta-Uspallata and Río Blanco basins of Argentina and the Paraná Basin in Brazil) provided an opportunity to show the effects of the local climate drivers in that region. A complete paleoclimate reconstruction using the Chemical Index of Alteration (CIA) as a proxy displays a dynamic climate transition for this region. The strata of the western active margin basins (i.e. Paganzo, Calingasta-Uspallata and Río Blanco basins) record a drastic shift in climate conditions from glacial to extreme desert conditions by the early Permian. Glaciation in these basins occurs solely along the Protoprecordilleran range, which was a significant uplift that separated the western interior retroarc-foreland basin (i.e. Paganzo Basin) from the western arc-related basins (i.e. Calingasta-Uspallata and Río Blanco basins). This uplift caused a rain shadow that prevented glaciation from occurring along the eastern margin of the Paganzo Basin. Later in the Pennsylvanian and Permian, the transition to an extremely arid environment can be linked to the shift in active tectonism and the development of a volcanic arc outboard of the western margin of Gondwana. Based on these findings, the main climate forcing mechanism in the western active margin basins was tectonism, which differs from the climate transition of the southeastern Paraná Basin in Brazil, which is along a similar paleolatitude. The

Paraná Basin experiences a shift from glacial climate to temperate climate almost 20 Ma later than the western margin basins.

1. Introduction

Global climate change is the result of interactions between the atmosphere, geosphere and hydrosphere. In climate change studies, as well as those of ancient climate systems, driving and feedback mechanisms are quite complex. Regions of Earth respond differently based on the interplay between global-scale and local-to-regional-scale drivers. Thus, regional-scale studies of deep time environmental transitions at high chronostratigraphic resolution add to our understanding of environmental responses to changing global climate. The climatic shift at the end of the Paleozoic is of significant interest because it is an analogue for current global change (cf. Gastaldo et al., 1996). The late Paleozoic ice age (LPIA) was the longest-lived ice age (approximately 360-255 million years ago) of the Phanerozoic (cf. Gastaldo et al., 1996; Montañez and Poulsen, 2013). Furthermore, the LPIA is the only example of when a vegetated and biologically complex Earth shifted from an icehouse to a greenhouse state (Gastaldo et al., 1996; Montañez et al., 2007; Fielding et al., 2008a; Isbell et al., 2012; Montañez and Poulsen, 2013; Limarino et al., 2014). Because of this, the LPIA has the potential to test driving mechanisms that influence changing climatic regimes, which in turn provide insight into how such drivers affect modern climate change, thus enabling the scientific community to understand natural versus anthropomorphic climate change.

Glaciation during the LPIA occurred episodically over intervals of one to several million years duration at different times across Gondwana. (Figs. 24, 25). The first LPIA glacial events occurred in northern South America and northern Africa during the late Devonian (the Frasnian

or Famennian; Caputo and Crowell, 1985; Isaacson et al., 2008). Glaciation then expanded across the western and southern basins of South America (e.g., Bolivia, western Argentina, Patagonia (cf. Caputo and Crowell, 1985; Isbell et al., 2003, 2012; Kołtonik et al., 2019; Rosa et al., 2019; Ezpeleta et al., 2020). In the western Argentine basins, the final glacial event ended during the early Bashkirian (Isbell et al., 2012; Limarino et al., 2014). While glaciation continued in eastern South America (i.e. Paraná, Sauce Grande and Chaco-Paraná basins) and Africa during the rest of the Carboniferous and into the Permian (Caputo and Crowell, 1985; Veevers and Powell, 1987; Eyles et al., 1993; López-Gamundí, 1997; Isbell et al., 2003, 2012; Caputo et al., 2008; Pérez Loinaze et al., 2010; Fielding et al. 2008a; Limarino et al., 2014; Mottin et al., 2018; Griffis et al., 2019), which suggest a diachronous development of glacial centers during the LPIA, followed by a stepped deglaciation across South America, and possibly the whole of Gondwana.

Studies have highlighted potential driving mechanisms for these changing climatic conditions, such as the drift of Gondwana across the paleo South Pole, changes in the configurations of the continental plates, changes in atmospheric CO₂, changes in insolation due to orbital parameters, and orogenic events (cf. Caputo and Crowell, 1985; Scotese and Barrett, 1990; Eyles et al., 1993; Heckel, 1994, 2008; Isbell et al., 2003, 2008; 2012; Royer et al., 2004; Montañez et al., 2007; Rygel et al., 2008; Horton and Poulsen, 2009; Tabor and Poulsen, 2008; Gulbranson et al., 2010; Montañez and Poulsen, 2013; Limarino et al., 2014). While global drivers account for some trends in the occurrence and disappearance of glacial centers across Gondwana, they cannot completely account for the glacial-interglacial periods within specific regions (i.e. South American glacial intervals vs. African intervals vs. Antarctic and Australian intervals) and they do not account for the disappearance of glacial centers in the western basins

of Argentina while glaciation at the same paleolatitude farther east continued. Instead, climatic changes during the Pennsylvanian in western Argentina are more likely the result of local, or regional, drivers (cf. Isbell et al., 2012; Montañez and Poulsen, 2013; Spalletti et al., 2012; Limarino et al., 2014). Therefore, studies of this region provide new insights into LPIA glaciations on a regional scale and the forcing and feedback mechanisms that caused them.

This paper presents a quantitative high-resolution record of paleoclimate during the Carboniferous-Permian transition of the sedimentary basins of southwestern Gondwana, focusing on the Paganzo and Calingasta-Uspallata basins of Argentina (Fig. 24). The western margin and retroarc basins of Argentina present a unique problem in that glacial ice developed during the Tournasian (Early Mississippian) and then disappeared in the Bashkirian (Early Pennsylvanian) while glaciation in other parts of Gondwana at similar paleo-latitudes, such as the southern Paraná Basin in Brazil, persisted to the end of the Carboniferous and possibly into the Earliest Permian (López-Gamundí et al., 1994; López-Gamundí, 1997; Holz et al., 2008; Caputo et al., 2008; Henry et al., 2008; Rocha-Campos et al., 2008; Limarino et al., 2014; Mottin et al., 2018; Griffis et al., 2019; Ezpeleta et al., 2020; Fig. 25). To demonstrate and evaluate this climate shift on a regional scale we: 1) create a high-resolution paleoclimate reconstruction for the late Paleozoic strata of the Paganzo and Calingasta-Uspallata basins using the Chemical Index of Alteration (CIA); 2) use these new data to test climate forcing and driving mechanisms regarding the drastic shift from a humid to arid environment; and 3) evaluate the current understanding of deglaciation across west central Gondwana, from the basins of western Argentina to the Paraná Basin of Brazil.

2. Regional Geologic Setting

2.1 Late Paleozoic basins of South America

Southern South America contains numerous late Paleozoic basins filled with sedimentary and volcanic rocks. Following the categorization of Limarino and Spalletti (2006), these basins are of two categories: intraplate basins (e.g. Chaco-Paraná and Paraná basins) and western active margin basins (e.g. Paganzo, Calingasta-Uspallata and Río Blanco basins). These eastern intraplate basins were separated from the western active margin basins by the Pampean Arch, and the western active margin basins were separated by a series of uplands that make up the current Sierras Pampeanas and the Precordilleran ranges (Limarino and Spalletti, 2006; Limarino et al., 2014; Fig. 24).

The Paganzo Basin spans an area of approximately 144,000 km² at its largest extent and is bounded today by the eastern Sierras Pampeanas to the east, north and south, and the Precordilleran range in the west (Fig. 24). The development and structure of the Paganzo Basin is still under debate. Some studies have identified it as a retroarc foreland basin (Ramos, 1988; Limarino and Spalletti, 2006; Limarino et al., 2014), a rift basin (Astini et al., 1995, 2009; Astini, 2010), or as a strike-slip pull-apart basin along the Panthalassan margin of Gondwana (Limarino et al., 2002a; Milana and Di Pasquo, 2019). Regardless of the exact type of basin, it was a significant catchment for late Paleozoic sediments, and records evidence of the glacial to post-glacial climate transition in the Carboniferous followed by extreme aridification in the early Permian (Limarino et al., 2014). Evidence from the middle Carboniferous sediments indicates that there were multiple separate depositional centers (cf. López-Gamundí et al., 1994; Pauls et

al., in review), that were in part separated by the various paleotopographic highs throughout the region (i.e. Pie de Palo Arch, Famatina Arch, and Sierras de Chepes, Los Llanos region; Fig. 24).

The Calingasta-Uspallata Basin is an arc-related basin formed in a tectonically and magmatically active region of the western Gondwana margin (Fig. 24). It is bounded to the east by the Protoprecordillera and to the west by a volcanic arc, which was located in present-day Chile (Azcu, 1999). Subsidence occurred in the basin from the Early Carboniferous until the early Permian ending during the San Rafael orogeny, which caused local metamorphism, deformation, and extensive magmatism (López-Gamundí et al., 1994; Azcu et al., 1999; Limarino et al., 2014). The basin fill is predominantly marine and contains a near complete succession of the glacial to post-glacial transition (Limarino et al., 2014).

The Paraná Basin stretches from present-day south-central Brazil southward into Paraguay, Uruguay, and Argentina, and during the late Paleozoic was adjacent to and extended into western Namibia, Africa (Eyles et al., 1993; França, 1994; Milani et al., 1994; Rocha-Campos et al., 2008). For this study, only the southern portion of the Paraná Basin (i.e. the area of Rio Grande do Sul State; Fig. 24) will be considered. This region over time experienced a wide variety of environments, ranging from glacial, to post glacial, to a perhumid environment with transgressions and regressions within an intracratonic sea.

2.2. Rise and fall of the Protoprecordillera

Evidence for middle Carboniferous glaciation in the western margin basins comes from an inferred paleotopographic high located in the Precordillera region of Argentina. This upland, known as the Protoprecordillera (cf. proto-Precordillera of Amos and Rolleri, 1965; González Bonorino, 1975; Fig. 24) or the Tontal Arch (cf. Milana and Berscowski, 1987, 1990, 1993;

Milana, 1988; Milana et al., 1987; Astini, 2010; Aquino et al., 2014; Valdez-Buso et al., 2017, 2020; Milana and di Pasquo, 2019) defined the western margin of the Paganzo Basin in what is now the Precordilleran region of the western Sierras Pampeanas and separated this basin from the Calingasta-Uspallata and Río Blanco basins on the west (López-Gamundí et al., 1994, 1997; Limarino et al., 2002a, 2002b, 2006; Kneller et al., 2004; Dykstra et al., 2006; Henry, 2007; Henry et al., 2008, 2010; Astini, 2010; Gulbranson et al., 2010; Césari et al., 2011; Isbell et al., 2012; Aquino et al., 2014; Alonso-Muruaga et al., 2018). This highland formed during the Chañic Orogeny (middle Devonian to earliest Mississippian; Fig. 26) due to the accretion of the Chilenia Terrane (Fig. 27). As a result, the obduction of the accretionary prism formed an uplifted fold and thrust belt, referred to here as the Protoprecordillera (González Bonorino, 1975; Ramos et al., 1984, 1986, 1998; Ramos, 1988; López-Gamundí et al., 1994; Limarino et al., 2002, 2006, 2014; Henry et al., 2008; Isbell et al., 2012; Moxness et al., 2018; Pauls et al., 2019; Fig. 27). It is interpreted that by the Visean at the latest, it was a significant and discontinuous mountain belt along the western margin of Argentine Gondwana (López-Gamundí et al., 1994; Limarino et al., 2002a, 2006, 2014; Henry et al., 2008; Isbell et al., 2012; Moxness et al., 2018; Pauls et al., 2019). This interpretation is based on evidence that incised paleovalleys, with up to 2,500 meters or more in relief, radiate from a high in the Precordilleran region of Argentina (cf. López-Gamundí et al., 1997; Limarino et al., 2002a, 2002b, 2006; Kneller et al., 2004; Dykstra et al., 2006; Henry, 2007; Henry et al., 2008, 2010; Astini, 2010; Gulbranson et al., 2010; Césari et al., 2011; Isbell et al., 2012; Aquino et al., 2014; Alonso-Muruaga et al., 2018; Pauls et al., in review). These paleovalleys contain glacial deposits at the base of each section that are at least of Visean-Serpukhovian age and indicate that this mountain belt was above the equilibrium-line altitude for its paleolatitude of approximately 50-60° (cf. Isbell et al., 2012).

Continued subduction along the western margin into the Pennsylvanian is recorded as volcanic rocks and ash layers that range in age from 320-280 Ma (Willner et al., 2005, 2008; Fig. 26) and is tied to an outboard volcanic arc. As the active subduction moved further westward during the Pennsylvanian, studies interpret the collapse of the Protoprecordilleran range as the barrier between the Panthalassan margin and the continental interior was breached (Ramos, 1988; López-Gamundí et al., 1994; Limarino et al., 2002a, 2006, 2014; Isbell et al., 2012; Spalletti et al., 2012). Evidence for the collapse and breaching of the mountain belt includes:

1. The stratigraphy of the region records the disappearance of glacial deposits and transition to transgressive packages in the arc-related basins (i.e. Calingasta-Uspallata and Río Blanco Basins) and in the western margin of the Paganzo Basin (Net and Limarino, 2006; Limarino et al., 2006). This facies trend is seen at all localities across the Paganzo Basin, with the development of coal deposits, and mudstones enriched in kaolinite (Limarino et al., 2014). The collapse of the Protoprecordillera would have removed the topographic barrier between the interior basins and the Panthalassan Ocean and created access to a significant moisture source from the continental margin to the interior. This is indicated by the increase in base level (i.e. local transgressive packages and coal measures; Limarino et al., 2014 and references therein).

2. There are marine faunas recorded at several localities of the Protoprecordillera (cf. López-Gamundí et al., 1994; Taboada, 1997; Henry et al., 2008; Milana and di Pasquo, 2019 and references therein). The presence of marine faunas within the Pennsylvanian units of the more central localities of the

Protoprecordilleran uplift can only be explained by a collapse in relief of the Protoprecordillera, which would have allowed for the flooding of these paleovalleys.

3. The incised paleovalleys along the Protoprecordillera, such as the one at Agua de Jagüel, contains approximately 2,500 m of late Paleozoic sedimentary successions (cf. Henry et al., 2008; this study) and are ultimately filled by the Bashkirian. Furthermore, near the top of Sequence 1 (glacial and glacially influenced sequence) in Henry et al. (2008), shallow water (i.e. hummocky cross-beds, sandstones) facies indicate that the paleovalley was at sea-level by the latest Mississippian. Upward in the Agua de Jagüel Formation, the strata of Sequence 2 and 3 progressively onlaps and overtops the valley walls. Sequence 3 is composed almost exclusively of prograding shallow marine parasequences. The occurrence of shallow marine deposits deep in the paleovalley in Sequence 1 and at the top of the paleovalley fill in Sequence 3 is only possible if subsidence was occurring due to the collapse of the mountain belt.

4. Sierras Pampeanas basement detrital material reached as far as the Andean Cordilleran region (cf. Spalletti et al., 2012). The presence of Sierras Pampeanas lithologies (i.e. Famatinian granites and gabbros) west of the Precordilleran range suggests that the mountain belt was breached during the late Mississippian-early Pennsylvanian.

3. Geology of late Paleozoic South American basins

The western margin basins of Gondwana are well-studied, with a focus on the units of the Paganzo, Calingasta-Uspallata and Río Blanco basins, as well as the associated depositional

processes and environments that extended across the region (i.e. Pazos, 2002; Gulbranson et al., 2010, 2015; Enkelmann et al., 2014). Here we provide a quantitative look at the Carboniferous-Permian climate transition by examining locations throughout the western basins on both sides of the Protoprecordilleran Range and comparing these locations through time to the climate recorded in the southeastern Paraná Basin in Brazil.

3.1. Strata of the western active margin basins

Strata of the western margin basins overlie the numerous terranes and accretionary prisms that make up the western margin of South America. In the eastern Paganzo Basin, Carboniferous-Permian strata overlie Pampean orogenic granitoids and Neoproterozoic-early Cambrian continental margin sedimentary deposits (Pankhurst et al., 2000). In the central portion of the Paganzo Basin, LPIA-related strata overlie Famatinian-aged granitic intrusions and metasedimentary units (Pankhurst et al., 1998, 2000; Net and Limarino, 2006). Along the Cuyania and Precordillera terranes, the basement rock is Mesoproterozoic in age along the eastern margin, and primarily Cambrian-Devonian continental margin and platform sedimentary rocks along the central and western portions (Keller, 1999; Willner et al., 2008; Thomas et al., 2015; Fig. 27). To the west of the Precordillera (i.e. Calingasta-Uspallata and Río Blanco basins, Andean Cordillera), time-equivalent strata overlie Ordovician and Devonian-aged sedimentary and metasedimentary packages (Willner et al., 2008; Spalletti et al., 2012; Limarino et al., 2014; Fig. 27).

The Paganzo Basin contains numerous stratigraphic units, most of which belong to the Paganzo Group (Fig. 25), but all are regarded as time-equivalent strata across the basin. The strata of the Calingasta-Uspallata and Río Blanco basins are known by different names

regionally (Fig. 25), but also contain a similar transition of depositional environments as the units in the Paganzo Basin (López-Gamundí et al., 1997; Henry et al., 2008, 2010; Isbell et al., 2012; Limarino et al., 2014). The various units are correlated using radiometric ages determined for units containing tuff and ash layers, as well as palynological and fossil plant records from the various sections and the facies associated with each succession (cf. Gulbranson et al., 2010, 2015; Césari et al., 2011).

Glaciomarine and glaciolacustrine deposition occurred during the Serpukhovian to early Bashkirian in deeply-incised paleovalleys that emanated from the Protoprecordilleran region into the surrounding Paganzo, Calingasta-Uspallata and Río Blanco basins (López-Gamundí et al., 1997; Limarino et al., 2002a, 2002b, 2006; Kneller et al., 2004; Dykstra et al., 2006; Henry, 2007; Henry et al., 2008, 2010; Astini, 2010; Gulbranson et al., 2010, 2015; Césari et al., 2011; Isbell et al., 2012; Aquino et al., 2014; Alonso-Muruaga et al., 2018). The glacial deposits are recorded in the basal units of the basins: the Guandacol, Jejenes, La Laja and Lagares formations in the western Paganzo Basin, and the lowermost Agua de Jagüel (i.e. Sequence 1 of Henry et al. [2008]) and Hoyada Verde formations in the Calingasta-Uspallata Basin (López-Gamundí et al., 1997; Limarino et al., 2002a, 2002b, 2006, 2014; Kneller et al., 2004; Dykstra et al., 2006; Henry et al., 2008, 2010; Astini, 2010; Gulbranson et al., 2010; Césari et al., 2011; Isbell et al., 2012; Aquino et al., 2014; Alonso-Muruaga et al., 2018). These Protoprecordilleran valleys contain glacial diamictites formed through subglacial, proglacial, glaciomarine, and distal processes (cf. López-Gamundí et al., 1997; Limarino et al., 2002a, 2002b, 2006; Kneller et al., 2004; Dykstra et al., 2006; Henry et al., 2008, 2010; Astini, 2010; Isbell et al., 2012; Aquino et al., 2014; Alonso-Muruaga et al., 2018).

However, the time-equivalent unit, the Malanzán Formation, in the eastern Paganzo Basin does not record evidence of glaciation (Moxness et al., 2018; Pauls et al., 2019, in review; Fig. 25). The Sierra de Chepes and Los Llanos regions were elevated enough that they could have been glaciated (cf. Enklemann et al., 2014; Moxness et al., 2018), and the paleoclimate was cold enough to have supported such a scenario. However, the depositional environment here was an alpine or intermontane valley filled with conglomerates formed through rock-falls, alluvial, and fluvial processes (cf. Moxness et al., 2018).

Glacial deposits disappear across the western margin localities, and are overlain by thick successions of post-glacial shales that represent a local transgressive event that is recorded in all sections (Limarino and Spalletti, 2006; Net and Limarino, 2006; Henry et al., 2008; Césari et al., 2011; Isbell et al., 2012; Limarino et al., 2014). A thick succession of mudrock in the Malanzán Formation is also recorded at the Olta-Malanzán locality (Moxness et al., 2018; Pauls et al., 2019). The tops of most of these units are conglomerates associated with the development of large gilbert-type deltas (cf. Moxness et al., 2018 and references therein).

The middle units of the Paganzo Group (i.e. Tupe, upper Lagares, and Loma Larga formations; Figs. 25) are comprised of fluvial deposits that succeeds the lowermost units (Andreis et al., 1986; Limarino et al., 2006; Guena et al., 2010; Tedesco et al., 2010; Limarino et al., 2014). Additionally, coal deposits exist in various levels within the middle units (Limarino et al., 2006; Guena et al., 2010; Tedesco et al., 2010; Limarino et al., 2014).

The latest Pennsylvanian-Permian units of the Paganzo Basin (i.e. Patquía, La Colina, De La Cuesta formations) represent processes associated with eolian, ephemeral riverine and playa depositional environments (Limarino et al., 2006; Guena et al., 2010; Césari et al., 2011; Limarino et al., 2014). Additionally, the red beds and large-scale (up to 10+ m thick) cross

bedded sandstone of the La Colina and Patquía Formations indicate the development of erg fields at a time when glacial deposits occurred in the Paraná Basin. In the Calingasta-Uspallata Basin, the uppermost Agua de Jagüel Formation (sequence 3 of Henry et al. [2008]) records multiple parasequence packages of shallow marine deposits, while the Tres Saltos Formation at Hoyada Verde records a similar transition to fluvial and shallow marine strata.

3.2. Paraná Basin strata

The late Paleozoic sedimentary deposits overlie various Neoproterozoic-Cambrian metasedimentary, and Devonian sedimentary rocks (Tedesco et al., 2019). In the Paraná Basin, the Itararé Group is composed of intercalations of shale, diamictite and sandstone of the Lagoa Azul, Campo Mourão, and Taciba/Rio do Sul formations (Fig. 25; Rocha-Campos et al., 2008). Each formation represents a megacycle of sandstones that are overlain by shales and diamictites (França and Potter, 1988; Rocha-Campos et al., 2008; Vesely et al., 2015). In the eastern Paraná Basin, the Itararé Group records a longer glaciation history than is preserved in the southern Paraná Basin localities (Mottin et al., 2018; Griffis et al., 2019; Rosa et al., 2019). A recent study by Rosa et al. (2019) indicate that glacial deposition of the Itararé Group started in the Viséan, and Griffis et al. (2017) provide ages that indicate glacial activity in the southern part of the basin ended in the latest Pennsylvanian. Overlying the uppermost Itararé Group strata (i.e. the Taciba Formation) is the Rio Bonito Formation, which consists of fluvial sandstones, estuarine sandstones and shales, and thicker coal packages. It is interpreted to represent the post-glacial succession and a shift to a more humid environment. The Palermo Formation interfingers with the Rio Bonito Formation in certain locations of the Paraná Basin, and contains deeper-water and

offshore marine deposits that are interpreted as an overall transgressive package. These units are Early Permian.

4. Bulk-rock major element geochemistry analyses

The paleoclimate of western Argentina has been long inferred from facies changes in the Paganzo Group strata, as well as strata in the Río Blanco and Calingasta-Uspallata basins. For this study, paleoclimate reconstructions of the Paganzo, Calingasta-Uspallata and southeastern Paraná basins were accomplished by using the CIA as a climate proxy, as it has been used in many studies to ascertain the humidity of an environment (cf. Nesbitt and Young, 1982; Maynard, 1992; Fedo et al., 1995; Bauluz et al., 2000; Price and Vebl, 2003; Sheldon, 2006; Soreghan and Soreghan, 2007; Retallack, 2009; Sheldon and Tabor, 2009; Goldberg and Humayun, 2010; Passchier and Erukanure, 2010; Passchier et al., 2013). The CIA was originally created in to determine the amount of chemical weathering that takes place during the deposition of clastic sediments in varying depositional environments (Nesbitt and Young, 1982). Nesbitt and Young (1982) developed the equation

$$\text{CIA} = (\text{Al}_2\text{O}_3 / \text{Al}_2\text{O}_3 + \text{CaO}^* + \text{Na}_2\text{O} + \text{K}_2\text{O}) \times 100$$

where CaO* represents the calcium content within silicate minerals. They operated under the assumption that the degradation of feldspars into clay minerals constitutes the main process during chemical weathering. This process is enhanced under humid climatic conditions, which leads to higher CIA values in muds deposited in these environments. Conversely, in arid environments, this degradation process would presumably be negligible, and therefore, these sediments would result in lower CIA values. Nesbitt and Young (1982) geochemically analyzed a variety of typical clastic sedimentary rock types and calculated average CIA values. For

average shale and mudstone, the values ranged from 70 to 75, while muds developed in tropical environments resulted in values from 80 to 100, and those deposits from glacial and arid environments had values ranging from 50 to 70 (Nesbitt and Young, 1982).

5. Geochemistry methods

A previous study conducted by Pauls et al. (2019) on one locality in the eastern Paganzo Basin at the Olta-Malanzán paleovalley system (OMPV) tested the applicability of using a paleoclimate proxy in this region. To broaden this analysis for a more regional comparison, the other units of the Paganzo Group strata were measured and sampled at three additional localities on either side of the Protoprecordilleran range: Cerro Guandacol (CG) in the north Paganzo Basin, the Agua Hedionda anticline (AH) section near the town of Huaco to the east of the Precordillera in the central Paganzo Basin, and the Agua de Jagüel (AJ) section along the southern section of the Protoprecordillera in the Calingasta-Uspallata Basin (Fig. 24). In addition to the samples collected from the western margin basins in Argentina, samples were also collected from the Itararé Group and Rio Bonito Formation in Rio Grande do Sul state of Brazil (Fig. 24). Field work was conducted in August of 2016 and 2017 and used standard stratigraphic and sedimentological techniques to examine four composite sections of late Paleozoic strata in La Rioja, San Juan and Mendoza Provinces of Argentina, and five sections in Brazil. To capture the full climate transition in the western margin basins, samples were collected from each locality in units that contained the mid-Carboniferous glacial facies and continued through the Carboniferous-Permian boundary (Table 3). Additional samples were taken at select locations from time-equivalent units (i.e. the Itararé Group, Rio Bonito and Palermo formations) in the southeastern portion of the Paraná Basin for comparison.

To reduce a weathering bias during sample collection, which could potentially skew the dataset towards low or high CIA values, only clay to silt-sized samples (i.e. < 0.004 – 0.0062 mm) were collected from trenches dug >10 cm into the outcrops, thus providing fresh, unweathered material. To reduce the effects created by hydraulic sorting, samples were collected from every unit that had the desired grain size (i.e. mudrocks) and rock units that contained outsized clasts were also avoided, so as not to create a “fresh-material” bias in the results (Sheldon and Tabor, 2009; Goldberg and Humayun, 2010). Sampling thus did not achieve an equal distribution of samples throughout the measured sections, especially within coarse-clastic horizons. Additionally, to ascertain that there was no metasomatism and illitization leading to increased K⁺ concentrations (cf. Fedo et al., 1995), the samples were plotted on A-CN-K ternary diagrams to show deviations from average weathering trends of basement materials (Nesbitt and Young, 1982, 1989; Passchier et al., 2013; Fig. 28).

The samples used for the CIA analysis were initially ground in a tungsten-carbide shatterbox for 30-45 seconds, and then were hand-ground in an agate mortar & pestle to achieve a uniform grain size. After grinding, all samples were placed overnight in a drying oven set to 105°C. A loss on ignition (LOI) analysis was performed to determine mass of the volatile components that would be lost during the fusion process, comparing the mass of a sample before and after ignition for 15 minutes in a 1050°C muffle furnace. Samples with a high LOI percentage (i.e. greater than 10%) were noted for later mass adjustment during the fusion process. All samples were then prepared for fusion according to the methods laid out in McHenry (2009), Byers et al. (2016) and McHenry et al. (2017).

Fused beads of each sample were prepared using the protocol described in McHenry (2009) in which 1.000 g of soil was added to 1 g of oxidizer (ammonium nitrate) and 10.000 g of

Claisse (Quebec, Canada) 50:50 lithium metaborate: lithium tetraborate flux containing 0.5% LiBr as a nonwetting agent. The material was fused in a Claisse M4 programmable fusion instrument. If a sample had a high LOI percentage, then 1.100 g of sample was used with 11.000 g of Claisse (Quebec, Canada) 50:50 lithium metaborate: lithium tetraborate flux. Fused beads were measured by a Bruker AXS, Inc. Pioneer S4 WD-XRF instrument using a custom measurement and calibration procedure based on eleven USGS sedimentary and igneous geological reference materials made in the same manner as samples prepared for this study, as described by McHenry (2009) and updated in Byers et al. (2016). The USGS geological reference materials used in this calibration routine are AGV-1, BCR-2, BHVO-2, BIR-1, DNC-1, DTS-2b, G-2, GSP-2, RGM-1, SGR-1 and STM-1.

6. CIA Analysis

The sampled section at Cerro Guandacol begins in the strata of the Tupe Formation (Table 3). In general, the CIA values in the Cerro Guandacol section range from 49 to 83, with an average of 65. The Tupe Formation at the base consists of interbedded mudstone and sandstones that increasingly coarsen upward, indicating the progradation of fluvial environments into the post-glacial marine environment of the upper Guandacol Formation. The values at the base of the Tupe are low (i.e. 49) but increase to 83 near the coal deposits. The CIA values decrease again to 65, as the section coarsens upward. The CIA increases again to 82 at the top of the Tupe Formation. As the Tupe Formation transitions into the Patquía Formation, the values decrease to 57, and then remain in the middle 60s for most of the Patquía Formation. At the very top of the section, the CIA values decrease once again to the 50s. Overall, the section resulted in CIA values that indicate minimal weathering.

The sampled section at Huaco starts in the glacial diamictites near the base of the Guandacol Formation and continues all the way through the uppermost Patquía Formation (Table 3; Fig. 29). The CIA values range from 55 to 88 (both values are in the Tupe Formation), and the section has an average value of 72. In the glacial diamictites of the Guandacol Formation, the values are 60s and lower 70s, and the values increase through the upper Guandacol Formation. Near the Guandacol-Tupe formations boundary, the CIA spikes to 80 before falling to 64 in the lowermost Tupe Formation. These interbedded mudstone and sandstone deposits represent transgressive-regressive deposits as fluvial facies prograde into the marine environment of the Guandacol Formation. Then, the rest of the Tupe Formation samples fluctuate between 85-60 and are highest (i.e. in the low 80s) near the coal deposits. As the section nears the Tupe-Patquía formations boundary, the values start to decrease from the 70s and 80s to the low value of 55. The values of the Patquía Formation range from 60 to 80, with an average of 71. These deposits represent fluvial, ephemeral fluvial and playa environments.

The strata at Agua de Jagüel were measured through all three sequences identified by Henry et al. (2008). The lower sequence (sequence 1) records glaciomarine facies throughout the lower third of the formation. The facies throughout the lower section includes glacial diamictites and marine shales with dropstones, and the CIA values range from 58-73. The middle and upper sequences (sequences 2 and 3) record fluvial shallow marine deposits and have CIA values that range from 66-78.

In the Paraná Basin, samples were collected in the upper Itararé Group strata (Taciba/Rio do Sul Formation) and lowermost Rio Bonito Formation. The Itararé Group strata incorporated glacial diamictites, rhythmites, mudstones and shales. The basal diamictite had a CIA value of 61, while the rhythmite and mudstone deposits were 69. The two upper Itararé Group samples

were 78 and 97, respectively. The Rio Bonito Formation contained paleosol and splay deposits and resulted in a CIA value of 98.

7. Paleoclimate of Southern South American Basins

The CIA trends for the western margin basins reflect an overall shift from glacial (arid) to post-glacial (temperate – humid) conditions to increasingly arid across the region, but each locality displays variations in this trend (Fig. 29). This climate transition is recorded ~20 Ma earlier in the western margin basins compared to the southeastern Paraná Basin strata.

7.1. Western Margin Basins

The mid-Carboniferous and Permian strata and facies of the western basins of Argentina have been traditionally used to determine changes in local tectonics and how they relate to the local climate transition because these rocks record a drastic shift from glacial conditions (i.e. glacially-related diamictites) to temperate and humid post-glacial conditions (i.e. coal deposits) to extreme aridity (i.e. eolian deposits) by the early Permian, documented in both facies as well as flora and pollen records (Gulbranson et al., 2010, 2015; Césari et al., 2011; Limarino et al., 2014).

While studies indicate that there was more restricted or localized deposition occurring in the retroarc or foreland Paganzo Basin (cf. Pauls et al., in review) during the latest Serpukhovian, the CIA values are relatively low across all localities (52-80), but not as low as is expected for glacial deposits (Nesbitt & Young, 1982; Bahlburg & Dobrzinski, 2011). Where there is evidence of glaciation (i.e. the presence of glacially striated pavements, clasts, and glacial diamictites in the Guandacol and Agua de Jagüel formations), the values (i.e. in the low 50s) are

on average lower than the lowermost Malanzán formation values (in the 60s) presented by Pauls et al. (2019). The CIA analysis indicates that the paleoclimate was dominated by cold and mostly dry conditions across the Paganzo Basin (cf. Nesbitt & Young, 1982; Bahlburg & Dobrzinski, 2011), but the higher values (i.e. 66-73) from the lower Agua de Jagüel Formation indicates more chemical weathering likely due to higher humidity along the Panthalassan margin. This is further supported by the glaciomarine nature of deposition of the Agua de Jagüel Formation during this time (López-Gamundí et al., 1994; López-Gamundí, 1997; Henry et al., 2008; Isbell et al., 2012; Limarino et al., 2014).

While all localities have relatively low CIA values during this timeframe, it is important to note that the Agua de Jagüel Formation records higher values than those values recorded at Cerro Guandacol, Agua Hedionda, and at Olta-Malanzán (cf. Pauls et al., 2019; Fig. 29). Additionally, a study conducted by Spalletti et al. (2012) presents geochemistry data for the Cerro Agua Negra Formation and is used here as another reference for climate on the western side of the Protoprecordillera. The Cerro Agua Negra Formation is recorded in the present Andean Cordillera region and would have been deposited further to the west than the Calingasta-Uspallata and Río Blanco basin localities (Spalletti et al., 2012; Limarino et al., 2014; Fig. 25). The mudstones of the middle Cerro Agua Negra Formation also display higher CIA values (in the 70s) than the interior Paganzo Basin strata, supporting the interpretation of weathering conditions associated with a higher humidity climate (Fig. 29).

Following the disappearance of the glacial deposits in the western Paganzo Basin localities and the Calingasta-Uspallata Basin, the strata records a local rise in base level. These local transgressive facies are interpreted as terminal glacial to post-glacial deposits (cf. Limarino et al., 2014; Pauls et al., 2019, in review). The CIA values increase at Huaco and OMPV, which

indicates an increase in humidity and therefore chemical weathering. The lag in timing between Huaco and OMPV may have more to do with a lack of precise correlation between the units than an actual time lag. This increase in humidity may have been simultaneous, but until better correlation between/among the Paganzo Group occurs, it is impossible to say with certainty. This increase in humidity is also recorded in the Agua de Jagüel Formation, which indicates that this transition to a humid terminal and post-glacial environment was a regional phenomenon.

Decreases in CIA values across the Paganzo Basin are recorded at all three localities (CG, AH, OMPV; Fig. 29) that corresponds to the transition from marine transgressive packages to more deltaic and fluvial deposits of both the Tupe and Loma Larga formations on either side of the basin (Limarino et al. 2002b, 2006; Tedesco et al., 2010; Pauls et al., 2019). During the Mid-Bashkirian, an increase in CIA values is recorded at all three localities, which corresponds to the development of coal deposits across the basin (Limarino et al., 2002b, 2006, 2014; Net et al., 2002; Tedesco et al., 2010; Pauls et al., 2019). An increase in CIA and the development of coal across each of the Paganzo Basin localities indicate a humid environment and the development of long-lasting bodies of water and/or wetlands across the region.

Additionally, the Agua de Jagüel section also reflects this same trend (Fig. 29), and therefore this transition to a warmer, humid climate is interpreted as a regional trend. This is also approximately the time frame during which the Protoprecordillera is interpreted to have been collapsing (cf. Limarino et al., 2014). If the mountain belt had collapsed by this time, then there would have been less of an orographic effect on the interior Paganzo Basin. Furthermore, evidence of breaching of the range (i.e. transgressive packages and coal measures at multiple locations) in the Paganzo Basin indicates a connection with the Panthalassan Ocean. This would have been a source of moisture to the interior of the Paganzo Basin that was not present during

the glacial stage (Visean-Bashkirian), and accounts for the higher humidity climate conditions reflected by the CIA values.

At the beginning of the middle Moscovian, CIA values decrease across the entire region (Fig. 29). From the middle to late Moscovian through the Kasimovian, the climate appears to stabilize with small fluctuations/vacillations indicating an overall temperate climate. This supports the interpretation that this time is marked by an increase in seasonality as some studies have suggested (cf. Limarino et al., 2014; Gulbranson et al., 2010, 2015). This trend occurs at Cerro Guandacol, Huaco and Olta-Malanzán (cf. Pauls et al., 2019; Fig. 29), but the values at Huaco are higher than the values recorded at Cerro Guandacol.

It is not until the latest Pennsylvanian that the climate trends across the entire region seem to differentiate or diverge. First, at Cerro Guandacol, the CIA values display a narrow range of values throughout both the Kasimovian and Gzhelian, which suggests that the climate does not vary much during this interval. However, the values suggest a decrease in weathering earlier than what is observed at the other studied sites, which is here interpreted as a relatively early increase in aridity. The lack of samples in the middle Patquía Formation is due to the absence of strata with the appropriate grain size for analysis (i.e. silt fraction or finer; Fig. 29). The dominance of eolian sand here indicates either minimal chemical weathering, or perhaps the fine-grained material at this location was transported out of the area during deposition. Overall, the lower CIA values indicate a drier climate at Cerro Guandacol, which varies slightly from that of the other Paganzo Basin localities, especially to that of Huaco as both of these localities are situated along the boundary between the Paganzo and the Calingasta-Uspallata and Río Blanco basins. Although these two localities share a similar paleogeographic location, it appears that their climate histories do not correlate directly. This could potentially be due to a more local

climate phenomenon, as Cerro Guandacol is located in a separate part of the discontinuous Protoprecordillera from Huaco (Amos and Rolleri, 1965; Gonzalez Bonorino, 1975; López-Gamundí et al., 1994; Limarino and Spalletti, 2006; Limarino et al., 2014; Pauls et al., in review). It is interesting to note that this climate transition at Cerro Guandacol is similar to findings of Gulbranson et al. (2010; 2015) in the nearby Río del Peñon locality of the Río Blanco Basin, where clay analyses indicate an increase in aridity starting as early as the Moscovian.

Second, at Huaco, while the climate was more humid in the Kasimovian, the CIA values in the early Gzhelian rapidly decrease, which indicates a rapid decrease in chemical weathering over a short period of time. This is interpreted here as an increase in overall climate aridity. This Gzhelian increase in aridity is not recorded at the Agua de Jagüel and Olta-Malanzán localities (Fig. 29). In contrast, the strata at Agua de Jagüel as well as the strata of the La Colina and Arroyo Totoral formations at Olta-Malanzán record an increase in humidity during the latest Carboniferous (cf. Pauls et al., 2019). Since the upper Agua de Jagüel Formation represents stacked prograding parasequence sets of shallow marine deposits, we attribute the higher humidity here to the proximity to the continental margin and marine conditions. On the other side of the Paganzo Basin, the higher humidity recorded during the latest Pennsylvanian at Olta-Malanzán (cf. Pauls et al., 2019) is not wholly unexpected, as the paleoclimate model proposed by Limarino et al. (2014) indicated that the eastern Sierras Pampeanas (i.e. the Sierras de Chepes and Los Llanos region) existed in a wet belt during this time. This is supported by evidence from the facies and paleoflora recorded in these strata. The strata here transition to coarse-grained sandstones in the middle La Colina Formation, and are finally overlain by eolian cross-beds (cf. Pauls et al., 2019). The lack of mudstones precluded further CIA analyses upward, but the presence of the eolian facies at the top of the section indicates a similar increase in aridity as is

recorded in the western localities, but probably at a later time. Further age constraint of the strata is needed to refine chronostratigraphic correlations of the Paganzo Group strata.

7.2. Paraná Basin

In contrast to the shift to a temperate-humid climate in the western margin basins of South American, the Southern Paraná Basin was still cold and dry during the late Pennsylvanian. It was also still experiencing glaciation (cf. França and Potter, 1988; França, 1994; Souza and Marques-Toigo, 2005; Guerra-Sommer et al., 2008; Vesely and Assine, 2006; Rocha Campos et al., 2008; Isbell et al., 2012; Griffis et al., 2019; Fedorchuk et al., 2019). Samples from a glacial diamictite of the upper Itararé Group (Taciba/Rio do Sul Formation) from southeastern Brazil resulted in a CIA value of 61, and reflect cold conditions with minimal chemical weathering, and is within the expected range for glacial deposits (50-70; Nesbitt and Young, 1982). Samples from rhythmites and mudstones above the glacial deposits of the upper Taciba Formation (upper Itararé Group) record CIA values of 69, which indicates some chemical weathering, but it is still within the glacial deposit range for CIA values (Nesbitt and Young, 1982).

Near the boundary with the Rio Bonito Formation, the uppermost Itararé Group strata records higher CIA values than the underlying strata. CIA values for the upper Taciba Formation (Itararé Group) increase to 78 and 97 at the boundary with the overlying Rio Bonito Formation. This shows that by the end of the Pennsylvanian, the southeastern part of the Paraná Basin was experiencing a more humid, post-glacial climate. The Rio Bonito sample from directly above the contact with the Taciba Formation also resulted in a high CIA value of 98, which indicates the continuation of extreme weathering as the result of a humid environment. This trend towards a

post-glacial humid environment occurs in the southern Paraná Basin almost 20 Ma later than in the western margin basins of Argentina.

8. Deglaciation of South American Gondwana during the LPIA

The late Paleozoic ice age has its beginnings in Brazil, Bolivia and Peru in South America, as well as basins in Africa, which experienced glaciation during the latest Devonian (late Famennian; cf. Caputo and Crowell, 1985; Díaz-Martínez, 1999; Isaacson et al., 1999; Díaz-Martínez et al., 2001; Veevers, 2004; Isaacson et al., 2008). Another brief episode of glaciation occurred in the late Tournaisian in basins of Brazil, Bolivia and Argentina (Caputo et al., 2008). These centers then diminished during the earliest Carboniferous (Caputo and Crowell, 1985; López-Gamundí, 1997; Díaz-Martínez, 1999; Isaacson et al., 1999, 2008; Díaz-Martínez et al., 2001; Isbell et al., 2003; Caputo et al., 2008).

During the middle Mississippian glaciation, local centers of ice resumed, as supported by evidence recorded in the basins of western Argentina (i.e. Río Blanco, Calingasta-Uspallata, and western Paganzo basins; López-Gamundí et al., 1994; López-Gamundí, 1997; Caputo et al., 2008; Isbell et al., 2003). It is important to note that although there are glacial deposits in the western Paganzo Basin, this glaciation only occurs along the Protoprecordilleran belt, and perhaps on other topographic highs just to the east (i.e. in the Sierra de Famatina region), but it does not appear any further east (Moxness et al., 2018; Pauls et al., 2019, in review). The Sierras de Chepes and Los Llanos region remained ice free during this time and record cold climate conditions (i.e. dropstones related to lake ice; Moxness et al. 2018), but do not present evidence that the location ever experienced long-lasting ice cover conditions.

Glaciation is also thought to have occurred, as larger ice sheets, in the Paraná Basin starting in the Viséan or Tournaisian at the earliest (Rosa et al., 2019; Fig. 30). Evidence for glaciation appears earlier in the eastern Paraná Basin Itararé Group strata than in the southern portion of the Paraná Basin (Mottin et al., 2018; Griffis et al., 2019; Rosa et al., 2019). With evidence of glacial activity across South America, this renewed development of glaciers is interpreted to be the onset of widespread glaciation across Gondwana (Caputo et al., 2008; Pérez-Loinaze et al., 2010; Limarino et al., 2014).

Nevertheless, as glaciation was continuing in Brazil, the ice centers in western Argentina began to diminish during the Serpukhovian, with the last glacial deposits recorded in the early Bashkirian in the Calingasta-Uspallata, Río Blanco and Paganzo basins (Limarino et al., 2014 and references therein). These last deposits are correlated across the western basins and are interpreted to have occurred concurrently in the region (cf. Gulbranson et al., 2010; Césari et al., 2011). Glaciation appears to have ended prior to 320 Ma (cf. Gulbranson et al., 2010; Césari et al., 2011; Valdez Buso et al., 2017, 2020) at most localities across the region. These ages are recorded in tuffites within the post-glacial transgressive packages at each location, indicating that volcanism had begun, coinciding with renewed subduction to the west (Willner et al., 2005, 2008). By this time in the Bashkirian, the Protoprecordilleran range would have been fully collapsed, and no longer served as a paleotopographic high. This also correlates well with the transition to a temperate and humid climate regime in the western margin basins during the Bashkirian and Moscovian (Fig. 30).

In the case of the Paraná Basin, most recent data show that the glaciation in the southern portion of the Paraná Basin lasted until the latest Carboniferous. (Griffis et al., 2017, 2019). Additionally, palynology reported by Mottin et al. (2018) suggests that glaciation may have

continued in the east central portion of the Paraná Basin until the Early Permian. The end of the Pennsylvanian in the Paraná Basin is marked by warmer and more humid conditions during deposition of coal in the Rio Bonito Formation (Goldberg and Humayun, 2010; Tesdesco et al., 2019; this study) than was recorded during the much-earlier Bashkirian transition to post-glacial conditions in the western margin basins (Pauls et al., 2019; this study).

Potential drivers for the end of glaciation in the basins of Argentina have been hypothesized and attributed to the drift of Gondwana across the South Pole, fluctuating CO₂ levels, or even tectonic and orogenic events (Powell and Li, 1994; Isbell et al., 2003, 2012; Royer et al., 2004; Montañez et al., 2007; Rygel et al., 2008; Horton and Poulsen, 2009; Tabor and Poulsen, 2008; Gulbranson et al., 2010; Montañez and Poulsen, 2013; Limarino et al., 2014). Studies have indicated that atmospheric CO₂ concentrations were steadily decreasing during the latter part of the Carboniferous (Royer, 2006; Montañez et al., 2007; Montañez and Poulsen, 2013; Fig. 31). If these models are true, then it would be reasonable to assume that atmospheric conditions would be cooling, and potentially favorable for long-lasting ice accumulation. In the western basins of Argentina, this is not found to be the case, as evidence of glacial activity disappears in the Bashkirian (earliest Pennsylvanian; López-Gamundí et al., 1994; López-Gamundí, 1997; Henry et al., 2008; Isbell et al., 2012; Limarino et al., 2014; Pauls et al., in review). Instead, other drivers must be considered for the phenomenon.

9. Tectonism as a control on climate change in southwestern Gondwana

Numerous studies have implicated the importance of topographic barriers on the transportation of moisture and atmospheric patterns across continental regions (Broccoli and Manabe, 1997; Ruddiman and Prell, 2007; Ruddiman et al., 1997; Newell et al., 1999; Tabor and

Poulsen, 2008; Godard et al., 2014; Isbell et al., 2012; Limarino et al., 2014). Mountain chains can affect a region's climate by disrupting the atmospheric circulation and in turn cause an orographic effect, with wet climate belts on the windward side and dry climate belts on the leeward side (Broccoli and Manabe, 1997; Partridge, 1997; Ruddiman and Prell, 1997; Ruddiman et al., 1997; Newell et al., 1999; Tabor and Poulsen, 2008; Isbell et al., 2012; Godard et al., 2014; Limarino et al., 2014). The Protoprecordillera and Famatina and Pie de Palo arches separated the interior Paganzo Basin from the Panthalassan margin, which would have prevented the transportation of moisture from the west to east (Fig. 31). Even though the Sierra de Chepes, Los Llanos regions were high enough that they could have been glaciated (cf. Enklemann et al., 2014; Moxness et al., 2018), and the paleoclimate was cold enough to have supported such a scenario, no evidence of glaciation exists in the Olta-Malanzán paleovalley. Instead, the depositional environment here represents a cold-climate alpine valley that may have experienced the occasional cover of surface ice (lake ice), but not glacial activity (cf. Moxness et al., 2018). The Protoprecordilleran valleys, on the other hand, contain numerous lines of evidence of glacial activity (cf. López-Gamundí et al., 1997; Limarino et al., 2002a, 2002b, 2006; Kneller et al., 2004; Dykstra et al., 2006; Henry et al., 2008, 2010; Astini, 2010; Isbell et al., 2012; Aquino et al., 2014; Alonso-Muruaga et al., 2018; Pauls et al., in review). This evidence of established glaciation, along with the higher values (i.e. 66-73) from the lower Agua de Jagüel Formation in the Calingasta-Uspallata Basin (i.e. western side of the Protoprecordillera) than its counterparts on the eastern and interior Paganzo Basin (i.e. in the 50s) supports the hypothesis that the Protoprecordillera was a significant topographic barrier that disrupted atmospheric circulation patterns in the region during the Serpukhovian glaciation. We assert here that the lack of glacial ice in the eastern region of the Paganzo Basin is most likely due to a rain shadow effect that the

Protoprecordilleran range, along with the Famatina and Pie de Palo arches had on the interior localities, much like the affect that the Andean cordillera has on the Famatina Range (Sierra de Famatina) today. At 20,000 ft, the Famatina Range should be glaciated like the nearby Andean cordillera, but it is not due to the rain shadow cast by the Andean orographic effect. However, it should be noted that it was glaciated in the Pleistocene.

The coincidence of the climate amelioration in the early Bashkirian with the loss of glacial indicators, and the appearance of local flooding packages can be directly tied to the complete collapse of the Protoprecordillera by this time. If the Protoprecordillera diminished in elevation, it could have dipped below the ELA (cf. Isbell et al., 2012) and therefore would not have been able to maintain glacial ice cover. This loss in elevation is recorded as an increase in subsidence all along the western margin localities, with flooding of the paleovalleys and the transition to thick transgressive packages (Limarino et al., 2014 and references therein). Furthermore, the appearance of ash layers and tuffites in these transgressive packages of the upper Guandacol, Jejenes formations indicates that not only was the Protoprecordillera collapsed, but the atmospheric circulation appears to have been restored, as these Carboniferous ages are related to volcanism occurring along the Chilean/western margin of Gondwana at this time (cf. Willner et al., 2008). Additionally, this change in topography as well as climate appears to have persisted until at least the middle-Moscovian to Gzhelian time, during which time volcanism increased along the margin (Willner et al., 2005, 2008).

This increase in volcanism is also recorded in strata of the Río Blanco Basin at the end of the Pennsylvanian and into the Permian, and it has been correlated to the accretion of a volcanic arc outboard of the western margin (cf. Limarino and Spalletti, 2006; Limarino et al., 2006; Spalletti et al., 2012; Limarino et al., 2014; Einhorn et al., 2015). This new paleotopographic

barrier would have once more cut the interior Paganzo Basin off from moisture sources, perhaps taking effect earlier in the northern parts of the basin, such as Cerro Guandacol, and other localities in the Río Blanco Basin (cf. Gulbranson et al., 2010, 2015).

In contrast to climate driving mechanisms for the western margin basins, active tectonism is not recorded in the Paraná Basin until much later in the Mesozoic (Milani and Ramos, 1998; Limarino and Spalletti, 2006; Rocha-Campos et al., 2008; Tedesco et al., 2019). Therefore, tectonism as a main driver for the climate transition from glacial to post-glacial conditions would not have affected climate conditions as it did in the western margin basins and cannot be considered as a mechanism for this region. Furthermore, the Paraná Basin was filled with an intracratonic seaway for most of the late Paleozoic (cf. Rocha-Campos et al., 2008), and therefore the highlands surrounding the basin would have had ample moisture for snow and ice to accumulate. Climate in the Paraná Basin was most likely influenced by global-scale drivers, such as the drift of Gondwana across the South Pole and a decrease in atmospheric CO₂ concentrations (Montañez et al., 2007), as well as local drivers like the seaway that allowed for a local moisture source.

Despite the fact that the western basins of Argentina and the Paraná Basin were located at a similar paleo-latitude, global drivers likely had a minimal effect on the disappearance of glacial ice in western Argentina. Upon compiling the latest research over the past decade, a better understanding of the late Paleozoic ice age emerges. The deglaciation of southwestern Gondwana was not sudden, but occurred in a step-like fashion, starting in northern and western Argentina and Bolivia, and migrated eastward through time (Caputo et al., 2008; Isbell et al., 2012). Based on the data gathered and presented here, it was likely that various climate drivers were at play and that regional drivers played the most significant role of when glaciation ended

within the regions of Gondwana that are located at similar paleolatitudes. For the climate transition recorded in the western margin basins, the most important driver appears to be related to the changes in the delivery of moisture to the region, which would have been controlled by tectonism along the western convergent margin of South America. A minor secondary influence was likely connected to the counterclockwise rotational drift of South American Gondwana north and westward away from the South Pole (cf. Powell and Li, 1994; Isbell et al., 2003, 2012; Lawver et al., 2008, 2011; Torsvik and Cocks, 2016). Together, the active tectonism in combination with the continental drift of Gondwana are responsible for the disappearance of glacial indicators in the western active margin basins. The same cannot be invoked for the eastern intraplate basins, which experienced a longer-lived glacial record than those along the western margin.

10. Conclusions

Bulk-rock major element geochemistry data provides the means to construct a paleoclimate model for the late Paleozoic basins of South American Gondwana. The western margin basins of Argentina (i.e. the Paganzo, Calingasta-Uspallata and Río Blanco basins) record a relatively early disappearance of glacial evidence when compared to the southern Paraná Basin, which is at a similar paleolatitude, but away from the active margin.

- The overall paleoclimate reconstruction for the western margin basins indicate that this region transitioned from cold and arid to warm and temperate-humid and finally back to arid at the Permian. Despite that fact, there were noticeable differences in the timing among the localities. The climate reconstruction for the

Paraná Basin indicates that the glacial to post-glacial humid climate did not occur until almost ~20 Ma later than the western margin basins.

- The basins on the western side of the Protoprecordillera range recorded higher overall CIA values throughout the late Serpukhovian-Bashkirian glacial phase than the Paganzo Basin localities, while still maintaining glacial activity. This gives clear evidence that the Protoprecordillera was a significant topographic barrier that caused an orographic effect on the easternmost Paganzo Basin (OMPV).
- The early Pennsylvanian climate amelioration recorded in the western margin basins can be tied to the collapse of the Protoprecordilleran range. Both stratigraphic, paleontological, and now this paleoclimatic reconstruction coincide with a loss in elevation and an increase in subsidence along the western margin of Gondwana during this time.
- Evidence for an increase in volcanism during the Pennsylvanian along the western active margin has been noted in the middle and upper units of the Paganzo Group and indicates a second orographic effect caused by the accretion of a volcanic arc. This resulted in the transition from a temperate-seasonal climate to an extremely arid one.
- Tectonism is the main climate driver for the relatively early disappearance of glacial activity in the western margin basins, whereas global drivers such as the rotation of Gondwana across the South Pole and decreasing atmospheric CO₂ concentrations seem to have exerted more control on the end of glaciation in the southern Paraná Basin.

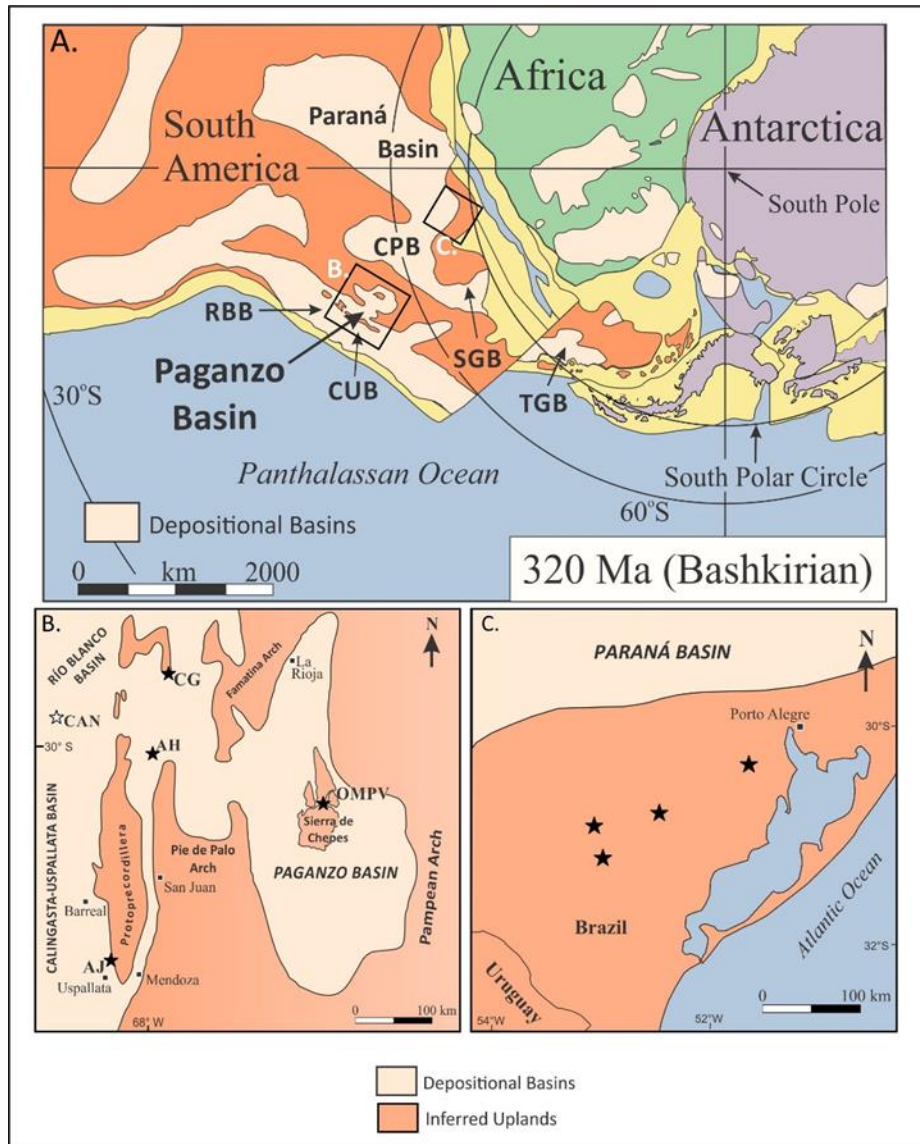


Figure 24 A. Map of plate reconstruction for the Bashkirian stage. RBB: Río Blanco Basin; CUB: Calingasta-Uspallata Basin; CPB: Chaco-Paraná Basin; SGB: Sauce Grande Basin. TGB: Tepuel-Genoa Basin. Reconstruction modified from Moxness et al. (2018). B. Plan-view map showing the interpreted outline of the Paganzo Basin. The localities for this study are marked by black stars: AH – Agua Hedionda anticline near Huaco; CG – Cerro Guandacol; OMPV - Olta-Malanzán paleovalley; AJ – Agua de Jagüel. White star indicates Cerro Agua Negra Formation from Spalletti et al., (2012), data used in comparison to this study. Map modified from Limarino et al. (2006). C. Map of reconstruction of southeastern Paraná Basin with localities marked by black stars used in this study.

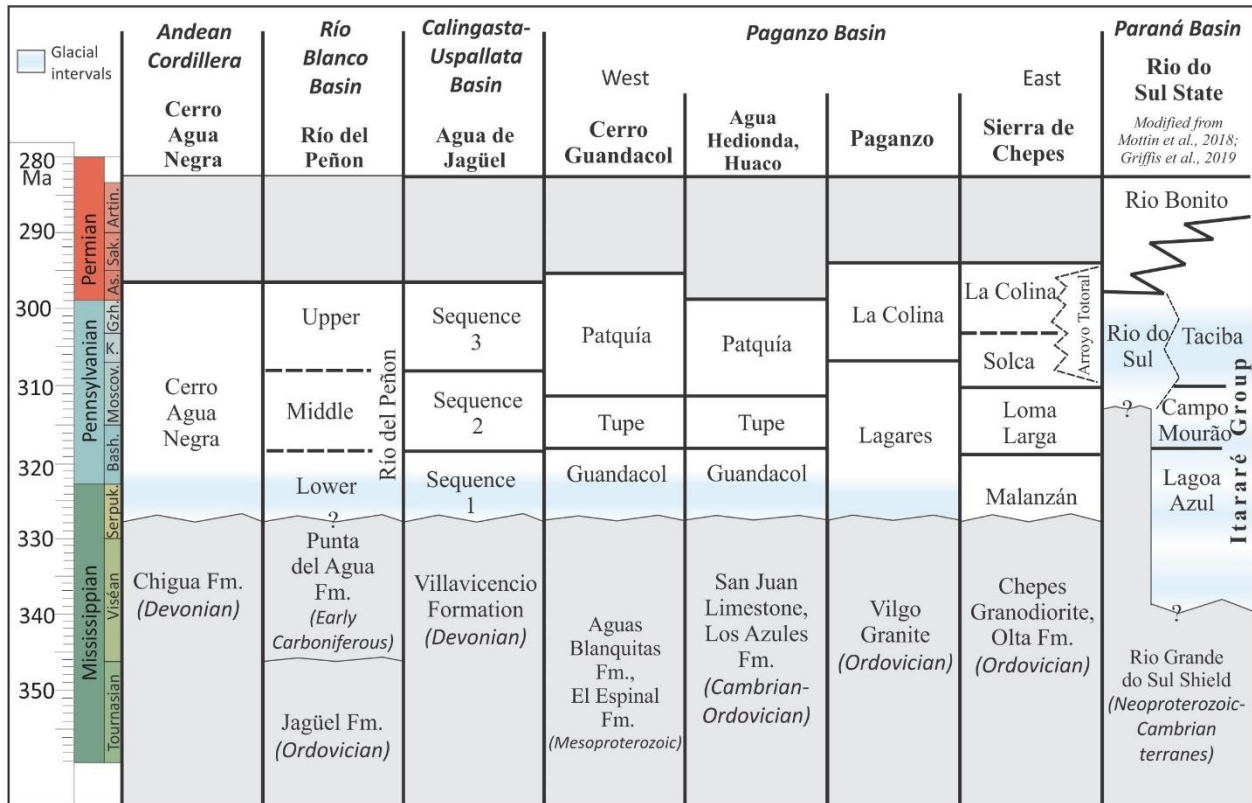


Figure 25. Generalized stratigraphic (white units) and basement rock (gray units) correlation chart for the western margin basins of Argentina and the Paraná Basin in Brazil. Modified from Limarino et al., 2014 with updated chronostratigraphic information for the Paraná Basin from Mottin et al. (2018) and Griffis et al. (2019).

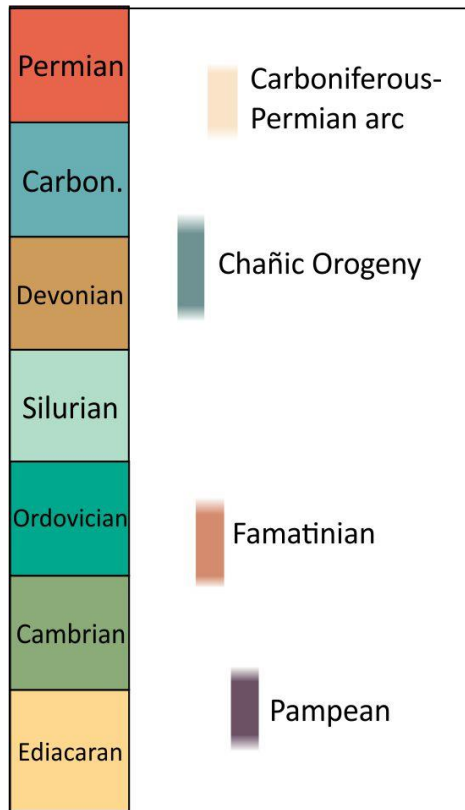


Figure 26 Time distribution of the orogenic events that occurred along the western margin of Gondwana. Pampean and Famatinian orogenies resulted from the collision of the Cuyania Terrane. The Chañic orogeny resulted from the obduction of the Precordilleran terrane. The Carboniferous-Permian arc resulted from the collision of the Chilenia Terrane. Modified from Ramos, 1988, 1999.

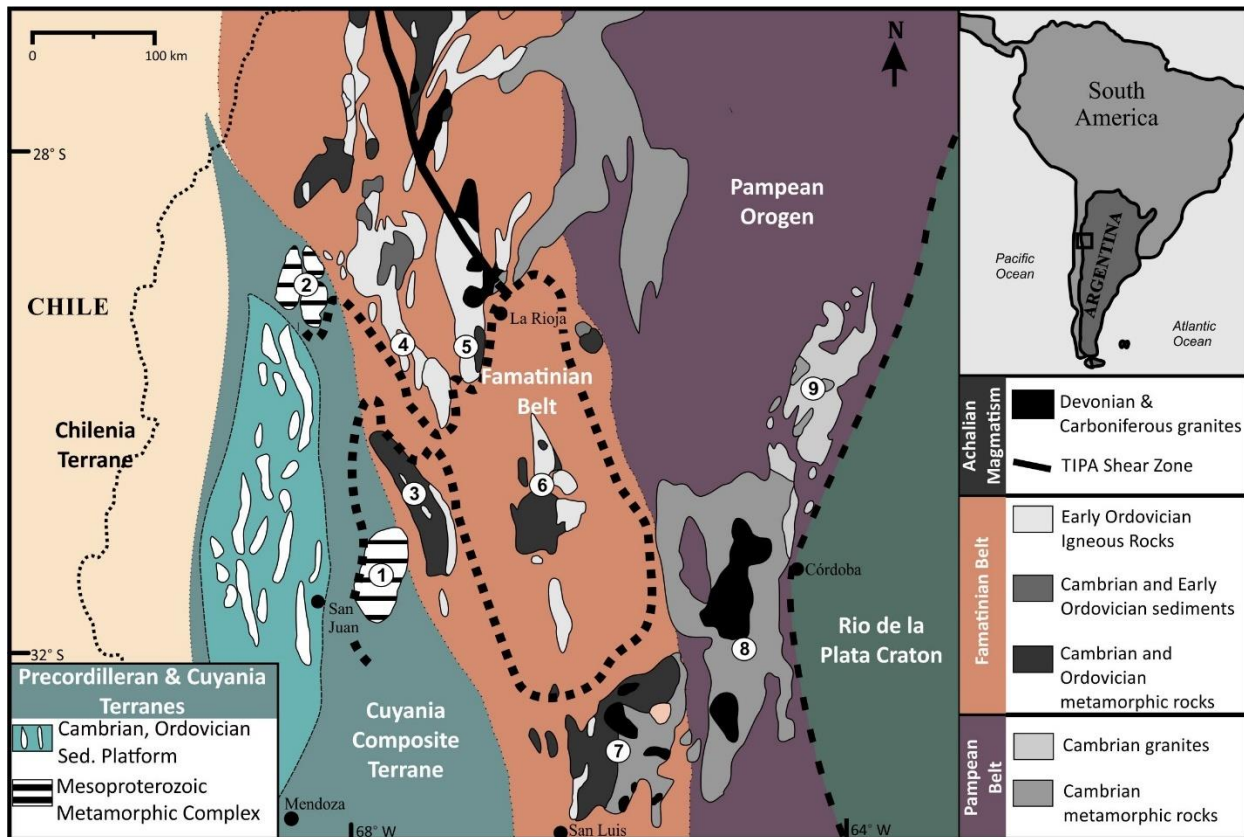


Figure 27. Mesoproterozoic-Carboniferous igneous and metamorphic provinces for the Paganzo Basin area (demarcated by the black dashed line). Map is modified from Dahlquist et al. (2010). The cited literature for this compilation is as follows: (1) Vujovich et al., 2004; Naipauer et al., 2010a (2) Varela et al., 2003, 2005 (3) Pankhurst et al., 2000 (4) Pankhurst et al., 2000 (5) Toselli et al., 2003; Pankhurst et al., 2000 (6) Pankhurst et al., 2000 (7) Vujovich and Ostera, 2003; Drobe et al., 2009 (8) Rapela et al., 1998, Pankhurst et al., 2000 (9) Leal et al., 20003; Llambías et al., 2003.

Table 3. Elemental abundances, loss-on-ignition (LOI), total analyzed abundances, and CIA values for samples from the sedimentary fill of the western margin basins and the southeastern Paraná Basin.

Sample ID	Formation	SiO ₂	TiO ₂	Al ₂ O ₃	Fe ₂ O ₃	MnO	MgO	CaO	Na ₂ O	K ₂ O	P ₂ O ₅	LOI	Total	CIA
Agua Hedionda (AH)														
HG0810-1C	Guandacol Fm.	62.90	0.76	15.69	6.80	0.15	2.83	1.15	1.95	3.40	0.16	3.68	99.58	65
HG0810-3C	Guandacol Fm.	55.70	0.74	19.60	6.19	0.07	2.13	0.98	0.18	5.75	0.19	8.35	100.09	71
HG0810-4C	Guandacol Fm.	55.70	1.05	20.10	8.29	0.11	1.03	0.38	0.89	4.60	0.17	6.80	99.27	75
HG0810-5C	Guandacol Fm.	55.20	0.81	16.2	7.31	0.12	2.45	3.49	1.35	3.12	0.19	9.36	99.73	59
CDH0923-1C	Guandacol Fm.	51.79	1.28	23.41	5.02	0.06	1.17	0.45	0.97	6.05	0.61	7.11	98.39	76
CDH0923-2C	Guandacol Fm.	62.37	1.13	21.36	2.39	0.02	0.53	0.20	0.24	4.55	0.18	6.35	99.50	80
CDH0923-4C	Tupe Fm.	54.09	1.06	18.30	7.68	0.07	1.76	2.21	1.69	3.71	0.19	7.82	98.74	64
CDH0923-6C	Tupe Fm.	58.03	0.99	18.75	7.12	0.05	2.23	0.50	1.73	3.47	0.17	5.53	98.72	73
CDH0923-7C	Tupe Fm.	54.92	1.13	21.23	6.68	0.06	2.30	0.25	0.66	4.06	0.06	7.43	98.93	79
CDH0923-8C	Tupe Fm.	68.62	0.90	18.95	0.91	0.01	0.13	0.16	0.27	1.87	0.03	7.10	99.04	88
CDH0923-9C	Tupe Fm.	60.32	0.99	21.87	4.29	0.05	0.93	0.32	0.50	3.01	0.03	6.99	99.43	83
CDH0923-10C	Tupe Fm.	50.42	0.82	19.77	15.10	0.05	1.01	0.56	0.30	2.68	0.08	7.87	98.79	82
CDH0923-11C	Tupe Fm.	53.32	0.88	21.27	10.74	0.06	1.11	0.38	0.38	2.70	0.05	7.82	98.80	84
CDH0923-12C	Tupe Fm.	54.37	0.97	26.41	2.64	0.01	0.61	0.16	1.88	1.94	0.03	3.14	98.79	83
CDH0923-13C	Tupe Fm.	61.63	0.80	16.90	5.82	0.04	2.10	0.76	2.77	3.84	0.14	11.10	106.03	63
CDH0923-14C	Tupe Fm.	51.60	0.91	24.52	4.85	0.05	1.46	0.42	1.72	2.79	0.05	10.50	98.97	79
CDH0923-15C	Tupe Fm.	58.69	0.90	21.70	3.50	0.07	0.74	1.47	0.92	2.93	0.04	7.24	98.31	75
CDH0923-16C	Tupe Fm.	60.99	0.83	17.25	8.16	0.02	0.94	0.58	1.13	3.93	0.04	8.48	102.45	71
CDH0923-17C	Tupe Fm.	53.10	0.79	17.85	8.76	0.10	1.10	2.65	0.61	3.03	0.03	6.45	94.56	66
CDH0923-18C	Tupe Fm.	63.16	0.84	18.55	4.34	0.04	0.99	0.83	1.33	2.53	0.07	6.17	98.95	75
CDH0923-19C	Tupe Fm.	65.53	0.69	16.17	4.96	0.09	1.27	0.99	1.39	2.48	0.08	5.75	99.51	71
CDH0923-20C	Tupe Fm.	55.89	0.88	19.19	9.02	0.07	1.30	0.32	1.78	3.27	0.06	6.77	98.67	74
CDH0923-21C	Tupe Fm.	51.16	0.99	23.68	9.69	0.04	0.90	0.79	0.55	2.75	0.24	8.13	99.03	83
CDH0923-22C	Tupe Fm.	71.04	0.36	14.29	0.84	0.02	0.45	0.74	5.01	1.23	0.03	11.10	98.54	55
CDH0923-23C	Tupe Fm.	56.46	0.21	19.36	7.20	0.02	1.72	1.33	3.57	2.79	0.03	5.16	97.94	64
CDH0923-25C	Tupe Fm.	59.24	0.68	19.82	5.76	0.04	1.69	0.90	1.80	3.52	0.03	5.23	99.04	70
CDH0923-26C	Tupe Fm.	55.53	0.86	21.90	5.60	0.04	1.60	0.60	2.68	3.49	0.03	6.65	99.09	70
CDH0923-27C	Patquía Fm.	51.38	0.98	24.24	7.16	0.05	1.16	0.74	1.84	3.59	0.13	7.17	98.60	75
CDH0923-28C	Patquía Fm.	56.06	0.90	21.47	6.86	0.08	1.64	0.40	1.37	3.44	0.13	6.49	98.97	77
CDH0923-29C	Patquía Fm.	76.33	0.71	11.19	2.79	0.01	0.89	0.51	2.30	1.95	0.02	5.88	102.69	62
CDH0923-30C	Patquía Fm.	56.70	0.93	20.79	6.54	0.07	1.66	0.51	1.40	3.40	0.22	6.08	98.38	77
CDH0923-31C	Patquía Fm.	54.31	0.89	22.23	7.04	0.07	1.74	0.19	1.81	3.64	0.04	6.64	98.76	76
CDH0923-32C	Patquía Fm.	59.46	0.80	18.87	6.68	0.06	1.74	0.74	1.19	3.31	0.04	5.38	98.47	74
CDH0923-33C	Patquía Fm.	74.57	0.80	12.17	3.64	0.02	0.95	0.41	1.85	1.92	0.02	2.82	99.28	68
CDH0923-34C	Patquía Fm.	74.21	0.80	12.35	3.65	0.02	0.97	0.54	1.83	1.96	0.02	2.89	99.36	67
CDH0923-35C	Patquía Fm.	56.53	0.75	17.82	7.42	0.07	1.60	0.59	0.96	2.91	0.05	2.53	91.35	76
CDH0923-36C	Patquía Fm.	75.82	0.73	11.10	2.91	0.01	0.89	0.80	2.27	1.96	0.02	2.43	99.07	60
CDH0924-1C	Patquía Fm.	66.80	0.86	15.70	5.62	0.03	0.86	0.42	2.07	3.12	0.03	3.47	99.10	68
CDH0924-2C	Patquía Fm.	64.05	0.87	15.60	5.74	0.02	0.75	0.46	1.61	3.20	0.03	3.67	96.11	69
CDH0924-3C	Patquía Fm.	72.95	0.75	13.47	4.08	0.01	0.49	0.41	1.96	2.44	0.03	2.71	99.39	67
CDH0924-4C	Patquía Fm.	71.76	0.85	14.25	4.20	0.01	0.59	0.39	1.87	2.66	0.07	3.52	100.28	69
CDH0924-5C	Patquía Fm.	74.22	0.80	12.94	3.80	0.01	0.47	0.32	2.00	2.21	0.03	2.50	99.39	68
CDH0924-7C	Patquía Fm.	58.03	0.84	18.09	6.75	0.03	0.96	0.48	1.56	3.23	0.03	8.02	98.12	72
CDH0924-8C	Patquía Fm.	60.13	0.89	19.50	7.15	0.02	0.97	0.29	1.41	3.58	0.05	4.76	98.86	75
CDH0924-9C	Patquía Fm.	66.87	0.83	15.34	7.66	0.01	0.37	0.23	1.28	1.80	0.04	3.98	98.53	78
CDH0924-10C	Patquía Fm.	60.02	0.95	19.16	7.54	0.03	0.92	0.38	1.60	3.05	0.04	5.04	98.84	80
CDH0924-11C	Patquía Fm.	60.70	0.92	19.05	7.14	0.02	0.95	0.67	1.20	3.04	0.04	5.32	99.18	75
CDH0924-12C	Patquía Fm.	58.37	0.88	16.56	8.70	0.06	2.70	0.66	2.37	5.08	0.09	3.14	98.73	61
CDH0924-13C	Patquía Fm.	50.24	0.87	24.51	5.44	0.06	1.36	0.27	1.88	2.65	0.04	11.10	98.54	79
CDH0924-15C	Patquía Fm.	59.96	0.87	17.53	6.68	0.04	1.83	0.76	2.89	3.87	0.11	3.28	97.95	64
Cerro Guandacol (CG)														
GDM0924-1C	Tupe Fm.	48.92	0.88	16.29	6.66	0.08	2.85	0.62	7.66	3.63	0.14	9.87	97.71	48
GDM0924-2C	Tupe Fm.	55.44	1.02	17.86	7.83	0.08	3.02	0.48	2.81	3.53	0.15	4.86	97.19	67
GDM0924-5C	Tupe Fm.	47.04	0.94	24.45	6.92	0.05	2.60	0.13	1.45	2.32	0.07	12.46	98.54	83
GDM0924-6C	Tupe Fm.	62.82	0.76	15.79	5.27	0.06	2.04	0.74	1.95	3.71	0.09	10.07	103.39	65
GDM0924-7C	Tupe Fm.	57.48	0.92	17.14	7.85	0.08	2.91	1.03	1.71	3.57	0.16	4.64	97.60	68
GDM0925-01C	Tupe Fm.	45.25	3.17	20.10	13.05	0.04	3.90	0.34	1.60	2.27	0.02	8.21	98.13	78
GDM0925-04C	Tupe Fm.	39.36	3.15	16.07	15.76	0.42	3.69	5.01	1.42	0.41	0.11	11.91	97.51	58
GDM0925-05C	Tupe Fm.	44.15	2.86	22.62	9.71	0.11	1.35	3.20	0.28	1.88	0.70	9.73	96.73	77
GDM0925-06C	Tupe Fm.	50.06	1.46	23.69	7.36	0.06	1.58	0.63	1.24	2.05	0.09	4.63	92.98	82
GDM0925-07C	Patquía Fm.	67.33	1.00	11.88	5.15	0.14	1.91	2.57	1.27	2.36	0.09	4.59	98.39	57
GDM0925-08C	Patquía Fm.	65.38	0.90	13.69	5.87	0.08	2.44	1.02	1.82	2.50	0.12	3.57	97.48	66
GDM0925-09C	Patquía Fm.	64.54	1.08	13.42	6.44	0.09	2.80	0.96	1.94	2.00	0.09	4.03	97.48	66
GDM0925-09C2	Patquía Fm.	67.00	0.73	14.19	4.84	0.06	1.67	0.95	2.18	2.88	0.05	2.90	97.54	63
GDM0925-10C	Patquía Fm.	63.18	0.81	16.40	5.28	0.06	1.77	0.69	2.70	3.28	0.04	3.00	97.31	64
GDM0925-11C	Patquía Fm.	66.26	0.74	14.79	5.15	0.06	1.48	0.42	2.92	3.05	0.06	2.76	97.79	63
GDM0925-12C	Patquía Fm.	64.69	0.79	15.27	5.43	0.07	1.93	0.67	2.28	3.19	0.07	3.32	97.81	65
GDM0925-13C	Patquía Fm.	65.29	0.77	14.64	4.95	0.06	1.61	1.15	2.01	3.25	0.06	3.43	97.32	63
GDM0925-15C	Patquía Fm.	62.64	0.77	16.04	5.78	0.06	1.79	1.12	2.25	3.83	0.09	3.48	97.95	62
GDM0925-17C	Patquía Fm.	67.17	0.59	12.83	2.06	0.15	1.14	1.46	3.45	2.90	0.08	4.71	96.79	53
GDM0925-19C	Patquía Fm.	65.32	0.63	14.45	4.23	0.06	1.51	0.57	3.82	2.91	0.04	3.52	97.13	58
Agua de Jagüel (AJ)														
ADJ0916-4C	Agua de Jagüel Fm.	86.09	0.63	5.06	2.60	0.05	0.58	0.81	1.13	0.50	0.07	1.66	99.23	58
ADJ0917-2MS	Agua de Jagüel Fm.	54.34	1.01	18.81	6.82	0.09	2.39	1.25	1.03	4.70	0.18	5.12	98.13	72

Table 3 continued. Elemental abundances, loss-on-ignition (LOI), total analyzed abundances, and CIA values for samples from the sedimentary fill of the western margin basins and the southeastern Paraná Basin.

ADJ0917-3C	Agua de Jagüel Fm.	56.22	0.99	17.68	8.17	0.15	2.70	2.10	1.37	3.81	0.18	4.51	97.84	72
ADJ0917-4C	Agua de Jagüel Fm.	56.09	0.51	9.04	6.82	0.08	2.43	1.17	0.70	2.08	0.19	4.94	98.44	66
ADJ0917-5C	Agua de Jagüel Fm.	53.38	1.00	19.01	6.57	0.10	2.24	2.90	1.00	4.60	0.17	5.31	95.80	72
ADJ0917-6C	Agua de Jagüel Fm.	53.01	0.98	19.60	8.12	0.08	2.97	1.04	0.97	4.73	0.17	5.10	97.76	72
ADJ0917-8C	Agua de Jagüel Fm.	57.60	1.02	17.81	6.52	0.26	5.75	9.60	1.20	3.86	0.28	4.56	99.58	73
ADJ0917-9C	Agua de Jagüel Fm.	50.47	1.03	19.52	9.24	0.09	2.37	0.61	0.88	4.38	0.17	6.04	97.65	72
ADJ0917-10C	Agua de Jagüel Fm.	64.51	0.69	14.67	8.94	0.10	3.03	0.54	1.74	2.85	0.18	3.80	97.53	66
ADJ0917-11C	Agua de Jagüel Fm.	62.59	0.99	14.94	5.10	0.44	4.85	7.20	1.64	2.98	0.27	4.13	98.60	66
ADJ0917-12C	Agua de Jagüel Fm.	56.80	1.03	16.27	9.38	0.10	2.63	0.64	1.58	3.23	0.16	5.49	97.38	63
ADJ0917-13C	Agua de Jagüel Fm.	62.97	0.97	14.89	9.20	0.15	2.88	0.66	1.80	2.78	0.18	4.21	97.65	66
ADJ0917-14C	Agua de Jagüel Fm.	58.91	0.88	14.00	8.43	0.08	2.69	0.49	1.45	2.86	0.18	5.60	98.07	58
ADJ0917-15C	Agua de Jagüel Fm.	56.57	1.03	17.42	9.63	0.10	3.19	1.00	1.15	3.91	0.17	5.14	96.59	70
ADJ0918-3C	Agua de Jagüel Fm.	57.22	0.93	16.82	6.32	0.10	1.26	0.79	1.54	3.78	0.18	5.38	98.29	66
ADJ0918-4C	Agua de Jagüel Fm.	55.57	0.96	17.17	6.18	0.06	1.94	0.74	1.71	3.38	0.17	4.66	98.43	71
ADJ0918-7C	Agua de Jagüel Fm.	64.74	1.02	15.44	6.85	0.06	1.76	1.21	1.04	2.83	0.17	4.66	97.66	74
ADJ0918-8C	Agua de Jagüel Fm.	58.15	0.96	17.80	7.95	0.11	2.37	1.39	0.91	3.41	0.22	6.22	97.84	78
ADJ0918-9C	Agua de Jagüel Fm.	57.03	0.95	18.62	8.56	0.07	3.05	0.69	0.88	3.83	0.24	5.37	96.23	74
ADJ0918-10C	Agua de Jagüel Fm.	64.44	0.79	15.27	5.65	0.05	1.49	0.63	1.45	2.90	0.17	4.66	97.82	70
ADJ0918-11C	Agua de Jagüel Fm.	61.31	0.95	17.32	7.43	0.01	1.10	0.23	1.34	3.52	0.21	4.76	96.57	71
ADJ0918-12C	Agua de Jagüel Fm.	62.95	0.94	14.94	7.98	0.04	1.90	0.64	1.61	2.37	0.16	4.67	97.53	68
Paraná Basin Samples														
FQ0820-1D	Itararé Gp.	71.97	0.63	12.53	3.89	0.07	1.42	0.83	1.96	3.60	0.19	3.83	100.92	61
STPA0822-2	Itararé Gp.	56.04	0.87	18.03	8.28	0.03	2.29	0.23	0.72	4.81	0.07	8.08	98.75	69
RR0820-1	Itararé Gp.	67.24	0.83	14.87	3.81	0.01	0.99	0.23	0.51	4.65	0.11	7.57	98.75	69
MP01	Itararé Gp.	68.99	0.98	15.33	0.68	0.05	0.27	0.01	0.05	4.16	0.12	4.85	95.49	78
ITA0823-1	Itararé Gp.	65.22	1.06	23.37	1.06	0.00	ND	0.02	0.00	0.68	0.03	1.02	92.46	97
RB0823-1	Rio Bonito Fm.	68.88	0.67	20.71	0.96	0.00	ND	0.01	ND	0.50	0.02	7.84	99.59	98
ND - not detected														

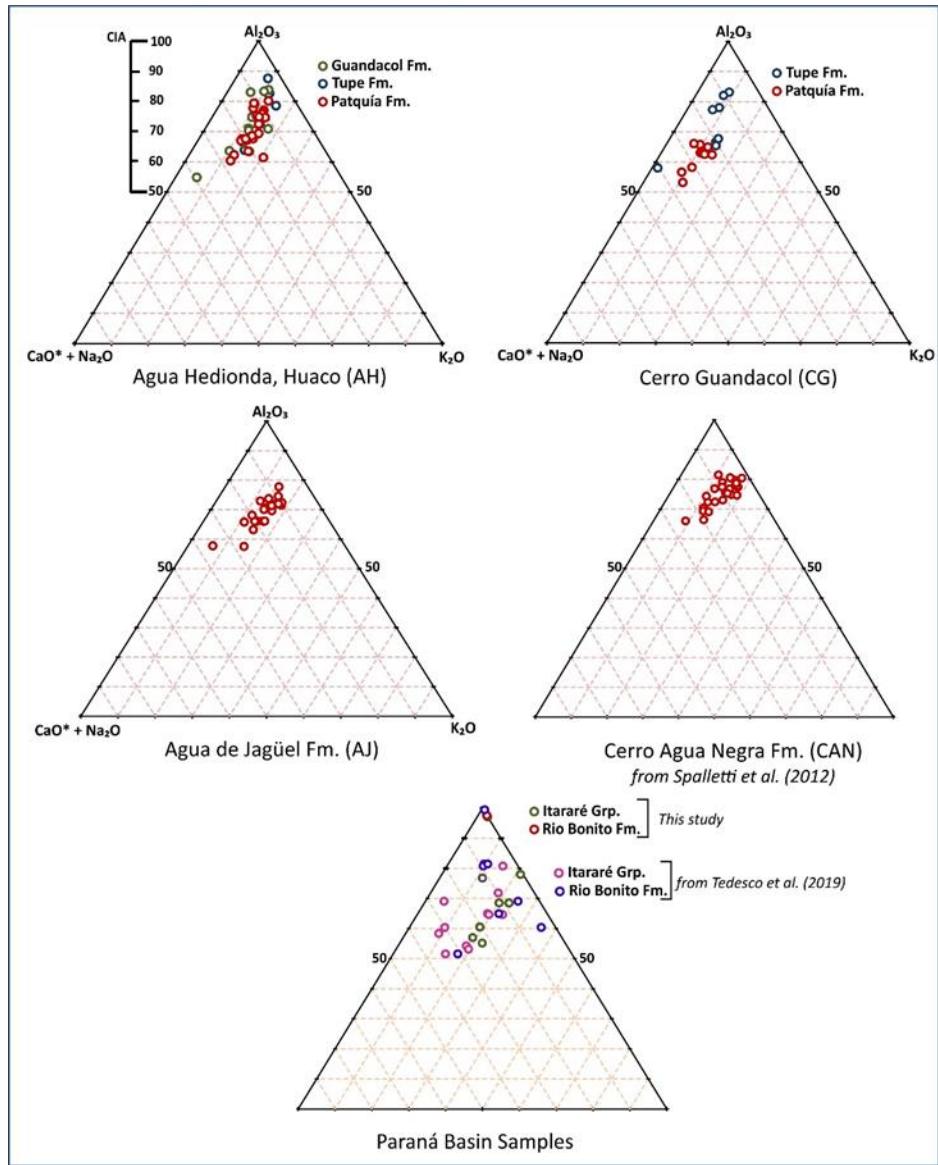


Figure 28. Ternary plots of Al_2O_3 vs. CaO^*+Na_2O vs. K_2O (A=CN-K) system (Nesbitt and Young, 1989). The distribution of data points at each locality is consistent with loss of alkalinity through chemical weathering. Cerro Agua Negra Formation data is from Spalletti et al. (2012), and comparison data for the Paraná Basin is from Tedesco et al. (2019).

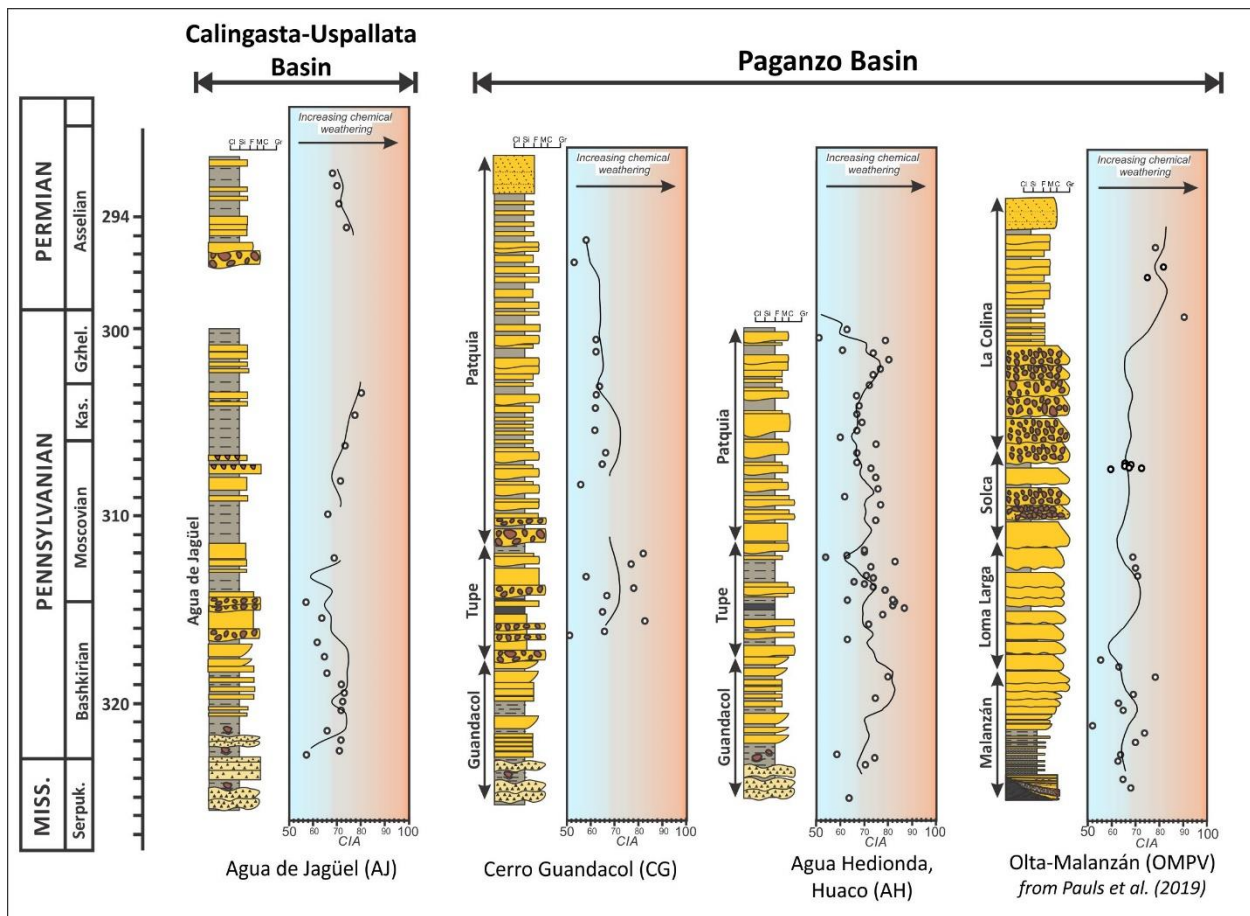


Figure 29. Generalized stratigraphic sections from Agua de Jagüel (AJ), Cerro Guandacol, Huaco (AH) based on the chronostratigraphic correlations from Césari et al. (2011), compared to the Olta-Malanzán Paleovalley (OMPV) data from Pauls et al. (2019). The Chemical Index of Alteration (CIA) values for each section have been plotted next to their approximate location within the succession and can also be found in Table 3. Left to right on the individual columns indicates increased chemical weathering and an inferred humid paleoclimate (i.e. blue is more arid and orange is more humid). The solid black line is a three-point moving average to give a better visual of the paleoclimate trend through time.

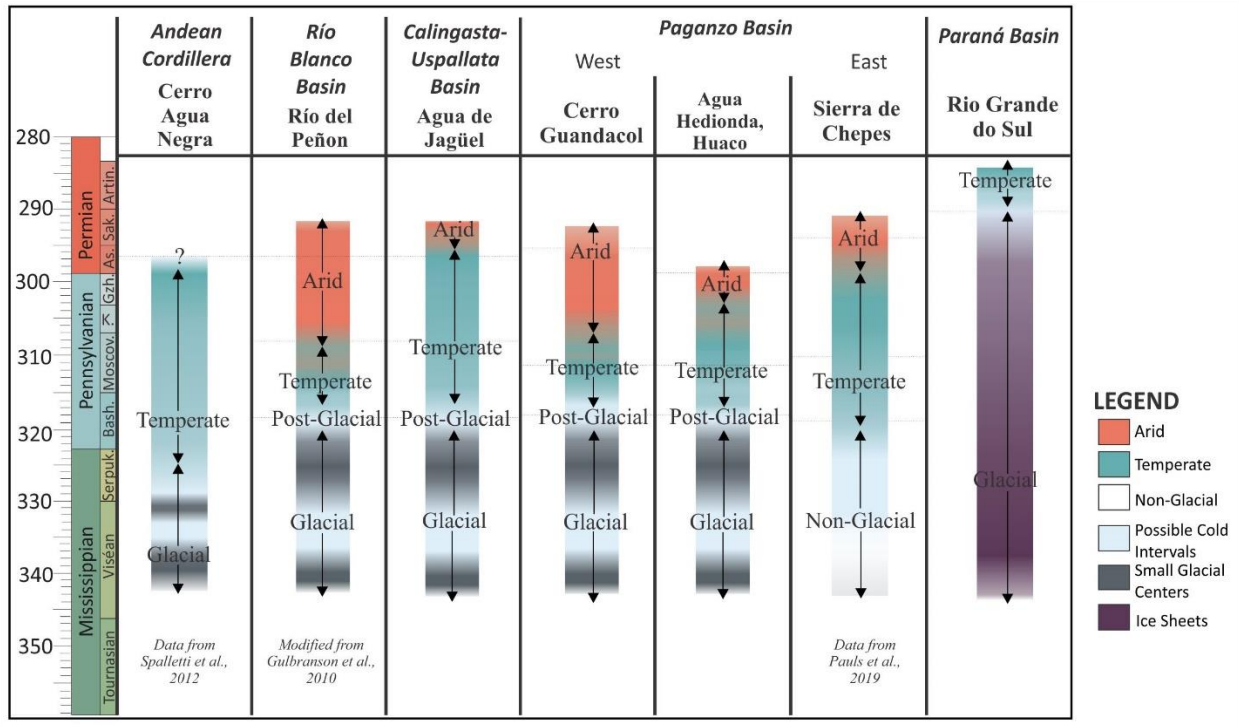
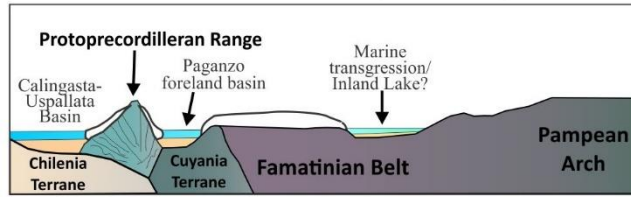
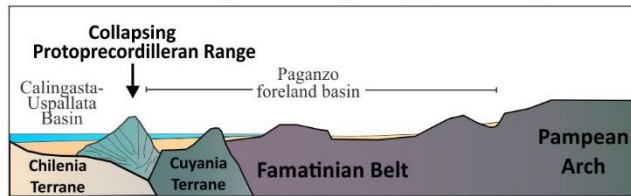


Figure 30. Glacial and cold intervals for South American Gondwana from west to east. Modified from Isbell et al. (2012), and based on data from Limarino and Spalletti (2006), Henry et al. (2008, 2010), Rocha-Campos et al. (2008), Gulbranson et al. (2010), Isbell et al. (2012), Limarino et al. (2014), Moxness et al. (2018), Fedorchuk et al. (2019), and Griffis et al. (2019).

A. Middle Carboniferous uplift and glaciation



B. Middle Pennsylvanian post-glacial deposition



C. Late Carboniferous-Permian back-arc extension

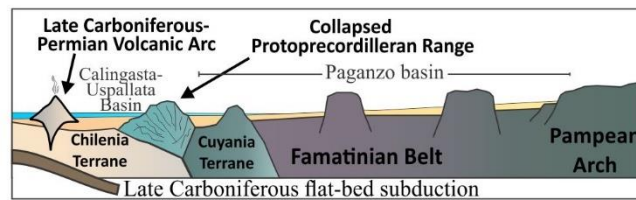


Figure 31. Cross-sectional view of the western margin of Gondwana and the proposed tectonism model during the middle Carboniferous to the Permian.

References

- Alonso-Muruaga, P.J., Limarino, C.O., Spalletti, L.A., Piñol, F.C., 2018. Depositional settings and evolution of a fjord system during the carboniferous glaciation in Northwest Argentina. *Journal of South American Earth Sciences* 369, pp. 28-45.
- Amos, A.J., and Rolleri, E., 1965. El Carbónico marino en el valle Calingasta-Uspallata, San Juan-Mendoza: *Boletín de Informaciones Petroleras* 368, pp. 50–71.
- Aquino, C.D., Milana, J.P., Faccini, U.F., 2014. New glacial evidences at the Talacasto paleofjord (Paganzo basin, W-Argentina) and its implications for the paleogeography of the Gondwana margin. *Journal of South American Earth Sciences* 56, pp. 278-300.
- Astini, R.A., Benedetto, J.L., & Vaccari, N.E. 1995. The Early Paleozoic evolution of the Argentine Precordillera as a Laurentian rifted, drifted and collided terrane: a geodynamic model. *Geological Society of America Bulletin*, 107, 253-273. doi:10.1130/0016-7606(1995)107<0253:TEPEOT>2.3.CO;2
- Astini, R.A., Martina, F., Ezpeleta, M., Dávila, F.D., Cawood, P.A., 2009. Chronology from Rifting to Foreland Basin in the Paganzo Basin (Argentina), and a Reappraisal on the "eo- and Neohercynian" Tectonics along Western Gondwana., XII Congreso Geológico Chileno, Santiago, Chile. Universidad de Chile, Santiago, Chile, pp. 1–4 Extended Abstracts S9 010.
- Astini, R., 2010. Linked basins and sedimentary products across an accretionary margin: the case for the late history of the peri-Gondwanan Terra Australis orogen through the stratigraphic record of the Paganzo Basin. In: Papa, C., Astini, R. (eds.), *Field Excursion Guidebook*, 18th International Sedimentological Congress. International Association of Sedimentologists, Mendoza, Argentina, pp. 58.
- Azcuy, C.L., Carrizo, H.A., Caminos, R., 1999. Carbonífero y Pérmico de las Sierras Pampeanas, Famatina, Precordillera, Cordillera Frontal y Bloque de San Rafael. *Instituto de Geología y Recursos Minerales Geología Argentina* 29, pp. 261-318.
- Bahlburg, H., Dobrzinski, N., 2011. A review of the Chemical Index of Alteration (CIA) and its application to the study of Neoproterozoic glacial deposits and climate transitions. In: Arnaud E., Halverson, G.P., Shields-Zhou, G. (Eds.) *The Geological Record of Neoproterozoic Glaciations*, Geological Society, London, *Memoirs* 36, p. 81-92.
- Bauluz, B., Mayayo, M.J., Fernandez-Nieto, C., Lopez, J.M.G., 2000. Geochemistry of Precambrian and Paleozoic siliciclastic rocks from the Iberian Range (NE Spain): implications for source-area weathering, sorting, provenance, and tectonic setting. *Chemical Geology* 168, pp. 135–150.
- Broccoli and Manabe, 1997. *Mountains and Midlatitude Aridity*: In Ruddiman, W.F. (ed.) *Tectonic uplift and climate change*, New York, NY, United States (USA), Plenum Press, New York, NY.

- Byers, H.L., McHenry, L.J., Grundl, T.J., 2016. Forty-Nine Major and Trace Element Concentrations Measured in Soil Reference Materials NIST SRM 2586, 2587, 2709a, 2710a and 2711a Using ICP-MS and Wavelength Dispersive-XRF. *Geostandards and Geoanalytical Research* 40, 3, pp. 433-445.
- Caputo, M.V., Crowell, J.C., 1985. Migration of glacial centers across Gondwana during Paleozoic Era. *Geological Society of America Bulletin* 96, pp. 1020-1036.
- Caputo, M. V., de Melo, J. H. G., Streef, M., Isbell, J. L., 2008. Late Devonian and Early Carboniferous glacial records of South America, in Fielding, C. R., Frank, T. D., and Isbell, J. L., eds., *Resolving the Late Paleozoic Ice Age in Time and Space*: Boulder, CO, Geological Society of America Special Publication, pp. 161-173.
- Césari, S.N., Limarino, C.O., Gulbranson, E.L., 2011. An Upper Paleozoic bio-chronostratigraphic scheme for the western margin of Gondwana. *Earth Science Reviews* 106, pp. 149-160.
- Díaz-Martínez, E., Vavrodova, M., Bek, J., Isaacson, P.E., 1999. Late Devonian (Famennian) Glaciation in Western Gondwana: Evidence from the Central Andes. In: R. Feist, J.A. Talent & A. Daurer (Eds.), *North Gondwana: Mid-Paleozoic Terranes, Stratigraphy and Biota*: *Abhandlungen Der Geologischen Bundesanstalt*, pp. 213-237.
- Dykstra, M., Kneller, B., Milana, J.P., 2006. Deglacial and postglacial sedimentary architecture in a deeply incised paleovalley–paleofjord — the Pennsylvanian (late Carboniferous) Jejenes Formation, San Juan, Argentina. *Geological Society of America Bulletin* 118, pp. 913–937.
- Einhorn, J.C., Gehrels, G.E., Vernon, A., and DeCelles, P.G., 2015. U-Pb zircon geochronology of Neoproterozoic–Paleozoic sandstones and Paleozoic plutonic rocks in the Central Andes (21°S–26°S), in DeCelles, P.G., Ducea, M.N., Carrapa, B., and Kapp, P.A., eds., *Geodynamics of a Cordilleran Orogenic System: The Central Andes of Argentina and Northern Chile*: Geological Society of America Memoir 212, pp. 115–124, doi:10.1130/2015.1212(06).
- Enkelmann, E., Ridgway, K.D., Carignano, C., Linnemann, U., 2014. A thermochronometric view into an ancient landscape: tectonic setting, and inversion of the Paleozoic eastern Paganzo basin, Argentina. *Lithosphere* 6, pp. 93–107.
- Eyles, C.H., Eyles, N., França, A.B., 1993. Glaciation and tectonics in an active intracratonic basin: The late Paleozoic Itararé Group, Paraná Basin, Brazil: *Sedimentology* 40, pp. 1–25, doi: 10.1111/j.1365-3091.1993.tb01087.x.
- Ezpeleta, M., Rustán, J.J., Balseiro, Dávila, F.M., Dahlquist, J.A., Vaccari, N.E., Sterren, A.F., Prestianni, C., Cisterna, G.A., Basei, M., 2020. Glaciomarine sequence stratigraphy in the Mississippian Río Blanco Basin, Argentina, southwestern Gondwana. Basin analysis and palaeoclimatic implications for the Late Paleozoic Ice Age during the Tournaisian. *Journal of the Geological Society*. doi:10.1144/jgs2019-214.

- Fedo, C.M., Nesbitt, H.W., Young, G.M., 1995. Unraveling the effects of potassium metasomatism in sedimentary rocks and paleosols, with implications for paleoweathering conditions and provenance. *Geology* 23, pp. 921-924.
- Fielding, C.R., Frank, T.D., Isbell, J.L., 2008. The late Paleozoic ice age—A review of current understanding and synthesis of global climate patterns, in Fielding, C.R., Frank, T.D., and Isbell, J.L., eds., *Resolving the Late Paleozoic Ice Age in Time and Space*. Geological Society of America Special Paper 441, pp. 343-354.
- França, A.B., Potter, P.E., 1988. Estratigrafia, ambiente deposicional e análise de reservatório do Grupo Itararé (Permocarbonífero), da Bacia do Paraná (Parte 1): *Boletim de Geociências da Petrobrás* 2, no. 2/4, p. 147–191.
- França, A.B., 1994. Itararé Group: Gondwanan Carboniferous-Permian of the Paraná Basin, Brazil, in Deynoux, M., Miller, J.M.G., Domack, E.W., Eyles, N., Fairchild, I.J., and Young, G.M., eds., *Earth's Glacial Record*: Cambridge, UK, Cambridge University Press, pp. 70–82.
- Gastaldo, R.A., DiMichele, W.A., Pfefferkorn, H.W., 1996. Out of the icehouse into the greenhouse: a late Paleozoic analogue for modern global vegetational change. *GSA Today* 10, pp. 1-7.
- Goldberg, K., Humayun, M., 2010. The applicability of the Chemical Index of Alteration as a paleoclimatic indicator: An example from the Permian of the Paraná Basin, Brazil. *Palaeogeography, Palaeoclimatology, Palaeoecology* 293, pp. 175-183.
- Gonzalez Bonorino, G., 1975. Acerca de la existencia de la Protoprecordillera de cuyo. in *actas. VI congreso geologico Argentino*. Bahia Blanca 1, pp. 101-107.
- Griffis, N.P., Montañez, I.P., Fedorchuk, N., Isbell, J., Mundil, R., Vesely, F., Weinshultz, L., Iannuzzi, R., Gulbranson, E., Taboada, A., Pagani, A., Sanborn, M.E., Huyskens, M., Wimpenny, J., Linol, B., Yin, Q.-Z., 2019. Isotopes to ice: Constraining provenance of glacial deposits and ice centers in west-central Gondwana. *Palaeogeography, Palaeoclimatology, Palaeoecology* 531. doi:10.1016/j.palaeo.2018.04.020.
- Guená, S.E., Escosteguy, L.D., 2010. Paleomagnetism of the Carboniferous-Permian Patquía Formation Paganzo basin, Argentina: implications for the apparent polar wander path for South America and Gondwana during the Late Paleozoic: *Geologica Acta* 8, 4, pp. 373-397.
- Gulbranson E.L., Montañez, I.P., Schmitz, M.D., Limarino, C.O., Isbell, J.L., Marensi, S.A., Crowley, J.L., 2010. High-precision U–Pb calibration of Carboniferous glaciation and climate history, Paganzo Group, NW Argentina. *Geological Society of America Bulletin* 122, pp. 1480–1498.
- Gulbranson, E.L., Montañez, I.P., Tabor, N., Limarino, C.O., 2015. Late Pennsylvanian aridification on the southwestern margin of Gondwana (Paganzo Basin, NW Argentina): A regional expression of a global climate perturbation. *Palaeogeography Palaeoclimatology Palaeoecology* 417, pp. 220-235.

- Heckel, P.H., 1994. Evaluation of evidence for glacio-eustatic control over marine Pennsylvanian cyclothems in North America and consideration of possible tectonic effects: In: Dennison, J.M., Ettensohn, F.R. (Eds.), *Tectonic and eustatic controls on sedimentary cycles*: Tulsa, Oklahoma, SEPM (Society for Sedimentary Geology) Concepts in Sedimentology and Paleontology 4, pp. 65–87.
- Heckel, P.H., 2008. Pennsylvanian cyclothems in midcontinent North America as far-field effects of waxing and waning of Gondwana ice sheets. In: Fielding, C.R., Frank, T., Isbell, J.L. (Eds.), *Resolving the Late Paleozoic Ice Age in Time and Space*: Geological Society of America Special Paper 441, pp. 275–289.
- Henry, L.C., 2007. Carboniferous glacial deposits of the Hoyada Verde and Tramojo Formations of the Calingasta-Uspallata Basin, west central Argentina: M.S. Thesis, University of Wisconsin-Milwaukee, 151 p.
- Henry, L.C., Isbell, J.L., Limarino, C.O., 2008. Carboniferous glacial deposits of the Protoprecordillera of west central Argentina. In: Fielding, C.R., Frank, T.D., Isbell, J.L. (Eds.), *Resolving the Late Paleozoic Ice Age in Time and Space*: Geological Society of America Special Paper 441, pp. 131–142.
- Henry L.C., Isbell, J.L., Limarino, C.O., McHenry, L.J., Fraiser, M.L., 2010. Mid-Carboniferous deglaciation of the Protoprecordillera, Argentina, recorded in the Agua de Jagüel paleovalley. *Palaeogeography, Palaeoclimatology, Palaeoecology* 298, pp. 112–129.
- Holz, M., Souza, P. A., Iannuzzi, R., 2008. Sequence stratigraphy and biostratigraphy of the Late Carboniferous to Early Permian glacial succession (Itarare Subgroup) at the eastern-southeastern margin of the Parana Basin, Brazil. *Special Paper - Geological Society of America* 441, pp. 115-129.
- Horton D.E., Poulsen, C.J., 2009. Paradox of late Paleozoic glacioeustasy. *Geology* 37, 715–718.
- Isbell, J.L., Miller, M.F., Wolfe, K.L. & Lenaker, P.A., 2003, Timing of late Paleozoic glaciation in Gondwana: was glaciation responsible for the development of northern hemisphere cyclothems?: in *Extreme depositional environments: mega end members in geologic time*, eds. M. A. Chan & A. W. Archer Boulder, Colorado: Geological Society of America Special Paper, pp. 5-24.
- Isbell, J.L., Fraiser, M.L., Henry, L.C., 2008. Examining the complexity of environmental change during the late Paleozoic and early Mesozoic: *Palaios* 23, 5-6, pp. 267-269.
- Isbell, J.L., Henry, L.C., Gulbranson, E.L., Limarino, C.O., Fraiser, M.L., Koch, Z.J., Ciccioli, P.L. & Dineen, A.A., 2012. Glacial paradoxes during the late Paleozoic ice age: Evaluating the equilibrium line altitude as a control on glaciation. *Gondwana Research* 22, pp. 1-19.

- Isaacson, P.E., Díaz-Martínez, E., Grader, G.W., Kalvoda, J., Babek, O., Devuyst, F.X., 2008. Late Devonian–earliest Mississippian glaciation in Gondwanaland and its biogeographic consequences. *Palaeogeography, Palaeoclimatology, Palaeoecology* 268, pp. 126–142. doi:10.1016/j.palaeo.2008.03.047.
- Isaacson, P.E., Hladil, J., Jian-Wei, S., Kalvoda, J., Grader, G., 1999. Late Devonian (Famennian) Glaciation in South America and Marine Offlap on other Continents. In: R. Feist, J.A. Talent & A. Daurer (Eds.), *North Gondwana: Mid-Paleozoic Terranes, Stratigraphy and Biota: Abhandlungen Der Geologischen Bundesanstalt*, pp. 239–257.
- Keller, M., 1999, Argentine Precordillera: Sedimentary and plate tectonic history of a Laurentian crustal fragment in South America: *Geological Society of America Special Paper* 341, 131 p., doi: 10.1130 /0-8137-2341-8.1.
- Kneller, B., Milana, J.P., Buckee, C., Al Ja'aidi, O.S., 2004. A depositional record of deglaciation in a paleofjord (Late Carboniferous [Pennsylvanian] of San Juan Province, Argentina): the role of catastrophic sedimentation. *Geological Society of America Bulletin* 116, pp. 348–367.
- Kołtonik, K., Isaacson, P.E., Piszczowska, A., Paszkowski, M., Augustsson, C., Szczerba, M., Slama, J., Budzyń, B., Stachacz, M., Krawczyński, W., 2019. Provenance of upper Paleozoic siliciclastics rocks from two high-latitude glacially influenced intervals in Bolivia. *Journal of South American Earth Sciences* 92, pp. 12–31. doi:10.1016/j.jsames.2019.02.023.
- Lawver, L.A., Dalziel, I.W.D., Norton, I.O., Gahagan, L.M., 2008. The Plates 2007 Atlas of Plate Reconstructions (750 Ma to Present Day), *Plates Progress Report No. 305–0307*. University of Texas Technical Report No. 195, 160 pp.
- Limarino, C.O., Marensi, S.A., Tripaldi, A., Caselli, A.T., 2002a. Evolution of the Upper Paleozoic basins of western Argentina during the maximum extent of Gondwana. 16th International Sedimentological Congress, Abstracts, 224–225.
- Limarino, C.O., Césari, S.N., Net, L.I., Marensi, S.A., Gutiérrez, P.R., Tripaldi, A., 2002b. The Upper Carboniferous postglacial transgression in the Paganzo and Río Blanco Basins (northwestern Argentina): facies and stratigraphic significance. *Journal of South American Earth Sciences* 15, pp. 445–460.
- Limarino, C.O., Spalletti, L.A., 2006. Paleogeography of the Upper Paleozoic basins of southern South America: an overview. *Journal of South American Earth Sciences* 22, pp. 134–155.
- Limarino, C.O., Tripaldi, A., Marensi, S., Fauqué, L., 2006. Tectonic, sea level, and climatic controls on late Paleozoic sedimentation in the western basins of Argentina. *Journal of South American Earth Sciences* 33, pp. 205–226.
- Limarino, C.O., Césari, S.N., Spalletti, L.A., Taboada, A.C., Isbell, J.L., Geuna, S., Gulbranson, E.L., 2014. A paleoclimatic review of southern South America during the late Paleozoic;

- A record from icehouse to extreme greenhouse conditions: *Gondwana Research* 25, pp. 1396-1421.
- López Gamundí, O.R., 1997. Glacial–postglacial transition in the late Paleozoic basins of southern South America. In: Martini, I.P. (Ed.), *Late Glacial and Postglacial Environmental Changes: Quaternary, Carboniferous–Permian, and Proterozoic*. Oxford University Press, Oxford, UK, pp. 147–168.
- López-Gamundí, O.R., Espejo, I.S., Conaghan, P.J., Powell, C.McA., Veevers, J.J., 1994. Southern South America. In: Veevers, J.J., Powell, C.McA. (Eds.), *Permian–Triassic Pangean basins and foldbelts along the Panthalassan margin of Gondwanaland*. Boulder, Colorado: Geological Society of America Memoir 184, 281–329.
- Maynard, J.B., 1992. Chemistry of modern soils as a guide to interpreting Precambrian paleosols. *Journal of Geology* 100, pp. 279–289.
- McHenry, L.J., 2009. Element mobility during zeolitic and argillic alteration of volcanic ash in a closed-basin lacustrine environment: case study Olduvai Gorge, Tanzania. *Chemical Geology* 265, pp. 540–552.
- McHenry, L.J., Carson, G.L., Dixon, D.T., Vickery, C.L., 2017. Secondary minerals associated with Lassen fumaroles and hot springs: Implications for martian hydrothermal deposits: *American Mineralogist* 102, pp. 1418-1434. doi:10.2138/am-2107-5839.
- Milana, J.P., 1988. Sedimentación estuarica carbonífera tardía en la Precordillera central, San Juan, Argentina. 2 Reunion Argent. Sedimentol. (Buenos Aires). Actas, pp. 185-188.
- Milana, J.P., Bercowski, F., 1987. Rasgos erosivos y depositacionales glaciales en el neopaleozoico de la precordillera central, San Juan, Argentina. 4a Reun. Internac. Work.roup PICG-211 (IUGS-UNESCO), St. Cruz Sierra, Bolivia, Abstracts, pp. 46-48.
- Milana, J.P., Bercowski, F., 1990. Facies y geometría de depositos glaciales en un paleovalle Carbonífero de Precordillera Central, San Juan, Argentina, 3 Reunion Argentina de Sedimentología (San Juan). Actas, pp. 199-204.
- Milana, J.P., Bercowski, F., 1993. Late Palaeozoic Glaciation in Paganzo Basin, Western Argentina: Sedimentological Evidence. *Comptes Rendus XII ICC-P, Bs. As, v.1*, pp. 325-335.
- Milana, J.P., di Pasquo, M.M., 2019. New chronostratigraphy for a Lower to Upper Carboniferous strike-slip basin of W-Precordillera (Argentina): its paleogeographic, tectonic and glacial importance. *Journal of South American Earth Sciences* 96. <https://doi.org/10.1016/j.jsames.2019.102383>.
- Milani, E.J., França, A.B., and Schneider, R.L., 1994. Bacia do Paraná: *Boletim de Geociências da Petrobras* 8, pp. 69–82.

- Montañez, I.P., Tabor, N.J., Niemeier, D., DiMichele, W.A., Frank, T.D., Fielding, C.R., Isbell, J.L., Birgenheir, L.P., Rygel, M.C., 2007, CO₂-forced climate and vegetative instability during late Paleozoic deglaciation: *Science* 315, pp. 87–91.
- Montañez, I.P., Poulsen, C.J., 2013, The late Paleozoic ice age: An evolving paradigm: *Annual Review of Earth and Planetary Sciences* 41, pp. 24.1-24.
- Mottin, T.E., Vesely, F.F., Rodrigues, M.C.N.L., Kipper, F., Souza, P.A., 2018. The paths and timing of late Paleozoic ice revisited: New stratigraphic and paleo-ice flow interpretations from a glacial succession in the upper Itararé Group (Paraná Basin, Brazil). *Palaeogeography, Palaeoclimatology, Palaeoecology* 490, pp 488-504. doi: 10.1016/j.palaeo.2017.11.031
- Moxness, L.D., Isbell, J.L., Pauls, K.N., Limarino, C.O., Schencman, J., 2018, Sedimentology of the mid-Carboniferous fill of the Olta paleovalley, eastern Paganzo Basin, Argentina: Implications for glaciation and controls on diachronous deglaciation in western Gondwana during the late Paleozoic Ice Age. *Journal of South American Earth Sciences* 84, p 127-148. doi/10.1016/j.jsames.2018.03.015
- Nesbitt, H.W., Young, G.M., 1982, Early Proterozoic climates and plate motions inferred from major element chemistry from lutites. *Nature* 199, pp. 715-717.
- Net, L.I., Alonso, M.S., Limarino, C.O., 2002. Source rock and environmental control on clay mineral associations, lower section of Paganzo group (Carboniferous), northwest Argentina. *Sedimentary Geology* 152, pp. 183–199.
- Net, L.I., Limarino, C.O., 2006. Applying sandstone petrofacies to unravel the Upper Carboniferous evolution of the Paganzo Basin, northwest Argentina. *Journal of South American Earth Sciences* 22, pp. 239–254.
- Newell, A.J., Tverdokhlebov, V.P., Benton, M.J., 1999. Interplay of tectonics and climate on a transverse fluvial system, Upper Permian, Southern Uralian Foreland Basin, Russia: *Sedimentary Geology* 127, pp. 11-29.
- Pankhurst, R.J., Rapela, C.W., Saavedra, J., Baldo, E., Dahlquist, J., Pascua, I., Fanning, C.M., 1998. The Famatinian magmatic arc in the Central Sierras Pampeanas: An early to mid-Ordovician continental arc on the Gondwana margin. In: Pankhurst, R.J., Rapela, C.W. (Eds.), *The Proto-Andean Margin of Gondwana*. Geological Society of London Special Publication 142, pp. 343-367.
- Pankhurst, R.J., Rapela, C.W., Fanning, C.M., 2000. Age and origin of coeval TTG, I- and S-type granites in the Famatinian belt of NW Argentina. *Earth and Environmental Science Transactions of the Royal Society of Edinburgh*, 91, pp. 151-168.
- Partridge, T., 1997. Late Neogene uplift in eastern and southern Africa and its paleoclimatic implications: In Ruddiman, W.F. (ed.) *Tectonic uplift and climate change*, New York, NY, United States (USA), Plenum Press, New York, NY.

- Passchier, S., Erukanure, E., 2010. Palaeoenvironments and weathering regime of the Neoproterozoic Squantum ‘Tillite’, Boston Basin: no evidence of a snowball Earth. *Sedimentology* 57, pp. 1526-1544.
- Passchier, S., Bohaty, S.M., Jiménez-Espejo, F., Pross, J., Röhl, U., van de Flierdt, T., Escutia, C., Brinkhuis, H., 2013. Early Eocene to middle Miocene cooling and aridification of East Antarctica. *Geochemistry Geophysics Geosystems* 14, 5. doi:10.1002/ggge.20106.
- Pauls, K.N., Isbell, J.L., McHenry, L., Limarino, C.O., Moxness, L.D., Schencman, L.J., 2019. A paleoclimatic reconstruction of the Carboniferous-Permian paleovalley fill in the Eastern Paganzo Basin: Insights into glacial extent and deglaciation of southwestern Gondwana. *Journal of South American Earth Sciences* 95. doi:10.1016/j.jsames.2019.102236.
- Pauls, K.N., Isbell, J.L., Limarino, C.O., Alonso-Muruaga, P.J., Malone, D.H., Schencman, L.J., Colombi, C.E., Moxness, L.D., in review. Constraining late Paleozoic ice extent in the Paganzo Basin of western Argentina utilizing U-Pb detrital zircon geochronology for the lower Paganzo Group strata. *Journal of South American Earth Sciences*.
- Pazos, P.J., 2002. The Late Carboniferous glacial to postglacial transition: facies and sequence stratigraphy, western Paganzo Basin, Argentina. *Gondwana Research* 5, pp. 467–487.
- Pérez Loinaze, V.S., Limarino, C.O., Césari, S.N., 2010. Glacial events in Carboniferous sequences from Paganzo and Río Blanco Basins (Northwest Argentina): palynology and depositional setting. *Geologica Acta* 8, 399–418.
- Powell, C.M., Li, Z.X., 1994. Reconstruction of the Panthalassan margin of Gondwanaland. In: Veevers, J., Powell, C. (Eds.), *Permian–Triassic Transantarctic Basin, Permian–Triassic Pangea Basins and Foldbelts Along the Panthalassan Margin of Gondwanaland: Geologic Society of America Memoir* 184, pp. 5–9.
- Price, J.R., Velbel, M.A., 2003. Chemical weathering indices applied to weathering profiles developed on heterogeneous felsic metamorphic parent rocks. *Chemical Geology* 202, pp. 397–416.
- Ramos, V.A., 1988. Tectonics of the Late Proterozoic–Early Paleozoic: a collisional history of Southern South America. *Episodes* 11, pp. 168–174.
- Ramos, V., Jordan, T., Allmendinger, R., Kay, S., Cortés, J., Palma, M., 1984. Chilenia: un terreno alóctono en la evolución paleozoica de los Andes Centrales. In: 10° Congr. Geol., vol. 2. Actas, Argentino, pp. 84–106.
- Ramos, V., Jordan, T., Allmendinger, R., Mpodozis, C., Kay, S., Cortés, J., Palma, M., 1986. Paleozoic terranes of the central Argentine-Chilean Andes. *Tectonics* 5, pp. 855–888.
- Ramos, V.A., 1999. Evolución tectónica de la Argentina. In: *Rasgos Estructurales del Territorio Argentino*. Instituto de Geología y Recursos Minerales, *Geología Argentina Anales* 29 (24), pp. 715-784.

- Rocha-Campos, A.C., dos Santos, P.R., Canuto, J.R., 2008. Late Paleozoic glacial deposits of Brazil; Parana Basin. In: Fielding, C.R., Frank, T.D., Isbell, J.L. (Eds.), *Resolving the Late Paleozoic Ice Age in Time and Space: Geological Society of America Special Paper 441*, pp. 97–114.
- Rosa, E.L.M., Vesely, F.F., Isbell, J.L., Kipper, F., Fedorchuk, N.D., Souza, P.A., 2019. Constraining the timing, kinematics and cyclicity of Mississippian-Early Pennsylvanian glaciations in the Paraná Basin, Brazil. *Sedimentary Geology* 384, pp. 29-49. doi:10.1016/j.sedgeo.2019.03.001.
- Royer, D. L., Berner, R. A., Montañez, I. P., Tabor, N. J., and Beerling, D. J., 2004, CO₂ as a primary driver of Phanerozoic climate: *GSA Today*, v. 14, no. 3, p. 4-10.
- Ruddiman, W. F., and Prell, W. L., 1997. *Introduction to the uplift-climate connection*. New York, NY, United States (USA), Plenum Press, New York, NY, Tectonic uplift and climate change.
- Ruddiman, W. F., Raymo, M. E., Prell, W. L., and Kutzbach, J. E., 1997. *The uplift-climate connection: a synthesis*. New York, NY, United States (USA), Plenum Press, New York, NY, Tectonic uplift and climate change.
- Rygel, M.C., Fielding, C.R., Frank, T.D., Birgenheier, L.P., 2008. The magnitude of late Paleozoic glacioeustatic fluctuations: a synthesis. *Journal of Sedimentary Research* 78, pp. 500–511.
- Scotese, C.R., Barrett, S. 1999. Gondwana's movement over the South Pole during the Palaeozoic: evidence from lithological indicators of climate. In: McKerrow, W.S., Scotese, C.R. (Eds.), *Palaeozoic Palaeogeography and Biogeography*, Geological Society, London, *Memoirs*, 12, pp. 75–85.
- Sheldon, N.D., 2006. Abrupt chemical weathering increase across the Permian–Triassic boundary. *Palaeogeography, Palaeoclimatology, Palaeoecology* 231, pp. 315–321.
- Sheldon, N.D., Tabor, N.J., 2009. Quantitative paleoenvironmental and paleoclimatic reconstruction using paleosols. *Earth Science Reviews* 95, pp. 1–52.
- Socha et al., 2014. Gondwana glacial paleolandscape, diamictite record of Carboniferous valley glaciation and preglacial remnants of an ancient weathering front in Northwestern Argentina, in *Gondwana Landscapes in southern South America*.
- Soreghan, M.J., Soreghan, G.S., 2007. Whole-rock geochemistry of upper Paleozoic loessite, western Pangaea: implications for paleo-atmospheric circulation. *Earth and Planetary Science Letters* 255, 117–132.
- Spalletti, L.A., Limarino, C.O., Piñol, F.C., 2012. Petrology and geochemistry of Carboniferous siliciclastics from the Argentine Frontal Cordillera: A test of methods for interpreting provenance and tectonic setting. *Journal of South American Earth Sciences* 36, pp. 32-54. doi:10.1016/j.jsames.2011.11.002.

- Taboada, A.C., 1997. Bioestratigrafía del Paleozoico Superior marino del Valle de Calingasta-Uspallata, provincias de San Juan y Mendoza. *Ameghiniana* 34, 2, 215–246.
- Tabor, N. J., and Poulsen, C. J., 2008, Palaeoclimate across the Late Pennsylvanian–Early Permian tropical palaeolatitudes; a review of climate indicators, their distribution, and relation to palaeophysiographic climate factors: *Palaeogeography, Palaeoclimatology, Palaeoecology*, v. 268, no. 3-4, pp. 293-310.
- Tedesco, A., Ciccio, P., Suriano, J., Limarino, C., 2010, Changes in the architecture of fluvial deposits in the Paganzo Basin (Upper Paleozoic of San Juan Province): an example of sea level and climatic controls on the development of coastal fluvial environments. *Geologica Acta*.
- Tedesco, J., Cagliari, J., Júnior, F.C., Girelli, T.J., Lana, C., 2019. Provenance and paleogeography of the Southern Paraná Basin: Geochemistry and U/Pb zircon geochronology of the Carboniferous-Permian transition. *Sedimentary Geology* 393-394. doi:10.1016/j.sedgeo.2019.105539
- Thomas, W.A., Astini, R.A., Mueller, P.A., and McClelland, W.C., 2015. Detrital-zircon geochronology and provenance of the Ordovician synorogenic clastic wedge, and Ordovician accretion of the Argentine Precordillera terrane: *Geosphere*, v. 11, no. 6, p. 1749–1769, doi:10.1130/GES01212.1.
- Torsvik, T.H., Cocks, L.R.M., 2016. *Earth History and Paleogeography*. University Printing House, Cambridge University, Cambridge, United Kingdom.
- Valdez Buso, V., Pasquo, M.D., Milana, J.P., Kneller, B., Fallgatter, C., Chemale, F.J., Paim, P.S.G., 2017. Integrated U-Pb zircon and palynological/palaeofloristic age determinations of a Bashkirian palaeofjord fill, Quebrada Grande (Western Argentina). *J. S. Am. Earth Sci.* 73, pp. 202–222.
- Valdez Buso, V., Milana, J.P., di Pasquo, M., Paim, P.S.G., Philipp, R.P., Aquino, C.A., Cagliari, J., Junior, F.C., Kneller, B., 2020. Timing of the Late Paleozoic glaciation in western Gondwana: New ages and correlations from Paganzo and Paraná basins. *Palaeogeography, Palaeoclimatology, Palaeoecology* 544. doi:10.1016/j.palaeo.2020.109624.
- Veevers, J.J., Powell, M., 1987. Late Paleozoic glacial episodes in Gondwanaland reflected in transgressive–regressive depositional sequences in Euramerica. *Geological Society of America Bulletin* 98, pp. 475–487.
- Vesely, F.F., Trzaskos, B., Kipper, F., Assine, M.L., Souza, P.A., 2015. Sedimentary record of a fluctuating ice margin from the Pennsylvanian of western Gondwana: Paraná Basin, southern Brazil. *Sedimentary Geology* 326, pp. 45–63.
- Willner, A.P., Thomson, S.N., Kröner, A., Wartho, J., Wijbrans, J.R., Hervé, F., 2005. Time Markers for the Evolution and Exhumation History of a Late Palaeozoic Paired

Metamorphic Belt in North–Central Chile (34°–35°30'S). *Journal of Petrology* 46, 9, pp. 1835-1858. doi:10.1093/petrology/egi036.

Willner, A.P., Gerdes, A., Massonne, H.-J., 2008. History of crustal growth and recycling at the Pacific convergent margin of South America at latitudes 29° -36° S revealed by a U-Pb and Lu-Hf isotope study of detrital zircon from late Paleozoic accretionary systems. *Chemical Geology* 253, pp. 114-129. doi:10.1016/j.chemgeo.2008.04.016.

Chapter 5. Provenance and paleogeography of the Paganzo Basin: Detrital zircon geochronology of the upper Paganzo Group strata

Abstract

U-Pb detrital zircon analyses of the upper Paganzo Group strata indicate a broadening of the Paganzo Basin, and a shift in sediment source through the end of the Carboniferous from more local sources to more distal sources indicating expansion of regional drainage. Two localities on either side of the Paganzo Basin are compared to determine the drainage development of the Paganzo Basin at the Carboniferous-Permian boundary. At Agua Hedionda near Huaco, the Patquía Formation shows sources that are very similar to the nearby Sierra de Valle Fértil range of the Famatina magmatic belt. The Tupe and Patquía formations here contain late Carboniferous detrital zircons which are linked to late Carboniferous-Permian volcanism to the west of the Precordillera region. At Olta-Malanzán, the detrital zircons of the Loma Larga and La Colina formations display a very similar phenomenon as their counterpart units in the west. The age-distributions from the Loma Larga to the La Colina indicate an eastern shift of the source region for the strata. The upper Paganzo Group strata facies records a drastic shift in climate conditions within the basin, from temperate and seasonal to extremely arid. The evidence from detrital zircon geochronology of selected Paganzo Group units (i.e. Malanzán, Loma Larga, La Colina formations along the eastern boundary and the Guandacol, Tupe and Patquía formations in the west) presented here may also have implications for the regional climate at the end of the Carboniferous.

1. Introduction

Detrital zircon geochronology studies have become an increasingly popular tool to elucidate provenance of late Paleozoic strata and to refine the extent of the glacial centers of Gondwana. However, few studies have been employed to track provenance through time with regards to paleoslope and basin development. Understanding basin development in South American Gondwana proves useful when evaluating climate transitions, as these could be related more to regional climate drivers rather than global climate drivers. The Paganzo Basin in Argentina provides an excellent location to analyze basin evolution using detrital zircon geochronology due to changing tectonic conditions along the convergent margin of western South America during the Carboniferous and Permian (Fig. 32).

Previous studies have conducted provenance analyses using petrology and major and minor elemental methods (cf. Net, 1999; Net et al., 2002; Net and Limarino, 2006; Spalletti et al., 2012), but none thus far have conducted a detrital zircon geochronology analysis of the Paganzo Group strata from the middle Carboniferous through the Permian strata (i.e. Tupe and Patquía formations and Loma Larga and La Colina formations; Fig. 33). These studies, too, have alluded to provenance shifts in the Paganzo Basin but are limited by the mineralogy of the strata, which can be problematic due to the widespread and similar igneous and metamorphic suites across the basin. Here, we present evidence that refines the understanding of potential source material for six units within the Paganzo Group.

In this study, we present new U-Pb detrital zircon ages of sedimentary rocks from the upper Paganzo Group (late Carboniferous-Permian) strata recorded in the easternmost and western margins of the Paganzo Basin in western Argentina. The main objectives of the study are

1) to understand the evolution of provenance and sediment dispersal patterns through the Carboniferous and Permian and 2) to identify changes in paleotopography or shifts in possible sources or uplands as the Paganzo Basin developed through time.

2. Regional Geologic Setting

The western margin of Gondwana records a long accretionary and depositional history. Late Paleozoic sedimentary basins overlie a multitude of terranes (i.e. the Pampia, Precordillera, Cuyania and Chilenia terranes), and associated volcanic and sedimentary successions (Fig. 34). The Paganzo Basin overlies basement rocks ranging from the Sierras Pampeanas in the east to the Precordillera and Cuyania terranes in the west (Pankhurst et al., 1998; Ramos et al., 1998, 2015; Rapela et al., 1998; Ramos, 1999, 2008, 2010; Rapalini, 2005; Dahlquist et al., 2010; Einhorn et al., 2015). Paleotopographic highs created by the accretion of the various terranes in this region have been implicated in the climate and depositional histories of the subsequent basins that developed in western Argentina (cf. Limarino et al., 2002, 2006).

The Sierras Pampeanas today make up most of the highlands between the Precordillera terrane and Cuyania terrane and the Río de la Plata craton, and are divided into magmatic or orogenic belts as they correspond to different accretionary events (Fig. 34). The easternmost Sierras Pampeanas were formed during the Cambrian, as the Pampia terrane docked against the Río de La Plata craton, and therefore contain igneous and metamorphic rocks with ages that range from 500 to 600 Ma (Rapela et al., 1998; Ramos et al., 2015). The upland ranges include the Sierra de Córdoba, Sierra del Norte de Córdoba, Sierra Ambato, Sierra Ancasti and others (Rapela et al., 1998; Leal et al., 2003; Llambías et al 2003; Toselli et al., 2003; Fig. 3).

The Sierras Pampeanas also contain Ordovician (490-450 Ma, with the main magmatism occurring between 490-470 Ma) granitic and metamorphic units associated with Famatina magmatism and the eastern portion of the Cuyania Terrane (Pankhurst et al., 1998, 2000; Keller, 1999; Ramos, 1999; Fig. 34). The Famatina orogenic belt runs north-south between the Pampean orogenic belt and the Cuyania composite terrane. In the Paganzo Basin region, evidence of Famatina magmatism can be found in the Sierras de Chepes, Los Llanos, Malanzán and Ulapes, Sierra de San Luis, Sierra de Velasco, Sierra Famatina, and Sierra de Valle Fértil (Pankhurst et al., 1998, 2000; Toselli et al., 2003; Vujovich and Ostera 2003; Dahlquist et al., 2010; Einhorn et al., 2015; Fig. 3). These ranges were paleotopographic highs during the deposition of late Paleozoic sedimentary rocks (Andreis et al., 1986; Buatois and Mangano, 1995; Sterren and Martinez, 1996; Limarino and Spalletti, 2006; Spalletti et al., 2012; Enkelmann et al., 2015; Enkelmann and Garver, 2015; Limarino et al., 2014; Pauls et al., in review).

The Famatina igneous and metamorphic suites are primarily the result of Ordovician intrusions and the thrusting and folding as the result of the docking of the Precordilleran Terrane during the Oclóyic Orogeny (Cambrian-Ordovician; Ramos et al., 1998; Keller, 1999; Ramos, 1999). In the eastern part of the Famatina belt is the Sierras de Chepes region, which contains crystallization ages from 477-497 Ma (Pankhurst et al., 1998; Stuart-Smith et al., 1999; Enkelmann et al., 2014). Additionally, these Ordovician granites were intruded by post-orogenic granitic bodies during the Devonian-early Carboniferous (365-345 Ma; Dahlquist et al., 2010; Martina et al., 2018).

To the west of the Sierra de Valle Fértil is the Cuyania terrane, which contains metamorphic units of Mesoproterozoic age along its easternmost boundary exposed at the surface in the Sierras de Pie de Palo, Umango, Maz and Espinol (Huff et al., 1998; Ottone et al.,

2001; Dahlquist et al., 2010; Sial et al., 2013; Verdecchia et al., 2014, 2018; Thomas et al., 2015; Fig. 3). Obducted onto the Cuyania terrane and the Chilenia terrane is the Precordilleran terrane, which occurred as the result of the Chañic orogeny (middle Devonian to earliest Mississippian) when Chilenia accreted to Gondwana's western margin (Ramos et al., 1984, 1986, 1988). Along the Precordillera, sedimentary packages from the Cambrian through Ordovician contain numerous ashes that are related to the Famatina magmatic arc, with ages ranging from 473-464 Ma (Huff et al., 1997, 1998; Astini, 1998; Ottone et al., 2001; Fanning et al., 2004; Astini et al., 2007; Thompson et al., 2012; Thomas et al., 2015). The Precordillera terrane is hypothesized to be part of a tectonic belt that made up either the Protoprecordilleran range or in some studies the Tontal Arch during the early Carboniferous (cf. Amos and Rolleri, 1965; González Bonorino, 1975; Limarino et al., 2006; Aquino et al., 2014; Valdez Buso et al., 2017, 2020; Milana and di Pasquo, 2019; Pauls et al., in review). This highland formed during the Chañic orogeny as a fold-and-thrust belt as the accretionary prism was obducted (González Bonorino, 1975; Ramos et al., 1984, 1986, 1988; López-Gamundí et al., 1994; Limarino et al., 2002, 2006, 2014; Henry et al., 2008; Isbell et al., 2012).

Subduction continued along the western margin of Gondwana during the Pennsylvanian and is recorded as volcanic rocks and ash layers that range in age from 320-280 Ma (cf. Willner et al., 2005, 2008). This active tectonism is tied to the development of an outboard volcanic arc. As the active subduction margin moved further westward during this time, studies have interpreted the collapse of the Protoprecordilleran range as the barrier between the Panthalassan margin and the continental interior (Ramos, 1988; López-Gamundí et al., 1994; Limarino et al., 2002a, 2006, 2014; Isbell et al., 2012; Spalletti et al., 2012). Therefore, the interior foreland

region was breached for a time prior to the end of the Pennsylvanian (López-Gamundí et al., 1994; Limarino et al., 2002a, 2006, 2014; Isbell et al., 2012; Spalletti et al., 2012).

Late Paleozoic strata in the Paganzo Basin were thus derived from these uplands and terranes and were distributed differentially within the basin. It has been long implied that the tectonic activity of the region has played a large role in the early disappearance of glacial activity within the basin, as well as the increase in aridity recorded in the rocks of the Paganzo Group. A thorough analysis of the units throughout the basin provides insight into the timing of the tectonism, and changes in source regions through time. Additionally, it aids in the overall understanding of the paleogeography of the foreland region during the Carboniferous-Permian climatic transition.

3. Late Paleozoic strata of the Paganzo Basin

The Paganzo Group strata make up the sedimentary fill of the Paganzo Basin, which is subdivided into formations of time-equivalent strata that are correlated using pollen, fossil plants, and radiometric ages from ash and tuff layers from various units (Gulbranson et al., 2010, 2015; Césari et al., 2011, 2019; Valdez Buso et al., 2020; Fig. 35). In the western portion of the Paganzo Basin, for example, the Paganzo Group is divided into the Guandacol (middle Serpukhovian-middle Baskirian), Tupe (middle Bashkirian-early Moscovian), and the Patquía (early Moscovian-early Permian) Formations (Limarino et al., 2006; Guena et al., 2010; Tedesco et al., 2010; Limarino et al., 2014). In the central Paganzo Basin, the Paganzo Group is divided into two formations: Lagares Formation (middle Serpukhovian-late Moscovian) and La Colina Formation (late Moscovian-Wuchiapingian) (Limarino et al., 2006; Guena et al., 2010; Tedesco et al., 2010; Limarino et al., 2014). In the eastern portion of the basin of the Sierras de Chepes

and Los Llanos region, the group is subdivided into the Malanzán Formation (middle Serpukhovian-middle Baskirian), Loma Larga Formation (middle Bashkirian-early Moscovian), Solca (middle Serpukhovian-late Moscovian), Arroyo Totoral (middle Serpukhovian-Wuchiapingian), and La Colina Formation (late Moscovian-Wuchiapingian; Crisafulli and Herbst, 2008; Césari et al., 2011; Limarino et al., 2014).

In the western Paganzo Basin, the base of the Guandacol Formation contains ice-proximal and subglacial deposits (Limarino et al., 2014; Fig. 35). Until a recent study by Moxness et al. (2018), it was thought that ice also existed along the eastern margin of the Paganzo Basin, as there were interpretations of glacial deposits at the base of the Malanzán Formation in the Sierra de Chepes region (Socha, 2006; Socha et al., 2014; Enkelmann et al., 2015; Enkelmann and Garver, 2015). These deposits have been reinterpreted as conglomerates related to alluvial, fluvial, and lacustrine processes in a cold climate environment (Moxness et al., 2018; Pauls et al., 2019). Moxness et al. (2018) also provided evidence as to why the Oltá-Malanzán paleovalley was not carved by glacial activity. This valley appears to have been ice-free during the Carboniferous and Permian. The early Pennsylvanian deposits represent the only evidence of glaciation within the western Paganzo Basin, and the middle to late Pennsylvanian is marked by progressively drier climates, while basins at similar paleolatitudes (i.e. the Chaco-Paraná and Paraná Basins) continue to record glaciation until the Carboniferous-Permian boundary (Henry et al., 2008; Rocha-Campos et al., 2008; Holz, 2010; Cesari et al., 2011; Limarino et al., 2014). On top of these diamictites and conglomeratic units, there are thick successions of post-glacial shales that represent a transgressive event that is recorded in all sections across the Paganzo Basin (Limarino et al., 2006, 2014; Césari et al., 2011).

The middle units (i.e. Tupe, upper Lagares, and Loma Larga formations; Fig. 4) are interpreted to be comprised of fluvial deposits that succeed the lowermost units (Andreis et al., 1986; Limarino et al., 2006; Guena et al., 2010; Tedesco et al., 2010; Limarino et al., 2014). Additionally, there are coal deposits described from various levels within the middle units, which has led to the interpretation of a more humid-post-glacial climate basin-wide (Limarino et al., 2006; Guena et al., 2010; Tedesco et al., 2010; Limarino et al., 2014).

In the eastern Paganzo Basin, the Solca Formation, which overlies the Loma Larga Formation (Fig. 35), consists of mostly conglomeratic units. It appears most similar in coloration (e.g. white sandstones alternating with red mudstones) and appearance to the lowermost Patquía Formation in the western part of the basin. The uppermost units, Patquía and La Colina Formations, are found throughout the Paganzo Basin, and are interpreted to be indicative of eolian, ephemeral riverine and playa depositional environments (Limarino et al., 2006; Guena et al., 2010; Cesari et al., 2011; Limarino et al., 2014).

In recent literature, most of what is written about the Paganzo Basin strata comes from the detailed studies of the western units of the Paganzo Group, (i.e. the Guandacol, Tupe, and Patquía Formations), and the associated depositional processes and environments are often then extrapolated basin-wide. This has led to confusion on the depositional environments across the basin (i.e. Pazos, 2002; Gulbranson et al., 2010, 2015; Enkelmann et al., 2014), but here we provide a quantitative look at the Carboniferous-Permian climate transition of the Paganzo Basin by examining locations on a whole-basin regional scale.

3.1. Agua Hedionda, Huaco locality

The Paganzo Group strata at the Agua Hedionda anticline locality are some of the best studied in the basin (cf. Bossi and Abdreis, 1985; López-Gamundí et al., 1994; Martínez, 1993; López-Gamundí and Martínez, 2000; Pazos, 2000, 2002a, b; Marensi et al., 2002; Limarino et al., 2002a; Marensi et al., 2005). Strata from the late Paleozoic outcrops on either side of the anticline record a glacial to post-glacial climate transition. Sections were measured along the eastern flank of the anticline, north and south of the Huaco River and Route 40 (Fig. 36). Strata were measured here as this section represents one of the most complete records of late Paleozoic strata in northwestern Argentina.

3.2. Olta-Malanzán paleovalley

The Olta-Malanzán paleovalley system (OMPV) is located within an isolated uplift of the Famatina orogenic belt of the Sierras Pampeanas (Fig. 36). The paleovalley system is thought to have developed in an alpine or mountain valley setting, either carved by glacial ice (cf. Sterren and Martinez, 1996; Enkelmann et al., 2014; Rabassa et al., 2014; Socha et al., 2014) or tectonically formed as a fault-bounded basin (Bracaccini, 1948; Andreis et al., 1986; Buatois and Mangano, 1995; Net and Limarino, 1999; Moxness et al. 2018), cutting down into and depositing over various granitic-granodioritic and metamorphic complexes (i.e. Chepes granodiorite, Tuaní and Asperezas granite suites, and the Olta schist and phyllite). Most recent evidence provided by Moxness et al. (2018) has shown that the valley was not carved by glaciers but did experience cold conditions. The late Paleozoic Paganzo Group strata here are currently being exhumed by the modern Río Olta and other tributary streams, which flows to the east, but paleocurrent measurements and the stratal dip of the sedimentary deposits indicate that the flow of the valley

was to the west during Carboniferous and Permian deposition (Andreis et al., 1986; Sterren and Martínez, 1996). The uplift itself is flanked on either end by two towns, Olta to the east and Malanzán in the west. The paleovalley is exposed in a synclinal extent, with the oldest (i.e. Serpukhovian-Bashkirian) material at the easternmost and westernmost ends, and the youngest (i.e. Permian) strata exposed toward the center (Fig. 36). Therefore, the paleovalley is often divided into two segments, the Olta paleovalley (OPV) and the Malanzán paleovalley (MPV).

4. Detrital zircon U-Pb geochronology analyses methods

Sections were measured in both segments of the OMPV paleovalley system to obtain a full understanding of upstream and downstream (proximal and distal) depositional environments. Sections were measured along the eastern flank of the anticline, north and south of the Huaco River and Route 40 (Fig. 36). To maintain assurance that provenance was restricted to local sources, we also sampled for detrital zircon analyses to track long-term provenance changes (Gehrels, 2000; Fedo et al., 2003; Anderson, 2005; Gehrels et al., 2008; Gehrels, 2011; Gehrels et al., 2011; Gehrels and Pecha, 2014). The ages obtained from the sedimentary rocks can then be compared to known dates of bedrock in the region, or of more distal sources to determine provenance and maximum depositional age of the sediments. Samples collected for detrital zircon analyses were used to assess changes in sediment source and dispersal patterns along the Protoprecordillera and Sierras Pampeanas (i.e. for the different formations in the Paganzo Group). The changing tectonic conditions (i.e. uplift and collapse of uplands) based on dispersal patterns and changing source terrains can be related to known climatic change in the basin, thus allowing for a better understanding of how these tectonic signatures affect climate within the overall regional and/or global climatic patterns.

This study makes use of previously published detrital zircon data for the strata in question, but to make a full comparison of provenance through time during the glacial-to-post-glacial transition, three additional sandstone samples were collected (CDH0923-5S, CDH0923-35S, LC0806-1S; Fig. 36). The samples were prepared using the methods of Gehrels (2011) and U-Pb ages were determined for all zircons at the University of Arizona LaserChron laboratory (ALC). Zircons were extracted by traditional methods of crushing and grinding, and were separated using a Wilfley table, heavy liquids, and a Frantz magnetic separator to remove high-U zircons that could yield discordant results (Sircombe and Stern, 2002; McKay et al., 2018). The samples analyzed at ALC contained 72, 183, and 178 zircons respectively, which were hand-picked and mounted from a sieved 63-250 μm size-fraction. U-Pb geochronology of the zircons was conducted by laser ablation inductively coupled plasma mass spectrometry (LA-ICPMS). The samples were analyzed using a Thermo Element2 single-collector ICPMS. Data collected at the ALC were reduced using their Excel age calculation program (see Gehrels et al., 2008; Gehrels and Pecha, 2014; ALC website: <https://sites.google.com/a/laserchron.org/laserchron/>). To eliminate results of analyses with common-Pb contamination or Pb loss, criteria for rejection included the following:

1. High errors (>10% uncertainty) of $^{206}\text{Pb}/^{207}\text{Pb}$ and $^{206}\text{Pb}/^{238}\text{U}$ isotope ratios
2. High ^{204}Pb values
3. Low $^{206}\text{Pb}/^{204}\text{Pb}$ ratios
4. High discordance (>20%) or reverse discordance (>5%)

The analyses that met these criteria were removed from interpretations, but are included in the full set of analyses in Appendix A.

Once the data was obtained, all accepted analyses were used to create Concordia diagrams using Isoplot 4.15, a Microsoft Excel add-in from Ludwig (2012; Fig. 37). The data here are discussed in the context of previously published ages from other strata of the Paganzo Group (cf. Enkelmann et al., 2014; Craddock et al., 2019). The data are also compared to published ages of igneous and metamorphic basement lithologies from the literature to determine provenance through time in the Paganzo Basin (e.g. Huff et al., 1998; Pankhurst et al., 1998; Rapela et al., 1998; Ottone et al., 2001; Dahlquist et al., 2010; Drobe et al., 2011; Verdecchia et al., 2011, 2014, 2018; Sial et al., 2013; Einhorn et al., 2015; Rapela et al., 2018).

5. Detrital Zircon Geochronology of the Paganzo Basin

CDH0923-5S, Tupe Formation, Huaco Locality, this study

One sandstone sample was collected from a trough-cross-bedded sandstone package from the lower Tupe Formation. The interpreted depositional environment for this sample is a fluvial system. 72 concordant detrital zircons were analyzed from this sample, ranging in age from 3095.6 ± 12.9 Ma to 286.7 ± 6.9 Ma (Fig. 38). Ordovician-aged zircons dominated this sample, with a primary age peak from 480-440 Ma. A secondary peak age occurs during the Mesoproterozoic, from 1400-960 Ma. In this sample, 8% were Carboniferous, 6% Devonian, 1% Silurian, 22% Ordovician, 6% Cambrian, 13% Neoproterozoic, 39% Mesoproterozoic, and 4% Paleoproterozoic (Fig. 39).

CDH0923-35S, Patquía Formation, Huaco Locality, this study

One sandstone sample was collected from a sandstone bed in an interbedded mudstone and sandstone facies succession interpreted as fluvial. The sample contained 183 zircons that range in age from 2690.5 ± 17.8 Ma to 305 ± 5.8 Ma. The primary age-peak is Ordovician, with

a minor peak in the Mesoproterozoic (Fig. 38). For this sample, 2% of the zircons were Carboniferous, 4% Devonian, 3% Silurian, 41% Ordovician, 9% Cambrian, 15% Neoproterozoic, 19% Mesoproterozoic, 7% Paleoproterozoic, and 1% Archean (Fig. 39).

LC0806, La Colina Formation, Olta-Malanzán Paleovalley Locality, this study

One sandstone sample was collected from a cross-bedded sandstone package from the upper La Colina Formation, here interpreted as an eolian dune complex. The sample had 178 analyzed zircons with an age range of 3325.5 ± 15.2 Ma to 361.5 ± 7.3 Ma. The sample shows a dominant peak in the Neoproterozoic-Cambrian, and a secondary peak in the Mesoproterozoic (Fig. 38). In this sample, 3% of the zircons analyzed were Devonian, 4% Ordovician, 20% Cambrian, 43% Neoproterozoic, 21% Mesoproterozoic, 6% Paleoproterozoic, and 3% Archean (Fig. 39).

6. Comparative detrital zircon sample

ARG175, Loma Larga Formation, Olta-Malanzán Paleovalley, Craddock et al., 2019

This sample was collected from a sandstone close to the town of Loma Larga, from a fluvial depositional environment (Fig. 36). The sample contained 44 concordant zircons, which range in age from 2133.8 ± 25.3 Ma to 412.4 ± 11.9 Ma (Fig. 38). In this sample, 2% of the zircons were Devonian in age, 4% Silurian, 32% Ordovician, 39% Cambrian, 16% Neoproterozoic, 5% Mesoproterozoic, and 2% Paleoproterozoic (Fig. 39).

CDH0923-3S, Guandacol Formation, Huaco Locality, Pauls et al. (in review)

One sandstone sample was collected from a wavy-bedded meter-thick sandstone package from within a shoreface succession in the uppermost Guandacol Formation (Fig. 36). This

sample contained 75 concordant zircons ranging in age from 2616.4 ± 8.9 Ma to 308.6 ± 11.1 Ma. A primary age peak ranges from 480-440 Ma (Ordovician), with a component from 500-600 Ma (Cambrian-late Neoproterozoic), and a secondary peak occurs at 1160-960 Ma (Fig. 38). In this sample, 1% of the zircons analyzed were Carboniferous, 5% Devonian, 3% Silurian, 20% Ordovician, 10% Cambrian, 27% Neoproterozoic, and 28% Mesoproterozoic.

ARG318, Lowermost Guandacol Formation, Huaco Locality (Craddock et al., 2019)

This sample was collected from a glacial diamictite at the base of the Guandacol Formation and is interpreted to be from a proglacial glaciomarine environment (Fig. 36). This sample contained 36 concordant zircons from 2059 ± 7.5 to 385.2 ± 5.9 Ma. For this sample, 3% of the zircons were Devonian, 20% Ordovician, 44% Cambrian, 19% Neoproterozoic, 8% Mesoproterozoic, and 3% Paleoproterozoic (Fig. 39).

29TR4, Lowermost Malanzán Formation, Olta-Malanzán Paleovalley (Enkelmann et al., 2014)

This sample was collected from a debris flow deposit at the base of the Malanzán Formation (Fig. 36). The sample contained 93 concordant detrital zircons with ages ranging from 2203 ± 36 Ma to 333 ± 4.5 . For this sample, 3% of the analyzed zircons were Carboniferous, 12% Devonian, 3% Silurian, 24% Ordovician, 29% Cambrian, 19% Neoproterozoic, 3% Mesoproterozoic, and 7% Paleoproterozoic (Fig. 39).

ARG203, Middle-Upper Malanzán Formation, Olta-Malanzán Paleovalley (Craddock et al., 2019)

This sample was collected from a sandstone within a succession of interbedded mudstones and sandstones interpreted to be a prograding/fluctuating delta front system (Fig. 36).

The sample contained 50 zircons that range in age from 937.3 ± 26.1 Ma to 362.7 ± 8.6 Ma. For this sample, 8% of the zircons were Devonian, 2% Silurian, 54% Ordovician, 20% Cambrian, and 16% Neoproterozoic (Fig. 39).

7. Provenance of the upper Paganzo Group Strata

Pauls et al. (in review) established that there were most likely separate depositional centers in the Paganzo Basin based on the detrital zircon analysis of the Guandacol and Malanzán formations, as the lowermost Guandacol Formation most likely represents a thorough mixing of the local western Precordillera basement materials (e.g., Los Azules Formation and the Mesoproterozoic basement of the Sierra de Pie de Palo complex; Huff et al., 1997, 1998; Ottone et al., 2001; Dahlquist et al., 2010; Sial et al., 2013; Verdecchia et al., 2014, 2018), while the Malanzán Formation detrital zircons are representative of the Sierra de Chepes granitoid complex (Pankhurst et al., 1998; Enkelmann et al., 2014). From the detrital zircon age population differences as well as paleoflow data presented in that study, it was concluded that there was most likely a paleotopographic barrier in the form of uplifted block(s) throughout the Paganzo Basin during the Visean-Bashkirian, most likely coinciding with the Famatina and Pie de Palo arches (i.e. Sierras Famatina and Sierra de Pie de Palo, respectively; Figs. 32, 39).

7.1. Agua Hedionda, Huaco Provenance

When compared to the Guandacol Formation sample of Pauls et al. (in review), the zircon grains from the Tupe and Patquía formations display some similarities in the age-distribution patterns, but a shift in the primary age peak requires separate provenance analysis. Based on the data provided in Pauls et al. (in review), the age-distribution patterns of the Guandacol compared

with the Tupe Formation data presented here are very similar, and therefore they are considered to have the same source (Fig. 39). The primary source was determined to be the nearby Sierra de Pie de Palo region, which contains the Mesoproterozoic-Ordovician ages (cf. Thomas et al., 2015 and references therein) found within the Guandacol Formation samples (ARG318, CDH0923-3S; Craddock et al., 2019; Pauls et al., in review; Fig. 39). However, there is an increase in the Mesoproterozoic zircon grains in the Tupe Formation (from 28% in the Guandacol Formation to 39% in the Tupe Formation; Fig. 39). This indicates either an unroofing of material in the area, or a shift in source region, that is pulling more from the eastern edge of the Cuyania terrane, such as the Mesoproterozoic aged rocks within Sierra de Pie de Palo region (Huff et al., 1997, 1998; Ottone et al., 2001; Dahlquist et al., 2010; Sial et al., 2013; Verdecchia et al., 2014, 2018; Rapela et al., 2018). We interpret this as a slight eastward shift in drainage for this location (Fig. 40).

When comparing the Tupe and Patquía formations age-distribution patterns, there is a more significant difference (Fig. 39). The main age peak in the Patquía Formation is overwhelmingly Ordovician, from 23% in the Tupe Formation to 41% in the Patquía Formation. This increase in Ordovician-aged detrital zircons suggest a change in source regions during the middle to late Pennsylvanian (Fig. 40). Net et al. (2006) indicated paleoflow to the west for both the Tupe and Patquía formations at the Agua Hedionda (Huaco) locality. When considered with paleoflow data provided by Net et al. (2006), the increase in Ordovician-aged zircons likely represents additional sediment sources from further to the east. The rocks of the Sierra de Valle Fértil are within the Famatina belt and are primarily Ordovician in age (468-486 Ma; Pankhurst et al., 2000; Dahlquist et al., 2010; Rapela et al., 2018; Fig. 39). We take this to show that by the Permian, this area of the Paganzo Basin was part of a larger drainage that incorporated rocks from farther away but still within the western margin of the Protoprecordilleran terrane (Fig. 40).

For both the Tupe and Patquía formations, the youngest zircon grains are late Carboniferous, with the youngest age zircon grain of the Tupe at 307.7 ± 12.8 Ma and the youngest-age zircon grain of the Patquía sample at 305.0 ± 5.8 Ma. For both of these formations, these are the youngest reported ages at this location, and both of these ages are concordant (Fig. 37). This new data provides better age constraint on the timing of deposition in the area. Both samples also contain zircon grains with an age of ~ 311 Ma, and the Tupe Formation also contains a few older Pennsylvanian aged-zircons with an average age of ~ 322 Ma (Appendix A). These zircon grains are interpreted here as volcanic ages that correspond to the latest Pennsylvanian-Permian arc that accreted to the western margin of Gondwana during this time (Casselli and Limarino, 2002; Limarino et al., 2006; Willner et al., 2008; Guena et al., 2010; Limarino et al., 2014).

7.2. Olta-Malanzán Provenance

Similarly to the transition from the Guandacol Formation to the Tupe Formation in the west, the primary age peak of the Loma Larga sample (ARG175; Craddock et al., 2019) is during the Cambrian and Ordovician, and does not differ greatly from the primary age peaks of the Malanzán Formation detrital zircon sample sets from previous studies (cf. Enkelmann et al., 2014; Craddock et al., 2019). This follows Enkelmann et al. (2014) thermochronometry evidence that the Sierra de Chepes region (477-497 Ma) was rapidly exhuming shortly before the deposition of the Malanzán Formation, which indicates active uplift prior to the middle Carboniferous deposition of the Paganzo Group strata. The uplifted basement in this region would have provided ample material for the late Paleozoic deposits and explains the dominance of Famatinian crystallization ages within the Malanzán and Loma Larga formations (Fig. 40).

The transition from the Loma Larga Formation to the La Colina Formation also displays a similar pattern in age-distribution as the upper Paganzo Group strata at Huaco. Here, the zircon age distributions shift to a greater population of older ages, from a predominance of Cambrian and Ordovician ages (74% in the upper Malanzán Formation, 73% in the Loma Larga Formation) to a dominance of Neoproterozoic and Mesoproterozoic ages (44% versus 24% of both Cambrian-Ordovician ages; Fig. 39). This older age-distribution coincides with older zircon crystallization ages found to the east of the Sierra de Chepes region, in rocks found in the Pampean orogenic belt (cf. Pankhurst et al., 2000). Our findings here also echo the results presented by Enkelmann et al. (2014), which suggested that the primary source for the La Colina Formation was also to the east of the depositional environment. We interpret the source region for the La Colina sediments to include a larger area that incorporates the Sierra de Córdoba, which lie directly to the east of the Sierras de Chepes and Los Llanos region (Fig. 39).

Unlike the Tupe and Patquía formations samples, the upper Paleozoic strata at Olta-Malanzán do not contain any late Carboniferous zircon grains (Fig. 39). This may indicate that the volcanic source for these ages found along the western margin was too distal to be deposited in this easternmost location of the basin.

8. Latest Pennsylvanian Paganzo Basin development

The Paganzo Basin appears to broaden in terms of source regions through the Pennsylvanian. In both regions of the basin, there seems to be a shift in provenance to the east. The biggest difference in provenance occurs at the same time on both margins: during the deposition of the middle Pennsylvanian strata: from the Tupe Formation to the Patquía Formation at Huaco and from the Loma Larga Formation to the La Colina Formation at OMPV.

This change in age populations corresponds with the interpretation that the Protoprecordillera collapsed during the Pennsylvanian (Limarino and Spalletti, 2006; Limarino et al., 2014). The collapse of the fold-and-thrust belt is attributed to the shift in tectonism along the western margin of Gondwana, with the development of an outboard magmatic arc that produced ash during the late Pennsylvanian and continued into the early Permian (Limarino et al., 2006; Willner et al., 2008; Tedesco et al., 2010; Einhorn et al., 2015; Sato et al., 2015). This shift in active tectonism certainly aligns with the change in detrital zircon provenance seen in the upper Paganzo Group strata. The barrier created by the Protoprecordillera would have been diminished, and flat-slab subduction would have caused extension of the foreland region westward. Exhumation rates slowed in the late Carboniferous, and with the extension of the foreland and collapse of the Protoprecordillera to the west, the source regions for the Paganzo Group strata migrated to the east. Detrital zircon populations in both the Patquía Formation (CDH0923-35S) and La Colina Formation (LC0806-1S) samples display primary peaks from basement material found east of each location (Fig. 39).

Additionally, both the Tupe and Patquía formations samples contain detrital zircon age populations that are much younger (i.e. late Carboniferous) than the Loma Larga and La Colina formations samples. These much younger grains fall within the range of ages associated with late Carboniferous volcanism (320-296 Ma; Willner et al., 2008; Sato et al., 2015). The presence of young zircon ages in the western units indicates proximity to and an increase in late Pennsylvanian volcanism along the continental margin (Limarino et al., 2006; Willner et al., 2008; Tedesco et al., 2010; Einhorn et al., 2015; Sato et al., 2015; Thomas et al., 2015). This evidence of volcanism suggests increased tectonism along the western margin of Gondwana and

may be tied to the collapse of the Protoprecordillera, but further data is needed to understand the timing of this collapse.

9. Implications for western Gondwana late Paleozoic climate

It is well documented that the Paganzo Group strata record a shift in climate during the late Paleozoic that differs from other basins in South American Gondwana (cf. Limarino et al., 2014 and references therein). An increase in the atmospheric concentrations of CO₂ during the early Permian may explain the warming trend in the rock record, as glaciers had receded out of the Parana Basin at that time. However, it does not necessarily explain the aridity trend recorded in western Argentina since at the same time the coal-bearing strata in the Rio Bonito Formation of the southern Paraná Basin suggest a humid climate ~2,000 km away in southern Brazil, which was located at the same paleolatitude. Instead, the active tectonics along the margin of Gondwana may be partially responsible. Previous studies have found that mountain belts play an extremely important role in the moisture flow patterns across the continents (Broccoli and Manabe, 1997; Ruddiman and Prell, 2007; Ruddiman et al., 1997; Newell et al., 1999; Tabor and Poulsen, 2008; Godard et al., 2014; Isbell et al., 2012; Limarino et al., 2014). Not only do the mountain belts affect regions via the orographic effect and contribute to rain shadow regions, but they also affect atmospheric circulation on a larger scale (Broccoli and Manabe, 1997 and references therein; Partridge, 1997; Ruddiman et al., 1997; Ruddiman and Prell, 2007). As the different paleotopographic highs, such as the Chilean volcanic arc, Protoprecordillera, and the Famatina and Pampeanas Systems (Fig. 9), change in importance and elevation, the various atmospheric patterns would have been disrupted and caused changes in regional climatic regimes (Ruddiman and Prell, 1997; Ruddiman et al., 1997; Newell et al., 1999; Broccoli and Manabe,

1997; Partridge, 1997; Tabor and Poulsen, 2008; Isbell et al., 2012; Godard et al., 2014; Limarino et al., 2014).

While the Sierras de Chepes and Los Llanos were most likely elevated enough to support glaciation (cf. de los Hoyos et al., 2011; Enkelmann et al., 2014; Enkelmann and Garver, 2015), there is no evidence of an accumulation of glacial ice (Moxness et al., 2018; Pauls et al., in review). This lack of glaciation could be in part due to the presence of the Protoprecordilleran range that separated, to some degree, the eastern domain of the Paganzo Basin from the Panthalassan Ocean during the latest Mississippian and Earliest Pennsylvanian. This topographic barrier could have created a rain shadow effect over the eastern part of the basin during the Visean-Serpukhovian glaciation of the Protoprecordilleran range (Moxness et al., 2018). In the Pennsylvanian, the climate has been reported to transition to a humid post-glacial environment (Limarino et al., 2014; Pauls et al., 2019, in prep.). While the detrital zircon populations do not show a significant change in age populations from the Guandacol and Malanzán to the Tupe and Loma Larga respectively, the strata of the Paganzo Group record a shift in climate, nonetheless. This shift has been attributed to the collapse of the Protoprecordillera as reported in numerous studies (Henry et al., 2008; Isbell et al., 2012; Spalletti et al., 2012; Limarino et al., 2014; Gulbranson et al., 2015; Moxness et al., 2018; Pauls et al., 2019). None of these studies, though, have been able to determine the exact timing or nature of the collapse. Further detrital zircon geochronology studies in basins along the western side of the Protoprecordillera (i.e. in the Calingasta-Uspallata and Río Blanco basins) are necessary to better refine our understanding of the timing of this event.

While the inferred collapse of the Protoprecordillera could explain the disappearance of alpine glaciers in the western part of the Paganzo Basin/Protoprecordillera and the transition to a

more humid post-glacial climate, it does not necessarily explain the appearance and development of the red beds (i.e. Patquía and La Colina Formations) in the Paganzo Basin. Many studies have provided evidence of a magmatic arc that develops on the outboard of the Panthalassic margin during the late Carboniferous-early Permian, and the detrital zircon populations presented here also support this scenario (cf. Limarino et al., 2006; Willner et al., 2008; Tedesco et al., 2010; Einhorn et al., 2015; Sato et al., 2015). In the western domain of the basin (i.e. Huaco locality), the Tupe and Patquía Formation detrital zircon populations contain a higher population of Carboniferous-aged zircons (Fig. 37, 39) and signify the presence of a volcanic arc accreting to the Panthalassan margin. This belt has been interpreted by several studies to have contributed to the increase in aridity recorded in the upper Paganzo Group strata (cf. Limarino et al., 2014; Pauls et al., 2019, in prep.). The accreting arc farther to the west would have potentially shifted orographically-controlled climatic belts westward expanding the rain shadow across all of the basin during the latest Pennsylvanian and into the Permian, thereby cutting off the moisture source to the interior basins. This would have allowed for the development of the eolian deposits recorded in the upper Paleozoic strata across all of the Paganzo Basin (i.e. Patquía, La Colina, De La Cuesta formations; Guena et al., 2010; Krapovickas et al., 2010; Limarino et al., 2014; Césari et al., 2019; Pauls et al., 2019).

10. Future considerations

While the data presented here points to a shift in tectonism during the middle Pennsylvanian, further data is needed to corroborate this evidence. Detrital zircon geochronology studies of all late Paleozoic strata should be expanded to other localities in the Paganzo Basin and surrounding regions to obtain a better understanding of source rocks for the different regions

of the basin. To better constrain/refine the timing of the collapse of the Protoprecordillera, which appears to have been an important control on local climate patterns, detrital zircon studies should be conducted on more localities along the eastern and western flanks of the fold-and-thrust belt: in the Paganzo and Calingasta-Uspallata basins. Furthermore, detrital zircon studies in the nearby Río Blanco Basin should also be considered to better refine the understanding of the affects the volcanic arc had on the northern region of the western margin basins.

11. Conclusions

Detrital zircon samples from the Huaco locality show a slight change in provenance through time, draining local basement materials during the early-middle Carboniferous, then shifting to a more Famatina-aged source, possibly the Sierra de Valle Fértil region. Additionally, late Carboniferous detrital zircons in the samples at Huaco indicate the presence of an outboard magmatic arc during the late Pennsylvanian-Permian. Detrital zircon samples from the eastern Sierras de Chepes and Los Llanos (OMPV), in contrast, show a shift in provenance from a source of local origin (i.e. Sierras de Chepes, Los Llanos, and Malanzán ranges) during the middle Carboniferous Malanzán and Loma Larga formations to an older-age-dominated zircon population in the La Colina Formation. The latest Pennsylvanian-Permian sediment source is likely coming from the eastern Sierras Pampeanas system, such as the Sierras de Córdoba.

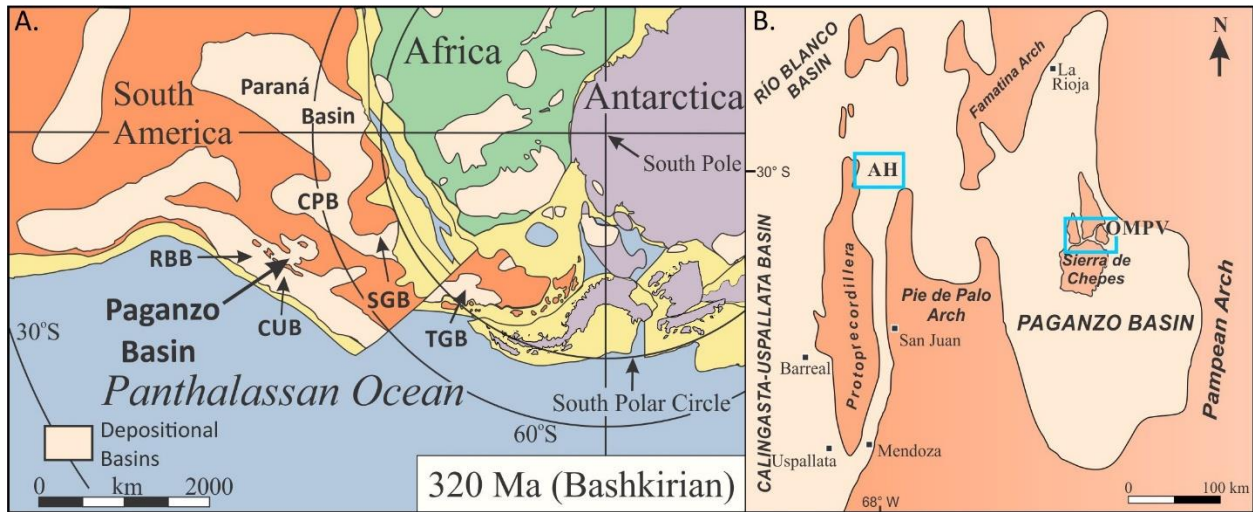


Figure 32. Map of plate reconstruction for Bashkirian. RBB: Río Blanco Basin; CUB: Calingasta-Uspallata Basin; CPB: Chaco-Paraná Basin; SGB: Sauce Grande Basin. TGB: Tepuel-Genoa Basin. Reconstruction modified from Moxness et al. (2018). B. Plan-view map showing the interpreted outline of the Paganzo Basin. The localities for this study are marked by blue rectangles: AH – Agua Hedionda anticline near Huaco; OMPV - Olta-Malanzán paleovalley. Map modified from Limarino et al. (2006).

Age (Ma)	Time Scale			Paganzo Basin		
	Period		Stage	Huaco	Paganzo	Sierra de Chepes
295	Permian	Cisuralian	Sakmarian			
			Asselian		La Colina/ Patquía	La Colina
300	Carboniferous	Pennsylvanian	Gzhelian	Patquía		
			Kasimovian			
			Moscovian			
			Bashkirian			
		315		Tupe		Loma Larga
		320		Guandacol		Malanzán
		325	Mississippian	Serpukhovian		
330	Viséan					
335						

Figure 33. Correlation chart for the late Paleozoic Paganzo Group strata for the sites in the Paganzo Basin, Argentina mentioned in the text. Ages and units are based on Limarino et al. (2002a, 2002b, 2006, 2014), Césari et al. (2011, 2019).

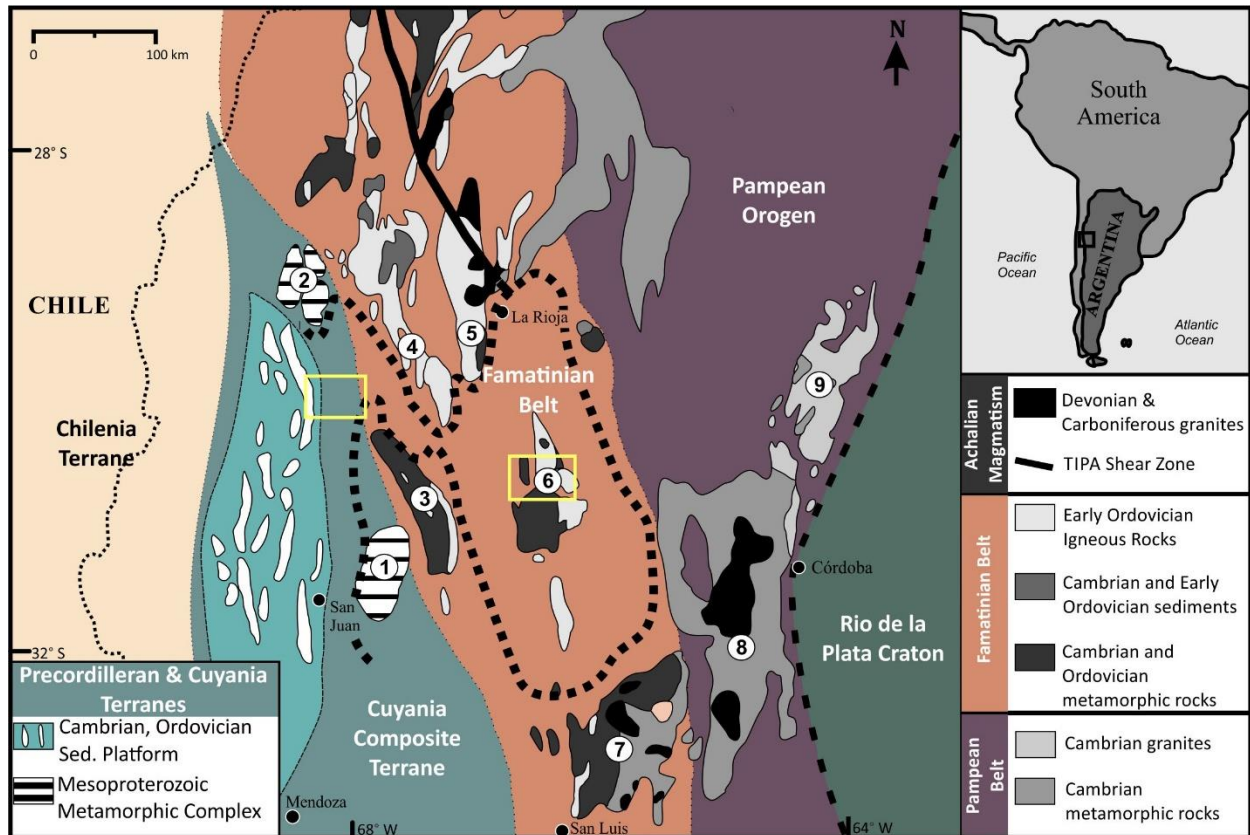


Figure 34. Map of the igneous and metamorphic basement units that serve as potential source terranes for the detrital zircon populations of the late Paleozoic Paganzo Group strata, outlined in yellow boxes. 1 – Sierras de Chepes and Los Llanos, 2 – Sierra de Valle Fertil, 3 – Sierra de Pie de Palo, 4 – Sierras de Umango, Maz and Espinal, 5 – Sierras Famatina, 6 – Sierra de Velasco, 7- Sierras de Córdoba, 8 – Sierra de San Luis. (Modified from Dahlquist et al., 2010). The dotted line is the approximate outline of the Paganzo Basin. (Modified from Limarino et al., 2006)

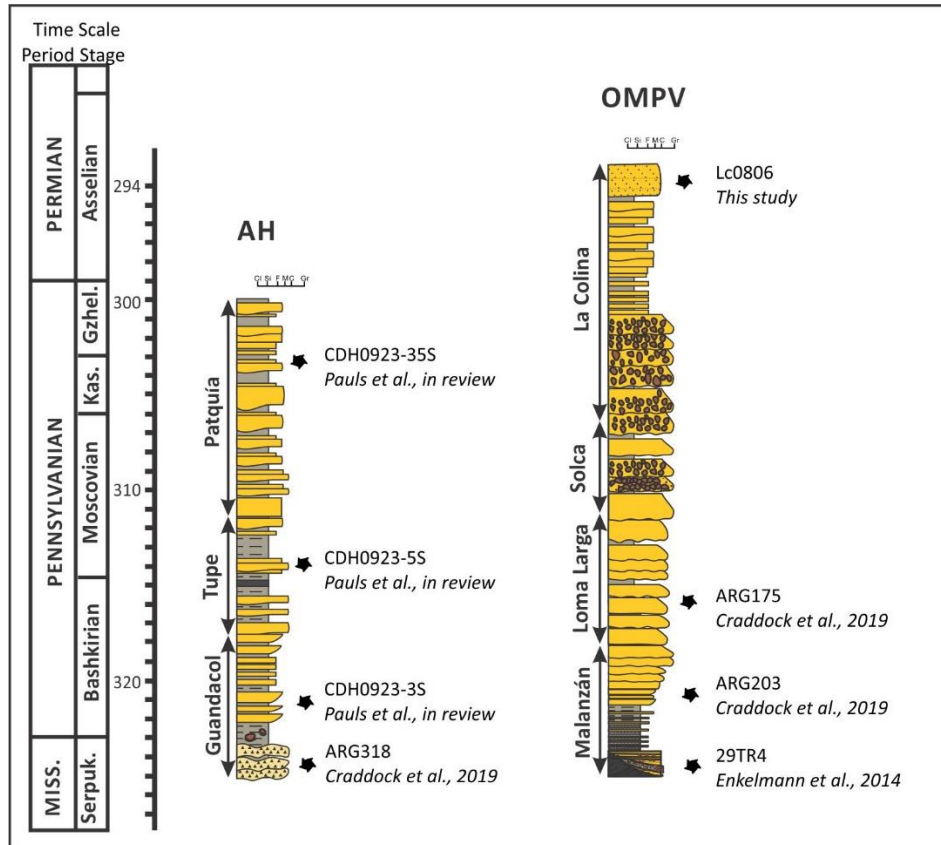


Figure 35. Simple stratigraphic column showing the selected Paganzo Group strata at the chosen localities. (Modified from Césari et al., 2011; Pauls et al., 2019).

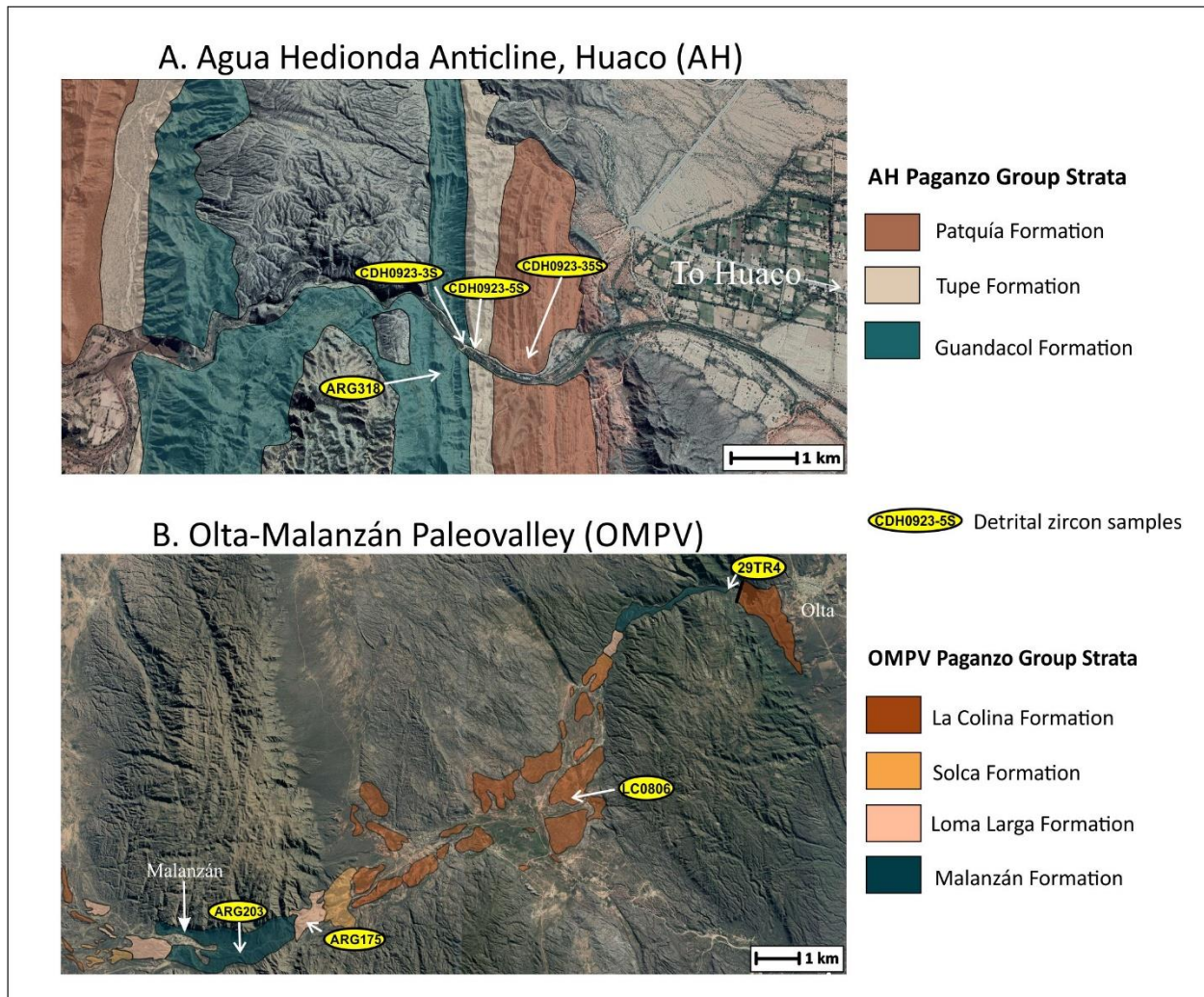


Figure 36. Google Earth aerial image with the geologic units of the Paganzo Group mapped showing the locations of the detrital zircon samples (yellow ellipsoids). A. The Agua Hedionda anticline, near the town of Huaco with the Guandacol, Tupe and Patquía formations. Detrital zircon sample ARG318 is from Craddock et al. (2019), and sample CDH0923-3S is from Pauls et al. (in review). B. The Olta-Malanzán paleovalley system (OMPV) with the Malanzán, Loma Larga, Solca, and La Colina formations. Detrital zircon samples ARG175 and ARG203 are from Craddock et al. (2019), and sample 29TR4 is from Enkelmann et al. (2014).

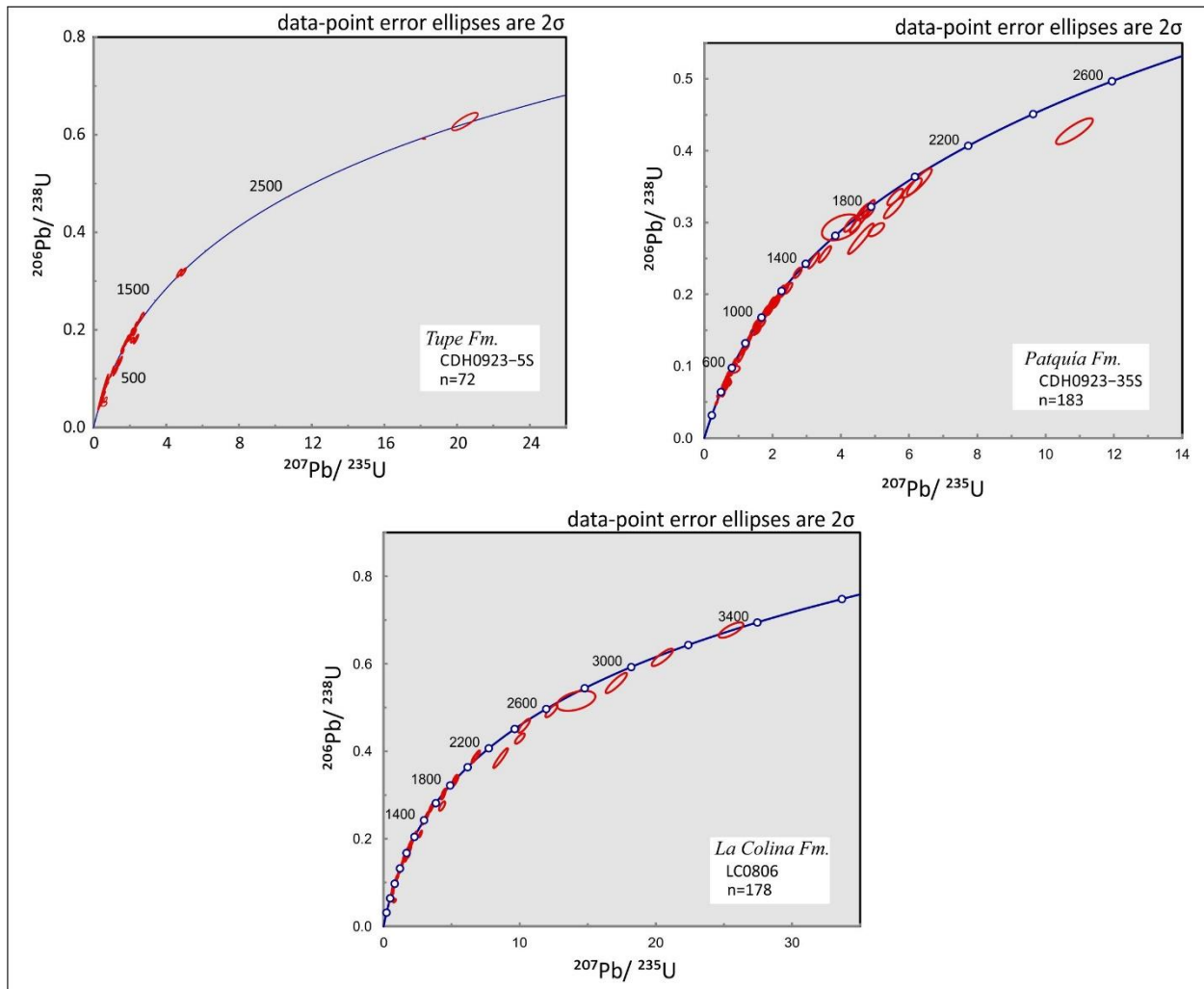


Figure 37. Concordia plot of all analyzed concordant zircon U-Pb measurements for detrital zircon sample CDH0923-5S from the Tupa Formation, CDH0923-35S from the Patquia Formation at the AH locality; and LC0806 of the La Colina Formation, OMPV locality. See Figure 5 for exact locations of each sample.

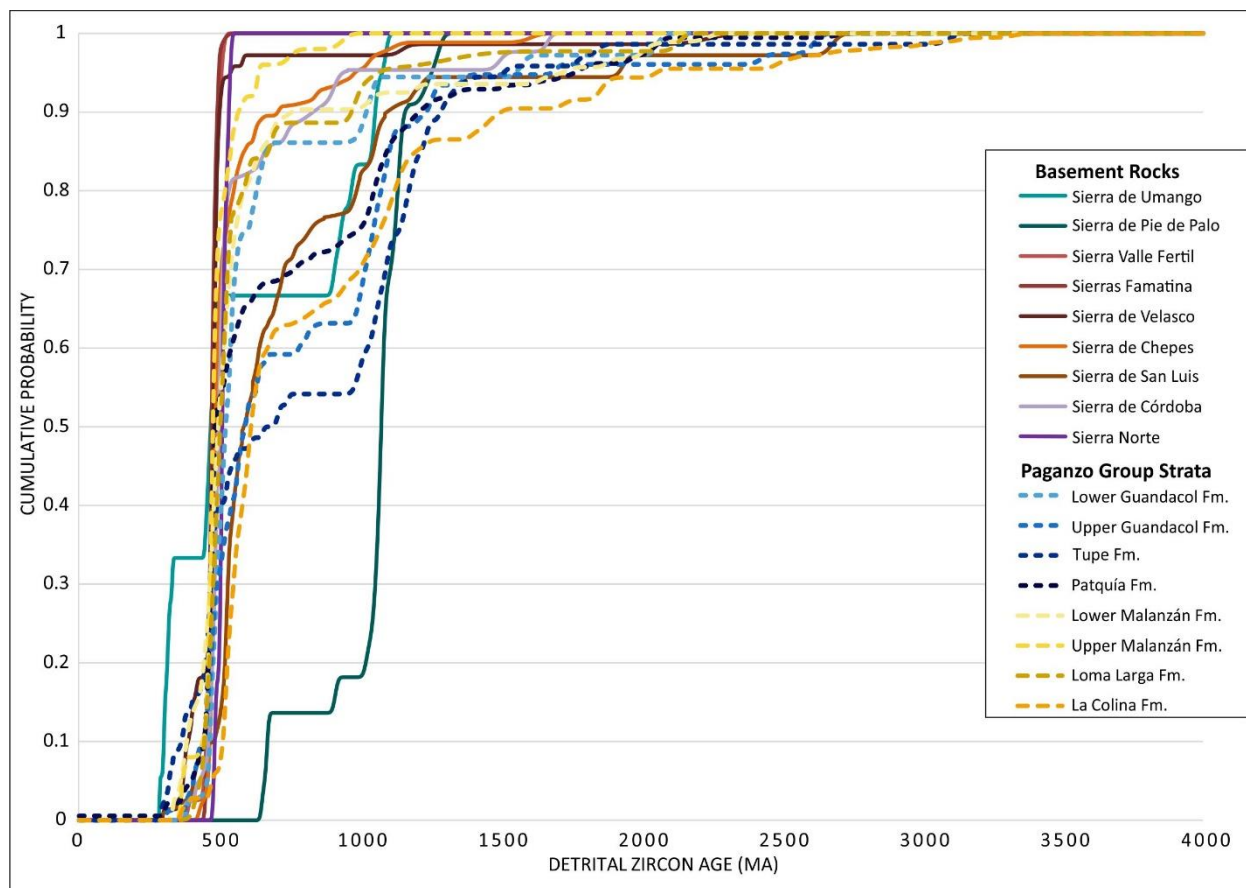


Figure 38. Cumulative probability distribution for the four Paganzo Group samples and the basement units in the region. Lower Paganzo Group strata samples are from other sources: Lower Guandacol Fm. – ARG318 (Craddock et al., 2019), Upper Guandacol Fm. – CDH0923-3S (Pauls et al., in review), Lower Malanzán Fm. – 29TR4 (Enkelmann et al., 2014), Upper Malanzán Fm. – ARG203 (Craddock et al., 2019). Upper Paganzo Group samples: Tupe Fm. – CDH0923-5S (this study), Patquía Fm. – CDH0923-35S (this study), Loma Larga Fm. – ARG175 (Craddock et al., 2019), La Colina Fm. – LC0806 (this study). The data for the igneous and metamorphic zircon compilation comes from the following literature: (1) Sierra de Pie de Palo - Vujovich et al., 2004; Naipauer et al., 2010a (2) Sierra de Umango - Varela et al., 2003, 2005 (3) Sierra de Valle Fétil - Pankhurst et al., 2000 (4) Sierra de Famatina - Pankhurst et al., 2000 (5) Sierra de Velasco - Toselli et al., 2003; Pankhurst et al., 2000 (6) Sierras de Chepes, Los Llanos - Pankhurst et al., 2000 (7) Sierra de San Luis - Vujovich and Ostera, 2003; Drobe et al., 2009 (8) Sierra de Córdoba - Rapela et al., 1998, Pankhurst et al., 2000 (9) Sierra Norte - Leal et al., 20003; Llambías et al., 2003.

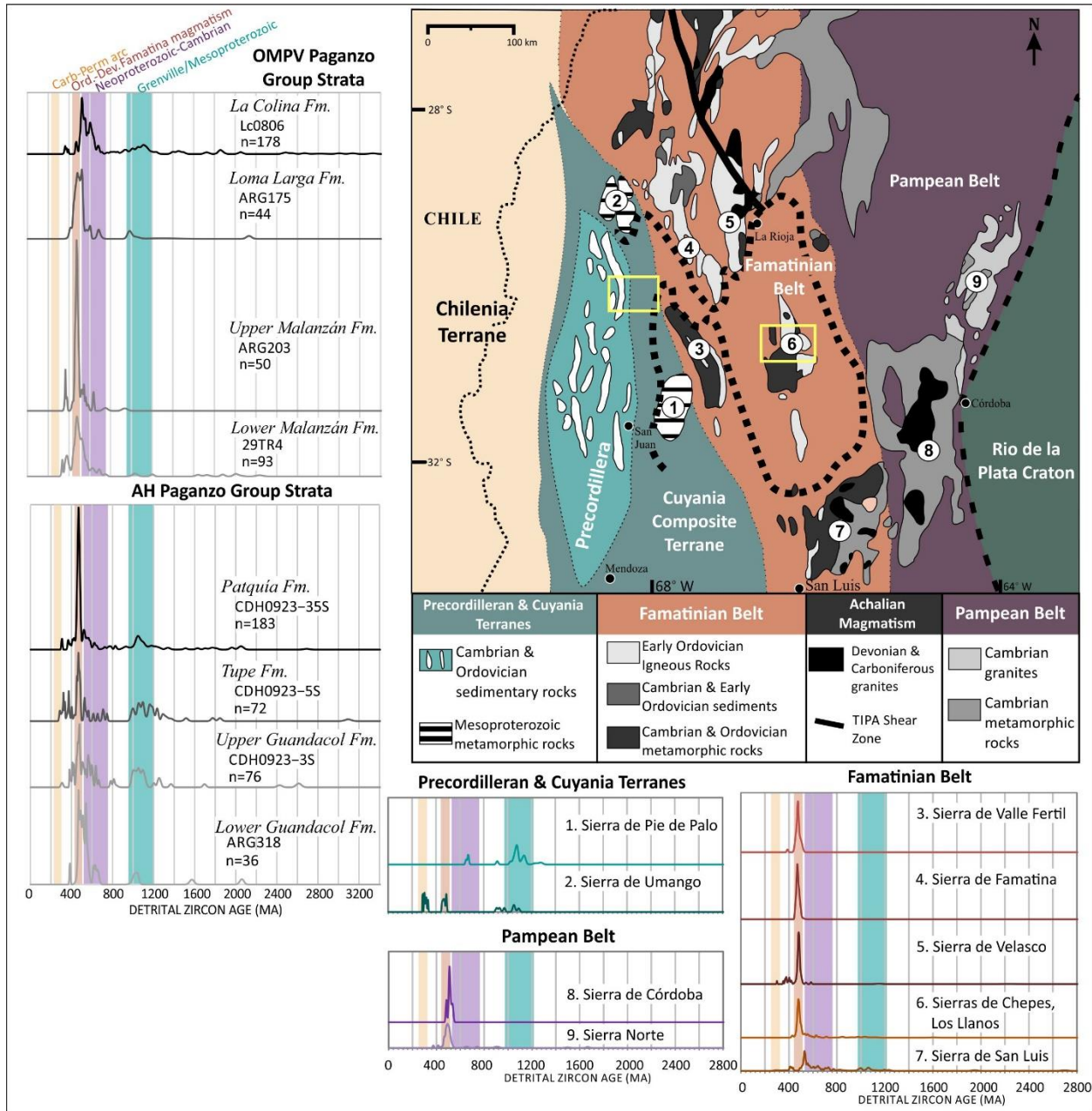


Figure 39. Mesoproterozoic-Carboniferous igneous and metamorphic provinces for the Paganzo Basin area (demarcated by the dotted line) and their available zircon geochronology (n=398). The studied sections are outlined by yellow boxes. Map is modified from Dahlquist et al. (2010). The cited literature for this compilation is as follows (1) Sierra de Pie de Palo - Vujovich et al., 2004; Naipauer et al., 2010a (2) Sierra de Umango - Varela et al., 2003, 2005 (3) Sierra de Valle Fértil - Pankhurst et al., 2000 (4) Sierra de Famatina - Pankhurst et al., 2000 (5) Sierra de Velasco - Toselli et al., 2003; Pankhurst et al., 2000 (6) Sierras de Chepes, Los Llanos - Pankhurst et al., 2000 (7) Sierra de San Luis - Vujovich and Ostera, 2003; Drobe et al., 2009 (8) Sierra de Córdoba - Rapela et al., 1998, Pankhurst et al., 2000 (9) Sierra Norte - Leal et al., 2000; Llambías et al., 2003.

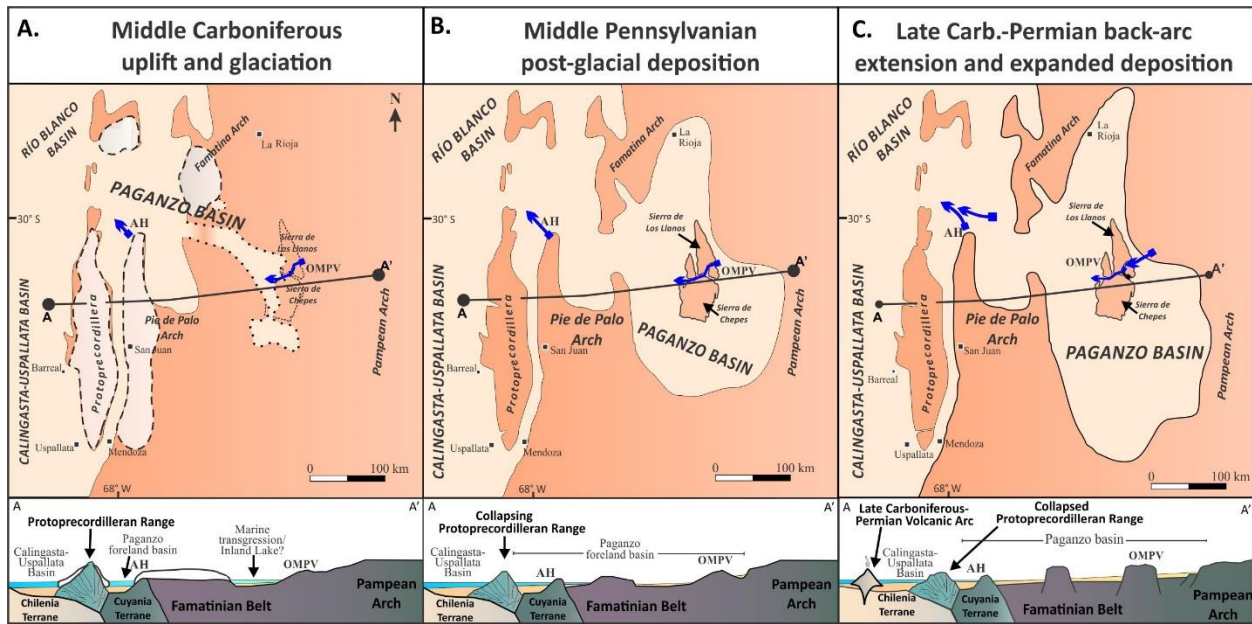


Figure 40. The proposed evolutive model of the Paganzo Basin development from the middle Carboniferous to the Permian.

References

- Amos, A.J., and Rolleri, E., 1965. El Carbónico marino en el valle Calingasta-Uspallata, San Juan-Mendoza: Boletín de Informaciones Petroleras 368, pp. 50–71.
- Anderson, T., 2005, Detrital zircons as tracers of sedimentary provenance: limiting conditions from statistics and numerical simulations: *Chemical Geology*, v. 216, p. 249-270.
- Andreis, R.R., Archangelsky, S., Leguizamón, R.R., 1986. El paleovalle de Malanzán: nuevos criterios para la estratigrafía del Neopaleozoico de la sierra de Los Llanos, La Rioja, República Argentina: *Boletín de la Academia Nacional de Ciencias (Córdoba)* 57, pp. 1-119.
- Aquino, C.D., Milana, J.P., Faccini, U.F., 2014. New glacial evidences at the Talacasto paleofjord (Paganzo basin, W-Argentina) and its implications for the paleogeography of the Gondwana margin. *Journal of South American Earth Sciences* 56, 278-300.
- Astini, R.A., 1998. Stratigraphical evidence supporting the rifting, drifting and collision of the Laurentian Precordillera terrane of western Argentina, in Pankhurst, R. J., and Rapela, C. W., eds., *The Proto-Andean Margin of Gondwana: Geological Society, London, Special Publication 142*, p. 11–33.
- Astini, R.A., Collo, G., and Martina, F., 2007, Ordovician K-bentonites in the upper-plate active margin of Western Gondwana, (Famatina Ranges): Stratigraphic and palaeogeographic significance: *Gondwana Research*, v. 11, p. 311–325, doi: 10.1016/j.gr.2006.05.005.
- Bossi, G. and Andreis, R.R., 1985. Secuencias deltaicas y lacustres del Carbonífero del centro-oeste argentino. X International Congress on Carboniferous Stratigraphy and Geology, Madrid, pp. 285-309.
- Braccacini, I.O., 1948. Los Estratos de Paganzo y sus niveles plantíferos en la sierra de los Llanos (provincial de La Rioja). *Revista de la Asociación Geológica Argentina* 1, 19-61.
- Broccoli and Manabe, 1997, Mountains and Midlatitude Aridity: In Ruddiman, W.F. (ed.) *Tectonic uplift and climate change*, New York, NY, United States (USA), Plenum Press, New York, NY.
- Buatois, L.A., Mángano, M.G., 1995. Post glacial lacustrine event sedimentation in an ancient mountain setting: Carboniferous Lake Malanzán (western Argentina). *Journal of Paleolimnology* 14, 1–22.
- Caselli, A.T., Limarino, C.O., 2002. Sedimentología y evolución paleoambiental de la Formación Patquía (Pérmico) en el extremo sur de la sierra de Maz y cerro Bola, provincia de La Rioja, Argentina. *Revista de la Asociación Geológica Argentina*, 57, 4, 415-436.
- Césari, S.N., Limarino, C.O., Gulbranson, E.L., 2011. An Upper Paleozoic bio-chronostratigraphic scheme for the western margin of Gondwana. *Earth Science Reviews* 106, pp. 149-160.

- Césari, S.N., Limarino, C.O., Spalletti, L.A., Piñol, F.C., Perez Loinaze, V.S., Ciccioli, P.L., Friedman, R., 2019. New U-Pb zircon age for the Pennsylvanian in Argentina: Implications in palynostratigraphy and regional stratigraphy. *Journal of South American Earth Sciences* 92, pp. 400-416. doi: 10.1016/j.jsames.2019.02.010
- Craddock, J.P., Ojakangas, R.W., Malone, D.H., Konstantinou, A., Mory, A., Thomas, R.J., Craddock, S.D., Pauls, K.N., Zimmerman, U., Botha, G., Rocha-Campos, A., de Pazos, P.R., Tohver, E., Riccomini, Cl., Martin, J., Redfern, J., Horstwood, M., Gehrels, G., 2019. Provenance of Permo-Carboniferous Diamictites across Gondwana. *Earth Science Reviews*. doi:10.1016/j.earscirev.2019.01.014
- Crisafulli, A., Herbst, R., 2008. Maderas gimnospérmicas de la Formación Solca (Pérmico Inferior), provincia de La Rioja, Argentina. *Ameghiniana* 45, 4, pp. 737-751.
- Dahlquist, J.A., Alasino, P.H., Nelson Eby, G., Galindo, C., Casquet, C., 2010. Fault controlled Carboniferous A-type magmatism in the proto-Andean foreland (Sierras Pampeanas, Argentina): Geochemical constraints and petrogenesis. *Lithos* 115, 65-81.
- Drobe, M., Lopez de Luchi, M.G., Steenken, A., Frei, R., Naumann, R., Siegesmund, S. & Wemmer, K. 2009. Provenance of the late Proterozoic to early Cambrian metaclastic sediments of the Sierra de San Luis (Eastern Sierras Pampeanas) and Cordillera Oriental, Argentina. *Journal of South American Earth Sciences*, 28, 239–262.
- Drobe, M., López de Luchi, M., Steenken, A., Wemmer, K., Naumann, R., Frei, R., Siegesmund, S., 2011. Geodynamic evolution of the Eastern Sierras Pampeanas (Central Argentina) based on geochemical, Sm–Nd, Pb–Pb and SHRIMP data. *Int. J. Earth Sciences* 100, 631-657.
- de los Hoyos, C.R., Willner, A.P., Larrovere, M.A., Rossi, J.N., Toselli, A.J., and Basei, M.A.S., 2011. Tectonothermal evolution and exhumation history of the Paleozoic proto-Andean Gondwana margin crust: The Famatinian belt in NW Argentina: *Gondwana Research*, v. 20, p. 309–324.
- Einhorn, J.C., Gehrels, G.E., Vernon, A., and DeCelles, P.G., 2015, U-Pb zircon geochronology of Neoproterozoic–Paleozoic sandstones and Paleozoic plutonic rocks in the Central Andes (21°S–26°S), in DeCelles, P.G., Ducea, M.N., Carrapa, B., and Kapp, P.A., eds., *Geodynamics of a Cordilleran Orogenic System: The Central Andes of Argentina and Northern Chile: Geological Society of America Memoir* 212, p. 115–124, doi:10.1130/2015.1212(06).
- Enkelmann, E., Ridgway, K.D., Carignano, C., Linnemann, U., 2014, A thermochronometric view into an ancient landscape: tectonic setting, and inversion of the Paleozoic eastern Paganzo basin, Argentina. *Lithosphere* 6, 93–107.
- Enkelmann, E., Garver, J.I., 2015, Low-temperature thermochronology applied to ancient settings. *Journal of Geodynamics*, v. 93, p. 17-30.
- Fanning, C.M., Pankhurst, R.J., Rapela, C.W., Baldo, E.G., Casquet, C., and Galindo, C., 2004. K-bentonites in the Argentine Precordillera contemporaneous with rhyolite volcanism in the

Famatinian Arc: *Journal of the Geological Society* [London], v. 161, p. 747–756, doi: 10.1144/0016-764903-130.

- Fedo, C.M., Sircombe, K., Rainbird, R., 2003, Detrital zircon analysis of the sedimentary record, in Hanchar, J.M., and Hoskin, P.W.O., eds., *Zircon: Reviews in Mineralogy and Geochemistry*, v. 53, p. 277-303.
- Gehrels, G.E., 2000, Introduction to detrital zircon studies of Paleozoic and Triassic strata in western Nevada and northern California, in Soreghan, M.J., and Gehrels, G.E., eds., *Paleozoic and Triassic paleogeography and tectonic evolution of western Nevada and northern California: Boulder, Colorado, Geological Society of America Special Paper 347*.
- Gehrels, G., 2011, Detrital Zircon U-Pb Geochronology: Current Methods and New Opportunities, in *Recent Advances in Tectonics of Sedimentary Basins*, C. Busby and A. Azor, editors, Blackwell Publishing.
- Gehrels, G.E., Valencia, V., Ruiz, J., 2008, Enhanced precision, accuracy, efficiency, and spatial resolution of U-Pb ages by laser ablation–multicollector–inductively coupled plasma–mass spectrometry: *Geochemistry, Geophysics, Geosystems*, v. 9, Q03017, doi:10.1029/2007GC001805.
- Gehrels, G., Blakey, R., Karlstrom, K., Timmons, M., Kelley, S., Dickinson, W., and Pecha, M., 2011, Detrital zircon U-Pb geochronology of Paleozoic strata in the Grand Canyon: *Lithosphere*.
- Gehrels, G., Pecha, M., 2014, Detrital zircon U-Pb geochronology and Hf isotope geochemistry of Paleozoic and Triassic passive margin strata of western North America: *Geosphere*, v. 10, p. 49-65.
- Gonzalez Bonorino, G., 1975. Acerca de la existencia de la Protoprecordillera de cuyo. in *actas. VI congreso geologico Argentino. Bahia Blanca 1*, 101e107.
- Godard, V., Bourlès, D.L., Spinabella, F., Burbank, D.W., Bookhagen, B., Burch Fisher, G., Moulin, A., Léanni, L., 2014, Dominance of tectonics over climate in Himalayan denudation: *Geology*, v. 42, no. 3, p. 243-246.
- Griffis, N.P., Mundil, R., Montañez, I.P., Isbell, J., Fedorchuk, N., Vesely, F., Iannuzzi, R., Qing-Zhu, Y., 2018. A new stratigraphic framework built on U-Pb single zircon TIMS ages with implications for the timing of the Penultimate Icehouse (Paraná Basin, Brazil): *Earth and Planetary Science Letters*.
- Guená, S.E., Escosteguy, L.D., 2010, Paleomagnetism of the Carboniferous-Permian Patquía Formation Paganzo basin, Argentina: implications for the apparent polar wander path for South America and Gondwana during the Late Paleozoic: *Geologica Acta*, v. 8, no. 4, p. 373-397.

- Gulbranson E.L., Montañez, I.P., Schmitz, M.D., Limarino, C.O., Isbell, J.L., Marensi, S.A., Crowley, J.L., 2010, High-precision U–Pb calibration of Carboniferous glaciation and climate history, Paganzo Group, NW Argentina. *Geological Society of America Bulletin* 122, 1480–1498.
- Gulbranson, E.L., Montañez, I.P., Tabor, N., Limarino, C.O., 2015. Late Pennsylvanian aridification on the southwestern margin of Gondwana (Paganzo Basin, NW Argentina): A regional expression of a global climate perturbation. *Palaeogeography Palaeoclimatology Palaeoecology* 417, pp. 220–235.
- Henry, L.C., Isbell, J.L., Limarino, C.O., 2008, Carboniferous glacial deposits of the Protoprecordillera of west central Argentina. In: Fielding, C.R., Frank, T.D., Isbell, J.L. (Eds.), *Resolving the Late Paleozoic Ice Age in Time and Space: Geological Society of America Special Paper*, 441, pp. 131–142.
- Holz, M., Franca, A. B., Souza, P. A., Iannuzzi, R., and Rohn, R., 2010. A stratigraphic chart of the Late Carboniferous/Permian succession of the eastern border of the Paraná Basin, Brazil, South America: *Journal of South American Earth Sciences*, v. 29, no. 2, p. 381–399.
- Huff, W.D., Davis, D., Bergström, S.M., Krekeler, M.P.S., Kolata, D.R., Cingolani, C.A., 1997. A biostratigraphically well-constrained K-bentonite U–Pb zircon age of the lowermost Darriwilian Stage (Middle Ordovician) from the Argentine Precordillera. *Episodes* 20, pp. 29–33.
- Huff, W.D., Davis, D., Bergström, S.M., Krekeler, M.P.S., Kolata, D.R., Cingolani, C.A., 1998. A biostratigraphically well-constrained K-bentonite U–Pb zircon age of the lowermost Darriwilian Stage (Middle Ordovician) from the Argentine Precordillera. *Episodes* 20, 29–33.
- Isbell, J.L., Henry, L.C., Gulbranson, E.L., Limarino, C.O., Fraiser, M.L., Koch, Z.J., Ciccioli, P.L. & Dineen, A.A., 2012. Glacial paradoxes during the late Paleozoic ice age: Evaluating the equilibrium line altitude as a control on glaciation. *Gondwana Research*, v. 22, p. 1–19.
- Keller, M., 1999, Argentine Precordillera: Sedimentary and plate tectonic history of a Laurentian crustal fragment in South America: *Geological Society of America Special Paper* 341, 131 p., doi: 10.1130 /0-8137-2341-8.1.
- Krapovickas, V., Mancuso, A.C., Arcucci, A., Caselli, A., 2010. Fluvial and eolian ichnofaunas from the Lower Permian of South America (Patquía Formation, Paganzo Basin). *Geológica Acta* 8, 4, pp. 449–462. doi: 10.1344/105.000001582.
- Leal, P.R., Hartmann, L.A., Santos, J.O.S., Miró, R.C., Ramos, V.A., 2003. Volcanismo postorogénico en el extremo norte de las Sierras Pampeanas Orientales: Nuevos datos geocronológicos y sus implicancias tectónicas. *Revista Asociación Geológica Argentina* 58, pp. 593–607.

- Limarino, C.O., Césari, S.N., Net, L.I., Marensi, S.A., Gutiérrez, P.R., Tripaldi, A., 2002. The Upper Carboniferous postglacial transgression in the Paganzo and Río Blanco Basins (northwestern Argentina): facies and stratigraphic significance. *Journal of South American Earth Sciences* 15, 445–460.
- Limarino, C.O., Spalletti, L.A., 2006. Paleogeography of the Upper Paleozoic basins of southern South America: an overview. *Journal of South American Earth Sciences* 22, 134–155.
- Limarino, C.O., Tripaldi, A., Marensi, S., Fauqué, L., 2006. Tectonic, sea level, and climatic controls on late Paleozoic sedimentation in the western basins of Argentina. *Journal of South American Earth Sciences* 33, 205–226.
- Limarino, C.O., Césari, S.N., Spalletti, L.A., Taboada, A.C., Isbell, J.L., Geuna, S., Gulbranson, E.L., 2014. A paleoclimatic review of southern South America during the late Paleozoic; A record from icehouse to extreme greenhouse conditions: *Gondwana Research*, v. 25, p. 1396-1421.
- Llambías, E.J., Gregori, D., Basei, M.A., Varela, R., Prozzi, C., 2003. Ignimbritas riolíticas neoproterozoicas en la Sierra Norte de Córdoba: ¿evidencia de un arco magmático temprano en el ciclo Pampeano?. *Revista Asociación Geológica Argentina* 58, 4, pp. 572-582.
- López-Gamundí, O.R., Limarino, C.O., Césari, S.N., 1992. Late Paleozoic paleoclimatology of central-west Argentina. *Palaeogeography, Palaeoclimatology, Palaeoecology* 91, pp. 305-329.
- López-Gamundí, O.R., Martínez, M., 2000. Evidence of glacial abrasion in the Calingasta–Uspallata and western Paganzo Basins, mid-Carboniferous of western Argentina. *Palaeogeography, Palaeoclimatology, Palaeoecology* 159, 145–165.
- Ludwig, K.R., 2012. *Isoplot 3.75, A Geochronological Toolkit for Excel*: Berkeley Geochronology Center Special Publication 5, 75.
- Marensi, S.A., Limarino, C.O., Césari, S.N., Tripaldi, A., Caselli, A.T., 2002. Glacial and postglacial sedimentation in western Paganzo Basin, Northwest Argentina. 16th International Sedimentological Congress, Abstracts, Johannesburg, pp. 236-237.
- Marensi, S.A., Tripaldi, A., Limarino, C.O., Caselli, A.T., 2005. Facies and architecture of a Carboniferous grounding-line system from the Guandacol Formation, Paganzo Basin, northwestern Argentina. *Gondwana Res.* 8, 187–202.
- Martina, F., Canelo, H.N., Dávila, F.M., Hollanda, M.H.B.M., Teixeira, W., 2018. Mississippian lamprphyre dikes in western Sierras Pampeanas, Argentina: Evidence of transtensional tectonics along the SW margin of Gondwana. *Journal of South American Earth Sciences* 83, pp. 68-80.
- Martínez, M., 1993. Hallazgo de fauna marina en la Formación Guandacol (Carbonífero) en la loc. de Agua Hedionda, San Juan, Precordillera Nororiental, Argentina, XII ICC-P, 2, pp. 291-296.

- McKay, M.P., Weislogel, A.L., Jackson, W.T., Jr., Dean, J., Fildani, A., 2018. Structural and magmatic controls on the turbidites of the Karoo Basin, South Africa. In: Ingersoll, R.V., Graham, S.A., Lawton, T.F. (eds), *Tectonics, Sedimentary Basins, and Provenance: A Celebration of William R. Dickinson's Career: Geological Society of America Special Paper 540*, 689-705.
- Milana, J.P., di Pasquo, M.M., 2019. New chronostratigraphy for a Lower to Upper Carboniferous strike-slip basin of W-Precordillera (Argentina): its paleogeographic, tectonic and glacial importance. *Journal of South American Earth Sciences* 96. <https://doi.org/10.1016/j.jsames.2019.102383>.
- Moxness, L.D., Isbell, J.L., Pauls, K.N., Limarino, C.O., Schencman, J., 2018. Sedimentology of the mid-Carboniferous fill of the Olta paleovalley, eastern Paganzo Basin, Argentina: Implications for glaciation and controls on diachronous deglaciation in western Gondwana during the late Paleozoic Ice Age. *Journal of South American Earth Sciences* 84, p 127-148. doi/10.1016/j.jsames.2018.03.015
- Net, L.I., 1999. Petrografía, diagénesis y procedencia de areniscas de la sección inferior del Grupo Paganzo (carbonífero) en la cuenca homónima. PhD Thesis, Universidad de Buenos Aires, p.49.
- Net, L.I., Limarino, C.O., 1999. Paleogeografía y correlación estratigráfica del Paleozoico Tardío de la Sierra de Los Llanos, provincia de La Rioja, Argentina: *Revista de la Asociación Geológica Argentina* 54 (3), 229–239.
- Net, L.I., Alonso, M.S., Limarino, C.O., 2002. Source rock and environmental control on clay mineral associations, lower section of Paganzo group (Carboniferous), northwest Argentina. *Sedimentary Geology* 152, 183–199.
- Net, L.I., Limarino, C.O., 2006. Applying sandstone petrofacies to unravel the Upper Carboniferous evolution of the Paganzo Basin, northwest Argentina. *Journal of South American Earth Sciences* 22, 239–254.
- Newell, A.J., Tverdokhlebov, V.P., Benton, M.J., 1999, Interplay of tectonics and climate on a transverse fluvial system, Upper Permian, Southern Uralian Foreland Basin, Russia: *Sedimentary Geology*, v. 127, p. 11-29.
- Ottone, E.G., Holfeltz, G.D., Albanesi, G.L., Ortega, G., 2001. Chitinozoans from the Ordovician Los Azules Formation, Central Precordillera, Argentina. *Micropaleontology* 47, 97-110.
- Pankhurst, R.J., Rapela, C.W., Saavedra, J., Baldo, E., Dahlquist, J., Pascua, I., Fanning, C.M., 1998. The Famatinian magmatic arc in the Central Sierras Pampeanas: An early to mid-Ordovician continental arc on the Gondwana margin. In: Pankhurst, R.J., Rapela, C.W. (Eds.) *The Proto-Andean Margin of Gondwana. Geological Society of London Special Publication 142*, 343-367.

- Pankhurst, R.J., Rapela, C.W., Fanning, C.M., 2000. Age and origin of coeval TTG, I- and S-type granites in the Famatinian belt of NW Argentina. *Earth and Environmental Science Transactions of the Royal Society of Edinburgh*, 91, 151-168.
- Partridge, T., 1997. Late Neogene uplift in eastern and southern Africa and its paleoclimatic implications: In Ruddiman, W.F. (ed.) *Tectonic uplift and climate change*, New York, NY, United States (USA), Plenum Press, New York, NY.
- Pauls, K.N., Isbell, J.L., McHenry, L., Limarino, C.O., Moxness, L.D., Schencman, L.J., 2019. A paleoclimatic reconstruction of the Carboniferous-Permian paleovalley fill in the Eastern Paganzo Basin: Insights into glacial extent and deglaciation of southwestern Gondwana. *Journal of South American Earth Sciences*.
- Pauls, K.N., Isbell, J.L., Limarino, C.O., Alonso-Muruaga, P.J., Malone, D.H., Schencman, L.J., Colombi, C.E., Moxness, L.D., in review. Constraining late Paleozoic ice extent in the Paganzo Basin of western Argentina utilizing U-Pb detrital zircon geochronology for the lower Paganzo Group strata. *Journal of South American Earth Sciences*.
- Pazos, P.J., 2000. Trace fossils and facies in glacial to postglacial deposits from the Paganzo Basin, (late Carboniferous) Central Precordillera, Argentina. *Ameghiniana* 37, pp. 23-38.
- Pazos, P.J., 2002a. The Late Carboniferous glacial to postglacial transition: facies and sequence stratigraphy, western Paganzo Basin, Argentina. *Gondwana Research* 5, pp. 467-487.
- Pazos, P.J., 2002b. Palaeoenvironmental framework of the glacial-postglacial transition (Late Paleozoic) in the Paganzo-Calingasta Basin (southern South America) and the Great Karoo-Kalahari Basin (southern Africa): ichnological implications. *Gondwana Research* 5, pp. 619-640.
- Rabassa, J., Carignano, C., Cioccale, M., 2014. A general overview of Gondwana landscapes in Argentina. In: Rabassa, J., Ollier, C. (Eds.), *Gondwana Landscapes in Southern South America: Argentina, Uruguay and southern Brazil*. Springer Earth System Science, Dordrecht, Heidelberg, New York, London, 201-245.
- Rapalini, A.E., 2005, The accretionary history of southern South America from the latest Proterozoic to the late Paleozoic: Some paleomagnetic constraints, in Vaughan, A.P.M., Leat, P.T., and Pankhurst, R.J., eds., *Terrane Processes at the Margins of Gondwana*: Geological Society, London, Special Publication 246, p. 305-328.
- Rapela, C.W., Pankhurst, R.J., Casquet, C., Baldo, E., Saavedra, J., Galindo, C., Fanning, C.M., 1998. The Pampean orogeny of the southern proto-Andes: evidence for Cambrian continental collision in the Sierras de Córdoba. In: Pankhurst, R.J., Rapela, C.W. (Eds.), *The Proto-Andean Margin of Gondwana*. *Geol. Soc. Lond.*, pp. 181-217.
- Rapela, C.W., Pankhurst, R.J., Casquet, C., Fanning, C.M., Baldo, E.G., González-Casado, J.M., Galindo, C., Dahquist, J., 2007. The Río de la Plata craton and the assembly of SW Gondwana. *Earth-Sci. Rev.* 83, 49-82.

- Rapela, C.W., Pankhurst, R.J., Casquet, C., Dahlquist, J.A., Fanning, M., Baldo, E.G., Galindo, C., Alasino, P.H., Ramacciotti, C.D., Verdecchia, S.O., Murra, J.A., Basei, M.A.S., 2018. A review of the Famatinian Ordovician magmatism in southern South America: evidence of lithosphere reworking and continental subduction in the early proto-Andean margin of Gondwana. *Earth-Science Reviews* 187, 259-285.
- Ramos, V.A., Dallmeyer, D. y Vujovich, G., 1998. Time constraints on the Early Paleozoic docking of the Precordillera, Central Argentina. In: Pankhurst, R. y Rapela, C. (Eds.): *The Proto-Andean Margin of Gondwana*, Geological Society, London, Special Publication, 142, 143-158.
- Ramos, V.A., 1999. Evolución tectónica de la Argentina. In: *Rasgos Estructurales del Territorio Argentino*. Instituto de Geología y Recursos Minerales, Geología Argentina Anales 29 (24), 715-784.
- Ramos, V.A., 2008. The basement of the Central Andes: the Arequipa and related terranes. *Annual Review Earth and Planetary Sciences* 36, pp. 289–324.
- Ramos, V.A., Vujovich, G., Martino, R. & Otamendi, J. 2010. Pampia: a large cratonic block missing in the Rodinia supercontinent. *Journal of Geodynamics*, 50, 243–255.
- Ramos, V.A., Escayola, M., Leal, P., Pimentel, M.M., Santos, J.O.S., 2015. The late stages of the Pampean Orogeny, C_ordoba (Argentina): Evidence of postcollisional Early Cambrian slab break-off magmatism. *Journal of South American Earth Sciences* 64, 351-364. doi: 10.1016/j.jsames.2015.08.002.
- Rocha Campos, A.C., dos Santos, P.R., Canuto, J.R., 2008. Late Paleozoic glacial deposits of Brazil; Parana Basin. In: Fielding, C.R., Frank, T.D., Isbell, J.L. (Eds.), *Resolving the Late Paleozoic Ice Age in Time and Space: Geological Society of America Special Paper*, 441, pp. 97–114.
- Ruddiman, W. F., and Prell, W. L., 1997, *Introduction to the uplift-climate connection*, New York, NY, United States (USA), Plenum Press, New York, NY, Tectonic uplift and climate change.
- Ruddiman, W. F., Raymo, M. E., Prell, W. L., and Kutzbach, J. E., 1997, *The uplift-climate connection: a synthesis*, New York, NY, United States (USA), Plenum Press, New York, NY, Tectonic uplift and climate change.
- Sato, A.M., Llambías, E.J., Basei, M.A.S., Castro, C.E., 2015. Three stages in the Late Paleozoic to Triassic magmatism of southwestern Gondwana, and the relationships with the volcanogenic events in coeval basins. *Journal of South American Earth Sciences*, 63, pp. 48-69. doi: 10.1016/j.jsames.2015.07.005.
- Sial, A.N., Peralta, S., Gaucher, C., Toselli, A.J., Ferreira, V.P., Frei, R., Parada, M.A., Pimentel, M.M., Pereira, N.S., 2013. High-resolution stable isotope stratigraphy of the upper Cambrian and Ordovician in the Argentine Precordillera: Carbon isotope excursions and correlations. *Gondwana Research* 24, 330-348.

- Sircombe, K.N., Stern, R.A., 2002. An investigation of artificial biasing in detrital zircon U-Pb geochronology due to magnetic separation in sample preparation. *Geochimica et Cosmochimica Acta*, 66 (13), 2379-2397.
- Socha, B.J., Carignano, C., Rabassa, J., Mickelson, D.M., 2014. Gondwana glacial paleolandscape, diamictite record of Carboniferous valley glaciation, and preglacial remnants of an ancient weathering front in northwestern Argentina. In: Rabassa, J., Ollier, C. (Eds.), *Gondwana landscapes in southern South America*. Springer, Dordrecht, pp. 331–363.
- Spalletti, L.A., Limarino, C.O., Piñol, F.C., 2012. Petrology and geochemistry of Carboniferous siliciclastics from the Argentine Frontal Cordillera: A test of methods for interpreting provenance and tectonic setting. *Journal of South American Earth Sciences* 36, pp. 32-54. doi:10.1016/j.jsames.2011.11.002.
- Sterren, A.F., Martínez, M., 1996. El paleovalle de Olta (Carbonífero): paleoambientes y paleogeografía. 13° Congreso Geológico Argentino y 3° Congreso Exploración de Hidrocarburos (Buenos Aires), Actas 2, 89-103.
- Tabor, N. J., and Poulsen, C. J., 2008. Palaeoclimate across the Late Pennsylvanian-Early Permian tropical palaeolatitudes; a review of climate indicators, their distribution, and relation to palaeophysiographic climate factors: *Palaeogeography, Palaeoclimatology, Palaeoecology*, v. 268, no. 3-4, p. 293-310.
- Tedesco, A., Ciccioli, P., Suriano, J., Limarino, C., 2010. Changes in the architecture of fluvial deposits in the Paganzo Basin (Upper Paleozoic of San Juan Province): an example of sea level and climatic controls on the development of coastal fluvial environments. *Geologica Acta*.
- Thomas, W.A., Astini, R.A., Mueller, P.A., and McClelland, W.C., 2015. Detrital-zircon geochronology and provenance of the Oclöyic synorogenic clastic wedge, and Ordovician accretion of the Argentine Precordillera terrane: *Geosphere*, v. 11, no. 6, p. 1749–1769, doi:10.1130/GES01212.1.
- Thompson, C.K., Kah, L.C., Astini, R., Bowring, S.A., and Buchwaldt, R., 2012. Bentonite geochronology, marine geochemistry, and the Great Ordovician Biodiversification Event (GOBE): *Palaeogeography, Palaeoclimatology, Palaeoecology*, v. 321–322, p. 88–101, doi: 10.1016/j.palaeo.2012.01.022.
- Toselli, A.J., Basei, M.A., Rossi de Toselli, J.N., Rudas, R., 2003. Análisis geoquímico-geocronológico de rocas granulíticas y calcosilicáticas de las Sierras Pampeanas Noroccidentales. *Revista de la Asociación Geológica Argentina*, 58, 4, pp. 629-642.
- Valdez Buso, V., Pasquo, M.D., Milana, J.P., Kneller, B., Fallgatter, C., Chemale, F.J., Paim, P.S.G., 2017. Integrated U-Pb zircon and palynological/palaeofloristic age determinations of a Bashkirian palaeofjord fill, Quebrada Grande (Western Argentina). *J. S. Am. Earth Sci.* 73, 202–222.

- Valdez Buso, V., Milana, J.P., di Pasquo, M., Paim, P.S.G., Philipp, R.P., Aquino, C.A., Cagliari, J., Junior, F.C., Kneller, B., 2020. Timing of the Late Paleozoic glaciation in western Gondwana: New ages and correlations from Paganzo and Paraná basins. *Palaeogeography, Palaeoclimatology, Palaeoecology* 544. doi:10.1016/j.palaeo.2020.109624.
- Varela, R., Basei, M.A.S., Sato, A.M., González, P.D., Siga Jr, O., Campos Neto, M.C., Cingloani, C.A., 2003. Grenvillian basement and Famatinian events of the Sierra de Umango (29°S): A review and new geochronological data. IV South American Symposium on Isotope Geology- Short Papers, pp. 304-306.
- Verdecchia, S. O., Casquet, C., Baldo, E. G., Pankhurst, R. J., Rapela, C. W., Fanning, M., Galindo, C., 2011. Mid- to Late Cambrian docking of the Rio de la Plata Craton to southwestern Gondwana; age constraints from U-Pb SHRIMP detrital zircon ages from Sierras de Ambato and Velasco (Sierras Pampeanas, Argentina). *Journal of the Geological Society of London* 168, 1061-1071.
- Verdecchia, S.O., Murra, J.A., Baldo, E.G., Casquet, C., Pascua, I., Saavedra, J., 2014. Geoquímica de las rocas metasedimentarias del Cámbrico medio al Ordovícico temprano de la Sierra de Los Llanos (Sierras Pampeanas, Argentina): Fuente de sedimentos, correlación y ambiente geotectónico. *Andean Geology* 41, 2, 380-400. doi: 10.5027/andgeoV41n2-a06.
- Verdecchia, S.O., Collo, G., Zandomeni, P.S., Wunderlin, C., Fehrmann, M., 2018. Crystallochemical indexes and geothermobarometric calculations as a multiproxy approach to P-T condition of the low-grade metamorphism: The case of the San Luis Formation, Eastern Sierras Pampeanas of Argentina. *Lithos*, pp. 385-401. doi: 10.1016/j.lithos.2018.11.021.
- Vujovich, G.I., Osters, H.A., 2003. Evidencias del ciclo Pampeano en el basamento del sector noroccidental de la sierra de San Luis. *Revista de la Asociación Geológica Argentina* 58, 4, pp. 541-548.
- Willner, A.P., Gerdes, A., Massonne, H.-J., 2008. History of crustal growth and recycling at the Pacific convergent margin of South America at latitudes 29° -36° S revealed by a U-Pb and Lu-Hf isotope study of detrital zircon from late Paleozoic accretionary systems. *Chemical Geology* 253, pp. 114-129. doi:10.1016/j.chemgeo.2008.04.

Chapter 6. Conclusions

Outcomes of stated project objectives

1. *Conduct a detailed sedimentologic and stratigraphic analysis of the deposits within the eastern Paganzo Basin to refine our understanding of the extent and timing of glaciation during the Carboniferous.*
 - Stratigraphic sections were measured at localities that contained glacial to post-glacial deposits, i.e., Agua de Jagüel (AJ) in the Calingasta-Uspallata Basin, Agua Hedionda (AH) anticline at Huaco in the west, and at the Olta-Malanzán paleovalley (OMPV) system in the Sierras de Chepes and Los Llanos of the eastern Paganzo Basin.
 - The depositional fill of the lower Paganzo Group strata indicated glacial deposits existed in the Huaco locality, but not in the Olta-Malanzán locality.
 - Ice most likely did not exist in the eastern Sierras Pampeanas, but did exist in the Protoprecordilleran and adjacent ranges of the middle-Carboniferous western Gondwana margin.
 - There were multiple depositional centers in the Paganzo Basin during the early-middle Carboniferous, as evidenced by the distinct detrital zircon populations from the eastern domain (i.e. OMPV) and the western domain (AH).

2. *Compare and contrast the glacial to post-glacial paleoclimate trends in southwestern Gondwana during the LPIA.*

- The CIA technique was successfully applied to the late Paleozoic sediments of the Paganzo Group strata, after testing at the Olta-Malanzán paleovalley system. The technique was then used for the remaining selected localities within the Paganzo Basin, and across the Protoprecordilleran region to the Calingasta-Uspallata Basin (i.e. at AJ).
- The climate trends of the three chosen localities of the Paganzo Basin (i.e. Cerro Guandacol, Huaco and Olta-Malanzán) all portray a humid post-glacial climate followed by a decrease in CIA values, indicating a transition to an arid climate through the late Carboniferous and into the Permian.
- The overall climate reconstructions indicate that the post-glacial transition of the early Pennsylvanian of the Paganzo Basin fluctuated. The cold conditions reflected in the values of the basal diamictites and conglomerates throughout the basin indicate that even as the glaciers were diminishing, cold conditions still persisted. Each of the sections in the basin contained other glacial diamictites (i.e. at Huaco and Cerro Guandacol), or non-glacial conglomerates and rare diamictites interstratified with shallow lacustrine deposits (i.e. at Olta-Malanzán). In all cases, the clasts in these basal deposits record little-to-no alteration of reworked or fresh basement or underlying materials.
- The late Carboniferous was fairly humid, and most likely represented a temperate climate prior to the increased aridification of the early Permian.

3. *Assess the role of tectonics as a driver for climate shifts recorded in the western basins of Argentina during the late Paleozoic.*
- Detrital zircon samples from the eastern domain of the Paganzo Basin (i.e. the Sierras de Chepes and Los Llanos [OMPV]), show a shift in provenance from a source in the very local Chepes Granodiorite (Ordovician in age) during the middle Carboniferous (Malanzán and Loma Larga formation samples), to an older-age dominated zircon population in the La Colina sample. The sediment source shifts eastward, and possibly sourced from the eastern Sierras Pampeanas system, such as the Sierras de Córdoba.
 - The provenance also changes through time in the western domain (i.e. at Huaco), and displays an eastward shift in drainage as well. Additionally, the Tupe and Patquía formations record the presence of late Carboniferous detrital zircons, which points to the existence of a magmatic arc outboard of the western margin of Gondwana during this time. Together, the results point to the extension of the basin westward, and the development of a magmatic arc through renewed subduction along the active tectonic margin.
 - Regional changes in paleotopography must have played some role in the drying out of the Paganzo Basin, as the paleoclimate reconstruction corresponds to the shifting provenance patterns in the late Carboniferous-early Permian. The development of a magmatic arc to the west of the basin and extension of the basin was likely in response to the convergence along the Panthalassan margin. Both of these factors could have created an extensive rain shadow that prevented moisture from reaching the interior of the Paganzo Basin.

Implications of early deglaciation in western Gondwana

Glaciation, or local centers of ice, are recorded in the basins of western Argentina (i.e. Río Blanco, Calingasta-Uspallata, and western Paganzo Basins) during the Mississippian (Visean), which is interpreted as the onset of widespread glaciation across Gondwana, including glaciation occurring in the Paraná Basin in Brazil (López-Gamundí et al., 1994; López-Gamundí, 1997; Caputo et al. 2008; Henry et al., 2008; Holz et al., 2008; Rocha Campos et al., 2008; Limarino et al., 2014; Rosa et al., 2019). While glaciation continued until the Carboniferous-Permian boundary in the Paraná Basin in Brazil, the western margin basins of Argentina at similar paleolatitudes (Paganzo, Calingasta-Uspallata, and Río Blanco Basins) experience a climate shift from glacial to humid and ever-wet conditions by the Bashkirian, which transitioned to arid conditions during the late Pennsylvanian (Henry et al., 2008; Rocha-Campos et al., 2008; Holz, 2010; Césari et al., 2011; Limarino et al., 2014). The data resulting from this study provide important information related to regional differences in climate change. This study pulls together the current understanding of the western margin of Gondwana and examines several hypotheses concerning glacial extent, as well as reasons for deglaciation and intense aridification of the Paganzo Basin. Furthermore, the findings from this project are consistent with a large body of work indicating that there were separate depositional centers in the basin during the glacial phase (Visean-Bashkirian), and that discrete ice centers existed rather than a large ice sheet centered in the eastern Sierras Pampeanas.

Paleoclimate in the western margin basins is driven primarily by active tectonism in the region that disrupted the atmospheric and moisture flow across the region. A secondary mechanism could be the rotational drift of Gondwana across the South Pole region, but further data is necessary to fully develop this idea. Evidence provided by this study shows that the early

Pennsylvanian climate amelioration in the western margin basins can be tied to the collapse of the Protoprecordillera range. The stratigraphic, paleontological and new paleoclimatic reconstructions coincide with the loss in elevation of the mountain belt during the latest Mississippian-early Pennsylvanian. This topographic change coincides with an increase in subsidence during this same time period. An increase in volcanism is also recorded in the western margin stratigraphic units and coincides with an increase in aridity throughout the region. The increase in volcanism is likely formed due to the development of the outboard volcanic arc, which may have caused an orographic effect during the late Pennsylvanian, therefore cutting the region off from a moisture source. Ergo, tectonism is the main climate driver for the relatively early disappearance of glacial activity in the western margin basins. However, global drivers such as the rotation of Gondwana across the South Pole and decreasing atmospheric CO₂ concentrations have more control on the end of glaciation in the southern Paraná Basin.

Future Directions

This project could be expanded in a few directions. The question remains as to whether or not the Protoprecordilleran was truly dissected, and if so, where, and how was it interconnected? Better correlations across the paleovalleys and paleofjords exposed in this region would be needed to test this. Some correlations across the Protoprecordilleran range to the deposits of the Calingasta-Uspallata and Río Blanco basin outcrops have been proposed (cf. Henry et al., 2008; Gulbranson et al., 2010; Césari et al., 2011), but some of these use biostratigraphic correlations. A more thorough detrital zircon geochronological analysis is needed to better ascertain exact glacial extent and the nature of the fold-and-thrust belt.

Furthermore, the source regions in the Paganzo Basin are similar in age, with some distinct differences. These differences could be better constrained and separated using an unmixing model (Konstantinou et al., 2014; Sundell and Saylor, 2017). This requires the creation of a database, using both from literature sources and additional samples from across the Paganzo Basin, much like the study conducted by Einhorn et al. (2015).

Lastly, the deglaciation and climate change dynamics of the Paganzo Basin are different than the Paraná Basin on the other side of the Pampean arch during the late Paleozoic. South American Gondwanan basins provide ideal locations for an in-depth study of the climate dynamics on a regional scale. This project only studied a small portion of the very large Paraná Basin. As both the Paganzo and Paraná basins contain glacial deposits and show variation in the duration and timing of these glacial episodes (cf. Crowell and Frakes, 1970; Visser, 1997; Isbell et al., 2003, 2012; Fielding et al., 2008a, 2008b; Rocha-Campos et al., 2008; Gonzalez and Diaz Saravia, 2010; Gulbranson et al., 2010; Limarino et al., 2014), more detailed analyses and comparisons in paleoclimate could help compare how the regions within each basin varied. Additional paleoclimate reconstructions for both the Calingasta-Uspallata and Río Blanco basins region could also be included for a more in-depth analysis of the timing of various climatic transitions during the Pennsylvanian.

The late Paleozoic ice age continues to provide opportunities to study the effects of climate drivers on global and regional scales. Thus, regional paleoclimate studies at a high chronostratigraphic resolution, such as this one, add to our knowledge of environmental responses to shifting global climate, and can potentially assist in our endeavor to understand how different mechanisms drive global climate change. The results of this project only represent a small corner of this vast world. There are still many paleoenvironmental aspects of the LPIA and

the ensuing transition into greenhouse conditions that are unknown, and continued studies, especially on a regional scale, will add to our understanding of the timing and environmental responses to changing global climate.

References

- Caputo, M.V., Crowell, J.C., 1985. Migration of glacial centers across Gondwana during Paleozoic Era. *Geological Society of America Bulletin* v. 96, p. 1020-1036.
- Césari, S.N., Limarino, C.O., Gulbranson, E.L., 2011. An Upper Paleozoic bio-chronostratigraphic scheme for the western margin of Gondwana. *Earth Sci. Rev.* 106, p. 149-160.
- Crowell, J.C., Frakes, L.A., 1970. Phanerozoic glaciation and the causes of ice ages. *American Journal of Science* 268, 193–224.
- Einhorn, J.C., Gehrels, G.E., Vernon, A., and DeCelles, P.G., 2015. U-Pb zircon geochronology of Neoproterozoic–Paleozoic sandstones and Paleozoic plutonic rocks in the Central Andes (21°S–26°S), in DeCelles, P.G., Ducea, M.N., Carrapa, B., and Kapp, P.A., eds., *Geodynamics of a Cordilleran Orogenic System: The Central Andes of Argentina and Northern Chile: Geological Society of America Memoir* 212, p. 115–124, doi:10.1130/2015.1212(06).
- Fielding, C.R., Frank, T.D., Isbell, J.L., 2008a. The late Paleozoic ice age—A review of current understanding and synthesis of global climate patterns, in Fielding, C.R., Frank, T.D., and Isbell, J.L., eds., *Resolving the Late Paleozoic Ice Age in Time and Space. Geological Society of America Special Paper* 441, p. 343-354.
- Fielding, C.R., Frank, T.D., Birgenheier, L.P., Rygel, M.C., Jones, A.T., Roberts, J., 2008b. Stratigraphic imprint of the Late Paleozoic Ice Age in eastern Australia: a record of alternating glacial and nonglacial climate regime. *Journal of the Geological Society, London*, v. 165, p. 129-140.
- González, C.R., Díaz Saravia, P., 2010. Bimodal character of the Late Paleozoic glaciations in Argentina and bipolarity of climatic changes. *Palaeogeography, Palaeoclimatology, Palaeoecology* 298, 101-111.
- Gulbranson E.L., Montañez, I.P., Schmitz, M.D., Limarino, C.O., Isbell, J.L., Marensi, S.A., Crowley, J.L., 2010. High-precision U–Pb calibration of Carboniferous glaciation and climate history, Paganzo Group, NW Argentina. *Geological Society of America Bulletin* 122, 1480–1498.
- Henry, L.C., Isbell, J.L., Limarino, C.O., 2008. Carboniferous glacial deposits of the Protoprecordillera of west central Argentina. In: Fielding, C.R., Frank, T.D., Isbell, J.L. (Eds.), *Resolving the Late Paleozoic Ice Age in Time and Space: Geological Society of America Special Paper*, 441, pp. 131–142.
- Holz, M., Franca, A. B., Souza, P. A., Iannuzzi, R., and Rohn, R., 2010. A stratigraphic chart of the Late Carboniferous/Permian succession of the eastern border of the Paraná Basin, Brazil, South America: *Journal of South American Earth Sciences*, v. 29, no. 2, p. 381-399.
- Isbell, J.L., Miller, M.F., Wolfe, K.L. & Lenaker, P.A., 2003. Timing of late Paleozoic glaciation in Gondwana: was glaciation responsible for the development of northern hemisphere

- cyclothems?: in Extreme depositional environments: mega end members in geologic time, eds. M. A. Chan & A. W. Archer Boulder, Colorado: Geological Society of America Special Paper, 5-24.
- Isbell, J.L., Henry, L.C., Gulbranson, E.L., Limarino, C.O., Fraiser, M.L., Koch, Z.J., Ciccioli, P.L. & Dineen, A.A., 2012. Glacial paradoxes during the late Paleozoic ice age: Evaluating the equilibrium line altitude as a control on glaciation. *Gondwana Research*, v. 22, p. 1-19.
- Konstantinou, A., Wirth, K.R., Vervoort, J.D., Malone, D.H., Davidson, C., Craddock, J.P., 2014. Provenance of quartz arenite of the early Paleozoic Midcontinent Region, USA. *The Journal of Geology* 122, doi: 10.1086/675327.
- Limarino, C.O., Tripaldi, A., Marensi, S., Fauqué, L., 2006. Tectonic, sea level, and climatic controls on late Paleozoic sedimentation in the western basins of Argentina. *Journal of South American Earth Sciences* 33, 205–226.
- Limarino, C.O., Césari, S.N., Spalleti, L.A., Taboada, A.C., Isbell, J.L., Geuna, S., Gulbranson, E.L., 2014. A paleoclimatic review of southern South America during the late Paleozoic: A record from icehouse to extreme greenhouse conditions: *Gondwana Research*, v. 25, p. 1396-1421.
- López Gamundí, O.R., 1997. Glacial–postglacial transition in the late Paleozoic basins of southern South America. In: Martini, I.P. (Ed.), *Late Glacial and Postglacial Environmental Changes: Quaternary, Carboniferous–Permian, and Proterozoic*. Oxford University Press, Oxford, UK, pp. 147–168.
- López-Gamundí, O.R., Espejo, I.S., Conaghan, P.J., Powell, C.McA., Veevers, J.J., 1994. Southern South America. In: Veevers, J.J., Powell, C.McA. (Eds.), *Permian–Triassic Pangean basins and foldbelts along the Panthalassan margin of Gondwanaland*. Boulder, Colorado: Geological Society of America Memoir 184, 281–329.
- Rosa, E.L.M., Vesely, F.F., Isbell, J.L., Kipper, F., Fedorchuk, N.D., Souza, P.A., 2019. Constraining the timing, kinematics and cyclicity of Mississippian–Early Pennsylvanian glaciations in the Paraná Basin, Brazil. *Sedimentary Geology* 384, pp. 29-49. doi:10.1016/j.sedgeo.2019.03.001.
- Rocha Campos, A.C., dos Santos, P.R., Canuto, J.R., 2008. Late Paleozoic glacial deposits of Brazil; Parana Basin. In: Fielding, C.R., Frank, T.D., Isbell, J.L. (Eds.), *Resolving the Late Paleozoic Ice Age in Time and Space: Geological Society of America Special Paper*, 441, pp. 97–114.
- Sundell, K. E., Saylor, J.E., 2017. Unmixing detrital geochronology age distributions, *Geochem. Geophys. Geosyst.*, 18, doi:10.1002/2016GC006774.
- Visser, J.N.J., 1997. Deglaciation sequences in the Permo-Carboniferous Karoo and Kalahari basins of southern Africa: a tool in the analysis of cyclic glaciomarine basin fills. *Sedimentology* 44, 507–521.

Appendix A: Detrital Zircon Geochronology Data

Table A1. CDH0923-3S U-Pb detrital zircon geochronologic analyses from Huaco (Guandacol Formation sandstone from AH locality described in Chapter 2).

Analysis	U (ppm)	$^{206}\text{Pb}/^{207}\text{Pb}$		U/Th	$^{206}\text{Pb}/^{207}\text{Pb}$		$^{206}\text{Pb}/^{235}\text{U}$		$^{206}\text{Pb}/^{238}\text{U}$		Err. corr.	$^{206}\text{Pb}/^{238}\text{U}$		$^{207}\text{Pb}/^{235}\text{U}$		$^{206}\text{Pb}/^{207}\text{Pb}$		Best age (Ma)	1 σ (Ma)	Conc. (%)
		1 σ	1 σ		1 σ	1 σ	1 σ	1 σ	1 σ	1 σ		1 σ	1 σ							
Spot 1	756	62866	4	13	1	2	1	0	1	1	1	1057	9	1055	8	1049	13	1049	13	101
Spot 10	183	16194	2	12	1	2	2	0	1	1	1	1003	13	1084	10	1251	14	1251	14	80
Spot 11	713	174825	1	12	1	2	1	0	1	1	1	1168	12	1180	9	1204	11	1204	11	97
Spot 12	411	14187	1	18	1	1	1	0	1	1	1	445	5	451	5	484	14	445	5	92
Spot 13	760	39334	11	18	1	1	1	0	1	1	1	480	5	483	5	496	14	480	5	97
Spot 14	434	22808	1	12	1	2	1	0	1	1	1	988	11	1079	8	1267	10	1267	10	78
Spot 15	895	548847	5	15	1	1	2	0	2	1	1	592	9	629	8	765	16	592	9	77
Spot 17	234	31015	1	14	1	1	1	0	1	1	1	812	8	845	8	934	18	812	8	87
Spot 2	59	26882	3	13	1	2	1	0	1	1	1	1009	8	1045	8	1120	17	1120	17	90
Spot 20	249	226275	3	13	1	2	1	0	1	1	1	1037	11	1052	9	1082	15	1082	15	96
Spot 21	336	1321082	2	18	1	1	1	0	1	1	1	463	5	468	5	493	17	463	5	94
Spot 22	392	24226	3	17	1	1	1	0	1	1	1	520	5	518	5	509	17	520	5	102
Spot 23	1471	341348	5	17	0	1	1	0	1	1	1	642	4	637	4	619	10	642	4	104
Spot 25	130	10075	1	17	2	1	2	0	1	1	1	503	6	519	8	590	36	503	6	85
Spot 27	395	17406	1	18	1	0	4	0	4	1	1	309	11	331	11	490	16	309	11	NA
Spot 28	200	26361	1	10	1	0	1	0	1	1	1	1492	14	1579	10	1697	12	1697	12	88
Spot 29	489	58376	2	14	1	2	1	0	1	1	1	971	7	975	6	983	12	983	12	99
Spot 3	151	208426	2	12	1	2	1	0	1	1	1	1114	10	1160	8	1248	13	1248	13	89
Spot 30	867	106427	2	14	1	2	1	0	1	1	1	1019	7	1012	6	996	11	996	11	102
Spot 31	308	15461	3	17	1	1	1	0	1	1	1	565	5	552	5	498	14	565	5	113
Spot 32	317	231755	5	13	1	2	1	0	1	1	1	1028	12	1039	9	1061	13	1061	13	97
Spot 33	478	21380	6	16	1	1	1	0	1	1	1	637	6	638	7	642	21	637	6	99
Spot 34	396	25779	5	17	1	1	1	0	1	1	1	605	7	605	6	604	16	605	7	100
Spot 35	782	135295	1	18	1	1	1	0	1	1	1	410	4	413	4	427	15	410	4	96
Spot 36	631	303018	5	14	1	1	3	0	3	1	1	827	22	854	18	926	29	827	22	89
Spot 37	443	126256	1	18	1	1	1	0	1	1	1	465	4	470	4	492	13	465	4	95
Spot 38	289	25655	2	18	1	1	1	0	1	1	1	460	4	463	4	481	17	460	4	96
Spot 39	295	24592	1	17	1	1	1	0	1	1	1	485	5	495	5	541	14	485	5	90
Spot 4	684	5336203	1	18	1	1	1	0	1	1	1	479	4	480	4	485	13	479	4	99
Spot 40	791	76354	4	16	1	1	1	0	1	1	1	635	5	634	5	634	12	635	5	100
Spot 41	366	7181	3	6	1	7	1	0	1	1	1	1837	14	2131	10	2428	11	2428	11	76
Spot 42	243	18350	1	17	1	1	1	0	1	1	1	512	5	511	4	506	14	512	5	101
Spot 43	384	14731	9	16	1	1	2	0	2	1	1	562	8	583	9	666	30	562	8	84
Spot 44	469	168238	5	18	1	1	1	0	1	1	1	480	4	478	4	470	14	480	4	102
Spot 45	36	9040	1	15	2	1	2	0	1	1	1	783	8	785	12	790	38	783	8	99
Spot 46	131	41743	1	6	1	12	1	0	1	1	1	2538	19	2582	10	2616	9	2616	9	97
Spot 47	421	12904	2	13	1	2	1	0	1	1	1	979	8	1021	7	1114	14	1114	14	88
Spot 49	915	66780	3	17	1	1	1	0	1	1	1	506	7	526	6	613	12	506	7	83
Spot 50	270	60685	2	13	1	2	1	0	1	1	1	1099	10	1098	8	1096	12	1096	12	100
Spot 51	1001	40374	3	17	1	1	1	0	1	1	1	540	5	542	5	549	12	540	5	98
Spot 52	304	204687	2	6	1	12	1	0	1	1	1	2512	28	2567	14	2611	9	2611	9	96
Spot 53	752	53305	2	17	1	1	1	0	1	1	1	450	4	459	5	503	18	450	4	90
Spot 54	296	35333	1	18	1	1	2	0	1	1	1	473	6	472	6	465	19	473	6	102
Spot 55	796	246891	11	17	1	1	1	0	1	1	1	560	5	571	5	616	14	560	5	91
Spot 56	184	164537	2	13	1	2	1	0	1	1	1	1017	11	1025	10	1044	18	1044	18	97
Spot 57	375	18148	2	18	1	0	2	0	2	1	1	394	7	401	6	440	19	394	7	NA
Spot 58	481	28077	1	18	1	1	1	0	1	1	1	477	6	479	5	486	16	477	6	98
Spot 59	808	40718	2	14	1	2	1	0	1	1	1	1033	11	1023	8	1003	12	1003	12	103
Spot 6	131	15807	1	18	1	1	2	0	1	1	1	453	5	456	6	471	24	453	5	96
Spot 60	955	34388	3	17	1	0	1	0	1	1	1	381	3	400	4	511	15	381	3	NA
Spot 61	1424	46098	8	18	1	1	1	0	1	1	1	426	4	434	4	478	12	426	4	89
Spot 62	555	1571684	1	18	1	0	1	0	1	1	1	409	4	409	4	410	15	409	4	100
Spot 63	288	299354	2	18	1	1	1	0	1	1	1	472	5	473	5	479	16	472	5	98
Spot 64	45	19359	5	13	1	2	1	0	1	1	1	1048	10	1064	9	1097	19	1097	19	96
Spot 65	269	52404	2	14	1	2	1	0	1	1	1	972	8	982	7	1004	12	1004	12	97
Spot 67	643	55935	26	17	1	1	1	0	1	1	1	567	6	568	6	573	15	567	6	99
Spot 68	244	193313	2	14	1	2	1	0	1	1	1	978	9	990	7	1019	12	1019	12	96
Spot 69	229	15208	2	17	1	1	1	0	1	1	1	595	5	596	5	602	15	595	5	99
Spot 7	244	30461	2	18	1	1	1	0	1	1	1	462	4	461	4	458	16	462	4	101
Spot 70	833	49207	18	17	1	1	1	0	1	1	1	544	7	546	6	555	17	544	7	98
Spot 71	99	15647	3	17	1	1	1	0	1	1	1	578	6	579	7	585	24	578	6	99
Spot 72	1231	53613	28	16	1	1	1	0	1	1	1	666	7	670	6	684	12	666	7	97
Spot 73	1152	67563	4	15	1	1	2	0	2	1	1	517	9	564	9	760	17	517	9	68

Spot 74	781	37971	2	13	1	2	1	0	1	1	982	7	1003	6	1047	12	1047	12	94
Spot 75	596	50100	3	14	1	2	1	0	1	1	1031	10	1029	8	1026	13	1026	13	100
Spot 76	580	26296	1	17	1	1	2	0	1	1	602	8	603	7	607	16	602	8	99
Spot 77	1001	30989	1	17	1	1	1	0	1	1	577	5	583	5	606	12	577	5	95
Spot 78	197	32780	3	13	1	2	1	0	1	1	1009	11	1037	9	1096	15	1096	15	92
Spot 79	158	109139	1	13	1	2	1	0	1	1	1047	11	1057	9	1080	17	1080	17	97
Spot 8	855	103011	2	18	1	1	1	0	1	1	422	4	433	4	488	12	422	4	86
Spot 81	608	210368	8	11	1	3	1	0	1	1	1270	14	1308	10	1369	15	1369	15	93
Spot 82	380	217577	3	18	1	1	1	0	1	1	491	5	487	5	468	21	491	5	105
Spot 83	364	12903	2	18	1	1	1	0	1	1	473	5	466	5	431	19	473	5	110
Spot 84	738	57199	2	14	1	2	1	0	1	1	1033	11	1031	8	1025	13	1025	13	101
Spot 86	197	23872	3	13	1	2	1	0	1	1	1042	9	1047	8	1058	14	1058	14	98
Spot 9	334	27649	2	17	1	1	1	0	1	1	529	5	528	5	525	16	529	5	101

Table A2. CDH0923-5S U-Pb geochronologic analyses from Huaco (Tupe Formation sandstone from AH locality described in Chapter 5).

Analysis	U (ppm)	²⁰⁶ Pb	U/Th	²⁰⁶ Pb	1σ	²⁰⁷ Pb	1σ	²⁰⁶ Pb	1σ	Err.	²⁰⁶ Pb	1σ	²⁰⁷ Pb	1σ	²⁰⁶ Pb	1σ	Best age	1σ	Conc.
		²⁰⁴ Pb		²⁰⁷ Pb		(%)		²³⁵ U			(%)		²³⁸ U		(%)				
Spot 7	670	5986	1.3	16.239	0.9	0.3859	2.6	0.0455	2.5	0.93	286.7	6.9	331.4	7.5	658.7	20.3	286.7	6.9	NA
Spot 39	347	1307	1.1	10.988	9.1	0.6133	10	0.0489	4.3	0.42	307.7	12.8	485.7	38.7	1446	173.3	307.7	12.8	NA
Spot 23	157	7479	0.7	14.511	1	0.4697	4.6	0.0495	4.5	0.98	311.2	13.6	391	14.8	895.3	20.3	311.2	13.6	NA
Spot 54	886	3679	1.2	15.037	0.8	0.4696	1.9	0.0512	1.7	0.91	322.1	5.4	390.9	6.2	821.4	16.4	322.1	5.4	NA
Spot 82	475	8124	1.3	16.455	0.8	0.4308	1.6	0.0514	1.4	0.86	323.3	4.4	363.8	5	630.2	18.1	323.3	4.4	NA
Spot 1	376	46052	1.3	17.26	0.7	0.428	1.3	0.0536	1.2	0.85	336.6	3.8	361.8	4.1	526.4	15.4	336.6	3.8	NA
Spot 72	549	1429	1.4	11.909	3.7	0.6647	5.7	0.0574	4.3	0.75	360	15	517.5	23	1291	72.8	360	15	NA
Spot 56	617	6285	3.3	15.021	0.9	0.5439	2.5	0.0593	2.3	0.93	371.2	8.3	441	8.8	823.5	19	371.2	8.3	NA
Spot 37	680	78965	1.5	17.995	0.7	0.4577	1.1	0.0598	0.9	0.79	374.1	3.2	382.6	3.6	434.3	15.1	374.1	3.2	NA
Spot 21	341	39953	0.8	18.631	1.9	0.4453	3.9	0.0602	3.4	0.88	376.8	12.4	374	12.1	356.3	41.8	376.8	12.4	NA
Spot 6	207	20317	1.5	17.993	0.9	0.4942	1.5	0.0645	1.2	0.79	403	4.6	407.7	5	434.6	20.2	403	4.6	92.7
Spot 47	768	22436	1.4	15.604	1.3	0.6118	2.8	0.0693	2.5	0.89	431.7	10.5	484.7	10.8	743.6	26.5	431.7	10.5	58.1
Spot 66	186	272643	1.9	17.323	0.8	0.5733	1.4	0.0721	1.1	0.78	448.6	4.6	460.2	5	518.4	18.6	448.6	4.6	86.5
Spot 15	562	19632	1.5	17.19	0.8	0.5842	1.2	0.0729	0.9	0.75	453.4	4.1	467.2	4.7	535.3	18	453.4	4.1	84.7
Spot 17	3275	71575	2.6	18.24	2.7	0.5508	20.8	0.0729	20.6	0.99	453.6	90.2	445.5	75	404.1	60	453.6	90.2	112.2
Spot 86	264	11264	1.1	16.032	0.8	0.6285	1.3	0.0731	1	0.77	454.8	4.4	495.1	5.2	686.1	18.1	454.8	4.4	66.3
Spot 3	185	36698	1.4	17.425	0.6	0.5799	1.1	0.0733	0.9	0.83	456.1	4.1	464.4	4.1	505.6	13.6	456.1	4.1	90.2
Spot 65	114	15261	1.9	17.815	0.9	0.5762	1.4	0.0745	1	0.72	463.1	4.5	462	5.1	456.7	21	463.1	4.5	101.4
Spot 84	151	45157	2.7	17.636	0.7	0.5847	1.2	0.0748	0.9	0.79	465.1	4.1	467.5	4.4	479	15.9	465.1	4.1	97.1
Spot 5	207	105265	1.4	17.436	0.9	0.5928	1.3	0.075	0.9	0.73	466.2	4.1	472.7	4.7	504.2	18.9	466.2	4.1	92.5
Spot 36	253	51956	1.7	17.734	0.6	0.5876	1.3	0.0756	1.2	0.89	469.9	5.4	469.3	5.1	466.7	13.7	469.9	5.4	100.7
Spot 80	341	32656	0.9	17.666	0.9	0.5904	1.5	0.0757	1.2	0.81	470.3	5.6	471.1	5.7	475.2	19.7	470.3	5.6	99
Spot 33	129	5674	1	18.204	1.1	0.573	1.4	0.0757	0.8	0.62	470.3	3.8	460	5	408.5	23.6	470.3	3.8	115.1
Spot 46	196	45281	1.9	17.66	0.9	0.595	1.4	0.0762	1.2	0.8	473.6	5.3	474	5.5	476.1	19.1	473.6	5.3	99.5
Spot 9	235	22365	1.4	17.602	0.8	0.6023	1.3	0.0769	1	0.78	477.8	4.7	478.7	5	483.3	18	477.8	4.7	98.9
Spot 85	359	18500	5.5	17.684	0.7	0.6031	1	0.0774	0.8	0.75	480.5	3.6	479.2	4	473.1	15.4	480.5	3.6	101.6
Spot 12	352	22530	1	17.686	0.8	0.6073	1.5	0.0779	1.3	0.85	483.7	5.9	481.8	5.7	472.8	17.4	483.7	5.9	102.3
Spot 42	308	40837	8.9	17.624	0.7	0.6103	1.2	0.078	1	0.81	484.5	4.6	483.8	4.7	480.5	15.7	484.5	4.6	100.8
Spot 30	417	38318	4.8	17.427	0.5	0.6244	1.1	0.079	1	0.88	489.9	4.7	492.6	4.4	505.4	11.7	489.9	4.7	96.9
Spot 4	444	422399	2.4	17.126	0.6	0.6799	1.1	0.0845	0.9	0.81	522.8	4.3	526.7	4.4	543.5	13.5	522.8	4.3	96.2
Spot 83	331	28850	1.6	17.304	0.8	0.68	1.3	0.0854	1	0.8	528.1	5.3	526.7	5.3	520.8	16.9	528.1	5.3	101.4
Spot 78	88	4086	1.5	16.984	1.4	0.6987	1.8	0.0861	1.2	0.66	532.5	6.1	538	7.5	561.6	29.5	532.5	6.1	94.8
Spot 34	138	38227	2.7	17.128	0.9	0.7121	1.5	0.0885	1.2	0.8	546.6	6.4	546	6.5	543.3	20.3	546.6	6.4	100.6
Spot 63	643	26792	3.4	15.907	0.9	0.795	1.3	0.0918	0.9	0.72	565.9	5.1	594	5.9	702.8	19.3	565.9	5.1	80.5
Spot 40	320	30869	2.7	16.592	0.6	0.8294	1.3	0.0999	1.2	0.91	613.6	7.1	613.3	6.1	612.3	12	613.6	7.1	100.2
Spot 68	292	46331	3.5	15.526	0.9	0.9506	1.5	0.1071	1.1	0.78	655.8	7.1	678.4	7.2	754.2	19.2	655.8	7.1	87
Spot 59	421	296156	3.2	14.669	1.5	1.0912	1.9	0.1161	1.2	0.65	708.3	8.4	749.1	10.2	872.9	30.2	708.3	8.4	81.1
Spot 11	244	21805	1.5	14.617	2.4	1.0977	2.9	0.1164	1.6	0.56	709.9	10.9	752.3	15.4	880.2	49.9	709.9	10.9	80.7
Spot 38	577	26093	1.9	15.065	0.6	1.1231	1.2	0.1228	1	0.86	746.5	7.3	764.5	6.5	817.5	12.6	746.5	7.3	91.3
Spot 61	529	55155	2.3	13.883	0.7	1.5949	1.1	0.1607	0.9	0.8	960.4	8.2	968.2	7.1	986	13.8	986	13.8	97.4
Spot 67	465	34768	5.2	13.84	0.8	1.3558	1.4	0.1362	1.2	0.82	822.9	8.9	870.1	8.3	992.2	16.5	992.2	16.5	82.9
Spot 32	217	30873	4.6	13.768	0.7	1.6497	1.3	0.1648	1.1	0.87	983.4	10.4	989.4	8.3	1002.8	13.3	1002.8	13.3	98.1
Spot 25	187	35462	5	13.737	0.7	1.5922	1.2	0.1587	0.9	0.81	949.5	8.3	967.1	7.3	1007.4	14	1007.4	14	94.3
Spot 62	320	70839	4.4	13.542	0.6	1.7764	1.4	0.1745	1.2	0.88	1037.1	11.5	1036.8	8.9	1036.4	13.1	1036.4	13.1	100.1
Spot 53	633	98901	3.4	13.435	0.5	1.7988	1.1	0.1753	1	0.87	1041.5	9.4	1045	7.3	1052.4	11	1052.4	11	99
Spot 71	122	39114	1.9	13.423	0.7	1.7814	1.2	0.1735	1	0.83	1031.4	9.2	1038.7	7.6	1054.1	13.1	1054.1	13.1	97.8
Spot 22	132	81604	2.8	13.422	0.7	1.8131	1.4	0.1766	1.3	0.88	1048.2	12.2	1050.2	9.4	1054.3	13.9	1054.3	13.9	99.4
Spot 79	104	37500	2.4	13.307	0.8	1.7868	1.2	0.1725	0.9	0.75	1026	8.4	1040.7	7.7	1071.6	15.6	1071.6	15.6	95.7
Spot 31	520	15378	0.9	13.261	0.8	1.2423	4.4	0.1195	4.3	0.98	727.9	29.9	819.9	24.8	1078.6	15.7	1078.6	15.7	67.5
Spot 29	67	7266	2.7	13.188	1	1.9361	1.4	0.1853	1	0.71	1095.7	9.7	1093.7	9.1	1089.5	19.2	1089.5	19.2	100.6
Spot 45	269	154124	2.8	13.145	0.6	1.6426	1.4	0.1567	1.3	0.91	938.2	11.2	986.7	8.9	1096.2	11.8	1096.2	11.8	85.6
Spot 10	1125	442737	5.7	13.13	0.5	1.8598	0.9	0.1772	0.8	0.82	1051.6	7.5	1066.9	6.2	1098.4	10.9	1098.4	10.9	95.7
Spot 74	42	7045	0.8	13.072	0.9	1.9258	1.2	0.1827	0.8	0.65	1081.5	8.1	1090.1	8.3	1107.3	18.8	1107.3	18.8	97.7
Spot 75	909	6087	1.3	12.99	1.6	1.2502	3.2	0.1178	2.7	0.86	718.1	18.6	823.5	17.9	1119.8	31.7	1119.8	31.7	64.1
Spot 48	1169	6709	2.2	12.748	0.7	1.3091	1.4	0.1211	1.2	0.86	736.8	8.3	849.7	8	1157.3	13.9	1157.3	13.9	63.7

Spot 44	113	32983	1.5	12.743	0.6	2.0409	1.2	0.1887	1	0.84	1114.4	10.2	1129.3	8	1158	12.6	1158	12.6	96.2
Spot 81	109	67195	3.4	12.703	0.6	2.1622	1.1	0.1993	0.9	0.81	1171.5	9.5	1169	7.6	1164.3	12.7	1164.3	12.7	100.6
Spot 2	521	5708	3.7	12.646	1.2	1.4858	3.2	0.1363	3	0.93	823.9	23.3	924.6	19.6	1173.1	23.2	1173.1	23.2	70.2
Spot 50	314	34550	1	12.59	0.7	2.1644	1.4	0.1977	1.3	0.87	1163	13.4	1169.7	10	1182	14.1	1182	14.1	98.4
Spot 64	816	20485	2.3	12.529	0.7	2.0256	1.2	0.1841	0.9	0.81	1089.6	9.4	1124.1	7.8	1191.6	13.4	1191.6	13.4	91.4
Spot 70	258	118594	2.6	12.515	0.6	2.0329	1.6	0.1846	1.4	0.92	1092.1	14.5	1126.6	10.7	1193.7	12	1193.7	12	91.5
Spot 73	257	3112170	2.8	12.281	0.6	2.3793	1.1	0.212	0.9	0.83	1239.5	10.7	1236.4	8.1	1231	12.3	1231	12.3	100.7
Spot 58	354	199563	3.5	12.253	0.6	2.3741	1.1	0.2111	1	0.87	1234.5	11.2	1234.8	8.1	1235.4	10.8	1235.4	10.8	99.9
Spot 14	90	39550	2.1	12.227	0.5	2.3277	1	0.2065	0.8	0.82	1210.1	8.6	1220.8	6.8	1239.6	10.7	1239.6	10.7	97.6
Spot 24	342	678584	4	11.944	0.4	2.5173	1.1	0.2182	1	0.92	1272.2	11.4	1277	7.8	1285.3	8.2	1285.3	8.2	99
Spot 49	269	56124	2.6	11.844	0.8	2.2777	1.7	0.1957	1.5	0.88	1152.4	15.7	1205.4	12	1301.7	15.8	1301.7	15.8	88.5
Spot 20	41	13758	1.3	11.69	0.9	2.7033	1.5	0.2293	1.2	0.8	1330.8	14.7	1329.4	11.4	1327	17.8	1327	17.8	100.3
Spot 35	88	8865	1.8	11.438	1.2	2.163	1.7	0.1795	1.2	0.72	1064.4	12.1	1169.2	11.9	1369	22.7	1369	22.7	77.7
Spot 60	227	12212	2.7	10.584	1	2.3669	2.3	0.1818	2.1	0.91	1076.7	20.8	1232.7	16.5	1516.9	18.3	1516.9	18.3	71
Spot 41	198	79539	1.1	9.2038	0.6	4.7438	1.2	0.3168	1.1	0.87	1774	16.7	1775	10.4	1776.1	11	1776.1	11	99.9
Spot 28	300	56261	1.3	8.8517	0.6	4.9707	1.1	0.3192	1	0.87	1786.1	15.5	1814.3	9.7	1847	10.2	1847	10.2	96.7
Spot 69	46	17618	1	4.229	0.8	20.454	1.4	0.6276	1.2	0.82	3140.2	29.1	3113.1	13.8	3095.6	12.9	3095.6	12.9	101.4

Table A3. CDH0923-35S U-Pb geochronologic analyses from Huaco (Patquia Formation sandstone from AH locality described in Chapter 5).

Analysis	U (ppm)	^{206}Pb		U/Th	^{206}Pb		1σ	^{207}Pb		1σ	^{206}Pb		1σ	^{207}Pb		1σ	^{206}Pb		1σ	Best age	1σ	Conc.
		^{204}Pb	^{204}Pb		^{207}Pb	(%)		^{235}U	(%)		^{238}U	(%)		corr.	^{238}U		(Ma)	^{235}U				
Spot 65	569	100811	2.4	18.8278	1.1	0.3547	2.2	0.0485	1.9	0.87	305	5.8	308.2	5.9	332.6	25.2	305	5.8	99			
Spot 22	273	29032	5.2	19.2655	1.4	0.3468	2.2	0.0485	1.7	0.77	305.2	5.1	302.3	5.9	280.3	33	305.2	5.1	100.9			
Spot 95	201	56035	1.7	18.5262	1	0.3688	1.9	0.0496	1.6	0.84	311.9	4.9	318.7	5.3	369.1	23.6	311.9	4.9	97.8			
Spot 35	546	48845	2.6	18.4689	0.9	0.4367	2	0.0585	1.8	0.9	366.6	6.5	367.9	6.3	376.1	20	366.6	6.5	99.6			
Spot 149	75	4369	2.1	19.3732	3.7	0.4164	3.9	0.0585	1.4	0.36	366.7	5	353.5	11.7	267.5	84	366.7	5	103.7			
Spot 79	348	10667	1.7	18.9215	1.2	0.4374	2.2	0.0601	1.8	0.85	376	6.7	368.4	6.7	321.4	26.2	376	6.7	102			
Spot 147	481	3361	2	15.065	1.9	0.5561	2.7	0.0608	2	0.71	380.4	7.2	449	9.9	817.5	40	380.4	7.2	84.7			
Spot 51	649	15776	1.3	16.8999	1	0.5124	1.6	0.0628	1.3	0.81	392.8	5.1	420.1	5.7	572.5	21.1	392.8	5.1	93.5			
Spot 40	580	9311	1.4	16.8287	1.2	0.5312	2.2	0.0649	1.8	0.83	405.2	7.1	432.6	7.6	581.6	25.9	405.2	7.1	69.7			
Spot 28	527	44054	1.4	18.3339	1	0.4924	1.6	0.0655	1.2	0.78	409	4.9	406.5	5.3	392.6	22.1	409	4.9	104.2			
Spot 162	459	5642	1.1	15.2936	1.7	0.6021	2.5	0.0668	1.9	0.75	416.9	7.6	478.6	9.5	785.9	34.7	416.9	7.6	53.1			
Spot 33	730	9707	1.5	16.1651	1.2	0.5784	2	0.0678	1.5	0.78	423.1	6.3	463.4	7.3	668.4	26.2	423.1	6.3	63.3			
Spot 167	459	3883	3.7	15.1751	1.3	0.6161	2.2	0.0678	1.7	0.81	423.1	7.1	487.4	8.3	802.2	26.7	423.1	7.1	52.7			
Spot 173	597	19780	2	16.9423	1	0.5623	2.1	0.0691	1.8	0.86	430.9	7.4	453	7.5	567	22.8	430.9	7.4	76			
Spot 61	517	6016	1.7	15.5321	3.3	0.6177	3.8	0.0696	1.9	0.51	433.8	8.1	488.4	14.8	753.3	69.3	433.8	8.1	57.6			
Spot 133	78	4439	1.5	18.2919	1.6	0.5342	2.5	0.0709	1.8	0.74	441.6	7.8	434.6	8.7	397.7	36.8	441.6	7.8	111			
Spot 122	501	10156	1.5	16.023	1.5	0.6198	2.3	0.0721	1.7	0.74	448.5	7.3	489.7	8.8	687.3	32.4	448.5	7.3	65.3			
Spot 63	174	8157	2	17.8321	1.3	0.5595	1.8	0.0724	1.2	0.66	450.5	5.2	451.2	6.5	454.5	29.8	450.5	5.2	99.1			
Spot 184	625	23531	45.2	17.4798	1.1	0.5729	2	0.0727	1.6	0.82	452.1	7	459.9	7.3	498.6	25	452.1	7	90.7			
Spot 15	186	13072	29.8	17.757	1	0.5639	1.6	0.0727	1.3	0.79	452.2	5.7	454.1	6	463.9	22.3	452.2	5.7	97.5			
Spot 159	68	3825	1.4	18.2626	1.5	0.5515	2.1	0.0731	1.5	0.7	454.7	6.5	446	7.6	401.3	34	454.7	6.5	113.3			
Spot 190	426	40318	1.4	17.5477	1.1	0.574	2	0.0731	1.6	0.83	454.7	7.1	460.6	7.3	490.1	24.3	454.7	7.1	92.8			
Spot 166	188	52975	20.2	17.377	1.1	0.58	1.8	0.0731	1.4	0.79	455	6.2	464.5	6.7	511.6	24.3	455	6.2	88.9			
Spot 158	272	32452	0.8	17.7051	0.9	0.5703	1.9	0.0733	1.6	0.86	455.8	7.1	458.2	6.9	470.4	20.7	455.8	7.1	96.9			
Spot 164	269	10570	2.5	18.0402	1.6	0.5599	2.2	0.0733	1.5	0.69	455.9	6.7	451.4	8	428.7	35.5	455.9	6.7	106.4			
Spot 54	183	8778	0.7	17.8845	1.1	0.5662	1.7	0.0735	1.4	0.79	457	6.1	455.5	6.4	448	23.7	457	6.1	102			
Spot 38	357	240979	1.3	17.381	1	0.5847	1.7	0.0737	1.3	0.79	458.6	5.9	467.5	6.3	511.1	22.5	458.6	5.9	89.7			
Spot 8	202	26001	1.8	17.4798	1.1	0.5814	1.7	0.0737	1.3	0.77	458.7	5.7	465.4	6.2	498.6	23.5	458.7	5.7	92			
Spot 81	166	5064	1.4	17.0345	1.6	0.5983	2.2	0.0739	1.4	0.66	459.9	6.4	476.1	8.3	555.2	35.7	459.9	6.4	82.8			
Spot 103	291	5507	1.5	17.1484	1.1	0.5956	1.8	0.0741	1.4	0.78	460.9	6.2	474.4	6.8	540.6	24.6	460.9	6.2	85.2			
Spot 77	447	31649	1.2	17.7482	1.2	0.5758	2	0.0742	1.6	0.81	461.1	7.2	461.8	7.4	465	26.1	461.1	7.2	99.2			
Spot 50	508	21205	31.2	17.5484	1	0.5825	2.1	0.0742	1.9	0.88	461.2	8.3	466	7.9	490	22	461.2	8.3	94.1			
Spot 128	321	36130	1.6	17.2983	1	0.5917	1.9	0.0743	1.6	0.84	461.8	7	471.9	7.1	521.6	22.5	461.8	7	88.5			
Spot 160	212	53435	6.5	17.6801	1.2	0.579	1.8	0.0743	1.3	0.76	461.9	5.9	463.8	6.6	473.5	25.6	461.9	5.9	97.5			
Spot 194	67	14115	1.3	17.8096	1.3	0.5749	1.9	0.0743	1.4	0.75	462	6.3	461.2	7	457.3	27.9	462	6.3	101			
Spot 146	641	45893	195.8	17.7577	0.9	0.577	1.8	0.0744	1.5	0.85	462.3	6.9	462.6	6.7	463.8	20.8	462.3	6.9	99.7			
Spot 169	383	12916	1.3	17.2176	1.2	0.5969	2	0.0746	1.6	0.8	463.6	7.1	475.3	7.6	531.9	26.4	463.6	7.1	87.2			
Spot 64	321	6857	1.8	17.0417	1.2	0.6038	1.9	0.0747	1.6	0.8	464.2	7	479.7	7.4	554.3	25.2	464.2	7	83.7			
Spot 39	217	20937	15.1	17.0215	1.3	0.6055	1.8	0.0748	1.4	0.73	464.9	6.1	480.7	7.1	556.9	27.3	464.9	6.1	83.5			
Spot 76	244	13455	2.9	17.975	0.9	0.5738	1.7	0.0748	1.5	0.85	465.2	6.5	460.5	6.3	436.8	20.3	465.2	6.5	106.5			
Spot 129	545	30905	2.6	17.8458	0.9	0.5783	2.1	0.0749	1.9	0.91	465.5	8.6	463.4	7.8	452.8	19.3	465.5	8.6	102.8			
Spot 100	61	10613	1.5	18.0728	1.7	0.5714	2.3	0.0749	1.6	0.68	465.8	7	458.9	8.4	424.7	37.2	465.8	7	109.7			
Spot 136	439	40872	3.9	17.7818	1	0.5814	2.1	0.075	1.8	0.88	466.3	8.2	465.4	7.7	460.8	21.3	466.3	8.2	101.2			
Spot 44	288	18273	2.9	17.7701	1	0.5827	1.7	0.0751	1.3	0.79	467	6	466.2	6.3	462.3	22.7	467	6	101			
Spot 85	284	35010	2.5	17.5987	1.2	0.5886	1.8	0.0752	1.4	0.78	467.2	6.5	470	7	483.7	25.7	467.2	6.5	96.6			
Spot 97	185	9177	2.2	18.1457	1	0.5709	1.8	0.0752	1.5	0.85	467.2	7	458.6	6.7	415.7	21.6	467.2	7	112.4			
Spot 115	310	31602	2.2	17.8766	1	0.5797	1.8	0.0752	1.4	0.82	467.4	6.5	464.3	6.5	449	22.5	467.4	6.5	104.1			
Spot 42	292	29661	3.1	17.4061	1.2	0.5955	1.8	0.0752	1.4	0.76	467.5	6.2	474.4	6.9	507.9	25.8	467.5	6.2	92			
Spot 163	226	67158	1.7	17.8434	1	0.5809	1.7	0.0752	1.4	0.81	467.5	6.2	465.1	6.3	453.1	21.9	467.5	6.2	103.2			
Spot 60	110	36748	1.1	17.7667	1.2	0.5839	1.7	0.0753	1.3	0.74	467.9	5.8	467	6.5	462.7	25.9	467.9	5.8	101.1			
Spot 80	699	90475	1.5	17.6115	0.9	0.5892	1.6	0.0753	1.3	0.82	468	6	470.4	6	482.1	20	468	6	97.1			
Spot 37	396	40851	1.5	17.6823	1	0.5871	1.8	0.0753	1.4	0.8	468.1	6.4	469	6.6	473.2	23	468.1	6.4	98.9			
Spot 150	244	34318	2.3	17.8671	1.1	0.5823	2	0.0755	1.7	0.85	469.1	7.7	465.9	7.5	450.1	23.7	469.1	7.7	104.2			
Spot 181	201	61301	3.7	17.9584	1.1	0.5794	2	0.0755	1.7	0.84	469.2	7.7	464.1	7.5	438.8	24.5	469.2	7.7	106.9			
Spot 127	245	74833	2.3	17.7743	1	0.5856	1.7	0.0755	1.3	0.78	469.3	6	468	6.3	461.7	23.2	469.3	6	101.7			
Spot 89	174	4078	1.4	17.3806	1.1	0.5989	1.7	0.0755	1.2	0.75	469.4	5.6	476.5	6.3	511.2	23.8	469.4	5.6	91.8			
Spot 84	218	26284	1.8	17.8385	1	0.5836	1.6	0.0755	1.3	0.8	469.4	5.9	466.8	6.2	453.7	22.2	469.4	5.9	103.5			

Spot 53	536	19162	3.9	17.5938	1.2	0.5917	2.3	0.0755	1.9	0.85	469.4	8.7	472	8.5	484.3	26.1	469.4	8.7	96.9
Spot 108	604	28325	2.3	17.211	1.1	0.6059	2.1	0.0757	1.8	0.85	470.2	8.1	481	8	532.7	23.9	470.2	8.1	88.3
Spot 117	106	11972	1	17.6725	1.4	0.5911	2	0.0758	1.4	0.72	471	6.5	471.6	7.5	474.4	30.2	471	6.5	99.3
Spot 24	227	21675	1.8	17.803	1.1	0.5875	1.5	0.0759	1	0.66	471.5	4.3	469.3	5.5	458.1	24.4	471.5	4.3	102.9
Spot 3	248	259516	1.3	17.4491	1.1	0.6	1.8	0.076	1.4	0.79	472	6.4	477.3	6.8	502.5	23.8	472	6.4	93.9
Spot 94	126	1944	2.5	15.1461	5.1	0.6914	5.7	0.076	2.5	0.43	472.1	11.2	533.6	23.6	806.2	107.1	472.1	11.2	58.6
Spot 20	481	36547	2.2	17.6774	1	0.5924	1.8	0.076	1.5	0.83	472.1	6.8	472.4	6.9	473.8	22.7	472.1	6.8	99.6
Spot 18	257	37821	1.6	17.2152	1	0.6086	1.8	0.076	1.6	0.86	472.3	7.2	482.7	7.1	532.2	20.9	472.3	7.2	88.8
Spot 105	150	30448	1.2	17.1853	1.3	0.6104	2	0.0761	1.6	0.79	472.9	7.3	483.8	7.8	536	27.5	472.9	7.3	88.2
Spot 68	151	8784	1.8	17.7608	1.1	0.591	1.7	0.0762	1.3	0.77	473.2	6.1	471.5	6.5	463.4	24.8	473.2	6.1	102.1
Spot 177	178	38102	2.4	17.6885	1.2	0.5936	1.8	0.0762	1.4	0.77	473.3	6.4	473.1	6.9	472.5	25.9	473.3	6.4	100.2
Spot 175	349	130482	5.6	17.4272	1.2	0.6025	1.8	0.0762	1.4	0.77	473.3	6.2	478.8	6.8	505.3	25.8	473.3	6.2	93.7
Spot 134	847	36106	1.8	17.7116	1.1	0.593	1.8	0.0762	1.4	0.8	473.4	6.4	472.8	6.7	469.5	23.5	473.4	6.4	100.8
Spot 41	130	91976	1.9	17.5919	1.1	0.5974	1.8	0.0763	1.3	0.76	473.7	6.1	475.6	6.7	484.5	25.2	473.7	6.1	97.8
Spot 113	240	13105	1	17.9757	1.5	0.586	2.4	0.0764	1.8	0.78	474.8	8.4	468.3	8.8	436.7	32.8	474.8	8.4	108.7
Spot 75	213	875505	1.8	17.5324	0.9	0.6009	1.8	0.0764	1.6	0.86	474.9	7.3	477.8	7	492	20.7	474.9	7.3	96.5
Spot 107	205	12733	2.3	17.935	1.5	0.5879	2.3	0.0765	1.7	0.75	475.2	7.8	469.5	8.5	441.7	33.2	475.2	7.8	107.6
Spot 27	122	32262	3	17.8847	1.2	0.5899	1.8	0.0766	1.4	0.76	475.5	6.3	470.8	6.9	448	26.5	475.5	6.3	106.2
Spot 88	817	32329	3.2	17.7161	1	0.5957	2.3	0.0766	2.1	0.89	475.6	9.4	474.5	8.8	469	23.1	475.6	9.4	101.4
Spot 172	198	10777	1.6	17.8204	1.4	0.5922	2.1	0.0766	1.6	0.74	475.7	7.1	472.3	8	456	31.6	475.7	7.1	104.3
Spot 111	305	40141	1.1	17.7895	1	0.5959	1.7	0.0769	1.3	0.81	477.7	6.2	474.6	6.3	459.8	21.4	477.7	6.2	103.9
Spot 47	139	94709	1.7	17.1939	1.1	0.6168	1.6	0.077	1.1	0.69	477.9	4.9	487.9	6	534.8	24.7	477.9	4.9	89.4
Spot 21	177	145664	1.4	17.9132	1.3	0.5923	1.8	0.077	1.3	0.71	478.1	5.8	472.3	6.8	444.4	28.2	478.1	5.8	107.6
Spot 142	247	50045	1.6	16.1666	1.5	0.6565	2	0.077	1.3	0.66	478.2	6.2	512.4	8.2	668.2	32.8	478.2	6.2	71.6
Spot 14	144	383416	2.9	17.5318	0.9	0.6069	1.8	0.0772	1.6	0.87	479.4	7.3	481.6	7	492.1	19.4	479.4	7.3	97.4
Spot 57	393	35444	1.2	17.5449	1.1	0.6076	2.2	0.0774	1.9	0.85	480.3	8.6	482.1	8.4	490.4	25	480.3	8.6	97.9
Spot 139	372	23654	1.3	17.5973	1.1	0.6063	1.7	0.0774	1.3	0.75	480.7	5.9	481.2	6.5	483.9	25.1	480.7	5.9	99.3
Spot 11	252	20633	0.9	17.7792	1.1	0.6012	1.7	0.0776	1.4	0.79	481.5	6.3	478	6.6	461.1	23.8	481.5	6.3	104.4
Spot 31	138	31837	1.9	17.4678	1.1	0.6143	1.7	0.0779	1.3	0.77	483.3	5.9	486.3	6.4	500.2	23.3	483.3	5.9	96.6
Spot 189	100	2653026	2.1	17.4574	1.1	0.6147	2	0.0779	1.7	0.83	483.3	7.8	486.5	7.8	501.5	24.9	483.3	7.8	96.4
Spot 32	216	15577	1.6	17.9217	1.1	0.6001	1.6	0.078	1.2	0.72	484.4	5.4	477.3	6.1	443.4	24.7	484.4	5.4	109.3
Spot 165	373	14336	2.6	17.8438	1.2	0.6039	1.8	0.0782	1.4	0.76	485.3	6.4	479.7	6.9	453	26	485.3	6.4	107.1
Spot 154	239	3228164	2.4	17.3825	1	0.62	1.5	0.0782	1.2	0.76	485.4	5.5	489.9	6	510.9	22.1	485.4	5.5	95
Spot 4	402	50148	2.5	17.9343	1.1	0.6013	2	0.0782	1.7	0.85	485.6	8.1	478	7.7	441.8	23.9	485.6	8.1	109.9
Spot 74	866	6739	3.4	15.0797	1.4	0.7162	2.5	0.0784	2.1	0.84	486.4	10	548.4	10.8	815.4	29.1	486.4	10	59.6
Spot 120	124	36939	1.6	17.2838	1.1	0.6268	1.7	0.0786	1.4	0.78	487.8	6.4	494.1	6.8	523.4	23.7	487.8	6.4	93.2
Spot 121	121	11411	1.1	18.0942	1.3	0.5989	2.2	0.0786	1.7	0.79	487.9	8.2	476.5	8.4	422	29.9	487.9	8.2	115.6
Spot 36	250	39203	1.3	17.5305	1.1	0.6187	1.7	0.0787	1.3	0.78	488.3	6.3	489	6.6	492.3	23.5	488.3	6.3	99.2
Spot 67	467	67914	10	17.2301	1.2	0.6298	2.2	0.0787	1.9	0.85	488.6	8.9	496	8.7	530.3	25.2	488.6	8.9	92.1
Spot 29	397	15306	5.6	17.3231	1.1	0.6358	2.1	0.0799	1.8	0.86	495.6	8.5	499.7	8.2	518.4	23.4	495.6	8.5	95.6
Spot 116	201	35747	1.8	17.4501	1	0.6494	2	0.0822	1.7	0.86	509.4	8.2	508.1	7.8	502.4	21.9	509.4	8.2	101.4
Spot 78	144	32710	1.6	17.2339	1.1	0.658	1.9	0.0823	1.5	0.82	509.8	7.5	513.4	7.5	529.8	23.7	509.8	7.5	96.2
Spot 196	136	34901	3.1	17.129	1.1	0.6701	1.7	0.0833	1.2	0.72	515.7	5.9	520.8	6.7	543.1	25.1	515.7	5.9	94.9
Spot 10	525	33874	2.6	16.5852	1	0.6929	2	0.0834	1.8	0.87	516.3	8.8	534.5	8.5	613.2	21.8	516.3	8.8	84.2
Spot 144	62	12520	1.1	17.7479	1.2	0.6525	1.7	0.084	1.2	0.73	520.1	6.2	510	6.8	465	25.7	520.1	6.2	111.8
Spot 125	201	9124	3.3	17.3954	1.7	0.6691	2.2	0.0844	1.5	0.68	522.6	7.7	520.1	9.2	509.3	36.4	522.6	7.7	102.6
Spot 19	229	93126	2.4	17.3012	0.9	0.6753	2	0.0848	1.7	0.87	524.5	8.6	523.9	8	521.2	20.8	524.5	8.6	100.6
Spot 16	672	22518	2.3	17.3897	1.2	0.6775	1.9	0.0855	1.5	0.79	528.8	7.8	525.3	8	510	25.9	528.8	7.8	103.7
Spot 71	244	316688	4.7	17.3558	1.2	0.6792	2	0.0855	1.5	0.79	529.1	7.8	526.3	8	514.3	26.4	529.1	7.8	102.9
Spot 145	332	40171	1.7	17.0063	1.2	0.696	1.8	0.0859	1.4	0.75	531.2	7.1	536.4	7.7	558.8	26.5	531.2	7.1	95
Spot 91	323	16011	2.4	17.0573	1.3	0.6966	2.1	0.0862	1.7	0.79	533.1	8.6	536.8	8.8	552.3	28.1	533.1	8.6	96.5
Spot 49	247	20859	17.5	16.5931	0.9	0.7343	1.6	0.0884	1.3	0.82	546.1	7.1	559.1	7	612.2	20	546.1	7.1	89.2
Spot 135	211	30683	2.2	17.6631	1	0.6903	1.9	0.0885	1.6	0.85	546.5	8.6	533	7.9	475.6	22	546.5	8.6	114.9
Spot 143	284	45258	2.5	17.1456	1.1	0.7143	2	0.0889	1.7	0.83	548.8	8.8	547.3	8.5	541	24.5	548.8	8.8	101.4
Spot 99	496	14326	7.5	15.5362	1.3	0.7998	2	0.0902	1.5	0.77	556.5	8.2	596.7	9	752.7	26.8	556.5	8.2	73.9
Spot 131	501	49722	3.4	16.7686	0.9	0.7435	2.3	0.0905	2.1	0.93	558.3	11.4	564.5	10	589.4	18.8	558.3	11.4	94.7
Spot 90	1045	30133	5.8	16.6261	1.1	0.7607	2	0.0918	1.7	0.82	566	9	574.4	8.8	607.9	24.7	566	9	93.1
Spot 151	242	27036	3.1	17.0753	1	0.7417	1.6	0.0919	1.2	0.78	566.7	6.7	563.4	6.9	550	21.5	566.7	6.7	103
Spot 2	430	55585	9	16.9097	1	0.7547	2.1	0.0926	1.8	0.87	570.9	9.8	570.9	9	571.2	22.2	570.9	9.8	99.9
Spot 59	616	12752	1.4	15.7881	1	0.8193	1.7	0.0939	1.3	0.81	578.3	7.4	607.6	7.6	718.7	20.9	578.3	7.4	80.5

Spot 119	228	13535	2.7	16.9731	1.1	0.7725	1.6	0.0951	1.2	0.75	585.9	6.8	581.2	7.2	563	23.6	585.9	6.8	104.1
Spot 62	47	3263	1.5	14.6568	5.9	0.9001	6.3	0.0957	2	0.32	589.3	11.4	651.8	30.2	874.6	123	589.3	11.4	67.4
Spot 26	187	21828	1.1	16.3767	0.9	0.8369	1.8	0.0994	1.5	0.86	611.1	8.9	617.4	8.2	640.5	19.5	611.1	8.9	95.4
Spot 114	357	345942	29.3	15.3736	1.6	0.9067	1.9	0.1011	1.1	0.57	621.1	6.4	655.3	9.1	774.9	32.7	621.1	6.4	80.2
Spot 25	1221	222407	4.6	16.179	0.8	0.8727	1.5	0.1024	1.3	0.86	628.7	7.9	637	7.3	666.6	17.2	628.7	7.9	94.3
Spot 104	288	22308	6.1	16.4881	1.2	0.8728	1.9	0.1044	1.5	0.79	640.3	9.3	637.1	9.1	625.9	25.1	640.3	9.3	102.3
Spot 83	580	121102	14.3	16.4415	1	0.8903	1.9	0.1062	1.6	0.86	650.7	10	646.5	9	632	20.8	650.7	10	103
Spot 183	221	46229	12.2	14.5933	1.8	1.0945	4.1	0.1159	3.7	0.9	706.9	24.9	750.7	21.9	883.6	36.8	706.9	24.9	80
Spot 23	277	733790	2.5	15.1247	0.8	1.0868	1.7	0.1193	1.5	0.87	726.4	10.3	747	9.1	809.1	17.8	726.4	10.3	89.8
Spot 198	236	30057	3.9	14.4194	0.9	1.1912	1.8	0.1246	1.6	0.86	757.2	11.1	796.5	10	908.3	19	757.2	11.1	83.4
Spot 1	196	9143	10.2	14.0485	1.2	1.2491	1.9	0.1273	1.5	0.76	772.6	10.6	823	10.7	961.8	25.1	772.6	10.6	80.3
Spot 157	297	132903	8.8	14.1846	0.9	1.2642	1.6	0.1301	1.3	0.82	788.5	9.8	829.8	9.1	942	19	788.5	9.8	83.7
Spot 141	196	63034	12.5	14.4505	1	1.3042	1.6	0.1367	1.3	0.79	826.2	9.7	847.6	9.1	903.8	19.9	826.2	9.7	91.4
Spot 130	537	222705	5	14.4198	1.1	1.317	2	0.1378	1.7	0.84	832.2	13.1	853.2	11.5	908.2	22.6	832.2	13.1	91.6
Spot 109	74	11563	1.1	14.4348	1.3	1.5069	1.9	0.1578	1.4	0.73	944.7	12.4	933.2	11.8	906.1	27.2	906.1	27.2	104.3
Spot 87	125	16086	5.4	14.2781	1.6	1.4265	2.3	0.1478	1.6	0.7	888.5	13.3	900.1	13.6	928.6	33.6	928.6	33.6	95.7
Spot 124	291	136779	5.5	14.2579	0.9	1.5523	1.8	0.1606	1.6	0.86	960.1	14	951.4	11.3	931.5	19.4	931.5	19.4	103.1
Spot 187	58	8902	1.6	14.1957	1.2	1.5117	1.7	0.1557	1.2	0.7	932.9	10.5	935.1	10.4	940.4	24.9	940.4	24.9	99.2
Spot 153	450	399753	4.4	13.905	1	1.5762	1.7	0.159	1.4	0.81	951.4	12.5	960.9	10.8	982.7	20.6	982.7	20.6	96.8
Spot 185	200	106438	2.5	13.7768	1	1.5683	1.9	0.1568	1.7	0.85	938.8	14.5	957.7	12.1	1001.5	20.7	1001.5	20.7	93.7
Spot 106	542	62528	4.8	13.6056	0.9	1.5424	1.6	0.1523	1.3	0.81	913.7	11.1	947.5	9.9	1026.8	19.2	1026.8	19.2	89
Spot 182	431	67530	2.5	13.5799	0.8	1.7219	1.9	0.1697	1.7	0.9	1010.3	15.8	1016.7	12.1	1030.7	16.5	1030.7	16.5	98
Spot 7	449	31964	3.4	13.5702	1	1.7934	2	0.1766	1.7	0.86	1048.3	16.7	1043.1	13.1	1032.1	21	1032.1	21	101.6
Spot 17	226	909905	0.8	13.5441	1.1	1.7733	1.7	0.1743	1.3	0.76	1035.6	12.6	1035.7	11.2	1036	22.4	1036	22.4	100
Spot 180	174	38508	3.4	13.504	0.8	1.711	1.6	0.1677	1.4	0.86	999.2	12.9	1012.7	10.4	1042	16.7	1042	16.7	95.9
Spot 178	489	74076	3.3	13.4828	1.1	1.7643	1.9	0.1726	1.5	0.81	1026.4	14.2	1032.4	12	1045.2	22.2	1045.2	22.2	98.2
Spot 140	223	28619	2.2	13.4803	1	1.6689	1.7	0.1632	1.3	0.8	974.7	12.1	996.8	10.5	1045.6	19.9	1045.6	19.9	93.2
Spot 197	313	1282713	3.5	13.4545	0.9	1.5341	1.9	0.1498	1.7	0.88	899.7	14.4	944.2	11.9	1049.4	18.2	1049.4	18.2	85.7
Spot 191	373	47454	5.2	13.446	0.9	1.7121	2	0.167	1.8	0.9	995.8	17	1013.1	13	1050.7	17.5	1050.7	17.5	94.8
Spot 12	247	34304	3.4	13.4453	1	1.7241	1.7	0.1682	1.4	0.82	1002.2	13.2	1017.6	11.2	1050.8	20.2	1050.8	20.2	95.4
Spot 192	133	27675	3.4	13.4385	1	1.7504	1.4	0.1707	1	0.72	1015.8	9.8	1027.3	9.3	1051.8	20.2	1051.8	20.2	96.6
Spot 186	290	37923	2.6	13.4243	0.9	1.6913	1.5	0.1647	1.2	0.8	983.1	11.3	1005.3	9.8	1054	18.5	1054	18.5	93.3
Spot 34	342	67987	7.3	13.3506	0.9	1.8365	1.6	0.1779	1.3	0.83	1055.5	12.7	1058.6	10.3	1065	17.5	1065	17.5	99.1
Spot 179	411	132933	4.8	13.3087	1	1.7296	2.1	0.167	1.8	0.88	995.7	16.8	1019.6	13.3	1071.4	19.6	1071.4	19.6	92.9
Spot 48	112	28979	2	13.2742	1.1	1.8537	1.6	0.1785	1.2	0.76	1059	12	1064.7	10.7	1076.5	21.4	1076.5	21.4	98.4
Spot 46	49	32188	2.5	13.1986	1.1	1.8521	1.6	0.1774	1.2	0.76	1052.6	12.1	1064.2	10.8	1088	21.5	1088	21.5	96.7
Spot 126	120	33760	2.7	13.1397	1	1.9813	1.8	0.1889	1.5	0.82	1115.4	15.6	1109.2	12.5	1097	21	1097	21	101.7
Spot 148	330	22901	1.2	13.1388	0.9	1.8228	1.9	0.1738	1.6	0.87	1032.9	15.5	1053.7	12.2	1097.1	18.5	1097.1	18.5	94.1
Spot 171	51	7423	2.5	13.1095	1.1	1.9339	1.7	0.184	1.3	0.77	1088.5	13.4	1092.9	11.6	1101.6	22.2	1101.6	22.2	98.8
Spot 43	322	28953	1.7	13.0974	1.2	1.5839	1.9	0.1505	1.5	0.78	903.9	12.6	963.9	11.9	1103.4	24	1103.4	24	81.9
Spot 13	204	38135	5.6	13.0766	0.9	1.8851	1.6	0.1789	1.3	0.83	1060.8	13.1	1075.9	10.7	1106.6	18.1	1106.6	18.1	95.9
Spot 66	103	13524	3.5	12.8678	1.2	1.713	1.7	0.1599	1.2	0.72	956.4	11.1	1013.4	11.1	1138.7	23.7	1138.7	23.7	84
Spot 152	91	11374	3.2	12.7698	1.6	2.0161	2.1	0.1868	1.3	0.65	1104	13.7	1120.9	14.2	1153.9	31.6	1153.9	31.6	95.7
Spot 102	823	45398	6.7	12.7127	1	1.931	1.9	0.1781	1.6	0.83	1056.7	15.2	1091.9	12.5	1162.8	20.6	1162.8	20.6	90.9
Spot 45	79	13443	3.4	12.5834	0.9	2.2516	1.6	0.2056	1.3	0.84	1205.2	14.4	1197.3	11	1183	16.8	1183	16.8	101.9
Spot 69	96	30742	3.6	12.579	1.1	2.1224	1.6	0.1937	1.2	0.74	1141.4	12.7	1156.1	11.3	1183.7	21.7	1183.7	21.7	96.4
Spot 118	203	79018	2.5	12.3947	1	2.2351	1.9	0.201	1.6	0.84	1180.8	17.2	1192.1	13.3	1212.8	20.1	1212.8	20.1	97.4
Spot 174	130	96652	2.8	12.3025	1	2.1076	1.8	0.1881	1.5	0.82	1111.3	15.3	1151.3	12.6	1227.5	20.6	1227.5	20.6	90.5
Spot 82	80	31817	2.8	12.2457	1.2	2.3041	1.9	0.2047	1.5	0.78	1200.6	16.4	1213.5	13.7	1236.5	23.8	1236.5	23.8	97.1
Spot 137	394	41972	3	12.0788	1.1	2.346	2.2	0.2056	1.9	0.88	1205.4	21.1	1226.3	15.6	1263.4	20.5	1263.4	20.5	95.4
Spot 112	123	47475	0.9	11.6411	1.1	2.4698	1.8	0.2086	1.5	0.8	1221.4	16.4	1263.2	13.2	1335.1	21	1335.1	21	91.5
Spot 193	42	15824	2.9	11.5837	1.2	2.7361	1.8	0.23	1.3	0.73	1334.3	15.5	1338.3	13.1	1344.7	23.2	1344.7	23.2	99.2
Spot 6	86	199657	3.7	10.6212	0.9	3.2034	2	0.2469	1.8	0.88	1422.3	22.7	1458	15.6	1510.3	17.9	1510.3	17.9	94.2
Spot 55	81	36788	5.5	10.0831	5.2	4.0082	5.8	0.2932	2.5	0.44	1657.7	36.9	1635.9	46.8	1607.8	96.4	1607.8	96.4	103.1
Spot 170	458	96131	9.7	9.9729	1	3.5326	2.1	0.2556	1.8	0.88	1467.4	23.9	1534.5	16.3	1628.3	18	1628.3	18	90.1
Spot 96	202	106618	2.3	9.5733	1	4.2867	1.8	0.2978	1.5	0.82	1680.2	21.9	1690.8	14.8	1704	18.8	1704	18.8	98.6
Spot 168	111	51057	1.7	9.2963	1.1	4.6709	1.9	0.3151	1.5	0.82	1765.6	23.9	1762	15.7	1757.8	19.5	1757.8	19.5	100.4
Spot 72	70	25633	2.1	9.1882	1	4.627	3.2	0.3085	3	0.95	1733.2	45.8	1754.2	26.6	1779.2	18.9	1779.2	18.9	97.4
Spot 110	211	23208	1.5	9.018	1	4.7978	1.5	0.3139	1.1	0.75	1760	16.8	1784.5	12.3	1813.2	17.7	1813.2	17.7	97.1
Spot 9	87	213434	1.5	8.3295	1.1	4.5897	3.3	0.2774	3.1	0.94	1578.2	43.8	1747.4	27.6	1956.3	19.3	1956.3	19.3	80.7

Spot 70	282	106836	3	8.2676	1	5.5938	1.7	0.3356	1.4	0.82	1865.3	22.3	1915.1	14.5	1969.6	17.4	1969.6	17.4	94.7	
Spot 161	276	33525	2.8	7.9523	1	5.5528	2.1	0.3204	1.9	0.88	1791.7	29.3	1908.8	18.2	2038.6	17.5	2038.6	17.5	87.9	
Spot 56	116	109810	5.3	7.9385	1.3	5.038	1.9	0.2902	1.3	0.69	1642.5	18.7	1825.7	15.7	2041.7	23.6	2041.7	23.6	80.4	
Spot 188	329	116526	2.1	7.8799	1.1	6.091	1.9	0.3483	1.6	0.83	1926.3	26.2	1989	16.5	2054.7	18.6	2054.7	18.6	93.7	
Spot 98	115	53267	2.5	7.8052	1	6.3012	2.4	0.3569	2.1	0.9	1967.3	35.8	2018.6	20.6	2071.5	18.2	2071.5	18.2	95	
Spot 138	228	39778	2.5	5.4284	1.1	10.8426	2	0.4271	1.7	0.85	2292.5	33.3	2509.7	18.9	2690.5	17.8	2690.5	17.8	85.2	
Spot 58*	162	1279	1.1	11.3959	4.8	0.939	5	0.0776	1.4	0.29	482	6.7	672.3	24.7	1376.2	92.4	1376.2	92.4	35	
Spot 155**	112	7036	1.4	18.1578	1.9	0.5876	2.5	0.0774	1.5	0.62	480.6	7.1	469.3	9.3	414.2	43.4	480.6	7.1	116	
Spot 93**	113	10038	1.8	18.1159	1.6	0.6004	2	0.0789	1.2	0.6	489.7	5.6	477.5	7.6	419.3	36	489.7	5.6	116.8	
Spot 156**	124	8772	1.3	18.1718	1.8	0.5931	2.1	0.0782	1	0.5	485.4	4.8	472.8	7.8	412.5	40	485.4	4.8	117.7	
Spot 132**	235	11747	1.4	18.2538	1	0.5799	1.9	0.0768	1.6	0.84	477.1	7.3	464.4	7	402.4	23	477.1	7.3	118.6	
Spot 30**	99	5516	1.7	18.2621	1.3	0.5833	1.6	0.0773	1	0.6	479.9	4.4	466.6	6	401.4	28.6	479.9	4.4	119.6	
Spot 86**	192	9562	1.6	18.3671	1.3	0.5751	1.9	0.0766	1.4	0.71	476	6.2	461.3	7	388.5	30	476	6.2	122.5	
Spot 199**	220	7876	1.6	18.4339	1.3	0.5647	1.9	0.0755	1.4	0.73	469.4	6.2	454.6	6.9	380.4	28.7	469.4	6.2	123.4	
Spot 92**	79	7287	1.6	18.4086	1.8	0.5827	2.3	0.0778	1.5	0.65	483.2	7	466.2	8.7	383.4	39.9	483.2	7	126	
Spot 73	180	6910	1.9	18.5391	1.4	0.5623	1.9	0.0756	1.3	0.7	470.1	6	453	7	367.5	30.8	470.1	6	127.9	
Spot 195**	174	586	3.4	29.6454	6.9	0.3583	7.1	0.0771	1.7	0.24	478.7	7.8	311	19.1	NA	NA	478.7	7.8	153.9	

*DISCORD

**REV DISCORD

Table A4. LC0806 U-Pb geochronologic analyses from OMPV (La Colina Formation sandstone from OMPV locality described in Chapter 5).

Analysis	U (ppm)	²⁰⁶ Pb/ ²⁰⁴ Pb		U/Th	²⁰⁶ Pb		²⁰⁷ Pb		²⁰⁶ Pb		error	²⁰⁶ Pb		²⁰⁷ Pb		²⁰⁶ Pb		Best age	1σ	Conc
		204	206		1σ	235U	1σ	238U	1σ	238U		1σ	235U	1σ	235U	1σ	(Ma)			
Spot 51	456	6917	4.8	18.5991	1.9	0.4274	2.8	0.0577	2.1	0.73	361.5	7.3	361.3	8.6	360.3	43.5	361.5	7.3	100	
Spot 135	488	31753	1.1	18.1344	1	0.4405	1.9	0.058	1.6	0.85	363.2	5.6	370.6	5.8	417.1	22.1	363.2	5.6	98	
Spot 13	1018	1005	1.3	10.0985	4.9	0.7998	5.7	0.0586	3	0.52	367.1	10.7	596.7	25.9	1605	91.2	367.1	10.7	61.5	
Spot 127	483	78814	1.5	18.621	1.3	0.4471	1.8	0.0604	1.3	0.71	378.1	4.8	375.2	5.7	357.6	28.9	378.1	4.8	100.8	
Spot 108	314	17352	1.1	18.1754	1.1	0.479	1.6	0.0632	1.2	0.74	394.9	4.7	397.4	5.4	412	24.6	394.9	4.7	99.4	
Spot 174	199	11759	1.7	17.4925	1.3	0.5874	1.7	0.0746	1.2	0.67	463.5	5.1	469.2	6.5	497	28.5	463.5	5.1	93.3	
Spot 186	621	6446	11.5	15.3825	2.1	0.6728	2.6	0.0751	1.4	0.56	466.7	6.4	522.4	10.5	773.7	45	466.7	6.4	60.3	
Spot 177	192	45568	1.6	17.5098	1.2	0.5977	1.8	0.0759	1.3	0.75	471.8	6.1	475.8	6.7	494.9	25.8	471.8	6.1	95.3	
Spot 49	226	29305	10.2	17.4223	1.2	0.6026	1.9	0.0762	1.5	0.79	473.3	7	478.9	7.4	505.9	26.1	473.3	7	93.5	
Spot 90	574	4858	5	15.8242	1.1	0.6651	2	0.0764	1.6	0.83	474.4	7.4	517.7	7.9	713.9	23.4	474.4	7.4	66.5	
Spot 146	280	168824	1.7	17.2116	1.2	0.6237	2	0.0779	1.6	0.8	483.6	7.4	492.2	7.7	532.6	26.2	483.6	7.4	90.8	
Spot 4	516	36293	121.4	17.0748	1.1	0.6543	1.5	0.0811	1.1	0.7	502.5	5.2	511.1	6.2	550.1	24	502.5	5.2	91.3	
Spot 183	373	23684	2	15.6119	1.1	0.717	1.8	0.0812	1.4	0.78	503.4	7	548.9	7.8	742.5	24.2	503.4	7	67.8	
Spot 74	341	45980	1	17.3219	1.1	0.6481	1.6	0.0815	1.2	0.76	504.8	6	507.3	6.5	518.6	23.2	504.8	6	97.4	
Spot 151	104	15786	1	17.3749	1.2	0.6504	1.8	0.082	1.3	0.76	508	6.5	508.7	7.1	511.9	25.4	508	6.5	99.2	
Spot 140	143	5511	1.7	17.8056	1	0.6391	2.1	0.0826	1.8	0.87	511.4	8.9	501.7	8.2	457.8	22.3	511.4	8.9	111.7	
Spot 63	1540	16236	24.1	16.309	0.8	0.7021	1.8	0.0831	1.6	0.9	514.5	7.8	540	7.4	649.4	16.8	514.5	7.8	79.2	
Spot 162	194	16135	3.2	17.4152	1.2	0.6587	1.8	0.0832	1.3	0.73	515.4	6.3	513.8	7.1	506.8	26.3	515.4	6.3	101.7	
Spot 157	335	21846	2	17.2592	1	0.6648	1.7	0.0833	1.3	0.79	515.5	6.6	517.6	6.9	526.6	23	515.5	6.6	97.9	
Spot 149	200	9970	1.9	17.2602	1.1	0.6649	1.6	0.0833	1.2	0.75	515.6	5.9	517.6	6.4	526.4	23.1	515.6	5.9	97.9	
Spot 166	312	79223	1.9	17.0807	0.9	0.675	1.8	0.0837	1.5	0.86	517.9	7.6	523.7	7.3	549.3	19.8	517.9	7.6	94.3	
Spot 60	170	32430	2	16.8987	1.2	0.6825	1.9	0.0837	1.5	0.77	518.1	7.3	528.3	7.8	572.7	26.3	518.1	7.3	90.5	
Spot 139	147	6983	1.7	17.7552	1.1	0.6523	1.6	0.084	1.2	0.73	520.2	5.9	509.9	6.4	464.1	24.2	520.2	5.9	112.1	
Spot 1	254	14667	2.2	16.5721	1	0.6994	1.4	0.0841	1	0.7	520.6	5	538.5	6.1	614.9	22.5	520.6	5	84.7	
Spot 14	337	21563	2.2	17.3039	1.3	0.6716	1.9	0.0843	1.4	0.73	521.9	6.9	521.7	7.8	520.9	28.7	521.9	6.9	100.2	
Spot 196	208	358571	2.6	16.9927	1	0.6845	1.6	0.0844	1.2	0.78	522.3	6.1	529.5	6.5	560.6	21.3	522.3	6.1	93.2	
Spot 147	222	159285	2.8	17.1714	1.1	0.6794	1.7	0.0846	1.3	0.76	523.8	6.3	526.4	6.8	537.7	23.9	523.8	6.3	97.4	
Spot 110	193	8003	2.2	17.5808	1.2	0.6641	1.7	0.0847	1.2	0.71	524.2	6.1	517.1	7	485.9	26.8	524.2	6.1	107.9	
Spot 18	485	24512	1.4	17.2253	1.1	0.6779	1.8	0.0847	1.4	0.79	524.2	7	525.5	7.2	530.9	23.3	524.2	7	98.8	
Spot 103	517	20118	1	17.2807	0.8	0.6758	1.3	0.0847	1	0.79	524.3	5.2	524.2	5.4	523.8	18	524.3	5.2	100.1	
Spot 29	639	32175	7.8	16.4772	1.3	0.7104	1.9	0.0849	1.3	0.71	525.5	6.7	545	7.9	627.3	28.5	525.5	6.7	83.8	
Spot 43	546	17328	2.1	16.8635	0.8	0.6959	1.6	0.0852	1.3	0.85	526.8	6.7	536.4	6.5	577.2	17.6	526.8	6.7	91.3	
Spot 180	152	7400	2.3	17.7632	1.3	0.6609	1.8	0.0852	1.3	0.71	527	6.6	515.1	7.4	463.1	28.9	527	6.6	113.8	
Spot 143	255	53540	2.7	16.3376	1.1	0.7191	1.9	0.0852	1.5	0.8	527.4	7.6	550.1	8	645.7	24.6	527.4	7.6	81.7	
Spot 34	140	18129	0.6	17.0939	1.1	0.6887	1.8	0.0854	1.4	0.79	528.4	7.2	532	7.5	547.6	24.2	528.4	7.2	96.5	
Spot 128	348	15010	1.6	17.5385	0.8	0.6715	1.4	0.0855	1.2	0.82	528.6	5.9	521.6	5.7	491.3	17.6	528.6	5.9	107.6	
Spot 168	187	14211	2.6	17.6681	1.2	0.667	1.7	0.0855	1.2	0.7	528.9	6	518.9	6.8	475	26.3	528.9	6	111.4	
Spot 9	417	196519	1.6	17.036	0.8	0.6936	1.3	0.0857	1	0.8	530.3	5.3	535	5.4	555	16.8	530.3	5.3	95.5	
Spot 91	491	30442	1.6	17.1087	1.1	0.6924	1.9	0.086	1.6	0.83	531.6	8.1	534.3	7.9	545.7	23.4	531.6	8.1	97.4	
Spot 94	129	8791	1.8	17.7608	1.3	0.6685	1.7	0.0862	1.2	0.69	532.8	6	519.8	7	463.4	27.8	532.8	6	115	
Spot 114	150	14611	2.3	17.4715	1.3	0.6814	1.7	0.0864	1.1	0.65	534.1	5.7	527.6	7	499.7	28.8	534.1	5.7	106.9	
Spot 16	740	29350	5	17.067	0.8	0.7005	1.6	0.0867	1.4	0.85	536.3	7	539.1	6.7	551.1	18.5	536.3	7	97.3	
Spot 163	470	9416	1.6	17.6816	1.5	0.6772	1.9	0.0869	1.1	0.6	537.1	5.7	525.1	7.6	473.3	33.1	537.1	5.7	113.5	
Spot 170	235	14207	3.8	17.1561	1.3	0.6992	2	0.087	1.6	0.77	538	8.1	538.3	8.5	539.7	28.3	538	8.1	99.7	
Spot 198	218	17901	2	17.2384	1	0.698	1.6	0.0873	1.3	0.78	539.6	6.6	537.6	6.8	529.2	22.3	539.6	6.6	102	
Spot 56	98	4832	1.6	16.6683	2.7	0.723	2.9	0.0874	1.1	0.39	540.4	5.9	552.5	12.4	602.4	58.2	540.4	5.9	89.7	
Spot 161	83	6586	1.9	17.5545	1.6	0.6882	2.2	0.0877	1.6	0.72	541.7	8.4	531.7	9.3	489.3	34.3	541.7	8.4	110.7	
Spot 48	223	36149	2.4	16.8593	1.1	0.7195	1.5	0.088	1	0.67	543.8	5.4	550.4	6.5	577.7	24.9	543.8	5.4	94.1	
Spot 15	281	11963	2.6	17.0639	1.1	0.7149	1.8	0.0885	1.4	0.79	546.8	7.3	547.7	7.5	551.4	23.4	546.8	7.3	99.2	
Spot 67	291	13627	4.8	17.4616	1.2	0.6999	1.6	0.0887	1	0.63	547.7	5.2	538.7	6.5	500.9	26.6	547.7	5.2	109.3	
Spot 197	317	36441	8	16.8295	1.2	0.7271	1.7	0.0888	1.3	0.73	548.3	6.7	554.8	7.4	581.6	25.4	548.3	6.7	94.3	
Spot 160	126	15161	1.7	16.9155	1.3	0.7253	2	0.089	1.5	0.74	549.8	7.7	553.8	8.5	570.5	29.2	549.8	7.7	96.4	
Spot 133	818	35355	17.1	17.2528	0.8	0.7124	1.8	0.0892	1.6	0.9	550.7	8.4	546.2	7.5	527.4	17.4	550.7	8.4	104.4	
Spot 195	588	24292	5	17.2845	1	0.7133	1.7	0.0895	1.3	0.8	552.3	7.1	546.7	7.1	523.3	21.8	552.3	7.1	105.5	
Spot 44	98	11057	1.4	16.7512	1	0.7378	1.7	0.0897	1.4	0.81	553.6	7.5	561.1	7.5	591.7	21.9	553.6	7.5	93.6	
Spot 3	407	38330	6.6	16.7193	1.1	0.7401	2.1	0.0898	1.7	0.84	554.2	9.2	562.4	9	595.8	24.6	554.2	9.2	93	
Spot 138	580	39108	75.9	16.99	0.9	0.7287	1.9	0.0898	1.7	0.89	554.5	8.9	555.8	8.1	560.9	19.1	554.5	8.9	98.9	
Spot 102	222	36214	1.7	17.12	1	0.7259	1.6	0.0902	1.2	0.77	556.5	6.6	554.1	6.8	544.3	22.4	556.5	6.6	102.3	
Spot 37	111	6525	2.4	17.0692	1.3	0.7292	1.8	0.0903	1.3	0.7	557.4	6.7	556.1	7.7	550.8	28.1	557.4	6.7	101.2	
Spot 187	1069	83090	4.5	17.0636	0.8	0.7314	1.7	0.0906	1.5	0.87	558.8	7.9	557.4	7.3	551.5	18.4	558.8	7.9	101.3	
Spot 45	190	28217	0.5	16.7533	1.3	0.7461	1.8	0.0907	1.3	0.7	559.6	6.7	566	7.8	591.4	27.9	559.6	6.7	94.6	
Spot 53	554	43451	5	16.7167	1.1	0.7477	1.6	0.0907	1.2	0.76	559.7	6.7	566.9	7.1	596.2	22.7	559.7	6.7	93.9	

Spot 20	466	37209	2.4	17.3003	1.2	0.7235	1.7	0.0908	1.2	0.71	560.4	6.5	552.7	7.3	521.3	26.7	560.4	6.5	107.5
Spot 84	202	4968	2	17.2766	1.2	0.7267	1.7	0.0911	1.2	0.72	562	6.5	554.6	7.2	524.3	25.7	562	6.5	107.2
Spot 36	557	30965	33.3	16.7956	0.9	0.749	1.7	0.0913	1.4	0.86	563.1	7.7	567.7	7.3	585.9	18.6	563.1	7.7	96.1
Spot 192	68	6127	1	17.0971	2.7	0.7482	3	0.0928	1.4	0.48	572.2	7.9	567.2	13.1	547.2	57.9	572.2	7.9	104.6
Spot 71	305	29116	1.8	17.0668	1	0.753	1.4	0.0932	1	0.69	574.7	5.4	569.9	6.2	551.1	22.7	574.7	5.4	104.3
Spot 55	65	13287	19.5	15.3854	1.9	0.838	2.4	0.0935	1.4	0.58	576.5	7.5	618	10.9	773.3	40.4	576.5	7.5	74.5
Spot 68	736	101112	22.9	16.6233	1	0.7757	1.5	0.0936	1.2	0.78	576.6	6.6	583	6.8	608.2	20.7	576.6	6.6	94.8
Spot 33	139	3928	2.2	17.5826	1.1	0.7371	1.8	0.094	1.4	0.77	579.4	7.5	560.7	7.6	485.7	24.7	579.4	7.5	119.3
Spot 136	254	26337	1.4	16.9933	1	0.7635	1.5	0.0941	1.2	0.77	580	6.4	576	6.6	560.5	20.9	580	6.4	103.5
Spot 21	198	9914	3	17.1819	1.6	0.761	2	0.0949	1.2	0.62	584.3	6.9	574.6	8.7	536.4	34	584.3	6.9	108.9
Spot 104	45	11174	0.6	16.6492	1.8	0.7865	2.3	0.095	1.4	0.63	585.1	8.1	589.2	10.2	604.9	38.4	585.1	8.1	96.7
Spot 121	332	39163	11	16.1699	1.1	0.8115	1.6	0.0952	1.2	0.74	586.3	6.6	603.3	7.2	667.7	22.8	586.3	6.6	87.8
Spot 191	1273	4261	13.1	13.9327	1.4	0.9522	2.1	0.0963	1.6	0.75	592.4	9	679.2	10.5	978.6	28.9	592.4	9	60.5
Spot 82	485	38472	2.8	16.7465	1	0.7931	1.5	0.0964	1.1	0.75	593.1	6.5	592.9	6.8	592.3	21.5	593.1	6.5	100.1
Spot 175	294	52017	3.8	16.2699	1	0.8217	1.9	0.097	1.6	0.85	596.9	9.1	609	8.6	654.6	21.3	596.9	9.1	91.2
Spot 42	150	20503	0.5	16.4887	1	0.812	1.5	0.0971	1.2	0.77	597.7	6.8	603.6	7	625.8	21.1	597.7	6.8	95.5
Spot 22	262	17277	1.3	16.5551	0.9	0.8093	1.5	0.0972	1.2	0.82	598	6.9	602	6.8	617.1	18.6	598	6.9	96.9
Spot 39	106	5855	1.2	17.1351	1.5	0.7821	1.9	0.0972	1.2	0.63	598.2	7	586.7	8.6	542.3	32.5	598.2	7	110.3
Spot 176	248	121043	4.6	16.6982	1.2	0.8072	1.9	0.0978	1.6	0.8	601.5	8.9	600.9	8.8	598.6	25.6	601.5	8.9	100.5
Spot 12	283	32075	2.3	16.7177	1	0.808	1.5	0.098	1	0.71	602.8	6	601.3	6.6	596	22.1	602.8	6	101.1
Spot 86	66	30389	2.4	16.1412	1.9	0.8376	2.2	0.0981	1.1	0.51	603.2	6.4	617.8	10.1	671.6	40.4	603.2	6.4	89.8
Spot 169	954	48865	16.7	16.6814	0.8	0.8163	1.7	0.0988	1.5	0.88	607.4	8.8	606	7.8	600.7	17.3	607.4	8.8	101.1
Spot 24	227	34748	3.2	16.5015	0.8	0.8261	1.4	0.0989	1.2	0.81	608	6.7	611.4	6.6	624.1	18.2	608	6.7	97.4
Spot 89	504	16187	1.3	15.9494	1.4	0.8558	2.6	0.099	2.2	0.85	608.8	13	627.8	12.4	697.1	29.9	608.8	13	87.3
Spot 46	195	10835	1.8	16.3166	0.9	0.8368	1.5	0.0991	1.2	0.8	609	6.9	617.4	6.8	648.4	19	609	6.9	93.9
Spot 31	190	16388	2.6	14.7901	1.8	0.9282	2.4	0.0996	1.5	0.62	612.1	8.5	666.7	11.5	855.8	38.3	612.1	8.5	71.5
Spot 172	136	19004	3.3	16.5695	1.3	0.8298	2	0.0998	1.5	0.76	613.1	8.9	613.5	9.3	615.3	28.1	613.1	8.9	99.6
Spot 54	1005	358281	3.3	16.6268	0.8	0.8275	1.7	0.0998	1.5	0.87	613.4	8.7	612.2	7.8	607.8	17.9	613.4	8.7	100.9
Spot 117	833	10746	7.1	15.2497	0.9	0.905	1.7	0.1001	1.4	0.84	615.2	8.3	654.4	8.1	791.9	19.2	615.2	8.3	77.7
Spot 80	661	24309	1.6	16.2369	0.8	0.8522	1.9	0.1004	1.8	0.91	616.8	10.4	625.9	9.1	658.9	17.4	616.8	10.4	93.6
Spot 193	1653	34050	8.2	16.2151	1	0.8542	1.9	0.1005	1.6	0.84	617.3	9.5	627	9	661.8	22.4	617.3	9.5	93.3
Spot 66	244	9221	5.4	16.7619	0.8	0.827	1.2	0.1006	0.9	0.74	617.8	5.4	611.9	5.7	590.3	18	617.8	5.4	104.7
Spot 70	317	138463	2.2	16.0058	1	0.8743	1.5	0.1015	1.1	0.76	623.4	6.8	637.9	7.2	689.6	21.2	623.4	6.8	90.4
Spot 92	737	104462	44.4	16.5308	0.9	0.8532	1.8	0.1023	1.5	0.85	628.1	8.9	626.4	8.3	620.3	20.4	628.1	8.9	101.3
Spot 165	127	11310	1.4	16.402	1	0.8621	2	0.1026	1.7	0.87	629.6	10.2	631.3	9.2	637.2	21.1	629.6	10.2	98.8
Spot 150	244	35951	1.5	16.5561	1.2	0.8555	1.9	0.1028	1.5	0.78	630.6	8.8	627.7	8.8	617	20.6	630.6	8.8	102.2
Spot 109	236	176599	10.4	15.5486	1.4	0.9126	2.1	0.103	1.5	0.71	631.7	8.8	658.4	10	751.1	30.4	631.7	8.8	84.1
Spot 154	114	5728	1.8	16.8313	1	0.8442	1.9	0.1031	1.6	0.84	632.6	9.4	621.5	8.7	581.3	22.3	632.6	9.4	108.8
Spot 23	477	25217	4	16.4429	1	0.8723	1.6	0.1041	1.3	0.79	638.2	7.7	636.8	7.5	631.8	20.8	638.2	7.7	101
Spot 0	714	48014	0.9	16.3417	0.8	0.8788	1.6	0.1042	1.4	0.85	639	8.3	640.3	7.6	645.1	18	639	8.3	99
Spot 8	1898	66219	41.2	16.1904	0.8	0.8955	1.6	0.1052	1.4	0.85	644.8	8.4	649.3	7.7	665.1	18.1	644.8	8.4	96.9
Spot 32	362	25607	2	16.1963	1	0.8979	1.9	0.1055	1.7	0.87	646.7	10.2	650.6	9.2	664.3	20.6	646.7	10.2	97.3
Spot 50	286	50233	2	16.3527	1	0.8906	1.6	0.1057	1.2	0.77	647.6	7.5	646.7	7.5	643.7	21.4	647.6	7.5	100.6
Spot 134	650	29158	3	15.3241	1	0.9693	1.9	0.1078	1.6	0.83	659.8	9.8	688.1	9.4	781.7	21.9	659.8	9.8	84.4
Spot 137	1068	54115	9.7	15.3573	1	0.9927	1.8	0.1106	1.5	0.83	676.3	9.7	700.1	9.1	777.1	20.9	676.3	9.7	87
Spot 10	303	16598	1.3	16.1214	1	0.9457	1.6	0.1106	1.2	0.79	676.4	8	675.9	7.8	674.2	20.8	676.4	8	100.3
Spot 167	649	68797	2.3	16.1717	1	0.9466	1.7	0.1111	1.4	0.81	679	9	676.3	8.5	667.5	21.6	679	9	101.7
Spot 27	455	22918	16.6	16.0355	0.8	0.9682	1.4	0.1127	1.1	0.83	688.1	7.4	687.5	6.9	685.6	16.5	688.1	7.4	100.4
Spot 40	182	18249	3.7	14.8407	0.9	1.0526	1.6	0.1133	1.3	0.82	692.2	8.7	730.2	8.4	848.7	19.4	692.2	8.7	81.6
Spot 185	884	54556	1.4	15.3926	0.8	1.0518	1.6	0.1175	1.5	0.88	716	9.9	729.8	8.6	772.3	16.4	716	9.9	92.7
Spot 19	283	19386	6.2	14.4147	1.1	1.2094	2.1	0.1265	1.8	0.85	767.8	13	804.9	11.8	909	23.3	767.8	13	84.5
Spot 188	308	43719	1.9	14.4903	0.8	1.2568	1.7	0.1321	1.5	0.87	800.1	11	826.5	9.5	898.2	17.5	800.1	11	89.1
Spot 158	365	31653	5	14.5142	1	1.293	1.8	0.1362	1.5	0.83	822.9	11.3	842.6	10.1	894.8	20.1	822.9	11.3	92
Spot 100	522	64600	8.7	14.296	0.9	1.3464	1.7	0.1397	1.4	0.83	842.7	11	866	9.8	926	19	842.7	11	91
Spot 116	574	46258	2.4	14.5248	0.9	1.3661	1.6	0.144	1.3	0.83	867.1	10.4	874.5	9.1	893.3	17.9	867.1	10.4	97.1
Spot 171	208	12462	1.5	14.3789	1.2	1.4125	1.9	0.1474	1.5	0.78	886.2	12	894.2	11.1	914.1	23.9	914.1	23.9	96.9
Spot 156	805	47386	3.5	14.3772	1.3	1.525	3	0.1591	2.7	0.89	951.7	23.6	940.5	18.3	914.4	27.7	914.4	27.7	104.1
Spot 95	381	362174	3.8	14.1956	0.8	1.4379	1.7	0.1481	1.5	0.87	890.3	12.3	904.8	10.2	940.4	17.4	940.4	17.4	94.7
Spot 124	264	29880	3.4	14.1812	0.9	1.4855	1.3	0.1529	0.9	0.72	916.9	7.9	924.5	7.8	942.5	18.5	942.5	18.5	97.3
Spot 83	663	76788	15.2	14.1158	1	1.5137	2	0.155	1.7	0.85	929.1	14.7	935.9	12.2	952	21.4	952	21.4	97.6
Spot 120	419	32564	4.1	14.0784	1	1.6123	1.7	0.1647	1.4	0.81	982.8	12.7	975	10.8	957.4	20.8	957.4	20.8	102.7
Spot 76	258	37294	4	13.7764	1	1.7224	1.9	0.1722	1.6	0.85	1024.1	15	1016.9	12	1001.6	20	1001.6	20	102.2
Spot 130	268	205141	1.3	13.7654	0.9	1.7565	1.2	0.1754	0.8	0.66	1042	7.9	1029.5	8.1	1003.2	19	1003.2	19	103.9
Spot 57	460	16621	0.8	13.734	0.9	1.6867	1.7	0.1681	1.5	0.86	1001.5	13.5	1003.5	10.7	1007.8	17.2	1007.8	17.2	99.4
Spot 7	548	21819	3.1	13.7148	0.9	1.6841	1.9	0.1676	1.6	0.88	998.8	15.3	1002.5	12	1010.7	18.2	1010.7	18.2	98.8

Spot 72	363	37629	2.4	13.6247	0.8	1.7155	1.6	0.1696	1.4	0.86	1009.9	12.9	1014.4	10.3	1024	16.5	1024	16.5	98.6
Spot 126	342	30997	4.5	13.6211	1	1.7284	1.6	0.1708	1.2	0.79	1016.6	11.5	1019.1	10	1024.5	19.3	1024.5	19.3	99.2
Spot 65	753	36047	4.4	13.4256	0.7	1.7376	1.4	0.1693	1.2	0.86	1008	11.5	1022.6	9.2	1053.8	14.6	1053.8	14.6	95.7
Spot 199	636	436821	2.7	13.3848	0.7	1.8992	1.8	0.1844	1.6	0.92	1091.2	16.4	1080.8	11.8	1059.9	14.1	1059.9	14.1	103
Spot 79	467	48772	6.3	13.3478	0.9	1.8992	1.6	0.1839	1.3	0.81	1088.4	12.9	1080.8	10.5	1065.5	18.6	1065.5	18.6	102.2
Spot 64	43	9584	1.8	13.3299	1.3	1.817	2	0.1757	1.5	0.75	1043.7	14.4	1051.6	13.1	1068.2	26.7	1068.2	26.7	97.7
Spot 178	261	40551	3.4	13.2858	1	1.9129	1.6	0.1844	1.2	0.77	1091	12.3	1085.6	10.6	1074.8	20.4	1074.8	20.4	101.5
Spot 6	249	33912	4.2	13.2762	1.2	1.7926	2	0.1727	1.6	0.81	1026.9	14.9	1042.8	12.7	1076.2	23.2	1076.2	23.2	95.4
Spot 61	413	48712	2.9	13.2649	1	1.6621	1.6	0.16	1.3	0.79	956.6	11.2	994.2	10.1	1078	19.4	1078	19.4	88.7
Spot 153	547	68066	7.9	13.1985	1	1.7645	1.8	0.169	1.5	0.83	1006.5	13.6	1032.5	11.5	1088	19.9	1088	19.9	92.5
Spot 101	276	40612	5	13.0673	0.9	1.9492	1.6	0.1848	1.3	0.83	1093.2	13	1098.2	10.5	1108	17.5	1108	17.5	98.7
Spot 17	490	33065	1.8	13.06	0.9	1.9595	1.7	0.1857	1.4	0.84	1098	14.4	1101.7	11.4	1109.1	18.3	1109.1	18.3	99
Spot 131	318	30219	1.4	13.0302	0.7	1.8132	1.5	0.1714	1.3	0.87	1020	12.3	1050.2	9.8	1113.7	14.5	1113.7	14.5	91.6
Spot 115	238	39945	0.8	13.0163	1	2.0275	1.6	0.1915	1.2	0.78	1129.4	12.9	1124.8	10.9	1115.8	20.3	1115.8	20.3	101.2
Spot 184	448	20366	2.1	12.9925	1	1.7642	1.8	0.1663	1.5	0.82	991.8	13.9	1032.4	11.8	1119.5	20.6	1119.5	20.6	88.6
Spot 155	271	182646	1.4	12.9842	1.1	2.0276	1.7	0.191	1.3	0.76	1126.9	13.8	1124.8	11.9	1120.8	22.5	1120.8	22.5	100.5
Spot 111	324	135715	2	12.9222	1	1.9848	1.6	0.1861	1.2	0.76	1100.2	11.9	1110.4	10.5	1130.3	20.1	1130.3	20.1	97.3
Spot 119	663	12800	2.7	12.8973	0.9	1.6998	1.9	0.1591	1.6	0.87	951.6	14.3	1008.5	11.9	1134.1	18.6	1134.1	18.6	83.9
Spot 189	232	32999	2.2	12.8149	1	1.6488	1.7	0.1533	1.4	0.81	919.5	11.8	989.1	10.8	1146.9	20.1	1146.9	20.1	80.2
Spot 106	441	225818	7.4	12.7999	1	1.8493	1.8	0.1718	1.5	0.83	1021.8	13.9	1063.2	11.6	1149.2	19.3	1149.2	19.3	88.9
Spot 142	591	14840	2.1	12.7911	0.9	1.9376	1.9	0.1798	1.7	0.88	1066	16.7	1094.2	12.9	1150.6	18.2	1150.6	18.2	92.7
Spot 173	418	13665	1.5	12.7582	1.6	1.8407	2.2	0.1704	1.5	0.69	1014.3	14.3	1060.1	14.6	1155.7	31.9	1155.7	31.9	87.8
Spot 159	734	84229	2	12.7301	1	2.0645	1.7	0.1907	1.4	0.81	1125.1	14.5	1137.1	11.9	1160	20.3	1160	20.3	97
Spot 125	180	35797	14.4	12.5534	1.1	1.9471	1.8	0.1774	1.4	0.8	1052.5	14.1	1097.5	12.2	1187.7	21.5	1187.7	21.5	88.6
Spot 164	217	13039	2.4	12.3993	1	2.3327	1.7	0.2099	1.4	0.79	1228.1	15.2	1222.3	12.2	1212	20.6	1212	20.6	101.3
Spot 97	483	9764	4.9	12.3811	2	1.8152	2.7	0.1631	1.9	0.68	973.8	16.8	1051	17.8	1215	38.9	1215	38.9	80.2
Spot 2	538	80402	3.9	12.203	0.7	2.3546	1.5	0.2085	1.3	0.87	1220.7	14.6	1228.9	10.7	1243.4	14.6	1243.4	14.6	98.2
Spot 78	67	24520	1.6	11.2556	0.9	2.938	1.6	0.2399	1.3	0.81	1386.4	16.3	1391.8	12.1	1400	17.8	1400	17.8	99
Spot 25	321	33373	2.3	11.2454	0.9	2.9923	1.5	0.2442	1.2	0.79	1408.3	15.6	1405.7	11.8	1401.7	18	1401.7	18	100.5
Spot 28	186	88677	1.5	11.0371	0.9	3.065	1.6	0.2455	1.3	0.81	1415	16.1	1424	11.9	1437.4	17.3	1437.4	17.3	98.4
Spot 75	263	62394	1.8	10.9413	1	3.2055	1.5	0.2545	1.2	0.79	1461.5	15.9	1458.5	11.9	1454	18.1	1454	18.1	100.5
Spot 5	187	75685	1.4	10.9049	0.8	3.206	1.3	0.2537	1	0.76	1457.4	13.1	1458.6	10.2	1460.4	16.1	1460.4	16.1	99.8
Spot 118	332	30795	2.1	10.7274	1.1	2.7108	1.8	0.211	1.5	0.81	1234.1	16.6	1331.4	13.6	1491.5	20.4	1491.5	20.4	82.7
Spot 113	404	63396	5.5	10.6551	1	3.5087	1.8	0.2713	1.5	0.83	1547.2	21	1529.2	14.6	1504.3	19.7	1504.3	19.7	102.9
Spot 87	135	73822	1.5	9.528	1	4.4346	1.5	0.3066	1.2	0.77	1723.9	17.5	1718.8	12.5	1712.7	17.9	1712.7	17.9	100.7
Spot 11	305	371562	4	9.3881	0.8	4.3773	1.4	0.2982	1.2	0.83	1682.2	17.2	1708.1	11.6	1739.9	14.4	1739.9	14.4	96.7
Spot 62	94	49413	1.5	8.8341	0.8	5.2638	1.3	0.3374	1	0.8	1874.2	16.9	1863	11.1	1850.6	14.1	1850.6	14.1	101.3
Spot 96	286	38076	2.3	8.8092	1	5.0851	1.6	0.325	1.3	0.78	1814.3	19.9	1833.6	13.6	1855.7	18.1	1855.7	18.1	97.8
Spot 35	258	10071	2.2	8.804	1.5	4.3036	2.2	0.2749	1.6	0.73	1565.7	22	1694.1	17.9	1856.7	26.8	1856.7	26.8	84.3
Spot 93	251	38198	0.7	8.7893	0.9	5.2629	1.5	0.3356	1.3	0.83	1865.6	20.9	1862.9	13.2	1859.8	15.4	1859.8	15.4	100.3
Spot 85	85	12972	0.6	8.6649	0.9	5.283	1.7	0.3321	1.4	0.83	1848.8	22.6	1866.1	14.4	1885.5	16.8	1885.5	16.8	98.1
Spot 88	221	495818	1.9	7.9186	0.8	6.6971	1.4	0.3848	1.2	0.84	2098.6	20.9	2072.2	12.3	2046.1	13.4	2046.1	13.4	102.6
Spot 123	422	287394	4.4	7.8566	0.8	6.8585	1.4	0.391	1.1	0.83	2127.4	20.3	2093.3	12	2060	13.3	2060	13.3	103.3
Spot 69	532	102737	2.6	6.1667	0.9	8.5962	2.5	0.3846	2.4	0.94	2097.9	42.8	2296.1	23.1	2477.6	14.4	2477.6	14.4	84.7
Spot 141	796	44205899	3.6	6.1175	0.9	10.3278	1.7	0.4584	1.4	0.84	2432.6	28.7	2464.6	15.6	2491.1	15.3	2491.1	15.3	97.7
Spot 26	239	56356	1.4	5.9107	0.9	10.0061	1.5	0.4291	1.1	0.77	2301.8	21.8	2435.3	13.4	2548.8	15.4	2548.8	15.4	90.3
Spot 81	189	177643	2.1	5.5021	0.8	12.3303	1.5	0.4923	1.2	0.83	2580.4	25.7	2629.9	13.8	2668.1	13.7	2668.1	13.7	96.7
Spot 59	184	1018	1.7	5.0205	3.7	14.1474	4.1	0.5154	1.8	0.44	2679.5	39.7	2759.6	38.8	2818.8	59.9	2818.8	59.9	95.1
Spot 190	529	36614	19.9	4.482	0.8	17.0988	1.9	0.5561	1.7	0.89	2850.3	38.6	2940.4	18	3002.6	13.7	3002.6	13.7	94.9
Spot 30	206	76068	1.8	4.1336	0.8	20.4861	1.6	0.6144	1.3	0.85	3087.7	32.2	3114.6	15	3131.9	13.2	3131.9	13.2	98.6
Spot 73	120	31094	5.3	3.6563	1	25.5213	1.4	0.6771	1.1	0.74	3333.1	27.7	3328.4	14.1	3325.5	15.2	3325.5	15.2	100.2
Spot 98	861	1469	2	10.2713	3.6	0.8733	5.2	0.0651	3.7	0.71	406.5	14.5	637.4	24.4	1573.3	67.8	1573.3	67.8	25.8
Spot 132	954	1096	6.1	9.2498	6.1	1.1065	6.8	0.0743	2.9	0.43	461.8	12.9	756.5	36.2	1767	112	1767	112	26.1
Spot 38	379	2909	3.8	12.8281	4.8	0.7118	5.4	0.0663	2.5	0.47	413.6	10.1	545.8	22.8	1144.9	94.9	1144.9	94.9	36.1
Spot 77	1204	3086	3.6	13.7748	1.6	0.8207	2.6	0.082	2	0.78	508.2	9.8	608.5	11.8	1001.8	32.9	1001.8	32.9	50.7
Spot 181	182	3504	2.1	18.2611	1	0.6397	1.6	0.0848	1.3	0.8	524.5	6.4	502.1	6.3	401.5	21.5	524.5	6.4	130.6
Spot 107	13	355	8.7	58.3295	106.3	0.2035	106.3	0.0861	1.7	0.02	532.7	8.5	188.1	184.6	NA	NA	532.7	8.5	NA

*DISCORD

**REV DISCORD

Appendix B. Bulk Rock Geochemistry Data

Table B2. Paganzo Basin: Agua Hedionda Anticline, Huaco (AH) Bulk-rock geochemistry

Sample	Formation Name	SiO2 (%)	TiO2 (%)	Al2O3 (%)	Fe2O3 (%)	Mn (%)	MgO (%)	CaO (%)	Na2O (%)	K2O (%)	P2O5 (%)	Y (PPM)	Zr (PPM)	V (PPM)	Zn (PPM)	Ni (PPM)	Cr (PPM)	Ce (PPM)	Sr (PPM)	Ba (PPM)	LOI	Sum (%)	CIA	
HG0810-1C	Guandacol Fm.	62.90	0.76	15.70	6.80	0.15	2.83	1.15	1.95	3.40	0.16	27	171	114	98	52	96	76	125	626	3.68	99.58	65	
HG0810-3C	Guandacol Fm.	55.70	0.74	19.60	6.19	0.07	2.13	0.98	0.18	5.75	0.19	34	101	113	77	44	97	67	67	221	601	8.35	100.09	71
HG0810-4C	Guandacol Fm.	55.70	1.05	20.10	8.29	0.11	1.03	0.38	0.89	4.60	0.17	33	115	165	113	73	117	67	67	417	530	6.80	99.27	75
HG0810-5C	Guandacol Fm.	55.20	0.81	16.20	7.31	0.12	2.45	3.49	1.35	3.12	0.19	29	164	111	82	41	95	66	387	569	9.36	99.73	59	
CDH0923-1C	Guandacol Fm.	51.79	1.28	23.41	5.02	0.06	1.17	0.45	0.97	6.05	0.61	43	176	288	45	34	118	56	3216	542	7.11	98.39	76	
CDH0923-2C	Guandacol Fm.	62.37	1.13	21.36	2.39	0.02	0.53	0.20	0.24	4.55	0.18	39	231	162	-	84	58	706	563	6.35	99.50	80		
CDH0923-4C	Tupe Fm.	54.09	1.06	18.30	7.68	0.07	1.76	2.21	0.69	3.71	0.19	36	117	223	144	51	124	53	182	569	7.82	98.74	64	
CDH0923-6C	Tupe Fm.	58.03	0.99	18.75	7.12	0.05	2.23	0.50	1.73	3.47	0.17	33	190	188	132	57	108	55	102	574	5.53	98.72	73	
CDH0923-7C	Tupe Fm.	54.92	1.13	21.23	6.68	0.06	2.30	0.25	0.66	4.06	0.06	38	125	239	167	64	97	59	99	601	7.43	98.83	79	
CDH0923-8C	Tupe Fm.	68.62	0.90	18.95	0.91	0.01	0.13	0.16	0.27	1.87	0.03	34	269	131	-	-	135	45	33	276	7.10	99.04	88	
CDH0923-9C	Tupe Fm.	60.32	0.99	21.87	4.29	0.05	0.93	0.32	0.50	3.01	0.03	36	353	204	57	31	88	46	48	376	6.99	99.43	83	
CDH0923-10C	Tupe Fm.	50.42	0.82	19.77	15.10	0.05	1.01	0.56	0.30	2.68	0.08	35	315	171	70	41	77	43	44	356	7.87	98.79	82	
CDH0923-11C	Tupe Fm.	53.32	0.88	21.27	10.74	0.06	1.10	0.38	0.38	2.70	0.03	49	204	51	40	60	38	48	281	7.82	98.80	84		
CDH0923-12C	Tupe Fm.	54.37	0.97	26.41	2.64	0.01	0.61	0.16	1.88	1.94	0.03	46	245	136	-	46	41	77	176	9.70	98.79	83		
CDH0923-13C	Tupe Fm.	61.63	0.80	16.90	5.82	0.04	2.10	0.76	2.77	3.84	0.14	42	151	168	88	31	78	45	101	406	11.12	106.03	63	
CDH0923-14C	Tupe Fm.	51.60	0.91	24.52	4.85	0.05	1.46	0.42	1.72	2.79	0.05	36	239	206	64	34	54	45	65	375	10.49	98.97	79	
CDH0923-15C	Tupe Fm.	58.69	0.90	21.70	3.50	0.07	1.74	1.47	0.92	2.93	0.04	36	292	155	-	72	43	75	351	7.24	98.31	75		
CDH0923-16C	Tupe Fm.	60.99	0.83	17.25	8.16	0.02	0.94	0.58	1.13	3.93	0.04	47	175	174	73	43	60	44	128	296	8.48	102.45	71	
CDH0923-17C	Tupe Fm.	53.10	0.79	17.85	8.76	0.10	1.10	2.65	0.61	3.03	0.03	29	180	42	31	59	38	94	254	6.45	94.56	66		
CDH0923-18C	Tupe Fm.	63.16	0.84	18.55	4.34	0.04	0.99	0.83	1.33	2.53	0.07	77	230	252	-	56	48	75	249	6.17	98.95	75		
CDH0923-19C	Tupe Fm.	65.53	0.69	16.17	4.96	0.09	1.27	0.99	1.39	2.48	0.08	36	208	165	59	38	58	46	75	378	5.75	99.51	71	
CDH0923-20C	Tupe Fm.	55.89	0.88	19.19	9.02	0.07	1.30	0.32	1.78	3.27	0.06	43	253	150	69	35	57	48	68	361	6.77	98.67	74	
CDH0923-21C	Tupe Fm.	51.16	0.99	23.68	9.69	0.04	0.90	0.79	0.55	2.75	0.24	70	192	198	50	38	65	58	82	292	8.13	99.03	83	
CDH0923-22C	Tupe Fm.	71.04	0.36	14.29	0.84	0.02	0.45	0.74	5.01	1.23	0.03	36	172	57	-	31	70	152	4.49	98.54	55			
CDH0923-23C	Tupe Fm.	56.46	0.21	19.36	7.20	0.02	1.72	1.33	3.57	2.79	0.03	37	199	111	-	-	30	135	146	5.16	97.94	64		
CDH0923-25C	Tupe Fm.	59.24	0.68	19.82	5.76	0.04	1.69	0.90	1.80	3.52	0.03	44	220	145	56	-	54	154	153	2426	5.23	99.04	70	
CDH0923-26C	Tupe Fm.	55.33	0.86	21.90	5.60	0.05	1.60	0.60	2.68	3.49	0.03	50	225	300	52	48	99	37	76	665	6.65	99.09	70	
CDH0923-27C	Patquia Fm.	51.38	0.98	24.24	7.16	0.04	1.16	0.74	1.84	3.59	0.13	45	261	148	59	33	50	50	541	317	7.17	98.60	75	
CDH0923-28C	Patquia Fm.	56.06	0.90	21.47	6.86	0.08	1.64	0.40	1.37	3.44	0.13	41	259	214	82	44	78	52	72	436	6.49	98.97	77	
CDH0923-29C	Patquia Fm.	76.33	0.71	11.19	2.79	0.01	0.89	0.51	2.30	1.95	0.02	29	435	130	-	53	39	98	281	5.88	102.69	62		
CDH0923-30C	Patquia Fm.	56.70	0.87	20.79	6.54	0.07	1.66	0.51	1.40	3.40	0.22	44	297	230	73	31	70	49	74	439	6.08	98.38	77	
CDH0923-31C	Patquia Fm.	54.31	0.83	22.23	7.04	0.07	1.74	0.19	1.81	3.64	0.04	50	206	152	66	39	60	43	66	369	6.64	98.76	76	
CDH0923-32C	Patquia Fm.	59.46	0.89	18.87	6.68	0.06	1.74	0.74	1.19	3.31	0.04	36	281	107	61	36	72	45	81	406	5.38	98.47	74	
CDH0923-33C	Patquia Fm.	74.57	0.80	12.17	3.64	0.02	0.95	0.41	1.85	1.92	0.02	30	419	69	-	67	35	99	243	2.82	99.28	68		
CDH0923-34C	Patquia Fm.	74.21	0.80	12.35	3.65	0.02	0.97	0.54	1.83	1.96	0.02	34	416	77	-	-	44	108	263	2.89	99.36	67		
CDH0923-35C	Patquia Fm.	56.53	0.75	17.82	7.42	0.07	1.60	0.59	0.96	2.91	0.05	43	197	181	46	37	56	48	110	339	2.53	91.35	76	
CDH0923-36C	Patquia Fm.	75.82	0.73	11.10	2.91	0.01	0.89	0.80	2.27	1.96	0.02	35	428	130	-	51	39	113	278	2.43	99.07	60		
CDH0924-1C	Patquia Fm.	66.80	0.86	15.70	5.62	0.03	0.86	0.42	2.07	3.12	0.03	38	343	128	-	70	41	108	311	3.47	99.10	68		
CDH0924-2C	Patquia Fm.	64.05	0.87	15.60	5.74	0.02	0.75	0.46	1.61	3.20	0.03	37	292	123	-	61	39	174	313	3.67	96.11	69		
CDH0924-3C	Patquia Fm.	72.95	0.75	13.47	4.08	0.01	0.49	0.41	1.96	2.44	0.03	31	424	130	-	46	39	91	265	2.71	99.39	67		
CDH0924-4C	Patquia Fm.	71.76	0.85	14.25	4.20	0.01	0.59	0.39	1.87	2.66	0.07	34	393	102	-	48	36	105	258	3.52	100.28	69		
CDH0924-5C	Patquia Fm.	74.22	0.80	12.94	3.80	0.01	0.47	0.32	2.00	2.21	0.03	31	420	117	-	61	35	102	162	2.50	99.39	68		
CDH0924-7C	Patquia Fm.	58.03	0.84	18.09	6.75	0.03	0.96	0.48	1.56	3.23	0.03	39	217	138	55	-	55	40	105	286	8.02	98.12	72	
CDH0924-8C	Patquia Fm.	60.13	0.89	19.50	7.15	0.02	0.97	0.29	1.41	3.58	0.05	46	219	153	63	30	73	45	132	347	4.76	98.86	75	
CDH0924-9C	Patquia Fm.	66.87	0.83	15.34	7.66	0.01	0.37	0.23	1.28	1.80	0.04	36	428	163	-	59	33	161	136	3.98	98.53	78		
CDH0924-10C	Patquia Fm.	60.02	0.95	19.16	7.54	0.03	0.92	0.38	1.60	3.05	0.04	41	306	180	61	36	69	43	133	306	5.04	98.84	80	
CDH0924-11C	Patquia Fm.	60.70	0.92	19.05	7.14	0.02	0.95	0.62	1.20	3.04	0.04	40	260	181	75	35	76	42	112	337	5.32	99.18	75	
CDH0924-12C	Patquia Fm.	58.37	0.88	16.56	8.70	0.06	2.70	0.66	2.37	5.08	0.09	42	60	250	143	42	79	35	76	323	3.14	98.73	61	
CDH0924-13C	Patquia Fm.	50.24	0.87	24.51	5.44	0.06	1.36	0.27	1.88	2.65	0.04	45	185	208	47	-	73	46	80	397	11.12	98.54	79	
CDH0924-14C	Patquia Fm.	50.23	0.87	15.96	7.87	0.09	2.49	6.93	3.48	3.52	0.10	45	44	260	115	34	50	40	122	292	7.87	99.52	42	
CDH0924-15C	Patquia Fm.	59.96	0.87	17.53	6.68	0.04	1.83	0.76	2.89	3.87	0.11	37	145	193	101	-	64	47	142	466	3.28	97.95	64	

Calibration Method for all Samples:
GEO-MAIORS-Ap08

** Significantly lower than the basement material, and therefore this CIA value is not used in analysis

Table B3. Paganzo Basin, Cerro Guandacol (G) Bulk-rock geochemistry

Sample	Formation Name	SiO2 (%)	TiO2 (%)	Al2O3 (%)	Fe2O3 (%)	Mn (%)	MgO (%)	CaO (%)	Na2O (%)	K2O (%)	P2O5 (%)	Y (PPM)	Zr (PPM)	V (PPM)	Zn (PPM)	Ni (PPM)	Cr (PPM)	Ce (PPM)	Sr (PPM)	Ba (PPM)	LOI	Sum (%)	ChA
GDM0924-1C	Tupe Fm.	48.92	0.88	16.29	6.66	0.08	2.85	0.62	7.66	3.63	0.14	39	98	175	89	36	84	49	89	438	9.87	97.71	48
GDM0924-2C	Tupe Fm.	55.44	1.02	17.86	7.83	0.08	3.02	0.48	2.81	3.53	0.15	33	182	216	74	41	86	50	87	417	4.86	97.19	67
GDM0924-5C	Tupe Fm.	47.04	0.94	24.45	6.92	0.05	2.60	0.13	1.45	2.32	0.07	44	119	225	82	34	92	47	72	314	12.46	98.54	83
GDM0924-6C	Tupe Fm.	62.82	0.76	15.79	5.27	0.06	2.04	0.74	1.95	3.71	0.09	38	161	128	67	33	78	37	116	189	10.07	103.39	65
GDM0924-7C	Tupe Fm.	57.48	0.92	17.14	7.85	0.08	2.91	1.03	1.71	3.57	0.16	33	122	218	97	51	73	47	97	436	4.64	97.60	68
GDM0925-01C	Tupe Fm.	45.25	3.17	20.10	13.05	0.04	3.90	0.34	1.60	2.27	0.02	38	242	546	105	278	379	32	71	106	8.21	98.13	78
GDM0925-04C	Tupe Fm.	39.36	3.15	16.07	15.76	0.42	3.69	5.01	1.42	0.41	0.11	28	199	526	109	236	342	39	261	173	11.91	97.51	58
GDM0925-5C	Tupe Fm.	44.15	2.86	22.62	9.71	0.11	1.35	3.20	0.28	1.88	0.70	38	316	364	91	96	168	33	203	128	9.73	96.73	77
GDM0925-06C	Tupe Fm.	50.06	1.46	23.69	7.36	0.06	1.58	0.63	1.24	2.05	0.09	35	228	282	105	56	78	42	75	281	4.63	92.98	82
GDM0925-07C	Patquia Fm.	67.33	1.00	11.88	5.15	0.14	1.91	2.57	1.27	2.36	0.09	33	274	109	39	47	82	33	62	232	4.59	98.39	57
GDM0925-8C	Patquia Fm.	65.38	0.90	13.69	5.87	0.08	2.44	1.02	1.82	2.50	0.12	34	272	108	41	65	94	35	84	204	3.57	97.48	66
GDM0925-9C	Patquia Fm.	64.54	1.08	13.42	6.44	0.09	2.80	0.96	1.94	2.00	0.09	30	208	153	77	63	80	33	67	149	4.03	97.48	66
GDM0925-9C2	Patquia Fm.	67.00	0.73	14.19	4.84	0.06	1.67	0.95	2.18	2.88	0.05	41	314	129	-	-	64	36	112	172	2.90	97.54	63
GDM0925-10C	Patquia Fm.	63.18	0.81	16.40	5.28	0.06	1.77	0.69	2.70	3.28	0.04	41	306	109	59	33	62	30	108	146	3.00	97.31	64
GDM0925-11C	Patquia Fm.	66.26	0.74	14.79	5.15	0.06	1.48	0.42	2.92	3.05	0.06	40	374	93	-	-	46	34	88	151	2.76	97.79	63
GDM0925-12C	Patquia Fm.	64.69	0.79	15.27	5.43	0.07	1.93	0.67	2.28	3.19	0.07	44	317	150	57	29	56	33	123	210	3.32	97.81	65
GDM0925-13C	Patquia Fm.	65.29	0.77	14.64	4.95	0.06	1.61	1.15	2.01	3.25	0.06	34	268	153	49	-	80	38	104	234	3.48	97.32	63
GDM0925-15C	Patquia Fm.	62.64	0.77	16.04	5.78	0.06	1.79	1.12	2.25	3.83	0.09	45	217	125	56	-	72	34	82	256	3.48	97.95	62
GDM0925-17C	Patquia Fm.	67.17	0.59	12.83	2.06	0.15	1.14	1.46	3.45	2.90	0.08	35	232	1704	40	30	156	31	121	184	4.71	96.79	53
GDM0925-19C	Patquia Fm.	65.32	0.63	14.45	4.23	0.06	1.51	0.57	3.82	2.91	0.04	42	322	86	86	39	48	32	78	105	3.52	97.13	58

Calibration Method for all Samples:

GEO-MAJORS-AP08

Table B4. Calingasta-Uspallata: Agua de Jagüel (AJ) Bulk-rock geochemistry

Sample	Formation Name	SiO2 (%)	TiO2 (%)	Al2O3 (%)	Fe2O3 (%)	Mn (%)	MgO (%)	CaO (%)	Na2O (%)	K2O (%)	P2O5 (%)	Y (PPM)	Zr (PPM)	V (PPM)	Zn (PPM)	Ni (PPM)	Cr (PPM)	Ce (PPM)	Sr (PPM)	Ba (PPM)	LOI	Sum (%)	CIA
AD0916-1C	Agua de Jagüel	78.99	0.69	5.04	2.24	0.09	0.49	4.95	1.21	0.54	0.09	22	165	68	-	-	-	27	86	196	4.94	99.35	31
AD0916-4C	Agua de Jagüel	86.09	0.63	5.06	2.60	0.05	0.58	0.81	1.13	0.50	0.07	20	147	80	-	-	-	49	46	101	1.66	99.23	58
AD0917-1M	Agua de Jagüel	48.21	0.62	9.62	6.52	0.26	5.75	9.60	0.42	2.52	0.28	34	123	147	85	39	48	44	243	442	15.66	99.58	32
AD0917-2MS	Agua de Jagüel	54.34	1.01	18.81	9.24	0.09	2.37	0.61	1.03	4.70	0.17	45	140	256	116	58	124	59	88	655	5.12	97.65	72
AD0917-3C	Agua de Jagüel	56.22	0.99	17.68	8.94	0.10	3.03	0.54	1.37	3.81	0.18	43	156	239	126	56	119	57	56	650	4.51	97.53	72
AD0917-4C	Agua de Jagüel	56.09	0.51	9.04	5.10	0.44	4.85	7.20	0.70	2.08	0.27	34	90	121	91	-	51	38	116	336	12.23	98.60	66
AD0917-5C	Agua de Jagüel	53.38	1.00	19.01	9.38	0.10	2.63	0.64	1.00	4.60	0.16	46	140	260	154	56	128	61	57	723	5.31	97.38	72
AD0917-6C	Agua de Jagüel	53.01	0.98	19.60	9.20	0.15	2.88	0.66	0.97	4.73	0.18	46	153	285	144	58	118	69	75	857	5.10	97.65	72
AD0917-8C	Agua de Jagüel	57.60	1.02	17.81	8.43	0.08	2.69	0.49	1.20	3.86	0.18	46	153	259	127	64	92	62	57	698	4.56	98.07	73
AD0917-9C	Agua de Jagüel	50.47	1.03	19.52	9.63	0.10	3.19	1.00	0.88	4.38	0.17	40	106	266	143	82	118	65	76	747	6.04	96.59	72
AD0917-10C	Agua de Jagüel	64.51	0.69	14.67	6.30	0.09	2.19	1.06	1.74	2.85	0.15	32	84	182	91	44	77	55	92	558	3.80	98.17	66
AD0917-11C	Agua de Jagüel	62.59	0.99	14.94	6.82	0.09	2.39	1.25	1.64	2.98	0.18	40	199	208	104	55	78	51	84	501	4.13	98.13	66
AD0917-12C	Agua de Jagüel	56.80	1.03	16.27	8.17	0.15	2.70	2.10	1.58	3.23	0.18	38	155	230	118	55	115	52	91	603	5.49	97.84	63
AD0917-13C	Agua de Jagüel	62.97	0.97	14.89	6.82	0.08	2.43	1.17	1.80	2.78	0.19	41	222	243	90	42	104	52	78	447	4.21	98.44	66
AD0917-14C	Agua de Jagüel	58.91	0.88	14.00	6.57	0.10	2.24	2.90	1.45	2.86	0.17	41	198	145	84	39	61	46	84	386	5.60	95.80	58
AD0917-15C	Agua de Jagüel	56.57	1.03	17.42	8.12	0.08	2.97	1.04	1.15	3.91	0.17	37	161	254	118	53	105	58	79	553	5.14	97.76	70
AD0918-3C	Agua de Jagüel	57.22	0.93	16.82	7.95	0.11	2.37	1.39	1.54	3.78	0.22	40	199	218	100	41	104	54	114	523	5.38	97.84	66
AD0918-4C	Agua de Jagüel	55.57	0.96	17.17	8.56	0.07	3.05	0.69	1.71	3.38	0.24	44	227	228	101	51	102	58	82	629	4.66	96.23	71
AD0918-7C	Agua de Jagüel	64.74	1.02	15.44	5.65	0.05	1.49	0.63	1.04	2.83	0.17	43	204	154	52	-	60	50	108	399	4.66	97.82	74
AD0918-8C	Agua de Jagüel	58.15	0.96	17.80	7.43	0.01	1.10	0.23	0.91	3.41	0.21	41	173	235	115	-	101	52	169	487	6.22	96.57	78
AD0918-9C	Agua de Jagüel	57.03	0.95	18.62	7.98	0.04	1.50	0.64	0.88	3.83	0.16	43	175	266	122	33	94	55	126	524	5.37	97.53	74
AD0918-10C	Agua de Jagüel	64.44	0.79	15.27	6.32	0.10	1.26	0.79	1.45	2.90	0.18	42	254	164	172	37	67	45	151	389	4.66	98.29	70
AD0918-11C	Agua de Jagüel	61.31	0.95	17.32	6.18	0.06	1.94	0.74	1.34	3.52	0.17	45	170	192	89	35	104	49	117	443	4.76	98.43	71
AD0918-12C	Agua de Jagüel	62.95	0.94	14.94	6.85	0.06	1.76	1.21	1.61	2.37	0.17	34	291	175	73	-	87	48	111	377	4.57	97.66	68

Calibration Method for all Samples:

GEO-MAIORS-Ap08

Table B5. Paraná: Brazil Samples Bulk-rock geochemistry

Sample	Formation Name	SiO ₂ (%)	TiO ₂ (%)	Al ₂ O ₃ (%)	Fe ₂ O ₃ (%)	Mn (%)	MgO (%)	CaO (%)	Na ₂ O (%)	K ₂ O (%)	P ₂ O ₅ (%)	Y (PPM)	Zr (PPM)	V (PPM)	Zn (PPM)	Ni (PPM)	Cr (PPM)	Ce (PPM)	Sr (PPM)	Ba (PPM)	LOI	Sum (%)	CIA
FQ0820-1D	Itararé Gp.	71.97	0.63	12.53	3.89	0.07	1.42	0.83	1.96	3.6	0.19	29	264	66	21	37	70	79	169	746	3.83	101.08	61
STRPAV0822-2	Itararé Gp.	56.04	0.87	18.03	8.28	0.03	2.29	0.23	0.72	4.81	0.07	41	192	149	111	78	95	274	146	3121	8.08	99.89	69
RR0820-1	Itararé Gp.	67.24	0.83	14.87	3.81	0.01	0.99	0.23	0.51	4.65	0.11	31	233	90	-	31	87	79	98	669	7.57	100.96	69
Mariana Pimentel	Itararé Gp.	68.99	0.98	15.33	0.68	0.05	0.27	0.01	0.05	4.16	0.12	39	195	96	-	-	52	97	401	738	4.85	95.66	78
ITA0823-1	Itararé Gp.	65.72	1.06	23.37	1.06	-	-	0.02	-	0.68	0.03	29	275	105	-	-	85	49	17	235	1.02	92.55	97
RB0823-1	Rio Bonito Fm.	68.88	0.67	20.71	0.96	-	-	0.01	-	0.5	0.02	31	215	57	-	-	65	51	35	152	7.84	99.66	98

Calibration Method for all Samples:
GEO-MAIORS-Ap08

CURRICULUM VITAE

Kathryn N. Pauls

Education

Augustana College, Rock Island, Illinois

Bachelor of Arts-Geology and Spanish, cum laude, May 2011

University of Wisconsin-Milwaukee, Milwaukee, Wisconsin

Master of Science-Geosciences, May 2014

Dissertation: Late Paleozoic climatic comparisons of mid-paleolatitude basins across southwestern Gondwana

Appointments

Field Museum, Chicago, IL

- IMLS Digitization Intern, Ordovician Collection

June-August 2019

Upper Iowa University, Milwaukee Center

- Adjunct Faculty

· ES 100: Introduction to Physical Geology, 2 terms; ES 161: Introduction to Environmental Science, 2 terms; ES 117: Natural Disasters

October 2016-Present

GSA GeoCorps of America Program, Badlands National Park

- Resource Education Interpretation, Paleontology Intern

June 2013-August 2013

Milwaukee Public Museum

- IMLS Digitization Intern

May 2018-May 2019, Present

- Geology Department Intern

February 2012-May 2012; July 2017-May 2018

University of Wisconsin-Milwaukee Department of Geosciences

- Distinguished Doctoral Dissertation R1 Fellow

2018-2019

- Science Bag Program Assistant

2015-present

- Graduate Research Assistant

Spring 2013, Spring 2015, 2016-2017

- Graduate Teaching Assistant

· GeoSci 100: Introduction to Geology, 9 semesters, 8 Lead TA; GeoSci 102: Historical Geology, 2 semesters; GeoSci 151: Ocean Sciences Laboratory, 1 semester; GeoSci 520: Introduction to Paleontology, 1 semester; GeoSci 511: Stratigraphy and Sedimentation, 3 semesters; GeoSci 697: Permian-Triassic Ecosystem Changes, 1 semester; Geosci 515: Physical Sedimentology, 1 semester;

· Geosci 185: Introduction to Earth Sciences for Teachers, Lecturer, 1 semester; Geosci 109: Dinosaurs, Online lecturer, 2 semester; Geosci 150: Oceanography, Online lecturer, 1 semester

August 2011-May 2020

United States Army Corps of Engineers – Rock Island District

- Student Cartographic Aid, GIS Department, Project Management Branch

May 2010-August 2011

University of Minnesota-Morris REU Program

- Research Assistant, Quaternary and LPIA Glacial Geology Project

June 2009-August 2009

Current Thesis Project and Timeline

Field work, data analysis:

Spring 2015 and Summer/Fall 2016

Dissertation proposal submission and defense, Qualifying Exams, field work:

Academic Year 2016-2017

Further field work and research, data analysis, manuscript submission:

Academic Year 2017-2018

Dissertation completion, defense, graduation anticipated:

Academic year 2019- 2020

Field Experiences (Research)

Mendoza, San Juan Provinces, Argentina	2017
Southern Ontario Province, Canada	2017
La Rioja and San Juan Provinces, Argentina;	
Rio Grande do Sul State, Brazil	2016
La Rioja Province, Argentina	2015
Southern Ontario Province, Canada	2014
Sierra de Tepuel, Patagonia, Argentina	2014
Sierra de Tepuel, Patagonia, Argentina	2012
Paraná State, Brazil	2009

Grants

UW-M Center for Latin American and Caribbean Studies Tinker Field Research Grant, 2016, 2017

Geological Society of America Graduate Student Research Grant, 2016

Wisconsin Geological Society Graduate Research Grant, 2015

Society for Sedimentary Geology (SEPM), Graduate Student Research Grant, 2012 & 2015

Awards and Scholarships

University of Wisconsin-Milwaukee

Graduate Student Research Excellence Award, 2016-2017

Outstanding TA of the Year Award, 2016

Graduate Student Excellence Fellowship Award, 2016

Department of Geosciences Summer Field Work Scholarship, 2015, 2016

Wisconsin Geological Society Scholarship, 2015, 2016

Center for Latin American and Caribbean Studies Student Research Travel Award, 2014-2017

Department of Geosciences Graduate Student Research Excellence Award, 2013

UWM Chancellor's Graduate Student Award, 2012-Present

Invited Talks and Presentations

Burpee Museum of Natural History

PaleoFest, March 2018, Paleogeology of a late Paleozoic high-latitude marine fauna: Insights into changes in diversity in a glacially influenced basin

Milwaukee Public Museum

Inside Out, April 2018, Using a Scanning Electron Microscope to learn the Stories of Sand Grains

Illinois State University

Geosciences Dept. Colloquium Series, October 2018, Late Paleozoic regional paleoclimate of the Protoprecordilleran Gondwana margin

Publications

Pauls, K.N., Isbell, J.L., Limarino, C.O., Colombi, C., Alonso-Muruaga, P., McHenry, L., Malone, D., Schencman, L.J., Moxness, L.D., in prep., Late Paleozoic paleoclimate reconstruction of the Paganzo Basin of western Argentina: Controls on diachronous deglaciation in western Gondwana.

Pauls, K.N., Isbell, J.L., Moxness, L.D., Limarino, C.O., Schencman, L.J., Malone, D., Colombi, C., Alonso-Muruaga, P., in prep., Constraining late Paleozoic ice extent in the Paganzo Basin of western Argentina.

Pauls, K.N., Gigstad, K., Fraiser, M.L., Isbell, J.L., Pagani, M.A., Taboada, A.C., Dineen, A.A., in prep. Paleocology of the Lanipustula Biozone of the Pampa de Tepuel Formation, Tepuel Basin, Patagonia, Argentina.

Pauls, K.N., Isbell, J.L., McHenry, L., Limarino, C.O., Moxness, L.D., Schencman, L.J., 2019. A paleoclimatic reconstruction of the Carboniferous-Permian paleovalley fill in the Eastern Paganzo Basin: Insights into glacial extent and deglaciation of southwestern Gondwana. *Journal of South American Earth Sciences*, vol. 95. <https://doi.org/10.1016/j.jsames.2019.102236>

Fedorchuk, N.D., Isbell, J.L., Griffis, N.P., Vesely, F.F., Rosa, E.L.M., Montañez, I.P., Mundil, R., Yin Q.-Z., Iannuzzi R., Roesler G., Pauls K.N., 2019. Carboniferous glaciotectionized sediments in the southernmost Paraná Basin, Brazil: Ice marginal dynamics and paleoclimate indicators. *Sedimentary Geology*. <https://doi.org/10.1016/j.sedgeo.2019.05.006>

Craddock, J.P., Ojakangas, R.W., Malone, D.H., Konstantinou, A., Mory, A., Thomas, R.J., Craddock, S.D., Pauls, K.N., Zimmerman, U., Botha, G., Rocha-Campos, A., de Pazos, P.R., Tohver, E., Riccomini, Cl., Martin, J., Redfern, J., Horstwood, M., Gehrels, G., 2019. Provenance of Permo-Carboniferous Diamictites across Gondwana. *Earth Science Reviews*. <https://doi.org/10.1016/j.earscirev.2019.01.014>

Moxness, L.D., Isbell, J.L., Pauls, K.N., Limarino, C.O., Schencman, L.J., 2018. Sedimentology of the Mid-Carboniferous fill of the Olta Paleovalley, eastern Paganzo Basin, Argentina: Implications for glaciation and controls on diachronous deglaciation in western Gondwana during the Late Paleozoic ice age. *Journal of South American Earth Sciences*, vol. 84, p. 127-148, doi: 10.1016/j.jsames.2018.03.015.

Fedorchuk, N.D., Isbell, J.L., Griffis, N.P., Montañez, I.P., Mundil, R., Iannuzzi, R., Vesely, F.F., Yin, Q.-Z., Pauls, K.N., Rosa, E.L.M., 2018. Origin of paleovalleys on the Rio Grande do Sul Shield (Brazil): Implications for the extent of late Paleozoic glaciation in central Gondwana. *Palaeogeography, Palaeoclimatology, Palaeoecology*, doi: 10.1016/j.palaeo.2018.04.013.

Professional Meeting Presentations and Abstracts

- Pauls, K.N., 2019. Using Your Head: MPM 8111 and the Pachycephalosaur Debate. Society for the Preservation of Natural History Collections Meeting, Chicago, IL.
- Coorough-Burke, P.J., Pauls, K.N., 2019. Digitizing the Ordovician collection: in between a rock and a new building. Society for the Preservation of Natural History Collections Meeting. Chicago, IL.
- Pauls, K.N., Isbell, J.L., Moxness, L.D., Limarino, C.O., Schencman, L.J., Colombi, C.E., Alonso-Muruaga, P.J., 2018. Late Paleozoic regional paleoclimate of the Protoprecordilleran Gondwana margin: a case study in the Paganzo Basin. Geological Society of America Abstracts with Programs. vol. 50, no. 6, doi: 10.1130/abs/2018AM-323895.
- Pauls, K.N., Isbell, J.L., Moxness, L.D., Limarino, C.O., Schencman, L.J., 2017. Late Paleozoic paleoclimatic comparisons of mid-latitude basins in Western Argentina: Controls on early Pennsylvanian deglaciation in Western Gondwana. Geological Society of America Abstracts with Programs, vol. 49, no. 6, doi: 10.1130/abs/2017AM-300103.
- Moxness, L.D., Isbell, J.L., Gulbranson, E.L., Pauls, K.N., 2016. Sedimentology of a late Paleozoic paleovalley in the eastern Paganzo Basin, La Rioja Province, Argentina. Geological Society of America Abstracts with Programs, vol. 48, no. 5 doi: 10.1130/abs/2016NC-275581.
- Pauls, K.N., Gulbranson, E.L., 2015. Carbohydrate cycling in evergreen and deciduous trees of SE Wisconsin: implications for high-resolution isotope analyses of growth rings of modern and fossil wood. Geological Society of America Abstracts with Programs, Vol. 47, No. 5, p. 18.
- Survis, Sarah R., Isbell, J.L., Pauls, K.N., Pagani, M.A., Taboada, A.C., 2015. Sedimentology and stratigraphy of high-latitude, shelf-edge and slope, glacial deposits from the late Paleozoic ice age in the Tepuel Basin, Patagonia, Argentina. Geological Society of America Abstracts with Programs, Vol. 47, No. 5, p. 86.
- Braun, N.L., Fraiser, M.L., Isbell, J.L., Pagani, M.A., Taboada, A.C., Pauls, K.N., 2014. Paleoecology of glacial and non-glacial Carboniferous faunas during the late Paleozoic ice age in Patagonia. Geological Society of America Abstracts with Programs, Vol. 46, No. 6, p. 137.
- Pauls, K.N., Fraiser, M.L., Isbell, J.L., Pagani, M.A., Taboada, A.C., 2013. Sedimentology and paleoecology of late Paleozoic high-latitude glacial deposits in the Tepuel Basin, Argentina. Geological Society of America Abstracts with Programs, Vol. 45, No. 7, p. 301.
- Isbell, J.L., Taboada, A.C., Gulbranson, E.L., Pagani, M.A., Pauls, K.N., Limarino, C.O., Ciccioli, P.L., Fraiser, M.L., 2013. Carboniferous and Permian glacial and nonglacial strata of the Tepuel-Genoa Basin, Patagonia, Argentina: A near-continuous, deep-water record of South Polar Gondwana during the late Paleozoic Ice Age: Geological Society of America Abstracts with Programs, v. 45, no. 7.
- Pagani, M.A., Taboada, A.C., Isbell, J.L., Fraiser, M.L., Dineen, A.A., Pauls, K.N., 2012, the Lanipustula Biozone in Patagonia: stratigraphic extension, faunal changes, paleoclimatology and paleoecology. Asociación Paleontológica Argentina Annual Meeting, General Roca.

Pauls, K.N., Fraiser, M.L., Isbell, J.L., Pagani, M.A., Taboada, A.C., 2012. Paleoecology and sedimentology of fossil-bearing, high-latitude glacial deposits in the Tepuel Basin, Argentina. *Geological Society of America Abstracts with Programs*, Vol. 44, No. 7, p. 398.

Pauls, K.N., Rocha-Campos, A.C., Cotter, J.F.P., 2011. An analysis of two Late Paleozoic sandstones of the Paraná Basin in Southern Brazil. *Geological Society of America Abstracts with Programs*, Vol. 43, No. 1, p. 114.

Pauls, K.N., Thomson, O.A., Rocha-Campos, A.C., Cotter, J.F.P., 2010. A grain-count analysis of the Late Paleozoic glacial deposits of the Paraná Basin, Witmarsum, Paraná State, Brazil. *Geological Society of America Abstracts with Programs*, Vol. 42, No. 2, p. 58.

Thomson, O.A., Pauls, K.N., Rocha-Campos, A.C., Cotter, J.F.P., 2010. Distinguishing between the sand units of the Carboniferous Itararé Subgroup and the Devonian Furnas Formation in Paraná State, Brazil. *Geological Society of America Abstracts with Programs*, Vol. 42, No. 3, p. 41.

Collaborators

Dr. John Isbell, UW-Milwaukee – Thesis Co-Advisor, PhD Advisor

Email: jisbell@uwm.edu

Dr. Margaret Fraiser, UW-Milwaukee – Thesis Co-Advisor

Email: mfraiser@uwm.edu

Dr. M. Alejandra Pagani, Museo Paleontológico Egidio Feruglio

Email: apagani@mef.org.ar

Dr. Arturo Taboada, (LIEB), Universidad Nacional de la Patagonia

Email: ataboada@unpata.edu.ar

Dr. C. Oscar Limarino (CONICET), Universidad de Buenos Aires

Email: oscarlimarino@gmail.com

Dr. Carina Colombi (CONICET), Universidad Nacional de San Juan

Email: ccolombi@unsj.edu.ar

Dr. L. Jazmin Schencman (CONICET), Universidad de Buenos Aires

Email: jazminsch@gmail.com

Dr. Pablo J. Alonso-Muruaga (CONICET), Universidad de Buenos Aires

Email: pablojoaquin3@gmail.com Kathryn N. Pauls